MONITORING AND CONTROL OF ELECTROTHERMAL SWING ADSORPTION BASED ON ELECTRICAL PROPERTIES OF THE ADSORBENT

BY

DAVID LEONARD JOHNSEN III

DISSERTATION

Submitted in partial fulfillment of the requirements
for the degree of Doctor of Philosophy in Environmental Engineering in Civil Engineering
in the Graduate College of the
University of Illinois at Urbana-Champaign, 2014

Urbana, Illinois

Doctoral Committee:

Professor Mark J. Rood, Chair & Director of Research
Professor Yuanhui Zhang
Professor Pierre Le Cloirec, Ecole Nationale Superieure de Chimie de Rennes, France
Assistant Professor Jeremy S. Guest

Abstract

Organic vapors and gases (e.g., toluene and isobutane, respectively) are used in industry to produce a variety of products (e.g., coatings and packaging materials). During production and use of these products, these vapors/gases are often emitted in dilute concentrations, causing adverse health effects and photochemical reactions that increase ground-level ozone concentration. Thermal oxidization is often used for vapor/gas disposal (ideal conversion to H_2O and CO_2). Capturing and recovering vapors/gases can reduce cost by providing feedstock for production and eliminate emissions from thermal oxidation.

A bench-scale electrothermal swing adsorption (ESA) system that uses activated carbon fiber cloth (ACFC) to selectively remove vapors/gases from gas streams and electrothermal heating to regenerate the ACFC was previously developed. This system concentrates a vapor/gas to > 50 % by volume allowing for condensation for reuse as a liquid. Typically, the end of an ACFC-ESA adsorption cycle and the heating part of a regeneration cycle are determined based on measurements from hydrocarbon sensors, which have capital costs and require periodic maintenance. Also, regeneration heating and cooling requires direct-contact thermocouple measurements to determine when to apply power and when cooling is complete to initiate an adsorption cycle, respectively. However, these thermocouples can lose contact with the ACFC or create an electrical short circuit during regeneration that damages the system and/or adsorbent.

For this research, a method was developed to monitor and control ACFC-ESA that eliminates the need for hydrocarbon and direct-contact temperature sensors. This method provides the ability to monitor the electrical properties of the ACFC and control adsorption cycles, regeneration cycles, and cyclic ESA based on these properties. This research is divided into five sections: 1) Characterize changes in ACFC electrical resistivity during adsorption for

ACFC samples with select physical and chemical properties, 2) characterize the effect of varying temperature and applied power profiles on the ACFC regeneration energy efficiency, 3) develop and test a new method to control ACFC regeneration heating based only on electrical resistance measurements, 4) characterize and control cyclic ESA based only on electrical measurements, and 5) compare the ESA system to existing abatement systems using a life cycle assessment and a cost assessment.

This method to monitor and control ESA based on the adsorbent's electrical properties is an improvement over current methods because it provides real-time adsorbed mass during adsorption cycles resulting in improved vapor/gas recovery efficiency and does not require direct-contact temperature or hydrocarbon sensors, which periodically fail and need to be calibrated, maintained, and replaced, reducing system run time and increasing operating costs. This study provides a method to increase ACFC-ESA vapor/gas capture and recovery efficiency and reduce energy demand and vapor/gas emissions (and their corresponding health effects) to improve the sustainability of the system. The unique contributions of this research include: 1) characterization of parameters affecting ACFC electrical resistance, 2) evaluation of regeneration temperature and power profiles for their effects on regeneration energy efficiency, 3) control of regeneration cycles based on electrical properties of the ACFC, 4) control of cyclic ESA based on electrical properties of ACFC, and 5) evaluation (life cycle assessment and cost assessment) of cyclic operation with this novel method to control ACFC-ESA for vapor/gas abatement compared to typical volatile organic compound abatement systems (i.e., granular activated carbon system and regenerative thermal oxidizer).

Acknowledgements

I would like to thank Dr. Mark J. Rood, my advisor and chair of my Ph. D. committee, for his continued guidance and constructive feedback throughout my doctoral studies. Dr. Rood provided me with encouragement and many opportunities to participate with a range of projects and activities to promote my academic and professional development. I would also like to thank my Ph.D. committee members Dr. Yuanhui Zhang, Dr. Pierre Le Cloirec, and Dr. Jeremy S. Guest for providing their revisions and comments to improve my doctoral dissertation.

Thanks to the Air Quality Engineering & Science research group for their support throughout my graduate studies and for their thorough feedback in group meetings and in the lab. I've had the opportunity to work closely on projects with many members within the group and it has been a great experience. Kaitlin Mallouk introduced me the experimental set-up that later developed into this project and has provided valuable feedback and discussion on many components of my dissertation research. Zhanquan Zhang aided me with performing X-ray diffraction and X-ray photoelectron spectroscopy and provided valuable insight about the electrical properties of activated carbon fiber cloth. Hamid Emamipour also contributed to many aspects of this research project including aiding with development of project proposals, adjustments to the experimental set-up, and providing insights into theoretical modeling pertaining to this work.

I would also like to thank Shaoying Qi, lab manager of the Environmental Engineering and Science Program, for his help with this project.

I would like to acknowledge financial support for this project including the National Science Foundation Chemical, Bioengineering, Environmental, and Transport Systems grant, the Air & Waste Management Association Milton Feldstein Memorial Scholarship, and the University of Illinois at Urbana-Champaign Department of Civil and Environmental Engineering Walter E. Deuchler and Graduate Assistant in Areas of National Needs fellowships. I would also like to acknowledge financial support for travel to professional conferences provided by the Lake Michigan States Sections of the Air & Waste Management Association and the Department of Civil and Environmental Engineering of the University of Illinois at Urbana-Champaign.

Table of Contents

List of Figures

List of Tables

Chapter 1: Introduction

1.1. Background Information

Volatile organic compounds (VOC)s are defined uniquely for outdoor and indoor environments because they can have different effects depending on where they are emitted. In an outdoor environment, they are classified by the United States Environmental Protection Agency (USEPA) as "any compound of carbon, excluding carbon monoxide, carbon dioxide, carbonic acid, metallic carbides or carbonates, and ammonium carbonate, which participates in atmospheric photochemical reactions" (USEPA, 2009). Outdoor VOC emissions are regulated because they react in the atmosphere to create ground-level ozone, which contributes to photochemical smog. For indoor environments, VOCs are generally defined as any organic compound with a composition that allows for evaporation at normal indoor pressure and temperature (USEPA, 2011a). Depending on the compound, VOC emissions in indoor environments cause eye, nose, and throat irritation, headaches, damage to the liver, kidney, and central nervous system, memory impairment, and cancer (USEPA, 2011a).

VOCs are used to produce a wide range of materials including paints, packaging materials, solvents, lubricants, and household cleaners and can be emitted as a gas from the material itself or during production of the material. VOC emissions resulting from evaporation are often released in dilute concentrations (i.e., < 5,000 ppm_v) that are mixed with the ambient indoor or outdoor air. Indoor emissions vary by building and, thus, need to be measured to determine the appropriate action to avoid adverse health effects. Outdoor emissions data are more readily available. Figure 1 describes the 2005 United States (US) outdoor atmospheric VOC emissions data separated by source. Anthropogenic point sources comprise > 36 % of the

total VOC emissions suggesting emissions can be significantly reduced with careful environmental practice at point sources (USEPA, 2011c).

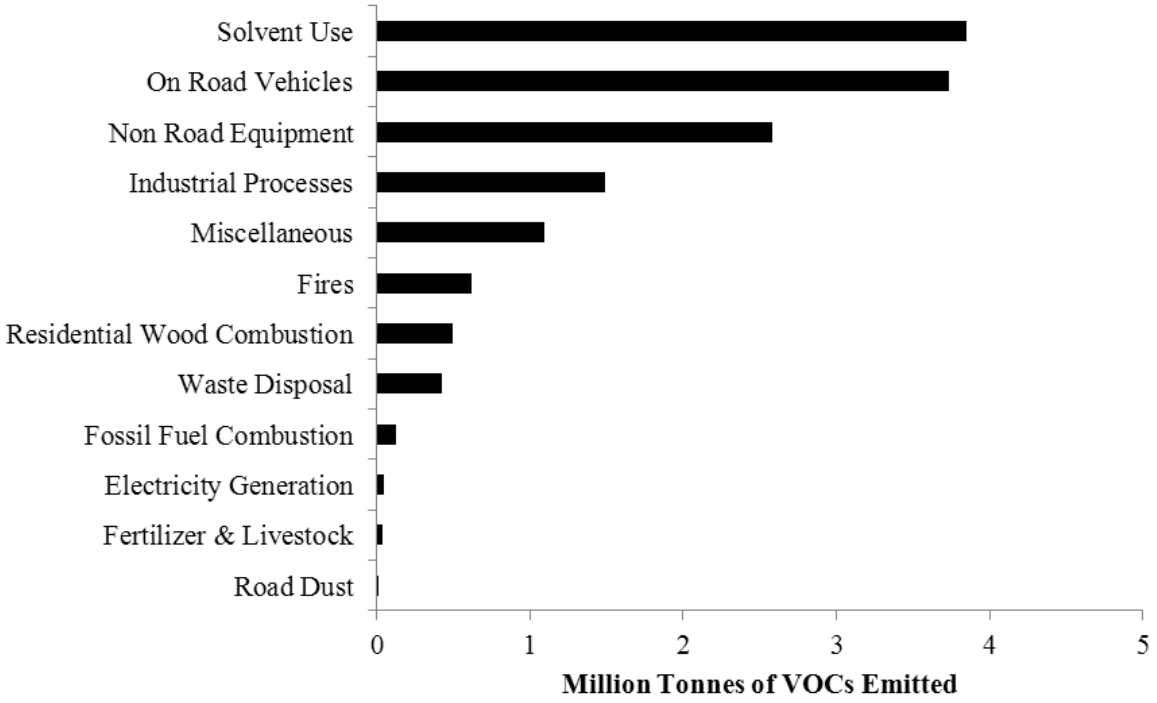

*Volatile organic compound (VOC), United States (US)
Figure 1: Sources of US VOC emissions in 2005 with data extracted from the US Environmental Protection Agency emissions inventory (USEPA, 2011c)

1.2. Organic Compound Abatement

There are a variety of methods for reducing VOC emissions to improve human health and meet air quality emissions standards. Process modification and substitution of materials are often the most desirable methods for organic compound abatement because they involve eliminating the pollutant source. When these options are not available, possibly due to cost or performance specifications, "end of the pipe" abatement techniques can be implemented to treat the gas streams containing VOCs before they are released into the ambient environment. These

techniques can be destructive and convert the compound into a different form (i.e., oxidation and biofiltration) or be non-destructive and recover the compound in the same form (i.e., direct condensation, membrane separation, absorption, and adsorption).

1.2.1. Oxidation

Oxidation of VOCs is an exothermic reaction that involves interaction between the organic gas and O_2 to primarily form H_2O and CO_2. Thermal oxidation requires high temperatures for combustion (i.e., 700 to 1200 °C), while catalytic oxidation involves a catalyst that lowers the required temperature (i.e., 340 to 590 °C) to oxidize the VOCs (Hunter and Oyama, 2000; Altwicker *et al.*, 1999). Benefits to lower combustion temperature include reduction of NO_x formation and lower operating costs because less auxiliary fuel is required (Noll, 1999). Trade-offs for catalytic oxidation include additional costs for the catalyst and maintenance for the catalytic unit (Noll, 1999). Thermal and catalytic oxidation are typically used for airstreams with VOC concentrations ranging from 100 to 2,000 ppm_v (Khan and Ghosal, 2000) and can achieve VOC removal efficiencies > 99.5 % (Cooper and Alley, 1986).

There are multiple trade-offs to using combustion to remove VOCs from gas streams. One trade-off is that combustion is destructive such that the VOC cannot be recovered as feedstock for reuse. Also, thermal and catalytic oxidation routinely require auxiliary fuel for complete oxidation of dilute concentrations of VOCs. This auxiliary fuel adds cost and results in additional mass of combustion products. Combustion forms CO_2 (i.e., a greenhouse gas) and products of incomplete combustion such as CO (i.e., a criteria pollutant) and NO (i.e., which is converted to the criteria pollutant NO_2 in the atmosphere). Additionally, combustion of halogenated VOCs can result in the formation of HCl, which is corrosive and toxic.

1.2.2. Biofiltration

Biofiltration is an abatement method that uses microorganisms to aerobically degrade VOCs in an airstream. This method is best suited for gas streams with VOC concentrations < 5,000 ppm_v (Khan and Ghosal, 2000). The gas stream passes through a biologically active support media, such as compost or soil that has a biofilm composed of microbial organisms, which consume VOCs and produce biomass, CO_2, and H_2O (Cooper and Alley, 1986). The advantages to biofiltration include high removal efficiency (i.e., > 90 %) and low operating cost for applications with stable VOC concentrations and flow rates (Leson and Winer, 1991). Biofiltration of easily degradable compounds costs \$0.25 to \$0.50 per 1,000 m^3 of gas treated, while biofiltration can cost as much as \$10 per 1,000 m^3 gas treated (Cooper and Alley, 1986). Biofiltration challenges include that the microorganisms require a large overall surface area and that operating conditions, such as inlet VOC concentration, moisture, and pH, must be maintained to sustain microorganism activity. Additionally, accumulation of biomass can cause non-uniform flow through the filter reducing the air flow that can be effectively treated, halogenated VOCs are difficult to treat with a biofilter, and biofiltration is a destructive process such that the VOC cannot be reused.

1.2.3. Condensation

Condensation is an abatement technique that can be used to remove VOCs from a gas stream for reuse that involves cooling and/or compressing the gas stream for the VOC to change from a gas to a liquid. To achieve condensation of the VOC, the gas stream is typically chilled with cold water, mechanical refrigeration, or cryogenic fluids. Another option for liquefaction of

VOCs is to use high pressure to compress the gas stream. The effectiveness of condensation depends on the concentration, saturation temperature, and saturation vapor pressure of the VOC. Condensation is generally used for high boiling point VOCs (i.e., > 38 °C) with concentrations > 5,000 ppm_v (USEPA, 2002). Extensive compression or chilling can be used to achieve condensation of low boiling point (e.g., organic gases) or dilute concentration (i.e., < 5,000 ppm_v) VOCs but the operation costs sharply increase (Khan and Ghosal, 2000).

1.2.4. Membrane Separation

Membrane separation involves the use of a pressure gradient across a semi-permeable membrane for the separation of two or more gases. The operating cost for this technique is nearly independent of the concentration of VOC to be removed, while it is largely dependent upon the volume of gas treated (Gales *et al*., 2011). Membrane separation is, thus, more effective for low flow rate gas streams (i.e., < few thousand m^3/h) and can have removal efficiencies from 90 to 99 % even for large VOC concentrations (i.e., > 5,000 ppm_v), but the power required to create the pressure gradient for higher flow gas streams is more costly (Khan and Ghosal, 2000; Gales *et al*., 2002). Membrane fouling from particles is also a challenge for membrane separation, so pretreatment devices are often necessary (Hunter and Oyama, 2000).

1.2.5. Absorption

Absorption of VOCs for air pollution abatement occurs when a gas stream interacts with a liquid absorbent causing mass transfer of the VOCs into the absorbent. A driving force and interaction between the gas and liquid are required for the absorption process to occur. The

driving force for absorption to occur within a wet scrubber is caused by the solubility of the pollutant gas into the liquid. The major advantage of a wet scrubbing system is that it can reach high VOC removal efficiencies (i.e., typically > 90 %) over a large range of gas stream flow rates (i.e., 0.25 to 35 m^3/s) and VOC concentrations (i.e., 250 to 10,000 ppm_v) (USEPA, 2012). One of the major challenges to VOC absorption is that for removal to occur, the VOC must be soluble in the absorbent (Wark *et al*., 1998). Another challenge is that the VOC is transferred into the scrubbing liquid, which must also be treated to separate the VOC from the liquid phase for recovery of the VOC (Hunter and Oyama, 2000).

1.2.6. Adsorption

Adsorption involves the interaction of a gas stream with an interface (adsorbent) that is preferred by the adsorbate (e.g., VOC), which causes mass transfer of the adsorbate onto the adsorbent. For this research, only solid adsorbents are considered. Adsorption can be classified as chemical or physical adsorption. For practical applications, chemical adsorption is irreversible because it involves a chemical reaction (e.g., formation of valence forces) between the VOC and the adsorbent (Wark *et al*., 1998). Physical adsorption involves intermolecular attractive forces (e.g., Van der Waals forces) that hold the VOCs to the adsorbent and does not involve a chemical change in the adsorbate/adsorbent (Wark *et al*., 1998) such that physical adsorption can be readily reversed by increasing temperature or lowering the pressure surrounding the adsorbent, which allows for desorption of VOCs as a concentrated gas stream that can be recovered. Physical adsorption is particularly effective for the removal of select VOCs in an air stream with concentrations ranging from 20 to 20,000 ppm_v (USEPA, 2002). VOC removal efficiencies > 98 % have been achieved with physical adsorption applications

(Dombrowski *et al.*, 2004; Mallouk *et al*., 2010), and the ability to regenerate the adsorbent allows for the recovery and potential reuse of the adsorbate.

1.3. Adsorption System

Adsorption systems use adsorption cycles to capture VOCs and regeneration cycles to recover the VOC for reuse or disposal. The adsorption cycle requires careful selection of an adsorbent to achieve adequate capture of the desired adsorbate. A range of regeneration cycle techniques can be used to regenerate the adsorbent and provide the desorbed VOC in a concentrated form so that it can be disposed of or reused for feedstock in a more effective manner. Additional post desorption treatment can then be performed to recover the VOC as a liquid so that it can be readily reused as feedstock.

1.3.1. Adsorption Cycle

As previously stated, adsorption is a physical process that involves the adhesion of an adsorbate to the surface of an adsorbent. For this work, the benchmark for controlling an adsorption cycle involves adsorption until the concentration downstream of the adsorption vessel reaches a concentration set-point, as measured with a hydrocarbon detector (e.g., photoionization detector). The following sections discuss a range of adsorbents and adsorbates and describe the benefits to selecting the adsorbent activated carbon fiber cloth (ACFC) for adsorbing the VOCs for this research. Adsorption isotherms, which are used to model the equilibrium adsorption capacity for an adsorbate/adsorbent combination, are also introduced.

1.3.1.1. *Adsorbents*

Adsorption capacity is affected by pore width, surface area, micropore volume, and surface polarity such that an ideal adsorbent has a pore width larger than the adsorbate diameter, large surface area, and large micropore volume (i.e., surface polarity will be addressed later in this section) (Noll *et al*., 1984; Ruthven 1984). Table 1 includes physical and chemical properties of commonly used adsorbents including silica gel, activated alumina, zeolites, and activated carbon. Silica gel and activated alumina are polar so they readily adsorb polar compounds such as water, alcohols, phenols, and amines through H_2 bonding (Ruthven, 1984). Polarity is useful for dehumidification applications, but results in limited VOC adsorption capacity when water is present due to competitive water vapor adsorption. Zeolites (i.e., molecular sieves) are aluminosilicates composed of Si, O, and Al with a crystal lattice of micropores that have a uniform pore size distribution (Ruthven, 1984). Zeolites are typically used for N, O, and organic compound separation but are generally more expensive than other adsorbents for VOC removal applications due to the cost of synthetically constructing a non-polar adsorbent with the appropriate pore size (Yang, 1999). Activated carbon is an effective adsorbent for VOCs because it can be treated to be non-polar and has a large micropore volume (i.e., 0.30 to 0.98 cm^3/g) (Table 1). Activated carbon is typically made by heating a carbonaceous material in an anoxic environment until the volatile material is removed. Then, the carbon is activated with steam or carbon dioxide at 700 to 1,100 °C to increase its surface area (Ponec *et al*., 1974). Granular activated carbon (GAC) is the most widely used activated carbon for VOC removal due to its high surface area (i.e., 600 to 1,600 m^2/g), hydrophobic nature for relative humidity (RH) < 50 %, and low cost (i.e., < $15/kg) (Noll, 1999; Khan and Ghosal, 2000).

Table 1: Physical and chemical properties of commonly used adsorbents

Adsorbent	Pore width (Å) [a]	Surface area (m^2/g) [a]	Micropore volume (cm^3/g)	Polarity[b]
Silica gel	20-70	300-900	0.45-1.0[d]	Polar
Activated alumina	35-140	90-400	0.30[d]	Polar
Zeolites	3-6	600-800	0.44[d]	Non-polar
Activated carbon[f]	5-100	500-2,500[c]	0.30-0.98[e,f]	Adjustable[g]
ACFC-15[e]	7	1,322	0.62	Adjustable[g]

[a](Noll *et al*., 1984), [b](Ruthven, 1984), [c](Hayes, 1981), [d](Do, 1998), [e](Lo *et al*., 2002), [f]Includes granular and spherical beads, tablets, powder, cylindrical pellets, fibers, and monoliths [e]ACC 5092-15, American Kynol, Inc. [f](0.52 cm^3/g for Calgon BPL granular activated carbon, Ramirez *et al*., 2004), [g]surface O groups can be readily added or removed to adjust polarity (Hashisho *et al*., 2009)

ACFC is analyzed here as a promising adsorbent that has been shown to have removal efficiencies of 99.4, 99.3, and 99.8 % for inlet concentrations of 940 ppm_v methyl ethyl ketone, 717 ppm_v methyl propyl ketone, and 970 ppm_v toluene in air, respectively (Ramirez *et al*., 2004). Benefits to ACFC include that it has faster heat and mass transfer kinetics and a larger adsorption capacity than traditional GAC (i.e., up to twice as large) because it tends to have a larger surface area (i.e., 1,322 m^2/g), microporosity (i.e., 0.94), total micropore volume (i.e., 0.621 cm^3/g), smaller external dimensions, and controllable morphology (Sullivan *et al.*, 2004b; Ramirez *et al*., 2004; Ruthven, 1984). Additionally, ACFC can be made from a synthetic feedstock that is free of ash (Hayes and Sakai, 2001), a common impurity in GAC that can catalyze chemical oxidation leading to fires and decomposition (Zerbonia *et al.*, 2000), and ACFC conducts electricity, which allows for novel adsorbent regeneration methods such as electrothermal heating (Sullivan *et al.*, 2001). Trade-offs of ACFC are that it is not as widely available and requires larger capital costs (i.e., 100 to 500 $/kg) when compared with GAC (i.e., < $15/kg) (Cheng, 2010; Hayes, 2010).

ACFC is commercially made from precursor materials such as Novoloid, pitch, cellulose, rayon, polyacrylonitrile, and saran polymer that are carbonized and activated to provide a carefully nano-engineered product with nano-tailored porosity and composition. Nippon Kynol manufactures Novoloid based carbons ACFC 10, 15, 20, and 25, which range in activation from ACFC 10 having the lowest activation to ACFC 25 having the highest activation. Table 2 shows the properties of each Nippon Kynol ACFC including N_2-Brunauer Emmett Teller (BET) surface area, micropore surface area, surface area microporosity, total pore volume, micropore volume, pore volume microporosity, mean pore width, and mean micropore width. The N_2-BET surface area is the total surface area of the ACFC determined with a N_2 adsorption isotherm and micro-pore properties pertain to all pores in the adsorbent with widths < 2 nm. Cost, surface area, and structural integrity of the cloth are directly related to activation level with ACFC 10 being the least expensive per unit mass, having the lowest surface area, and being able to withstand the largest amount of stress. Because each activation level of ACFC provides adequate structural integrity for this study, ACFC 15, which is 95 % C with the balance containing H, O, and N, (Lordgooei *et al.*, 1996) was selected for this study based on its surface area and cost.

Table 2: Properties of American Kynol activated carbon fiber cloth (ACFC) determined using N_2 adsorption at 77 K, where ACC-5092-10 is the least activated and ACC-5092-25 is the most activated (Lo, 2002)

ACFC sample	N_2 - BET surface area (m^2/g)	Micro-pore surface area (m^2/g)	Surface area micro-porosity (%)	Total pore volume (cm^3/g)	Micro-pore volume (cm^3/g)	Pore volume micro-porosity (%)	Mean pore width (Å)	Mean micropore width (Å)
ACC-5092-10	810	790	97.5	0.402	0.385	95.8	6.1	6.1
ACC-5092-15	1,322	1,279	96.7	0.658	0.621	94.4	7.0	6.9
ACC-5092-20	1,604	1,540	96.0	0.803	0.746	92.9	7.4	6.9
ACC-5092-25	1,864	1,786	95.8	0.931	0.859	92.2	8.9	8.8

*Brunauer–Emmett–Teller (BET)

1.3.1.2. *Adsorbates*

The physical properties of isobutane, acetone, and toluene, which are the VOCs/adsorbates used in this study, are included in Table 3. These adsorbates were selected for their molecular structures and wide range of boiling points (-11.7 °C to 110.6 °C), which both affect the intermolecular and adsorbate/adsorbent interaction during adsorption (Masel, 1996). Isobutane is used as an inert blowing agent to produce packaging materials and is emitted as a waste product that is typically thermally oxidized before emission to the atmosphere. Sheet foam packaging material manufacturing operations within the US can potentially recover and reuse > 13 Gg/yr of blowing agents if a capture and recovery technology was used in place of thermal oxidizers (USEPA, 2013). Acetone is primarily used as a solvent to make poly(methyl

methacrylate), a shatter resistant plastic that is an alternative to glass. Acetone is also used as a solvent in surface coatings and is used in the production of methacrylates and bisphenol-A (Dow, 2012). Toluene is a solvent used to make paint, paint thinner, and gasoline. Similar to isobutane, acetone and toluene are both emitted to the atmosphere during production of products and are off-gassed during curing. Capture and recovery of these compounds converts a waste product into a valuable feedstock that can be reused for production.

Table 3: Chemical properties of isobutane, acetone, and toluene

Property	**Isobutane**	**Acetone**	**Toluene**
Molecular form	Alkane	Ketone	Aromatic
Molecular formula	C_4H_{10}	$(CH_3)_2CO$	C_7H_8
Molecular weight (g/mol)[a]	58.1	58.1	92.1
Boiling point (°C)[a]	-11.7	56.2	110.6
Critical temperature (°C)[a]	152.0	235.5	320.8
Critical pressure (bar)[a]	37.5	47.0	41.6
Electrical resistivity (Ω-cm)[b]	-[c]	5e6[d]	>1e13[e]
Surface diffusivity (m^2/s)[f]	5.6e-8	5.6e-8	4.5e-8

[a](Handbook of Chemistry and Physics, 1983), [b]20 °C and 1 atm, [c]isobutane is a gas at the stated conditions, indicating its resistivity is infinite unless ions are present, [d](Shell Oil, 2010), [e](Shell Oil, 2007), [f]Knudsen surface diffusivity for ACC-5092-15 (i.e., described in Table 2) at 20 °C assuming slit shaped pores (Do and Do, 2001)

1.3.1.3. *Adsorption Isotherms*

Adsorption isotherms describe the mass of an adsorbate that adheres to an adsorbent once equilibrium conditions are reached at a specific temperature, pressure, and adsorbate concentration. There are five different types of isotherms, as classified by the Brunauer system (Figure 2), that describe adsorption for different adsorbate/adsorbent pairs (Brunauer *et al*., 1940). The Type I isotherm is the Langmuir isotherm, which involves monolayer adsorption and

occurs during the adsorption of gases onto microporous solids. The type II isotherm is commonly observed when gases adsorb onto nonporous or macroporous adsorbents. Type III isotherms also occur with nonporous or macroporous adsorbents but when the adsorption interaction is weak. Type IV isotherms occur when a gas adsorbs onto a mesoporous material and type V isotherms are common for weak interactions between a gas and a microporous or mesoporous adsorbent. Adsorption isotherms can be modeled based on properties of the adsorbent/adsorbate or empirically to predict the adsorption capacity for a specified partial pressure, as seen with the Dubinin-Radushkevich (DR) and Toth equations, respectively.

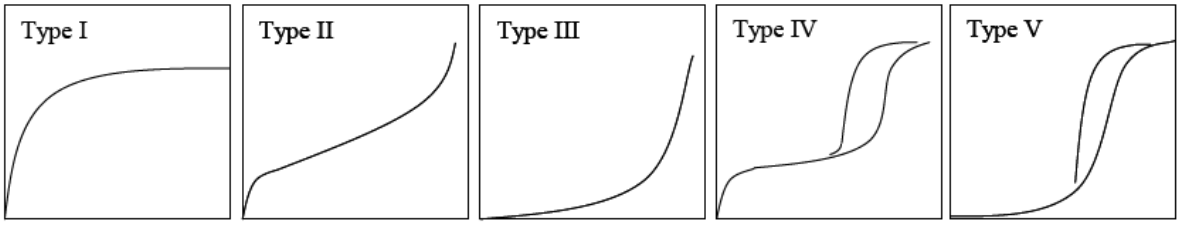

Figure 2: Brunauer classification of adsorption isotherms (i.e., x-axis is partial pressure of adsorbate and y-axis is adsorbed mass)

1.3.1.4. *Isosteric Heat of Adsorption*

Physical adsorption of organic compounds onto ACFC is a reversible exothermic process such that heat is released during adsorption and energy is required for desorption. The isosteric heat of adsorption represents the energy that is released during adsorption. It is important to consider this heat that is released during adsorption to avoid operating adsorption systems at adsorbent temperatures that significantly reduce adsorption capacity or cause bed fires (Zerbonia *et al*., 2000). The isosteric heat of adsorption is also valuable for determining energy balances to predict the total energy required to regenerate ACFC (Sullivan *et al*., 2004a).

1.3.2. Regeneration Cycle

Desorption of mass (e.g., vapors or gases) that is adsorbed to ACFC can be achieved through decreasing the pressure surrounding the adsorbent with pressure swing adsorption (PSA) or increasing the temperature of the adsorbent with thermal swing adsorption. PSA has been demonstrated for gas separation but the mechanical energy required for vacuum of dilute concentrations of VOCs can be more expensive than direct heating and the adsorbate can be recovered at low purity (Ruthven, 1984). There are a variety of different methods to achieve thermal regeneration of an adsorbent. The most common thermal desorption method involves passing steam through the adsorption vessel; however, the water from steam desorption can cause corrosion to system components and heat is lost to system components (Yang, 1999). A heated inert gas can be used as a substitute to steam to avoid corrosion but heat is still lost to the system components. Additionally, controlling the concentration of the desorption gas stream can be challenging with steam and heated inert gas regeneration because adsorbent heating is dependent on the flow rate of the heating gas. Alternative methods that provide heat directly to the adsorbent without corrosion include microwave swing adsorption (MSA) and electrothermal swing adsorption (ESA). MSA regeneration uses microwave heating to selectively heat an adsorbent and has the potential to selectively heat an adsorbate (Hashisho *et al*., 2005). However, MSA is in a developmental state and has been shown to be less energy efficient than an ESA system for methyl ethyl ketone recovery (Emamipour *et al*., 2007).

ESA has been studied since the 1970s and involves applying electrical voltage across the activated carbon, which acts as an electrical resistor that dissipates heat as current passes through the adsorbent (Fabuss and Dubois, 1970). ESA is a particularly attractive regeneration method because the power applied to the adsorbent is controlled independently from the carrier gas flow

rate providing increased control of the concentration ratio (the outlet adsorbate concentration generated during a regeneration cycle divided by the inlet adsorbate concentration during the preceding adsorption cycle). For example, studies of ACFC adsorption systems have shown maximum concentration ratios of 63, 100, 240, and 1,050 (Lordgooei *et al*., 1996; Subrenat and Le Cloirec, 2000; Mallouk *et al*., 2010; Luo *et al*., 2006, respectively).

Additional benefits of ACFC-ESA are that it does not require steam (eliminating the use of water and generation of wastewater), energy is delivered directly to the adsorbent, and the heat and mass transfer rates of the adsorbent are rapid (Lordgooei *et al*., 1996; Subrenat *et al*., 2001; Sullivan *et al*., 2004b). ESA also has been demonstrated for a variety of different adsorbate/adsorbent combinations in the literature, including treatment of gas streams at the pilot scale (Das *et al.*, 2004; Emamipour *et al.*, 2007; Petkovska *et al.*, 1991; Snyder and Leesch, 2001; Subrenat and Le Cloirec, 2006; Sullivan *et al.*, 2001; Yu *et al.*, 2004). Another benefit to ESA is that it allows for rapid feedback control of applied voltage for heating the adsorbent separate from the carrier gas flow rate, which has been utilized to provide constant VOC concentrations during regeneration cycles (i.e., at 496 ± 3 ppm_v and 4,962 ± 32 ppm_v, provided as mean ± standard deviation) (Emamipour *et al.*, 2007). Careful control of the adsorbent's temperature is also desirable when high VOC concentrations are required for post-desorption combustion for disposal or for condensation to recover the VOC. High VOC concentrations during electrothermal heating have been achieved for activated carbon beads (Luo *et al*., 2006), fiber cloths (Subrenat *et al*., 2001) and monoliths (Yu *et al*., 2007) by increasing desorption temperature, although a practical upper temperature limit for increasing VOC concentration has been demonstrated (Das *et al*., 2004). Increasing the heating duration and electrical energy application has been shown to increase the total mass desorbed, while increasing electrical

current with constant power had no effect (An *et al*., 2010). Experiments were also performed, in which 7 V direct current (DC) were initially applied to ACFC for desorption and then 4 VDC were applied once the adsorbent reached 110 °C (Petkovska *et al*., 1991). The desorption rate was higher with this initially increased voltage than when applying a constant 4 VDC suggesting that increased power application during initial heating achieves higher desorption concentrations.

Electrothermal heating regeneration cycles typically involve heating to a constant regeneration set-point temperature based on direct-contact temperature measurements (e.g., thermocouples) until the concentration downstream of the vessel decreases to a set-point concentration, as determined with a hydrocarbon detector (e.g., flame ionization detector). This method serves as the benchmark for a regeneration cycle for this work. While ESA has been analyzed at specific temperatures for select adsorbents/adsorbates, differences in desorption properties resulting from maintaining a time-weighted mean adsorbent temperature while oscillating the real-time adsorbent temperature or power applied to the adsorbent have not been characterized. Feedback control techniques, which increase the rate of initial heating through increasing power application, have the potential to increase desorption rates and reduce energy requirements to regenerate an adsorbent, but such an approach has not been characterized. Additionally, alternative heating control methods that do not require temperature measurements have not been characterized.

After thermal regeneration, the adsorbent experiences cooling until it reaches a temperature that is adequate for adsorption. For dual vessel adsorption systems, it is advantageous for the duration of the regeneration cycles (heating and cooling) to be equal or less than the duration of the adsorption cycle to maximize adsorbent usage. However, without active cooling, cooling can have large time requirements that limit the amount of time that the system

can be online for adsorption. The time required for cooling can be reduced by using a cooling system with a refrigerant, which has been demonstrated with a variety of different activated carbon systems (Askalany *et al*., 2012). However, the increased pressure drop that occurs from these active cooling systems can result in adsorbent deterioration, requiring adsorbent replacement (Wang *et al*., 2010). The duration for cooling can also be reduced by increasing the convective heat transfer by increasing the flow rate of the ambient air surrounding the adsorption vessel with a fan (Johnsen and Rood, 2011a). This technique is beneficial because it increases the cooling rate without degrading the adsorbent. Additionally, cooling is typically ended based on measurements from direct-contact temperature sensors (e.g., thermocouples). This control method based on thermocouple measurements, combined with active fan cooling, serves as the benchmark for the cooling portion of an ESA regeneration cycle for this work.

Regeneration cycles for ACFC-ESA systems typically have smaller gas flow rates than adsorption cycles because these cycles primarily use gas flows to maintain an inert environment and displace the desorbed gas from the vessel. Starting adsorption cycles at higher temperatures than ambient temperature can be more energy efficient than starting at ambient temperature because the adsorbent can be rapidly cooled by the larger flow rate adsorption gas stream, reducing the duration of cooling and thus vessel size requirements. However, care must be taken to avoid starting an adsorption cycle at temperatures that are high enough to ignite the gas stream. For example, cooling was successfully ended at the start of an adsorption cycle) at 60 °C for adsorption of 2,000 ppm_v isobutane (Mallouk *et al*., 2010) and at 40 °C for 1,000 ppm_v methyl ethyl ketone (Hashisho *et al*., 2005), allowing for smaller vessels to operate with shorter adsorption and regeneration cycles.

1.3.3. Liquid Recovery

It is often desirable to recover a VOC as a liquid for reuse as a feedstock for the process that originally emitted the VOC. Gases (e.g., a VOC in a gas stream) condense to liquid when their partial pressure reaches their saturation vapor pressure. The factors that affect this relationship include VOC composition, concentration, total pressure, and temperature. Careful control of the regeneration conditions during ESA can provide a highly concentrated gas stream (e.g., 94 % by volume for isobutane) at ambient temperature and pressure (Mallouk *et al*., 2010). These conditions allow VOCs with high boiling points (e.g., > 40 °C) to liquefy by condensing on the adsorption vessel wall without active cooling (Dombrowski *et al*., 2004). Pressure and/or temperature of the desorption gas stream can also be controlled to obtain conditions to achieve liquid recovery of low boiling point VOCs (Mallouk *et al*., 2010).

1.4. ACFC Electrical Resistance

ACFC has unique electrical properties due to its nanographitic structure, providing a desirable material for environmental sensing applications. This section first discusses ACFC's nanographitic structure with respect to resistivity and then the potential for using ACFC's resistivity as a temperature and adsorbed mass sensor.

1.4.1. Nanographitic Structure

ACFC is an effective gas adsorbent and has unique electrical properties due to its local nanographitic structure. ACFC is comprised of a disordered 3-D nanographitic structure of nanographite domains, each consisting of 3 to 4 stacked nanographene sheets of 250 to 350

carbon atoms that are arranged similar to an aromatic polycyclic molecule, as shown in Figure 3 (Hao *et al*., 2012). The nanographite domains have mean in-plane dimensions of 2 to 3 nm and typically have an interlayer spacing between nanographene sheets of 0.38 nm (Kempinksi *et al*., 2005; Fung *et al*., 1993a; Suzuki and Kaneko, 1988). These nanographite domains are bound to each other in a disordered manner via bonds between sp^3 hybridized carbon atoms (Kaneko *et al*., 1992) resulting in micropores between domains that provide large surface areas (up to 2600 m^2/g) for the adsorption of gaseous species (Oshida *et al*., 1995).

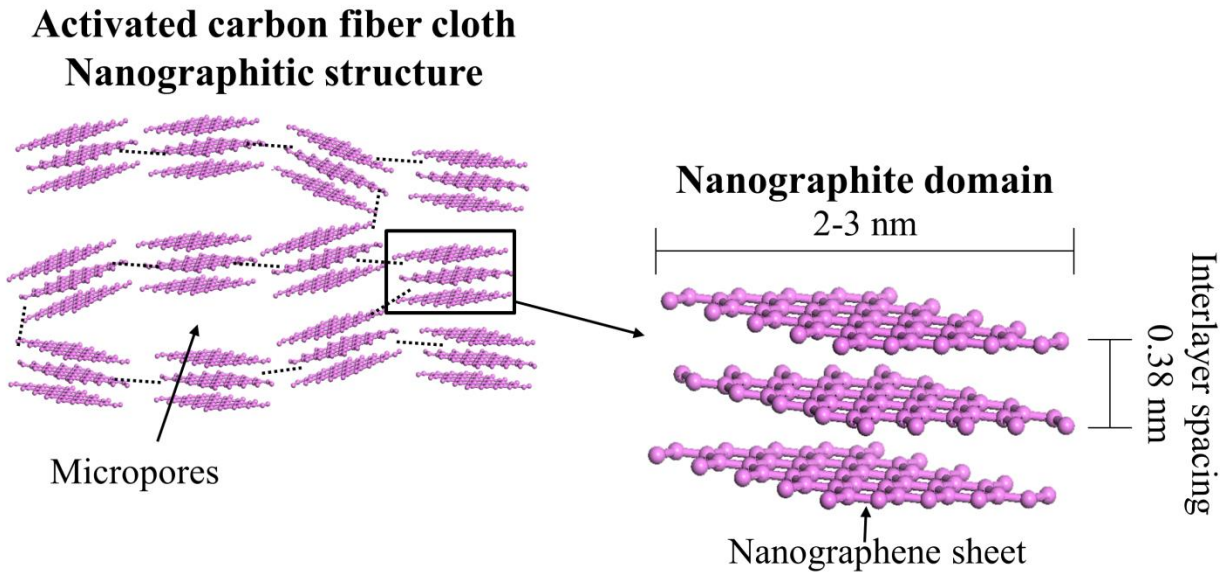

Figure 3: Schematic of the nanographitic structure of activated carbon fiber cloth (broken lines represent bonds between sp^3 hybridized carbon atoms) and increased magnification of a single nanographitic domain

The relationship between ACFC's temperature and resistivity closely follows the Coulomb-gap variable range hopping model for granular metallic materials, in which electrons hop between the highly conductive nanographite domains (Fung *et al*., 1994; Kempinski *et al*.,

2006; Shibayama *et al*., 2000). For this model, the probability of electron hopping increases with increasing temperature due to added energy. Electron transport by hopping is dependent on the dimensions of and distance between the metallic grains (i.e., nanographite domains for ACFC) as well as the concentration of localized electrons within the grains. The dimensions and distance between ACFC's nanographite domains can be readily altered through heat treatment (Fung *et al*., 1993b). The resistivity of ACFC is also largely affected by electron hopping that occurs at the edges of the nanographite domains (Enoki *et al*., 2008). The edges of the nanographene sheets (single sheet of the nanographite domain) are either comprised of energetically stable armchair edges or zigzag edges with localized nonbonding π-electrons (Enoki *et al*., 2008). The localized nonbonding π-electrons create energetically favorable sites for surface functional groups or for physical adsorption (Enoki *et al*., 2008). Thus, the electrical resistivity of ACFC is particularly interesting because it can be affected by heat treatment, surface functional groups, and physical adsorption as described below.

Heat treatment of a carbon-based precursor can affect the resistivity of the material by altering its physical and chemical structure. Moderate heat treatment of carbon (e.g., 450 to 900 °C) in CO_2 or steam alters the size and alignment of the nanographite domains, resulting in increased porosity (Daud *et al*., 2002). This increased porosity decreases the cross section of the sample for current flow and increases the distance electrons travel to pass through the material and the distance for electron hopping between domains, resulting in increased resistivity (Hashisho *et al*., 2009). Heat treatment to higher temperatures (e.g., 2000 °C) graphitizes the carbon by increasing alignment of the nanographite domains (Fung *et al*., 1993b; Mrowsowski, 1952), resulting in a more ordered nanographitic structure with lower resistivity. Thus, the

temperature of the heat treatment affects the spatial configuration of the nanographite domains and the resistivity of ACFC.

Adding surface functional groups to ACFC can result in charge transfer that affects ACFC's electrical resistivity. For example, doping of the ACFC's surface with electron acceptors or electron donors decreases or increases the concentration of localized electrons in the ACFC, respectively. O is a particularly important electron acceptor because the edges of nanographene sheets readily react with O resulting in O functional groups, such as carboxyl, carbonyl, and phenol groups, in which charge transfer occurs from the nanographene sheets to the O groups (Sumanasekera *et al*., 2010; Hao *et al*., 2008). For example, O functional groups can be added to ACFC with HNO_3 treatments (Hashisho *et al*., 2009; Ramos *et al*., 2008). These surface O functional groups accept ACFC electrons, reducing electron hopping between the nanographite domains (Joly *et al*., 2010; Hao *et al*., 2008). By contrast, H_2 treatment is used to remove O functional groups from ACFC, decreasing ACFC resistivity (Hashisho *et al*., 2009). Thus, ACFC resistivity can be nano-tailored by altering the amount of surface O functional groups on the sample (e.g., with HNO_3 or H_2 treatment).

Physical adsorption through van der Waals interactions alters ACFC's physical structure, which also affects ACFC's electrical resistivity. The interlayer spacing between the nanographene sheets of as-prepared ACFC is typically 0.38 nm, while the corresponding spacing for graphite is 0.335 nm, because edge effects create a less stable structure that allows these sheets to spread (Suzuki and Kaneko, 1988). X-ray diffraction (XRD) (Kaneko *et al*., 1992; Suzuki and Kaneko, 1988) and electron spin resonance (ESR) (Kobayashi *et al*., 1998; Sato *et al*., 2007) studies have revealed that select physically adsorbed molecules reduced the interlayer spacing between the nanographene sheets, thus increasing the distance between nanographite

domains and increasing electrical resistivity. This compression of the nanographite domains is particularly pronounced during water adsorption onto activated carbon fibers, in which the interlayer spacing decreases from 0.38 to 0.34 nm (determined with XRD), within 1.5 % of the interlayer spacing for graphite (Suzuki and Kaneko, 1988). Another XRD study revealed that the physical adsorption of benzene onto cellulosic activated carbon fibers increased the interlayer spacing between the nanographene sheets, suggesting attraction between the benzene and nanographene sheet (Suzuki and Kaneko, 1988). Other organic molecules without hydroxyl groups decreased the resistivity of activated carbon, which is likely due to alterations of the nanographitic structure of the ACFC but additional studies would strengthen this research area.

To summarize, heat treatment, surface functional groups, and physical adsorption each affect the electrical resistivity of ACFC. Heat treatment affects electrical resistivity by altering the alignment and distance between nanographite domains, which affects the distance for electron travel and electron hopping. Adding surface functional groups to ACFC affects its resistivity by altering the amount of localized electrons. Physical adsorption affects resistivity by altering the interlayer spacing of the nanographite domains, which affects the distance for electron hopping between nanographitic domains.

1.4.2. Temperature Sensing based on Resistivity

Temperature control during electrothermal regeneration typically requires a temperature sensor to determine the amount of voltage to apply to the ACFC to achieve a specified temperature. Thermocouples and resistance temperature detectors are commonly used to measure ACFC temperature and perform best if they have direct-contact with the adsorbent for rapid and accurate representation of the adsorbent's temperature (Ramirez *et al*., 2011). This

measurement requires the sensor to be electrically isolated from the ACFC during electrothermal heating, which makes temperature measurement more complicated. It can also be challenging to achieve and sustain direct-contact between the sensor and the ACFC during the movement of the ESA system to different treatment sites. Another characteristic of direct-contact temperature sensors is that they provide point measurements, which may not be representative of the mean spatial temperature of the adsorbent. For example, the coefficient of variance of ACFC surface temperature ranged from 0.04 to 0.32 when electrothermally heating select ACFC samples from 60 to 130 °C (Subrenat and Le Cloirec, 2003).

Alternative sensors that have measured carbonaceous adsorbent temperature include an infrared camera (Subrenat and Le Cloirec, 2003), a dilation liquid thermometer (Bourdin, 1998), and a fiber optic sensor (Hashisho *et al*., 2009). Each of these sensing techniques has its own advantages and disadvantages, but each requires the purchase and maintenance of the sensor. It has been well documented that ACFC acts as a semiconductor at temperatures that are relevant for ESA (20 to 160 °C), such that resistance decreases as temperature increases (Johnsen *et al*., 2011a; Petkovska *et al*., 1991; Subrenat *et al*., 2001). A method that treats an entire ACFC cartridge as a resistance temperature detector to control its temperature based on remote measurements reduces the need for local temperature sensors; thus, potentially reducing the costs for maintenance and the replacement of system components, while increasing system run time.

1.4.3. Adsorbed Mass Sensing based on Resistivity

The change in ACFC resistivity that occurs during physical adsorption allows ACFC to potentially be used as a gas sensor. Electrical resistance has been shown to increase (Dacey *et al*., 1966; McIntosh *et al*., 1946), decrease (Baudu *et al*., 1992; Johnsen and Rood, 2012a;

Saysset *et al*., 1999), or initially increase and then decrease as adsorbed mass increases (Tobias *et al*., 1986). For example, activated carbon resistance has been shown to decrease by 3.1 % after isobutane adsorption and increase by 0.9 % after ethylene oxide adsorption (McIntosh *et al*., 1946).

Many experimental studies have been performed to characterize the changes in electrical resistance of carbonaceous adsorbents during adsorption cycles. For example, Smeltzer and McIntosh, 1953 observed that the change in resistance during hydrocarbon adsorption onto activated carbon rods is proportional to the number of carbon atoms in the adsorbate. They speculated that the hydrocarbons may create surface complexes that provide excess electrons, reducing the resistance. In 2002, experiments were performed that involved CO_2 adsorption onto activated carbon in an adsorption column, and the square of the change in electrical resistivity was observed to be proportional to the mass adsorbed (Del Vecchio *et al*., 2002). The authors suggested that electrical resistance measurements can be used to predict the amount of adsorbed mass and published additional results for the adsorption of methyl chloride onto a molecular sieve and water vapor onto basic alumina, which showed similar trends to the CO_2/activated carbon system (Del Vecchio *et al*., 2004). The Del Vecchio *et al*., 2004 study involved point measurements of resistance, which allowed for tracking of the mass transfer zone but was unable to demonstrate a consistent change in electrical resistance of the adsorbent per unit mass of methyl chloride adsorbed onto a molecular sieve over repeated adsorption/regeneration cycles. The electrical resistance of an adsorbent must remain consistent or be predictable with respect to adsorbed mass to be a reasonable method for detecting adsorbed mass. ACFC has been shown to maintain VOC adsorption capacity of 0.08 g toluene/g ACFC after 300 heating cycles (Yao *et al*., 2009) for an inlet toluene concentration of 115 ppb_v in air with 20 to 22 % RH. It would be

valuable to confirm that the electrical resistance also remains consistent over repeated electrothermal heating cycles because the proposed ACFC-ESA control method requires consistent electrical resistance values.

1.5. Life Cycle Assessment

A life cycle assessment (LCA) is an iterative evaluation that considers all the environmental burdens throughout the lifetime of a product or process, which include the burdens from the producing, manufacturing, transportation, use, and disposal of materials (USEPA, 2006). This holistic approach is beneficial because it prevents a positive assessment for a change that simply shifts the environmental burden (e.g., a VOC abatement system that largely increases NO_x and CO_2 emissions). A LCA typically includes four components: goal and scope definition, inventory analysis, impact assessment, and interpretation (Figure 4). The goal and scope definition includes defining the product or process, the LCA boundaries, the functional unit for comparison, and desired environmental effects to analyze. Next, inventory analysis involves compiling a list of the energy and materials that are used over the life of the product or process. For impact assessment, the environmental impacts of the inventory are considered for a range of indicators. A LCA typically includes impact indicators such as acidification potential, ozone depletion potential, global warming potential, eutrophication potential, photochemical ozone creation potential, and gross energy requirements (De Benedetti *et al*., 2010; ISO 14040, 2006; ISO 14044, 2006). The interpretation includes evaluating the information from each component to determine the specific areas with the largest impact on a product or process and to determine which product or process has the smallest impacts.

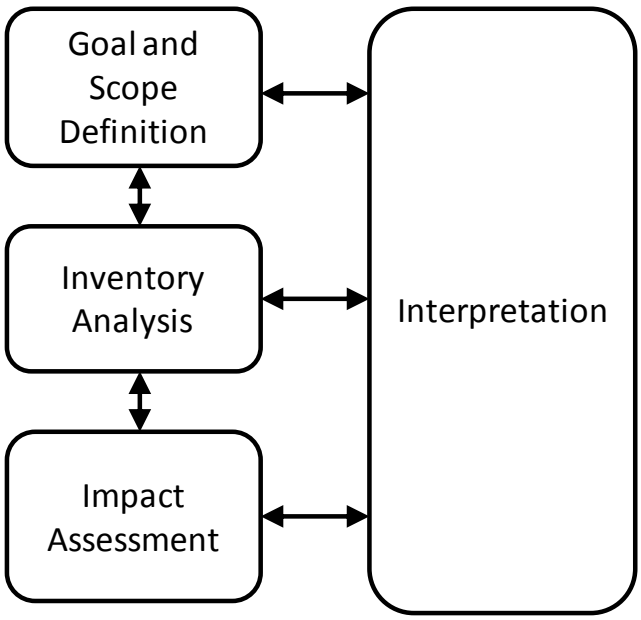

Figure 4: Life cycle assessment framework (ISO 14040, 2006)

1.6. Research Objectives and Significance

This study characterizes the electrical resistance of ACFC during adsorption and regeneration cycles and is the first work to demonstrate a method to operate cyclic ESA based on remote electrical measurements. This new ESA monitoring and control method is safer, simpler, and more cost effective than that used for current ACFC-ESA systems, because it ends adsorption cycles before breakthrough occurs to improve VOC abatement efficiency and eliminates the need for direct-contact temperature and hydrocarbon sensors for adsorption and regeneration cycles, which are typically required for ACFC-ESA systems (Figure 5). Developing, testing, and assessing this new method to operate an ESA system is divided into five chapters, as described in Figure 6. Chapter 2 involves characterization of ACFC resistance during an adsorption cycle based on ACFCs nanographitic structure, chemical properties, and physical properties. Chapters 3 and 4 involve characterization of parameters that affect the energy efficiency of regeneration heating cycles and automatically operating these cycles based

on electrical resistance measurements, respectively. Chapter 5 builds on the results from Chapters 1-3 to, for the first time, develop and automate a method to monitor and control an ACFC-ESA system based on electrical resistance measurements. Finally, Chapter 6 evaluates this ACFC-ESA system compared to conventional VOC abatement systems using a life cycle assessment and a cost assessment. The objectives and significance of each of these chapters (i.e., chapter 2 to 6) are described in sections 1.6.1 to 1.6.5, respectively.

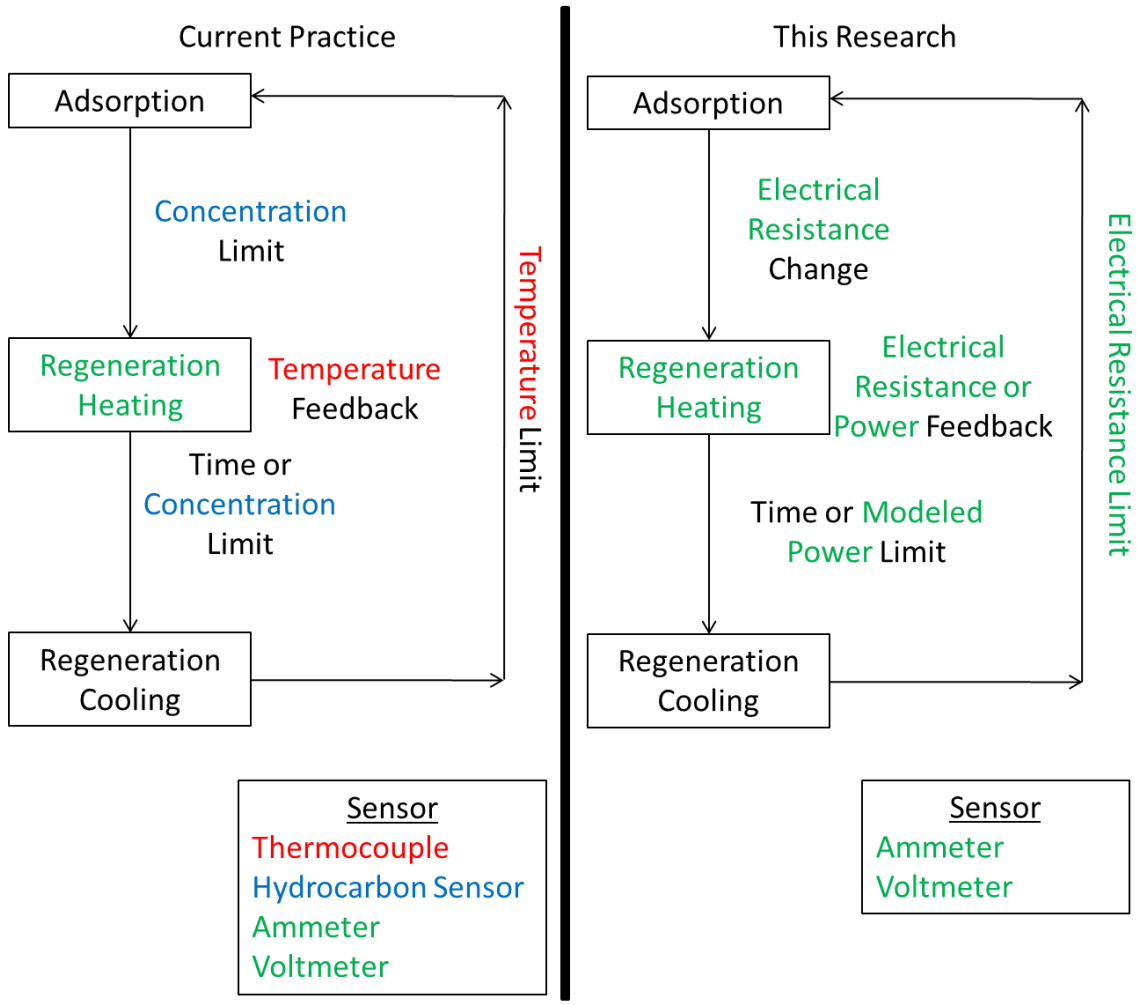

Figure 5: Comparison of current practice and this research method for automatically controlling activated carbon fiber cloth electrothermal swing adsorption with concentration, temperature, and electrical sensors in blue, red, and green, respectively

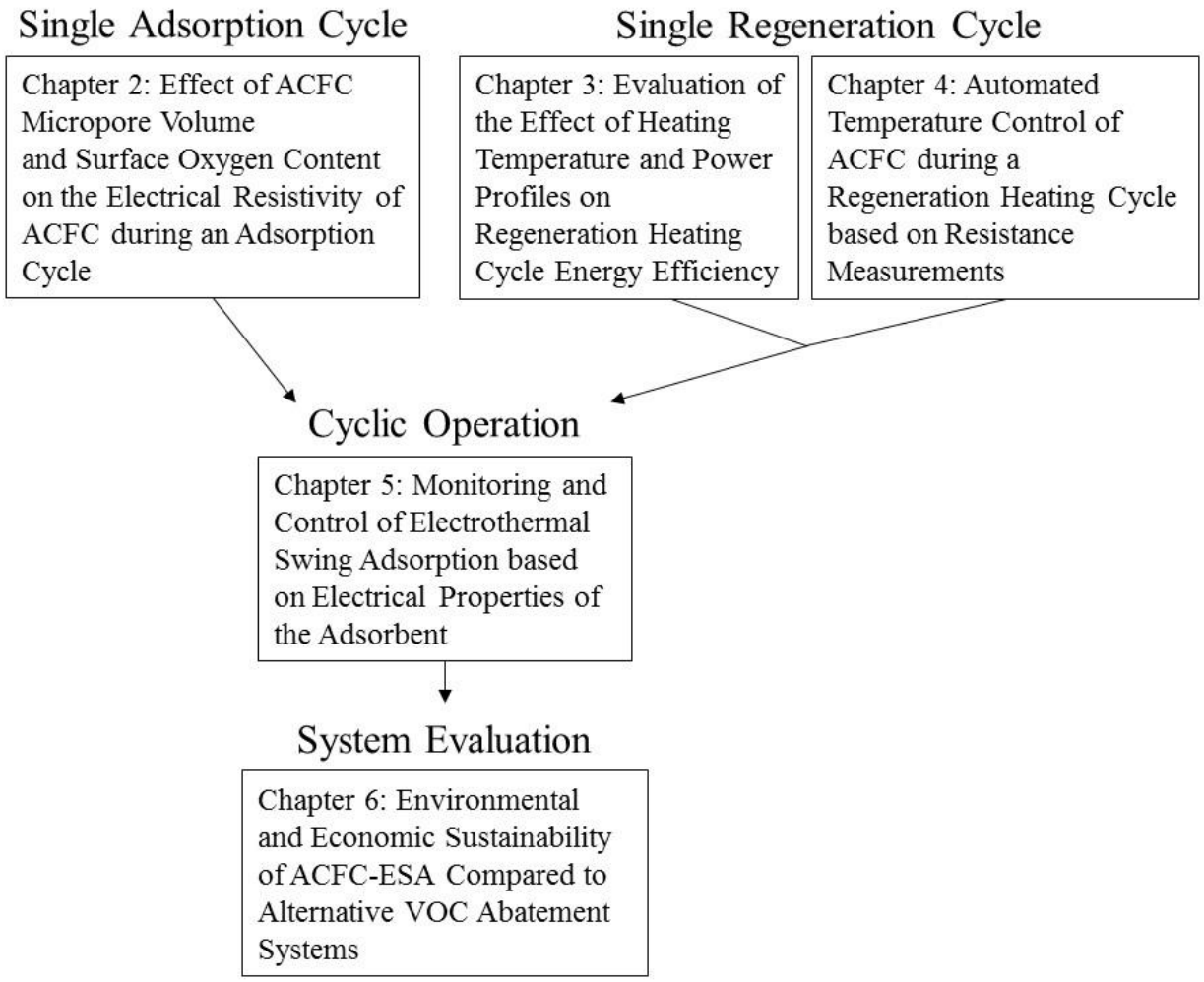

*Activated carbon fiber cloth (ACFC), electrothermal swing adsorption (ESA), volatile organic compound (VOC)

Figure 6: Flow chart of the research performed to develop, test, and evaluate a new method to operate ACFC-ESA based on electrical measurements

1.6.1. Effect of ACFC Micropore Volume and Surface Oxygen Content on the Electrical Resistivity of ACFC during an Adsorption Cycle

The nanographitic structure of ACFC samples with select micropore volumes and surface O contents was analyzed and related to the electrical resistivity of the samples as well as the change in electrical resistivity that occurs during an isobutane adsorption cycle (Johnsen *et al.*,

2013a; Johnsen *et al*., 2013b; Johnsen *et al*., 2014a; Johnsen *et al*., 2014b). This is the first research to describe the change in electrical resistivity that occurs during isobutane adsorption based on ACFCs nanographitic structure, micropore volume, and surface O content. *These contributions provide valuable insight into the factors that improve the response of ACFC resistivity to adsorbed VOC, which can be used to prepare ACFC samples with select properties to detect adsorbed mass based on resistivity measurements. These results can be used to end an ACFC-ESA adsorption cycle before adsorbate breakthrough occurs, which improves capture efficiency by reducing emissions to the atmosphere, and to remove the need for hydrocarbon detectors.*

1.6.2. Evaluation of the Effect of Heating Temperature and Power Profiles on Regeneration Heating Cycle Energy Efficiency

Control logic was developed and tested to provide a range of regeneration heating temperature and applied power profiles to determine the regeneration energy efficiency of each profile (Johnsen *et al*., 2011a). For the first time, control of temperature oscillations, frequency of power spikes, and magnitudes of the initial heating rate were tested to determine their effects on the total regeneration energy consumption and desorbed mass. *These contributions are valuable because they characterize select electrothermal heating temperature and power profiles to determine the profile characteristics that improve regeneration energy efficiency. These results can be used to select regeneration temperature and power profiles that reduce energy consumption for a regeneration heating cycle, which can be used to reduce the total energy consumption for ACFC-ESA making this a more economically feasible VOC abatement strategy.*

1.6.3. Automated Temperature Control of ACFC during a Regeneration Heating Cycle based on Resistance Measurements

ACFC resistance was modeled based on the resistivity of the ACFC (without adsorbate), cartridge geometry, and temperature and a new method was developed and demonstrated to control an automated regeneration heating cycle based on remote electrical resistance measurements (Johnsen and Rood, 2011b; Johnsen and Rood, 2012a). Additionally, the stability of ACFC's electrical resistance values were characterized over 900 electrothermal heating cycles. *This contribution is valuable because it provides a method to predict the resistance of an ACFC cartridge and a method to electrothermally heat the cartridge based on rapid remote electrical resistance measurements. This method eliminates the need for direct-contact temperature or hydrocarbon sensors, and demonstrates consistency of resistance values showing that the proposed control technique can be used for extended regeneration heating cycles for practical applications such as ACFC-ESA.*

1.6.4. Monitoring and Control of Electrothermal Swing Adsorption based on Electrical Properties of the Adsorbent

Cyclic bench-scale ACFC-ESA of VOCs based on remote electrical resistance measurements was developed and demonstrated for the first time (Johnsen and Rood, 2012b). The electrical properties of the ACFC were characterized during adsorption and regeneration cycles. Then, adsorption and regeneration cycles were operated cyclically and controlled based on the electrical properties of the adsorbent to characterize and demonstrate this novel technique for controlling ESA. *These contributions are valuable because they demonstrate proof of concept for cyclic ACFC-ESA of VOCs based on remote electrical measurements. This method*

is beneficial because it does not require direct-contact temperature or hydrocarbon sensors and has improved capture efficiency from ending an adsorption cycle before adsorbate breakthrough occurs compared to existing ESA providing a more economically competitive method to operate ESA.

1.6.5. Environmental and Economic Sustainability of ACFC-ESA Compared to Alternative Volatile Organic Compound Abatement Systems

A life cycle assessment and a cost assessment were performed to compare the environmental and economic implications of using the ACFC-ESA system from this research to a regenerative thermal oxidizer (RTO) or GAC system for treating the exhaust gas stream from packaging manufacturing. Evaluation of cyclic operation is critical from a practical standpoint, because cyclic ACFC-ESA operation provides continuous treatment of a VOC-laden gas stream, which is often required for industrial applications. *This contribution is valuable because it evaluates the feasibility of using this new ESA control method based on a life cycle assessment and cost assessment. This result demonstrates that ACFC-ESA is environmentally and economically competitive with existing VOC abatement systems for treating the exhaust gas from packaging manufacturing and identifies areas to improve the design of the ACFC-ESA system.*

Chapter 2: Effect of ACFC Micropore Volume and Surface Oxygen Content on the Electrical Resistivity of ACFC during an Adsorption Cycle

2.1. Abstract[1]

This chapter characterizes ACFC's electrical resistivity and the change in electrical resistivity that occurs during isobutane adsorption for ACFC samples with select micropore volumes (0.35 to 0.92 cm^3/g) and surface O contents (1.7 to 7.7 at. %). The resistivity of all samples decreased with increasing temperature, which is attributed to the thermal energy (i.e., provided by electrothermal heating) increasing the occurrence of the electrons having enough energy to hop between nanographite domains. Increasing micropore volume resulted in a larger decrease in resistivity after an isobutane adsorption cycle, which is attributed to increased adsorption capacity with increasing micropore volume. However, increasing surface O increased the change in resistivity per unit mass of adsorbed isobutane. Increasing O for lower O content samples increased the percent change in resistivity due to isobutane adsorption, while increasing O for moderately oxygenated samples had no effect on this value. Thus, increasing surface O improves ACFC's ability to sense adsorbed mass based on resistivity up to a threshold O value. These results provide valuable insight into the factors affecting ACFC resistivity due to adsorption, which can be used to detect the amount of adsorbed mass and to determine the remaining adsorption capacity of the adsorbent.

[1]Reproduced in part with permission from Johnsen DL, Emamipour H, Zhang Z, Yan Z, Rood MJ. Electrical resistance of activated carbon fiber cloth during acetone and isobutane adsorption. *Carbon*. 2014a; 76:435-45. Copyright 2014 Elsevier.

2.2. Experimental Apparatus and Methods

2.2.1. ACFC Samples

Results using ACFC-10-V, ACFC-15-V, and ACFC-20-V are reported in this chapter. The last letter of the ACFC abbreviation describes the sample treatment, in which V denotes the untreated samples. For this chapter, 4 cm by 8 cm ACFC rectangular samples were treated with H_2 or HNO_3 to achieve nano-tailored physical and chemical properties.

2.2.1.1. *H_2 Treatment*

H_2 treatment was performed in a controlled-tube temperature furnace with 5.1 cm inner diameter (Lindberg, model 54232) to remove O functional groups from the ACFC samples. First, the samples were heated to 200 °C in 0.5 standard liter per minute N_2 (SLPM, standard conditions of 25 °C and 1 atm) for 1 h to remove volatile adsorbates (e.g., water vapor). Then, the samples were heated to 900 °C in 0.1 SLPM H_2 for > 8 h to remove surface O functional groups (Hashisho *et al*., 2009; Sullivan *et al*., 2007). This H_2 treatment was performed on ACFC samples with select activation levels and the resulting samples are denoted as ACFC-10-H, ACFC-15-H, and ACFC-20-H.

2.2.1.2. *HNO_3 Treatment*

HNO_3 treatments were performed to add surface O functional groups to ACFC-10-V. First, the ACFC-10-V sample was submerged in a 100 mL aqueous solution containing 5.3 M HNO_3 in distilled water for > 8 h at 25 °C. The sample was then removed from the solution and washed with deionized water until neutral pH was achieved as measured with pH level indicator

strips. The sample was then heated to 150 °C in 0.5 SLPM N_2 for 30 min in a controlled-temperature tube furnace (Lindberg, model 54232) to remove water vapor and then to 350 °C for an additional 2 h to remove adsorbed nitrate groups (Atkinson *et al*., 2013). The prepared sample with added surface O functional groups is denoted as ACFC-10-O.

2.2.2. Adsorbent Characterization

2.2.2.1. *Pore Structure*

ACFC pore structure was determined with N_2 adsorption isotherms performed with a surface analyzer (Micromeritics, ASAP 2020). Samples (i.e., 150 to 210 mg) were degassed for 3 h at 300 °C and an absolute pressure of 500 mm Hg. The adsorption isotherms were obtained at 77 K and 10^{-6} < relative pressure < 1. The BET method was used to fit the adsorption data from 0.003 < relative pressure < 0.03 to achieve high correlation coefficients (r^2) and positive values for the BET constant (C) with software provided by the surface analyzer. Micropore volumes and pore size distributions were determined with the 3D model (Sun *et al*., 1998). The pore widths were weighted based on volume to determine the mean pore width.

2.2.2.2. *Elemental Composition*

Surface elemental content (C, N, and O) of the ACFC samples was determined with an X-ray photoelectron spectrometer (Kratos, Axis Ultra) under ultrahigh vacuum (10^{-9} Torr) at the Frederick Seitz Materials Research Laboratory Central Facilities (University of Illinois). Monochromatic Al Kα (1486.6 eV) radiation was used as the primary x-ray source to excite photoelectrons. The emitted electron signal was plotted as a spectrum of binding energies, which

were used to determine the elemental composition and chemical state of the sample at a maximum probe depth of 2 to 5 nm and a lateral resolution of 1 mm. The energy scale was adjusted to a C1s (graphite) spectrum at 284.8 eV. Surface N was not reported because it was less than the instrument quantification limit (< 0.1 at. %) for each of the samples.

Bulk elemental composition for C, H, N, and O was determined with an elemental analyzer (Exeter Analytical Inc., CEE-440) at the Microanalysis Laboratory in Noyes Lab (University of Illinois). A brief description of the process for elemental analysis is provided here while a more detailed description is available in Hashisho *et al.*, 2009. ACFC samples (2 mg) were degassed for 8 h at 100 °C in air at atmospheric pressure and then injected into the elemental analyzer's high temperature furnace. A burst of O_2 was then added to ensure total combustion of all inorganic and organic substances (i.e., ACFC does not contain ash). The combustion gases were then mixed and passed through a series of gas traps and high-precision thermal conductivity detectors to determine the mass content of C, H, and N in the sample. The mass of O was determined as the difference between the initial dry sample gravimetric mass in the instrument and the mass of the measured elements.

2.2.2.3. *Nanographitic Structure*

The nanographitic structure of the amorphous ACFC samples was characterized with an x-ray diffractometer (Siemens/Brukar, D-5000) with Cu Kα radiation (λ = 0.15418 nm) at 40 kV and 30 mA at the Frederick Seitz Materials Research Laboratory Central Facilities (University of Illinois). A scan rate of 2°/min with a scan step size of 0.2° was used over 2θ values ranging from 10° to 60°. Samples were mounted onto a quartz support to reduce background noise. The x-ray spectra were analyzed with EVA software (Brukar) to describe the nanographitic structure

of the ACFC. The $K\alpha_2$ radiation and background intensity were removed and then the EVA software was used to determine the location of the peaks of the XRD spectra (i.e., 2θ values). The location of the peaks (i.e., 2θ values) describes the nanographitic structure of the sample and is thus unique for each ACFC sample. The average interlayer spacing (d_{002}, nm) between the nanographene sheets was calculated with Bragg's law using the 2θ value of the 002 peak of the spectra.

$$d_{002} = \frac{\lambda}{2\sin(\theta)} \qquad \text{(Equation 1)}$$

where λ is the x-ray wavelength (nm) and θ is the incidence angle (°).

The XRD tests were performed in ambient air. For tests involving ACFC with isobutane, the ACFC sample was first placed in a glass vessel with a 5 SLPM 100 % isobutane gas stream passing through the vessel for 5 min to ensure equilibrium conditions were reached. The sample was then inserted into the XRD and was thus exposed to air while the spectra were determined.

2.2.2.4. *Electrical Resistivity*

The electrical resistivity of ACFC was determined based on the sample's geometry, temperature, and resistance. First, the sample length (L, m), width (W, m), and height (H, m) were measured. The resistance of the sample was then determined at select temperatures using a 4-point probe method to eliminate wire and contact resistance (Heaney, 2003). The sample was supported across its width by a set of stainless steel electrodes (i.e., exterior electrodes). A second interior set of stainless steel electrodes were connected to the sample and the distance between these electrodes was measured (L_I, m). The 4-electrode supported sample was then inserted into a 1.85 L interior volume Pyrex vessel (Figure 7). The sample was electrothermally

heated to 200 °C in 1 SLPM N_2 (i.e., controlled with Tylan mass flow controller) for 1 h to desorb volatile adsorbates by applying voltage from a DC power supply (Tenma, Model 72-2085) across the ACFC through the exterior electrodes. ACFC temperature was measured with a Type K ungrounded thermocouple (1.6 mm diameter, Omega Inc.) contacting the ACFC at the center of the sample. The ACFC was then electrothermally heated to select temperatures from 25 to 200 °C with the DC power supply. The electrical current was measured in series with the power supply with a multimeter (Fluke, Model 45). Voltage was simultaneously measured with a second multimeter that was connected to the interior electrodes (Newport, HHM290/N).

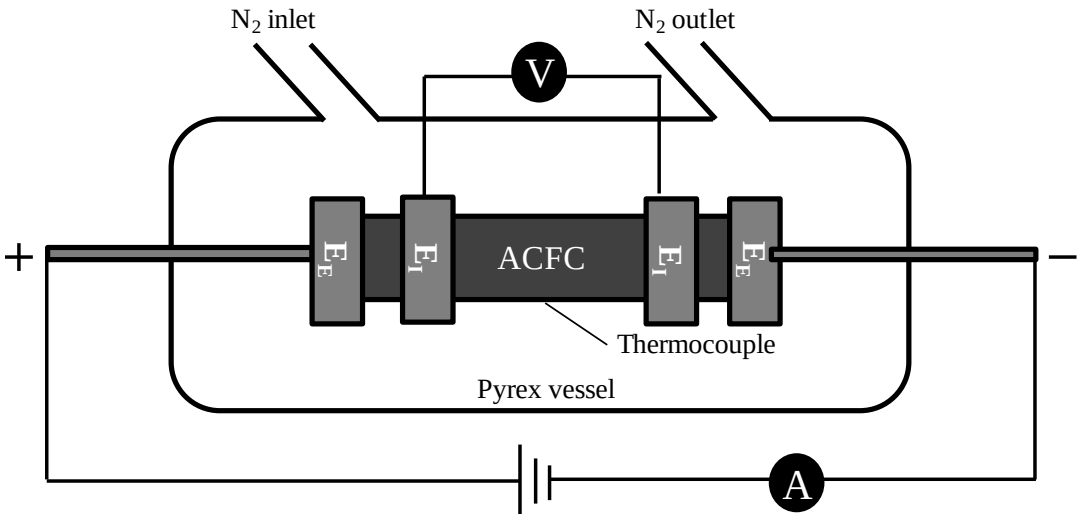

V	Volt meter
A	Ammeter
E_I	Interior electrode
E_E	Exterior electrode

Figure 7: 4-point probe apparatus for characterizing electrical resistivity of rectangular activated carbon fiber cloth (ACFC) samples

The measured current and voltage values at select ACFC temperatures were used to calculate resistance (R, Ω) based on Ohm's law and then resistivity ($\rho(T)$, Ω-m) was calculated based on the relationship between resistance, temperature, and geometry (Hashisho *et al*., 2009).

$$\rho(T) = R\frac{HW}{L_I} \quad \text{(Equation 2)}$$

A linear least square regression between resistivity and temperature was used to determine the sample resistivity as a function of temperature.

$$\rho(T) = \rho_R[1 + \alpha_R(T - T_R)] \quad \text{(Equation 3)}$$

where ρ_R is the resistivity at the reference temperature (Ω-m), α_R is the thermal coefficient of resistivity (°C^{-1}), which is the change in resistivity for a 1 °C change in temperature, T is temperature (°C), and T_R is the reference temperature (0 °C for this study for comparison with previous studies (Hashisho *et al*., 2009; Johnsen and Rood, 2012a)). The linear model was used to describe the relationship between temperature and resistivity because measurements occurred over high temperatures (i.e., 273 to 473 K), of which ACFC temperature is typically linear with resistivity (Fung *et al*., 1993a). Additionally, the linear model fit the data well for the samples in this study (i.e., $r^2 \geq 0.95$ for all samples in this study).

A 1 SLPM gas stream with 1 ± 0.02 % (nominal value ± certified maximum deviation from nominal value) isobutane by volume and remainder N_2 was passed through the vessel allowing the adsorption of isobutane onto ACFC samples that were initially 25 °C. The electrical resistance of the ACFC was calculated before adsorption and after achieving equilibrium conditions and the change in resistivity during a complete adsorption cycle was calculated. The temperature of the ACFC increased by up to 1 °C during isobutane adsorption and then decreased back to the initial temperature before the end of the adsorption cycle.

Screening tests were performed with inlet isobutane concentrations ranging from 1,000 ppm_v to 1 % by volume to determine the inlet isobutane concentration for this study. The change in ACFC resistivity per change in unit mass of adsorbed isobutane was independent of inlet concentration (i.e., for the screening concentrations), while the total adsorbed mass increased with increasing inlet concentration. Thus, an inlet isobutane concentration of 1 % by volume was selected for this study because it provided the largest change in resistivity and adsorbed mass (i.e., for the screening concentrations), while still being representative of results (i.e., change in resistivity per change in adsorbed mass) for inlet concentrations as low as 1,000 ppm_v. The concentration of the adsorbate was measured downstream of the adsorption vessel with a photoionization detector (RAE Systems, Inc., PDM-10A). The downstream concentration was within 2 % of the inlet concentration after < 10 min of adsorption but all adsorption experiments were performed for 20 min to ensure equilibrium conditions were achieved.

The experimental procedure and conditions described in the previous paragraph were then repeated with 1 cm by 1 cm ACFC samples to determine their adsorption capacity. These ACFC samples were placed in a gravimetric balance (Cahn, model C-2000) to measure the initial mass of each degassed ACFC sample and the adsorbed mass at equilibrium. The adsorption capacity of ACFC samples (g adsorbate/g ACFC) was then calculated for each sample. Triplicate tests were performed for each ACFC sample to obtain mean and standard deviations for resistivity and adsorption capacity values.

2.3. Results and Discussion

2.3.1. ACFC Characterization

2.3.1.1. *Pore Structure of ACFC Samples*

The pore structures for each ACFC sample in this chapter are presented in Table 4. These results are briefly discussed because the samples are similar to those used in a previous study (Sullivan *et al*., 2007). The ACFC samples with higher activation levels have a more porous structure as indicated by their higher BET surface area, micropore volume, total pore volume, and mean pore width. Additionally, the pore structure values for the ACFC-10 samples were largely unaffected by H_2 or HNO_3 treatment (i.e., BET surface areas and micropore volumes within 5 % before and after treatment) demonstrating that these treatments did not impact the microporous structure of the sample.

Table 4: Pore structure of ACFC samples

Sample	**BET surface area (m^2/g)**	**Micropore volume (cm^3/g)**	**Total pore volume (cm^3/g)**	**Mean micropore width (nm)**
ACFC-10-V	854	0.37	0.37	0.59
ACFC-10-H	859	0.35	0.36	0.64
ACFC-10-O	854	0.36	0.36	0.59
ACFC-15-V	1464	0.59	0.62	0.71
ACFC-15-H	1304	0.53	0.56	0.72
ACFC-20-V	1836	0.81	0.87	0.84
ACFC-20-H	1919	0.92	0.95	0.91

*Brunauer–Emmett–Teller (BET)

2.3.1.2. *Chemical Composition of ACFC Samples*

The elemental composition (surface and bulk) of the prepared ACFC samples is provided in Table 5. The carbon and O contents of the ACFC samples follow the same trends when analyzing the surface and bulk values such that H_2 treatment reduces O content, while HNO_3 treatment increases O content, in agreement with previous ACFC studies (Sullivan *et al*., 2007; Hashisho *et al*., 2009). The surface O contents are within 2.4 at. % of the bulk O contents for all samples. The difference in surface and bulk O contents may be due to differences in the measurement techniques (i.e., X-ray photoelectron spectroscopy (XPS) and elemental analysis, respectively). For example, XPS cannot detect H while elemental analysis measures H, which affects the measured at. % of each element. Additionally, XPS measures O based on electron binding energy while elemental analysis does not directly measure O (i.e., difference method is used to determine O). Types of ACFC O groups (e.g., graphitic, phenol, carbonyl, and carboxyl) with corresponding Boehm titration results for select ACFC samples are described in a previous study but were not considered for this study (Atkinson *et al*., 2013).

Table 5: Elemental composition of activated carbon fiber cloth samples

Sample	Surface composition		Bulk composition			
	C (at. %)	**O (at. %)**	**C (at. %)**	**H (at. %)**	**N (at. %)**	**O (at. %)**
ACFC-10-V	95.3	4.7	89.3	6.3	0.0	4.4
ACFC-10-H	97.8	2.2	91.8	6.4	0.2	1.7
ACFC-10-O	92.3	7.7	87.4	5.6	0.9	6.2
ACFC-15-V[a]	95.3	3.8	93.6	3.5	0.3	2.6
ACFC-15-H	98.3	1.7	92.9	5.6	0.0	1.4
ACFC-20-V[a]	94.1	5.0	93.5	3.5	0.3	2.6
ACFC-20-H	97.5	2.6	94.1	4.4	0.1	1.4

[a]Hashisho *et al*., 2009

2.3.1.3. *Nanographitic Structure of ACFC Samples*

XRD patterns of select ACFC samples are provided in Figure 8. All of the samples have a broad peak with a 2θ value at 21-24° (i.e., disordered graphitic (002) plane) and at 43-44° (i.e., overlapped (100) and (101) planes), while the exact 2θ value of these peaks are determined for each ACFC sample. These broad peaks represent an amorphous system of nanographite domains (Suzuki and Kaneko, 1988; Liu and Zhao, 2012).

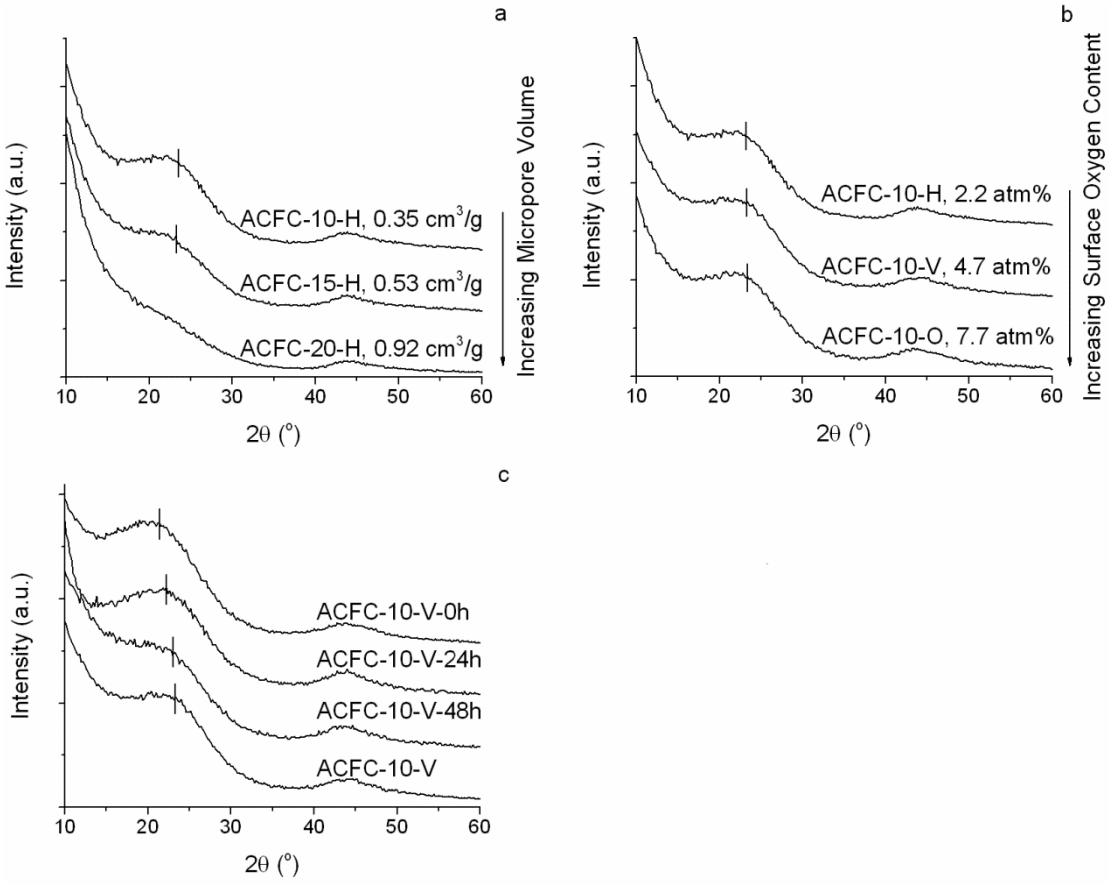

Figure 8: X-ray diffraction patterns of activated carbon fiber cloth samples with: a) select micropore volumes, b) select O contents, and c) with initially adsorbed isobutane and varying levels of ACFC regeneration as described in Table 6, in which vertical lines show peak locations for determining interlayer spacing except for ACFC-20-H due to an indistinguishable peak compared to the instrumental noise

XRD patterns of H_2 treated ACFC samples with select micropore volumes (i.e., 0.35 to 0.92 cm^3/g) and similar elemental compositions (i.e., surface O contents from 1.7 to 2.6 at. %) are provided in Figure 8a. The samples with higher activation levels have smaller peak intensities, showing less order of the nanographitic structure. This decrease in order of the nanographitic structure with increased activation level is attributed to the more intense heat treatments creating a more porous structure (as indicated by their larger micropore volumes) with an increased level of disorder of the nanographite domains, similar to that observed for ACFs made from a liquefied wood precursor (Liu and Zhao, 2012) For the sample with the largest

micropore volume (ACFC-20-H), the (002) peak is indistinguishable, demonstrating a highly disordered material. These results confirm that the heat treatments used to activate these samples were well below temperatures required to achieve graphitization of the samples.

XRD patterns of ACFC samples with similar micropore volumes (0.35 to 0.37 cm^3/g) and select O contents (2.2 to 7.7 at. %) are provided in Figure 8b. The interlayer spacing for each of the treated ACFC-10 samples was within 0.6 % of that for the untreated sample, which was 0.382 nm. Thus, even the sample with the smallest O content (1.7 at. %) has enough O to expand the interlayer distance between the nanographene sheets when compared to graphite, which has an interlayer spacing of 0.335 nm. The strong similarity between XRD patterns of the prepared ACFC-10 samples provides evidence that although the H_2 and HNO_3 treatments altered the O content of the ACFC, these treatments did not affect the nanographitic structure of the samples when compared to the untreated sample.

XRD results describing differences in the nanographitic structure of ACFC-10-V samples with adsorbed isobutane and after varying levels of isobutane adsorption are shown in Figure 8c and Table 6. The peak for the (002) plane shifts to a smaller 2θ value when isobutane is adsorbed onto ACFC-10-V. It should be noted that the mass of adsorbed isobutane is not constant during generation of the XRD pattern due to desorption of isobutane into the air during sampling. However, there is a clear trend that adsorbed isobutane increases the interlayer spacing because the interlayer spacing of the sample with the initially adsorbed 0.12 g isobutane/g ACFC (ACFC-10-V-0h) is 9 % larger than that of the initial sample (ACFC-10-V) without isobutane. Also, the interlayer spacing between the nanographene sheets of the regenerated ACFC (ACFC-10-48h) is within 1 % of that of the initial sample (ACFC-10-V) without isobutane suggesting that most of the isobutane was desorbed. A previous study of

benzene adsorption onto activated carbon fibers provided similar interlayer spacing trends (i.e., increased from 0.38 nm to 0.44 nm after adsorption) despite benzene being a vapor and isobutane being a gas (i.e., boiling points of 80 and -12 °C, respectively) (Suzuki and Kaneko, 1988). It is likely that the increased interlayer spacing between the nanographene sheets observed during adsorption of isobutane and benzene is due to attraction between the organic compound and the nanographite domains.

Table 6: Nanographite domain interlayer spacing for ACFC-10-V samples with initially adsorbed isobutane and varying levels of sample regeneration

Sample	**Adsorbate**	**Regeneration conditions**	**Nanographite domain interlayer spacing (nm)**
ACFC-10-V-0h	Isobutane	None	0.415
ACFC-10-V-24h	Isobutane	24 h at 25 °C in air	0.400
ACFC-10-V-48h	Isobutane	24 h at 25 °C in air and 24 h at 100 °C in air	0.385
ACFC-10-V	None	Pure sample	0.382
Graphite	None	Pure sample	0.335

2.3.2. ACFC Electrical Resistivity

2.3.2.1. *Dependence of ACFC Electrical Resistivity on Micropore Volume and Surface Oxygen Content between 25 °C and 200 °C*

The dependence of ACFC electrical resistivity on temperature is provided in Table 7 and Figure 9. Resistivity increases with surface O for ACFC samples with a select activation level (i.e., ACFC-10, ACFC-15, or ACFC-20) in agreement with Hashisho *et al*., 2009. The previously discussed XRD results (Figure 8b) demonstrate that the nanographitic structure of the ACFC-10 samples were unaffected by the treatments to add or remove surface O such that the interlayer spacing and orientation of the nanographite domains remained constant. Thus, the

increase in resistivity with surface O is attributed to the O groups localizing electrons, which prevents these electrons from hopping between nanographite domains (Hao *et al*., 2012; Hashisho *et al*., 2009).

Table 7: Electrical resistivity parameters and linear regression coefficient of activated carbon fiber cloth (ACFC) samples (mean ± standard deviation)

Samples	$\boldsymbol{\rho_R}$ **(Ω-cm)[a]**	$\boldsymbol{\alpha_R \cdot 10^3}$ **(°C^{-1})[b]**	**r^2 (-)[c]**
ACFC-10-V	0.54±0.02	-2.67±0.08	0.95
ACFC-10-H	0.19±0.00	-1.66±0.16	0.98
ACFC-10-O	0.74±0.02	-2.74±0.02	0.96
ACFC-15-V	0.53±0.01	-2.66±0.05	0.97
ACFC-15-H	0.31±0.00	-1.89±0.08	0.99
ACFC-20-V	0.87±0.00	-2.92±0.06	0.96
ACFC-20-H	0.37±0.01	-2.06±0.05	0.95

[a]Equation 3 [b]r is the linear correlation coefficient describing the dependence of ACFC's resistivity on ACFC temperature

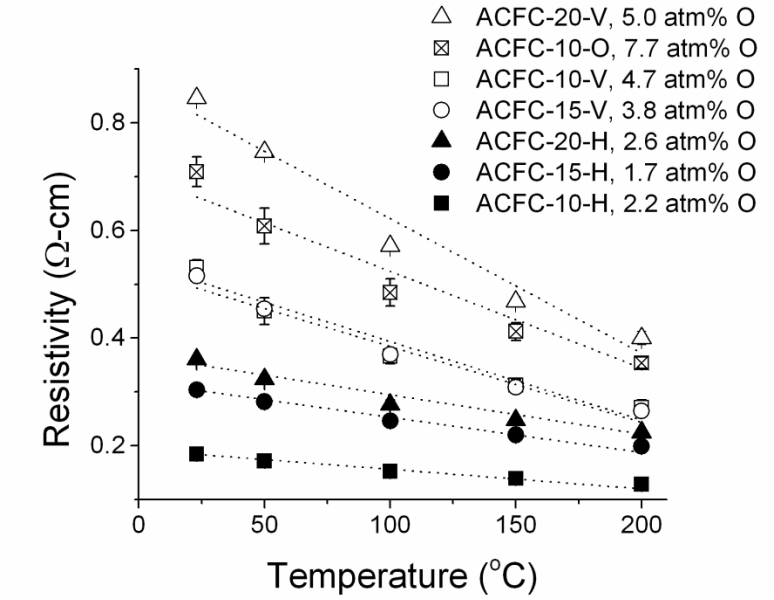

Figure 9: Electrical resistivity of activated carbon fiber cloth with respect to temperature with standard deviations of the resistivity values shown with vertical error bars

ACFC resistivity increased with activation level, as seen with ACFC-10-H, ACFC-15-H, and ACFC-20-H, which all have similar O contents (1.7 to 2.6 at. %). Increasing activation level did not affect the interlayer spacing of the nanographite domains (i.e., diffraction pattern peak locations in Figure 8a) and was not expected to affect the number of localized electrons since the O contents of the samples are consistent. However, increasing activation level results in increased disorder of the nanographitic structure, as evidenced through the higher porosity and the previously discussed diffraction patterns (Table 4 and Figure 8a). A more disordered material requires the electrons to travel farther to circumvent pore space when compared to a more graphitic material. Additionally, higher porosity can increase hopping distance between the nanographite domains. Thus, the increased resistivity for samples with higher activation levels is attributed to the increased travel distance and hopping distance between nanographite domains. It should be noted that ACFC-10-V has a similar resistivity to ACFC-15-V (0.54 and 0.53 Ω-cm, respectively) despite the difference in activation level, which has also been observed

in a previous study (Hashisho *et al*., 2008). This result is attributed to the competing effects from ACFC-10-V having a larger surface O content than ACFC-15-V (i.e., 4.7 and 3.8 at. %, respectively) and ACFC-10-V having a smaller micropore volume than ACFC-15-V (i.e., 0.37 and 0.59 cm^3/g, respectively).

All samples have a negative thermal coefficient, which has been documented in literature for ACFCs and is attributed to the localization of electrons with decreasing temperature (Fung *et al*., 1994; Hashisho *et al*., 2009). As previously stated, ACFC resistivity follows the Coulomb-gap variable range hopping model (Fung *et al*., 1994; Kempinski *et al*., 2006; Shibayama *et al*., 2000) such that the localization of electrons results in a more pronounced change in resistivity for a change of 1 °C. Thus, for a given activation level, the ACFC samples with higher O content likely have a larger thermal coefficient because the O localizes electrons.

2.3.2.2. *Dependence of ACFC Electrical Resistivity on Micropore Volume and Surface Oxygen Content Before and After Isobutane Adsorption*

ACFC electrical resistivity before and after complete isobutane adsorption cycles for ACFC samples with specified ranges of micropore volumes and surface O contents is provided in Figure 10 and isobutane adsorption capacities are provided in Table 8. Resistivity decreased by 5.1 to 9.7 % after a complete isobutane adsorption cycle demonstrating that adsorption of isobutane can be sensed based on resistivity and such sensing can be improved with careful selection of micropore volume and surface O content of the ACFC sample. Both the initial resistivity and the absolute change in resistivity that occurs after a complete isobutane adsorption cycle increased with increasing ACFC micropore volume and surface O content.

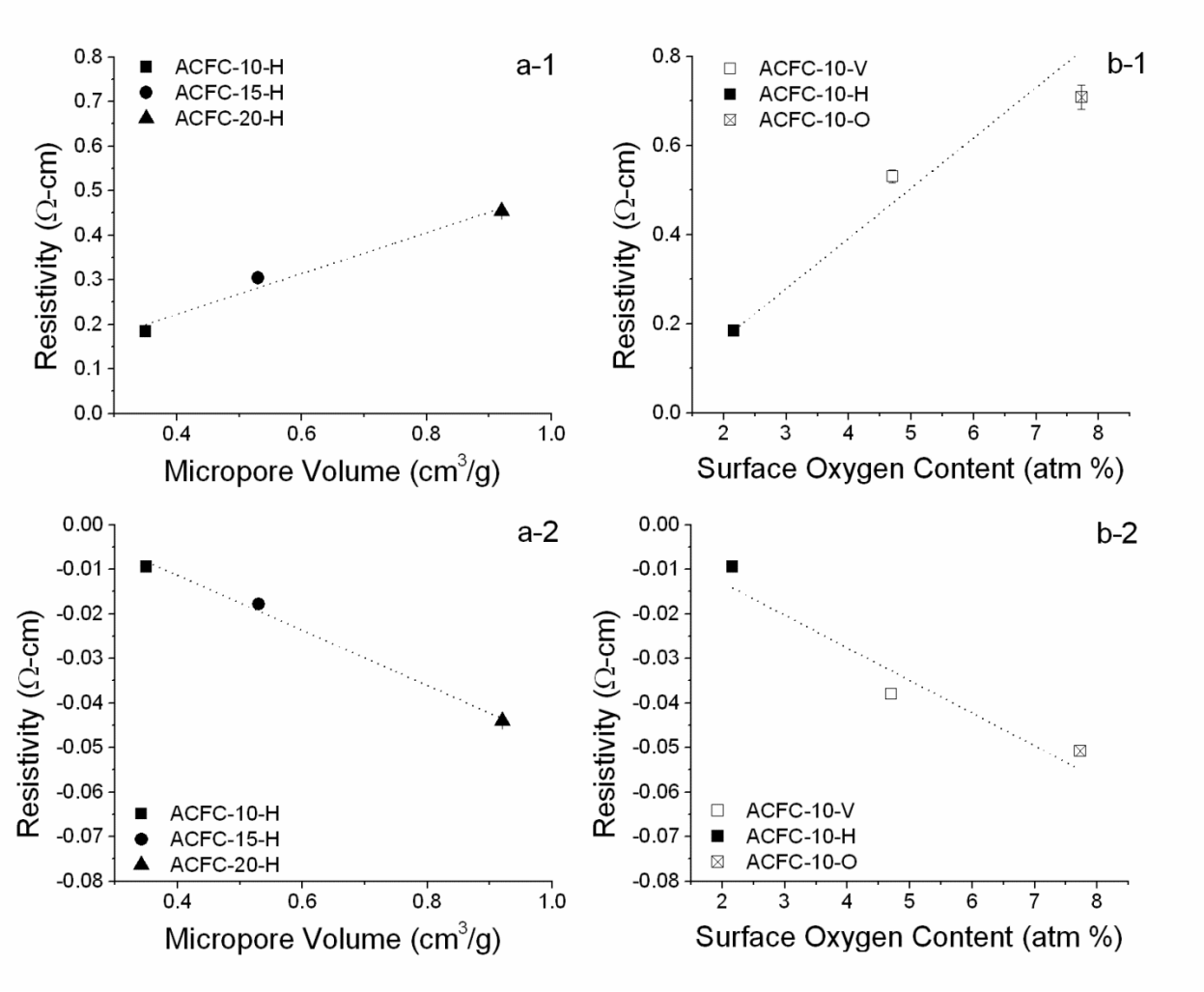

Figure 10: Initial resistivity of activated carbon fiber cloth samples at 25 °C (a-1 and b-1) and change in ACFC resistivity after a complete adsorption cycle of 1 % isobutane (by volume) (a-2 and b-2) compared to sample: a) micropore volume and b) surface O content where standard deviations are represented with vertical error bars

Table 8: Adsorption capacity of 1 % isobutane by volume in N_2 onto activated carbon fiber cloth (ACFC) samples (mean ± standard deviation)

Sample	Adsorption capacity (g isobutane /g ACFC)
ACFC-10-V	0.100 ± 0.001
ACFC-10-H	0.118 ± 0.001
ACFC-10-O	0.102 ± 0.003
ACFC-15-V	0.176 ± 0.004
ACFC-15-H	0.174 ± 0.007
ACFC-20-V	0.210 ± 0.003
ACFC-20-H	0.202 ± 0.006

Statistical analysis was used to compare sample adsorption capacity to its micropore volume and surface O content. First, a multiple linear regression was performed to describe adsorption capacity based on micropore volume, surface O content, and the interaction between micropore volume and surface O content. This regression confirmed that there was no statistically significant interaction between micropore volume and surface O content at a significance level of 0.05 (i.e., independent parameters for predicting adsorption capacity). A multiple linear regression was then used to compare adsorption capacity to micropore volume and surface O content (i.e., multiple linear regression without interaction). At a significance level of 0.05, micropore volume was a statistically significant predictor of adsorption capacity while surface O content was not. The increased absolute change in resistivity after an adsorption cycle with increasing micropore volume is thus attributed to the increased adsorption capacity (i.e., more adsorbed isobutane that reduces the spacing between ACFC's nanographite domains resulting in increased electron hopping). The change in isobutane adsorption capacity was not affected by surface O content (0.10 to 0.12 g isobutane/g ACFC for the adsorption capacity of samples with similar micropore volumes of 0.35 to 0.37 cm^3/g and surface O contents ranging

from 2.2 to 7.7 at. %). Thus, the increased change in resistivity after an adsorption cycle with increasing surface O content is attributed to the ACFC surface O content increasing the absolute change in resistivity per unit mass adsorbed, resulting in a better sensor for adsorbed isobutane. This trend is attributed to the surface O localizing electrons and the adsorbed isobutane providing energy to release localized electrons.

The percentage change in resistivity during an adsorption cycle was then normalized based on the percentage change in ACFC mass (before and after adsorption) and compared to surface O content in Figure 11. This figure provides the following benefits: 1) Normalizing the resistivity based on adsorbed mass accounts for the difference in sample adsorption capacity resulting from ACFC samples having different micropore volumes and 2) providing percentage change of resistivity per percentage change in mass allows for relative comparisons for the adsorbent as a whole. The magnitude of the percentage change in resistivity per percentage change in mass increases by 100 % when increasing surface O from 1.7 to 3.8 at. % but remains constant (i.e., within 14 %) for samples with higher surface O contents (i.e., 3.8 to 7.7 at. %). Combining this result with the resistivity magnitudes from Figure 9 leads to the following conclusions: 1) At low surface O content (i.e., < 3.8 at. %), increasing surface O increases the initial resistivity of the sample and also increases the percentage change in resistivity per percentage change in mass of adsorbed isobutane. 2) At higher surface O content (i.e., 3.8 to 7.7 at. %), increasing surface O increases the initial resistivity of the sample and does not change the percentage change in resistivity per percentage change in mass of adsorbed isobutane.

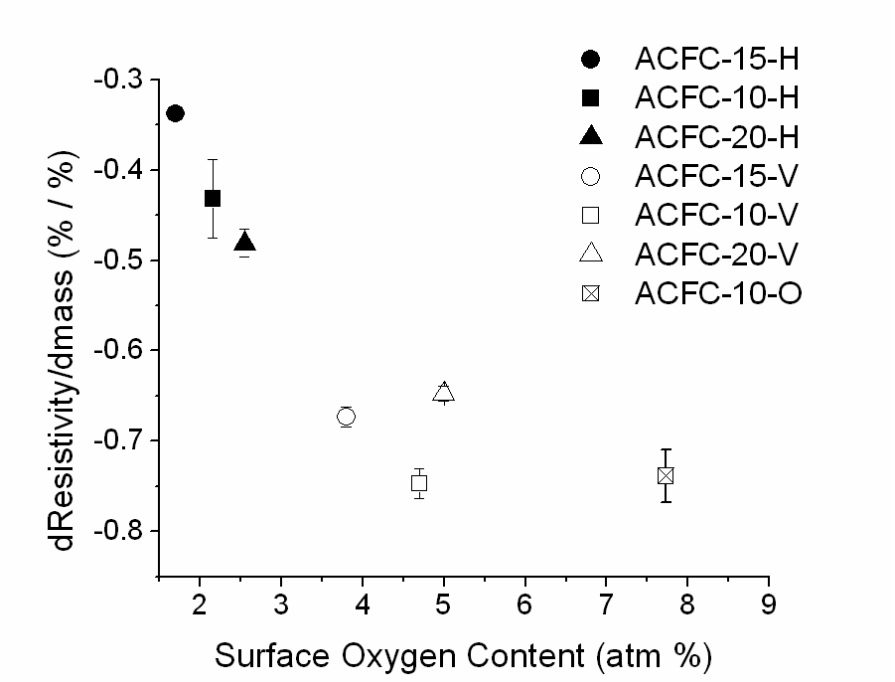

Figure 11: Percentage change in resistivity of activated carbon fiber cloth (ACFC) samples after a complete adsorption cycle of 1 % isobutane (by volume) normalized by percentage change in ACFC mass compared to sample surface O content where standard deviations are represented with vertical error bars

An explanation of the change in resistivity of ACFC samples that occurs during isobutane adsorption also requires comparison with the nanographitic structure of ACFC. As previously discussed, isobutane adsorption onto the prepared ACFC samples increases the interlayer spacing between the nanographene sheets, which decreases the distance between nanographite domains. The observed decrease in resistivity during isobutane adsorption is attributed to an increase in the interlayer spacing between the nanographene sheets resulting in a decreased spacing between domains. Samples with higher micropore volumes have a higher adsorption capacity and more adsorption sites that are occupied by the isobutane, resulting in a larger decrease in the resistivity. The samples with different surface O contents had nearly identical nanographitic structures (treated samples had interlayer spacing within 0.6 % of the untreated samples). However, the resistivity of ACFC samples with higher O contents were more affected by

isobutane adsorption, which is thus attributed to the O localizing electrons and the adsorbed isobutane providing energy to release localized electrons, improving electron transport.

A linear regression was used to quantify the resistivity of the ACFC samples from Table 7 with respect to ACFC micropore volume (W_o, cm^3/g), surface oxygen content ($O_{\%}$, at. %), and adsorbed mass of isobutane ($m_{a,iso}$, g adsorbed/g ACFC). Micropore volume, surface oxygen content, and adsorbed mass were statistically linearly independent from each other at the 0.05 significance level supporting the use of this linear regression.

$$\rho = -0.190 + 0.558(W_o) + 0.096(O_{\%}) - 0.268(m_{a,iso}) \quad \text{(Equation 4)}$$

This empirical model provides a linear fit to the resistivity data from the samples in this study ($r^2 = 0.88$) to provide quantitative weighting of select factors affecting ACFC resistivity but is not intended to be a predictive model for alternative ACFC samples. For, example, the negative y-intercept in Equation 4 results from the regression and does not have a physical meaning (i.e., should not be used to infer the resistivity of graphitic carbon). Equation 4 was determined to provide relative magnitudes of the effects of micropore volume, surface oxygen content, and adsorbed mass of isobutane on the resistivity of ACFC and the linear model provides a good approximation for the tested ACFC samples and conditions(i.e., as previously mentioned $r^2 = 0.88$). Despite the surface oxygen content term having the smallest coefficient, the surface oxygen content term was the largest term (i.e., compared to the adsorbed mass and micropore volume terms) in Equation 4 for five of the seven ACFC samples. The micropore volume term was the largest term for ACFC-15-H and ACFC-20-H. The adsorbed mass term was the smallest for all ACFC samples. This equation demonstrates the importance of ACFC surface oxygen content and micropore volume on its resistivity. Alternative non-linear models

describing ACFC resistivity that included polynomial terms (i.e., input variables to the powers of 0.33, 0.5, 2, and 3) and interaction terms were analyzed but there was not a significant improvement in the r^2 value of any of these models (i.e., r^2 value from 0.60-0.90 depending on the model) compared to the linear model in equation 4 (i.e., $r^2 = 0.88$). Thus, the linear model is presented in this work as the simplest model that provides a good fit to the measured ACFC resistivity data. Future work should be performed to develop a physical model describing the effects of micropore volume, surface oxygen content, and adsorbed mass on the resistivity of ACFC to provide a predictive model for a wider range of adsorbent properties and conditions.

Chapter 3: Evaluation of the Effect of Heating Temperature and Power Profiles on Regeneration Heating Cycle Energy Efficiency

3.1. Abstract[2]

ESA of organic gases generated by industrial processes can reduce atmospheric emissions and allow for re-use of recovered product. Desorption energy efficiency can be improved through control of adsorbent heating allowing for cost-effective separation and concentration of these gases for reuse. ACFC-ESA experiments with an air stream containing 2,000 ppm_v isobutane were performed in this chapter to evaluate regeneration energy consumption. Control logic based on temperature feedback achieved select temperature and power profiles during regeneration cycles while maintaining the ACFC's mean regeneration temperature at 200 °C. Energy requirements for regeneration were independent of differences in temperature/power oscillations (i.e., 1,186 to 1,237 kJ/mol isobutane). Additional logic that increased the maximum power application at lower ACFC temperatures resulted in a 36 % decrease in energy consumption. Implementing such control logic improves energy efficiency for separating and concentrating organic gases for post-desorption liquefaction of the organic gas for reuse reducing the energy requirements for ACFC-ESA.

[2]Reproduced in part with permission from Johnsen DL, Mallouk KE, Rood MJ. Control of electrothermal heating during regeneration of activated carbon fiber cloth. *Environmental Science & Technology*. 2011;45(2):738-43. Copyright 2011 American Chemical Society.

3.2. Experimental Apparatus and Methods

3.2.1. ACFC Cartridge Experimental Apparatus and Methods

Experiments were performed with a 3.5 L interior volume stainless steel vessel containing two annular ACFC cartridges (ACFC-15) electrically connected in series with a total of 183.3 g ± 0.85 g of ACFC (i.e., mean ± standard deviation) as shown in Figure 12. Gas flow rates were controlled with mass flow controllers (air: Aalborg, model GFC571S; isobutane/N_2: Tylan Inc.). Gas streams for adsorption cycles were generated by mixing isobutane (Aeropres Corp., 97.8 % isobutane, vapor withdrawal) with house compressed air that passed through silica gel and a high efficiency particulate air filter to remove water and particles. A 50 SLPM gas stream containing 2,000 ppm_v isobutane was directed into the vessel until the exhaust stream reached a breakthrough concentration of 1,000 ppm_v isobutane (i.e., 50 % breakthrough) as measured with a photo ionization detector (PID, RAE Systems, Inc., PDM-10A). After breakthrough, the vessel was purged of O_2 with 15 L N_2 (S.J. Smith, 99.95 % N_2) at 5 SLPM. The N_2 flow rate was then reduced to 0.5 SLPM and a feedback controller was activated to heat the ACFC. All controllers were designed with LabVIEW^{TM} 6.1 software and controlled DC voltage to a silicon controlled rectifier (SCR, Robicon, Model 440 102.10), which supplied up to 120 V alternating current (AC) that was then reduced with a variable voltage transformer (Variac, Powerstat) and applied to the ACFC for heating. Direct contact Type K thermocouples (0.81 mm diameter, Omega Inc.) measured ACFC temperature during heating. The concentration of isobutane in the exhaust gas stream during regeneration cycles was continuously measured with a flame ionization detector (FID, MSA Inc., Series 8800) because the concentration was above the PID measurement range. The PID and FID hydrocarbon detectors were calibrated before each test using controlled adsorbate inlet concentrations (i.e., 0, 500, 1000, 1500, 2000,

3000, 4000 ppm_v isobutane remainder air for the PID and 0, 20 %, 40 %, 60 %, 80 %, and 100 % isobutane by volume remainder N_2 for the FID). Root mean square (RMS) voltage and RMS current applied to the ACFC were measured with a potentiometer (Omega, Inc.) and a current transformer (Split Core) connected to an ammeter (Omega, Inc.), respectively. All measurements were continuously stored at 1 Hz with National Instruments Fieldpoint™ hardware.

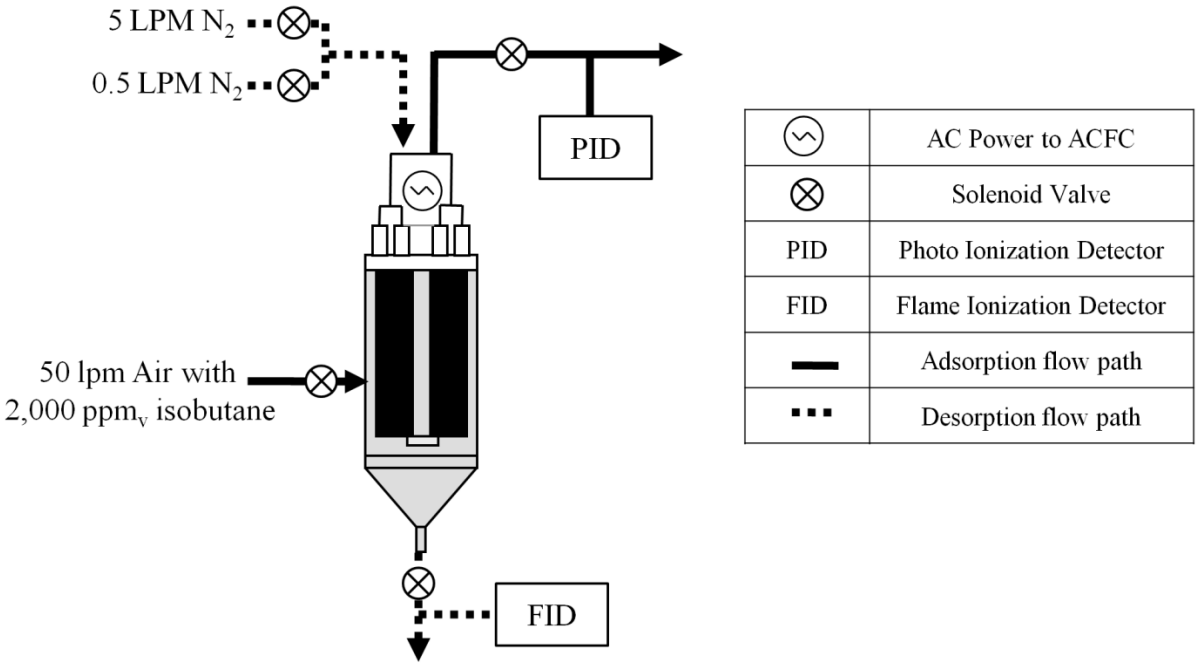

Figure 12: Activated carbon fiber cloth adsorption/desorption vessel for temperature feedback control

FID measurements were utilized to determine the mass of isobutane that desorbed from the ACFC (m_d, g), which is proportional to the area under the desorption concentration profile.

$$m_d = \sum_{i=0}^{t_f} M \left[\frac{P Q_{N_2} Y_{iso,t_i}}{R_g T}\right] (t_i - t_{i-1}) \qquad \text{(Equation 5)}$$

where M is molecular weight (g/mol), P is pressure (atm), Q_{N_2} is the flow rate of N_2 during desorption (SLPM), R_g is the ideal gas constant (L-atm/mol-K), T is temperature (K), t is time (min), t_f is the final time (min), and Y_{iso,t_i} is the isobutane to N_2 mole ratio at t_i (-).

3.2.2. Development of Temperature Feedback Controllers

Thermocouple feedback was used here to determine the energy efficiency of different regeneration temperature and power profiles. All feedback controllers were developed with LabVIEW™ 6.1 software based on the set-point and measured temperatures (thermocouple) of the ACFC and, as previously mentioned, they control the 0 to 5 VDC signal that is sent to the SCR to control electrothermal heating of the ACFC. Select temperature feedback controllers were tested for heating the ACFC to a set-point of 200 °C, which are titled an On-Off, proportional integral derivative (P-I-D), P-I-D delay, and P-I-D delay with a secondary P-I-D controller.

The On/Off, P-I-D, and P-I-D delay controllers are primary controllers that receive temperature feedback from a thermocouple and control voltage applied to the ACFC to achieve and maintain a temperature set-point (Figure 13). The On/Off controller applies 5 VDC to the SCR when the ACFC temperature is lower than the set-point temperature and 0 VDC when the ACFC's temperature is higher than the set-point temperature. The P-I-D controller, which applies 0 to 5 VDC to the SCR, was initially tuned with the Ziegler-Nichols method (Ziegler *et al.*, 1993) and additional adjustments were made to the constants. The P-I-D delay controller applies 5 VDC to the SCR until the ACFC is within 2 % of the set-point temperature, and then a P-I-D controller is activated.

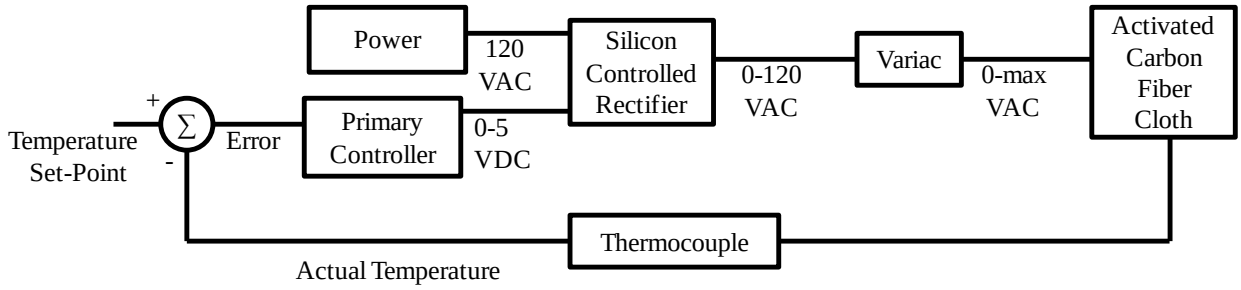

*Alternating current voltage (VAC), direct current voltage (VDC)
Figure 13: Control loop for activated carbon fiber cloth regeneration controller based on temperature feedback

For initial ACFC heating from the ambient temperature to the set-point temperature, each controller applies the maximum output voltage, determined by the SCR. ACFC acts as a typical semiconductor such that increased temperature results in decreased resistance and thus, an increase in current. The maximum current applied for regeneration heating was limited to 30 A as a safety protocol to avoid damaging the system's hardware or the ACFC. Thus, the SCR maximum voltage setting is determined to maintain current < 30 A at high temperatures, which resulted in current < 15 A at ambient temperature. The secondary P-I-D controller receives electrical current feedback from the ammeter and controls the maximum signal voltage for the primary controller (Figure 14). The secondary P-I-D constants were tuned to adjust the voltage to maintain a current of 26 A as the temperature increases, allowing for a higher SCR maximum voltage setting. Thus, the secondary P-I-D allows for larger power application at low temperatures resulting in faster initial heating, while reducing the voltage to maintain the current < 30 A at high temperatures.

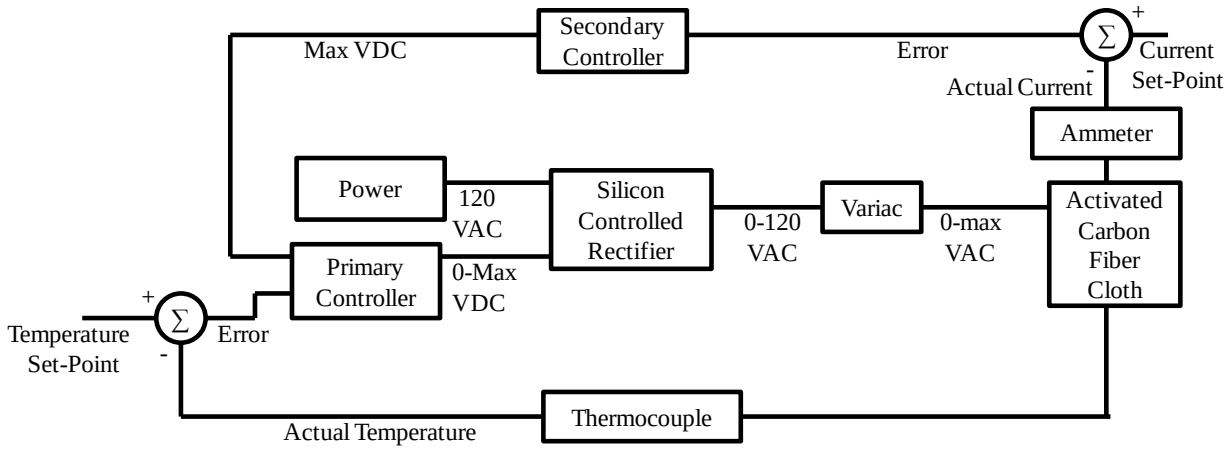

*Alternating current voltage (VAC), direct current voltage (VDC)
Figure 14: Control loop for activated carbon fiber cloth regeneration with primary and secondary controllers based on temperature and current feedback, respectively

The rate of temperature change, temperature settling time, temperature overshoot, and the absolute average percent difference (AAE) between actual and set-point temperatures were determined to characterize the controllers. The rate of temperature change (dT/dt) is the change in temperature of the ACFC per unit time while heating from 10 % to 90 % of the ACFC's temperature set-point. The settling time is the time for the ACFC to heat and stabilize within 4 % of the set-point temperature. Overshoot is the percentage difference between the maximum actual temperature and the set-point temperature. AAE is the absolute average percent difference between two data sets.

$$\mathrm{AAE} = \frac{100}{n}\sum_{i=1}^{n}\frac{|x_1 - x_2|}{x_2} \qquad \text{(Equation 6)}$$

where x_1 are the values from data set 1 (e.g., measured values), x_2 are the values from data set 2 (e.g., set-point or modeled values), and *n* is the number of matched measured and set-point or modeled values (-). Temperature AAE in this chapter compares measured and set-point values

and is calculated from the time when the ACFC first reaches the set-point until 60 s after reaching the set-point.

3.3. Results and Discussion

Each controller was designed to heat ACFC to provide specified temperature and power profiles to determine the effect of these profiles on the regeneration energy efficiency (Figure 15, Table 9). The On/Off controller provides precise temperature control with frequent large power oscillations (Figure 15a-b). The P-I-D controller provides large temperature oscillations with small power oscillations. The P-I-D delay controller provides precise temperature control with small power oscillations. The P-I-D delay with secondary P-I-D controller provides a larger power application during initial heating to the set-point temperature and then functions as a P-I-D delay controller providing precise temperature control with small power oscillations.

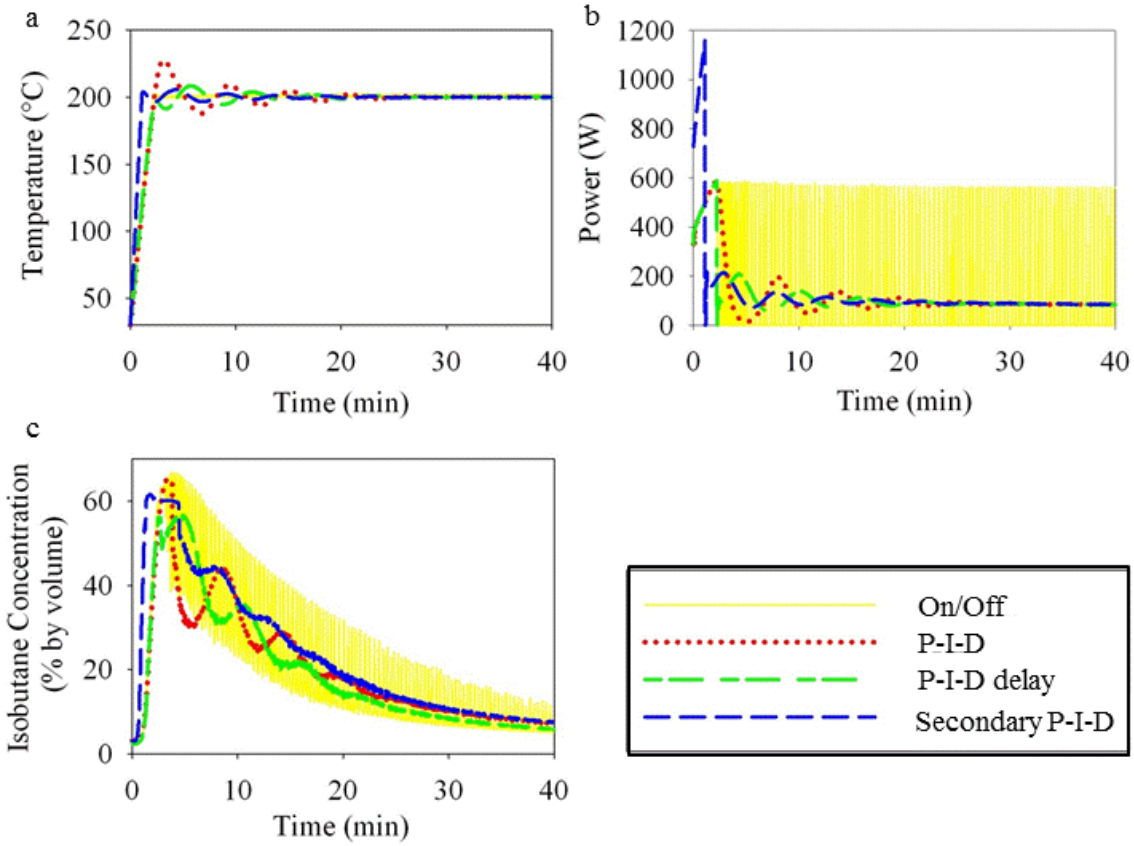

*Proportional-integral-derivative (P-I-D)

Figure 15: Temperature (a), power (b), and outlet isobutane concentration (c) profiles during activated carbon fiber cloth regeneration at a 200 °C set-point with 0.5 SLPM N_2 with select feedback controllers

Table 9: Controller responses (mean ± standard deviation) for heating activated carbon fiber cloth with isobutane to 200 °C

Regeneration Properties	On-Off	P-I-D	P-I-D Delay	Secondary P-I-D
Initial temperature (°C)	30.8 ± 3.9	31.8 ± 3.0	32.3 ± 0.9	30.9 ± 0.4
Overshoot (%)	1.5 ± 0.1	13.5 ± 0.6	4.5 ± 0.4	2.8 ± 0.1
AAE (%)[a]	0.6 ± 0.1	9.6 ± 0.9	2.5 ± 0.3	1.4 ± 0.4
Settling time (s)	132 ± 1	503 ± 120	372 ± 9	64 ± 1
dT/dt (°C/s)[b]	1.14 ± 0.01	1.62 ± 0.08	1.12 ± 0.01	2.27 ± 0.05
Maximum power to heat ACFC[c] with adsorbed isobutane (W/g ACFC)	3.27 ± 0.07	3.19 ± 0.02	3.24± 0.04	6.30 ± 0.04
Total energy including isobutane desorption and heat loses to the system (kJ)	288 ± 3	294 ± 6	285 ± 2	299 ± 3
Mass desorbed (g)	14.1 ± 0.7	14.0 ± 1.7	13.3 ±1.0	19.0 ± 3.7
Energy (Total energy including isobutane desorption and heat loses to the system)/mole desorbed (kJ/mol)	1,186 ± 72	1,211 ± 118	1,237 ± 83	908 ± 170
Total energy to heat ACFC without isobutane (kJ)[c]	257 ± 9	258 ± 2	254 ± 2	265 ± 6

*Proportional-integral-derivative (P-I-D), absolute average percent difference (AAE), activated carbon fiber cloth (ACFC)

[a]Equation 6, [b]Change in temperature per change in time, [c]Measurement performed without isobutane loading

ACFC temperature profiles during regeneration cycles with a set-point of 200 °C are included in Figure 15a. For all controllers, the ACFC temperature stabilized to the set-point temperature over time. The P-I-D controller has the largest settling time, overshoot, and oscillations about the set-point (described by AAE): 503 s, 13.5 %, and 9.6 %, respectively. The On/Off controller provides small oscillations of temperature with a small overshoot for the entire regeneration cycle resulting in the smallest AAE and overshoot (0.6 % and 1.5 %, respectively), which suggests this controller achieves the most precise temperature control after reaching the set-point temperature. The P-I-D delay controller has settling time, AAE, and overshoot values that are between the On/Off and P-I-D controller values. The P-I-D delay with secondary P-I-D

controller has a large dT/dt and small settling time while maintaining a small overshoot and small AAE, suggesting that it provides precise control with an increased rate of initial heating (2.27 °C/s, 64.4 s, 2.8 %, 1.4 %, respectively). Thus, the On/Off, P-I-D delay, and P-I-D delay with secondary P-I-D controllers provide precise temperature control and the P-I-D delay with secondary P-I-D provides the quickest initial heating.

The power application and outlet isobutane concentration profiles during the regeneration cycles are included in Figure 15b and Figure 15c, respectively**.** The On/Off controller causes the most frequent and largest magnitude power oscillations throughout the regeneration cycle. For a small averaging time (e.g., 30 s), the mean power applied by the On/Off controller is closer to the total mean power than the other controllers resulting in continuous rapid temperature oscillations about the set-point with the smallest magnitude (< 1 °C). The secondary P-I-D controller allows for larger power application to the ACFC at lower temperatures, and thus, has the largest energy consumption during initial heating. However, the initial heating period is < 2 min in comparison to the total 40 min regeneration cycle so the increase in total energy consumption was < 5 % for adding the secondary P-I-D to the P-I-D delay controller. The frequent, yet smaller, magnitude temperature oscillations provided by the On/Off controller cause frequent oscillations in isobutane concentration with large amplitudes due to the rapid temperature change from heating with full power (3.27 W/g). The mean outlet isobutane concentration declines over time in a similar manner for each controller and each has a maximum isobutane concentration of 55 % to 66 % by volume (1 min averaging time). Due to increased initial power application, the P-I-D delay with secondary P-I-D reached the peak concentration in 1.4 ± 0.1 min (i.e., mean ± standard deviation), which was 49 % faster than the other controllers. The energy/mole isobutane desorbed (908 kJ/mol to 1,237 kJ/mol) during the

40 min regeneration cycles is of the same order of magnitude as reported for acetone (924 kJ/mol to regenerate ACFC that treated 1,000 ppm_v acetone in air) during 3.5 min regeneration cycles (Dombrowski *et al.*, 2004). The On/Off, P-I-D, and P-I-D delay controllers had energy/mole values within 4 % suggesting that, in the tested conditions, the regeneration energy efficiency is independent of power oscillations and ACFC temperature oscillations. The increased initial power application, provided by adding the secondary P-I-D controller, increased the mass of desorbed isobutane by 43 % resulting in an improved regeneration energy efficiency over the P-I-D delay controller by 36 %. Because both controllers operate the same after initial heating, this increased mass indicates that increased power application during initial heating increases the regeneration energy efficiency, which is consistent with results obtained during the desorption of CO_2 from ACFC in N_2 carrier gas (An *et al*., 2010). The improved regeneration energy efficiency is likely due to the reduced energy losses that result from more quickly reaching the set-point temperature. In summary, power oscillations and temperature oscillations do not affect regeneration energy efficiency, while increasing initial power application improves efficiency. Additionally, the outlet concentration decreases towards the end of the regeneration cycle resulting in a lower regeneration energy efficiency. For continuous adsorption/regeneration cycles, a high initial power application (> 5.4 W/g ACFC) and shorter regeneration time (< 15 min) are suggested to improve regeneration energy efficiency.

Chapter 4: Automated Temperature Control of Activated Carbon Fiber Cloth during a Regeneration Heating Cycle based on Resistance Measurements

4.1. Abstract[3]

During ACFC-ESA, local temperature measurement (e.g., thermocouple) is typically used to monitor/control the heating portion of adsorbent regeneration cycles. Remote electrical resistance measurement is evaluated in this chapter as an alternative to local temperature measurement. ACFC resistance that was modeled based on its physical properties was within 10.5 % of measured resistance values during electrothermal heating. Resistance control was developed based on this measured relationship and used to control temperature to within 2.3 % of regeneration set-point temperatures. Isobutane laden adsorbent was then heated with resistance control. After 2 min of heating, the temperature of the adsorbent with isobutane was 13 % less than the adsorbent without isobutane. This difference decreased to 2.1 % after 9 min of heating showing desorption of isobutane with this new method. An ACFC cartridge was also heated to 175°C for 900 heating cycles with its resistance and adsorption capacity values remaining within 3 % and 2 %, respectively. Thus, this new regeneration heating method, based on rapid sensing of the adsorbent's resistance, removes the need for direct-contact temperature sensors providing a simple, cost-efficient, and long-term regeneration technique for ESA systems.

[3]Reproduced in part with permission from Johnsen DL, Rood MJ. Temperature Control during Regeneration of Activated Carbon Fiber Cloth with Resistance-Feedback. *Environmental Science & Technology*. 2012;46(20):11305-12. Copyright 2012 American Chemical Society.

4.2. Experimental Apparatus and Methods

4.2.1. Resistivity of Flat Sheets of ACFC

Resistivity of ACFC-15 was determined based on the mean of resistance measurements from five rectangular ACFC samples (7.4 cm x 3.9 cm) from different sections of the same lot of material using the 2-point probe apparatus shown in Figure 16. Each rectangle was supported across its width by stainless steel electrodes. The vessel was purged with 2 SLPM N_2 for 30 min, while voltage was applied across the ACFC with a DC power supply (Tenma, Model 72-2085) to maintain the ACFC at 200 °C to desorb volatile adsorbates (e.g., water vapor) from the ACFC. ACFC temperature was measured with a Type K thermocouple (1.6 mm diameter, Omega Inc.) contacting the ACFC at the center of the sample. The ACFC was then heated from 50 to 210 °C in 20 °C increments and current and voltage were measured concomitantly with a multimeter (Fluke, Model 45). Current and voltage were used to calculate ACFC's resistance and then resistivity (ρ, Ω-m) was calculated based on the relationship between resistance, temperature, and geometry (Sullivan *et al.,* 2001).

$$\rho = R\frac{CSA_E}{L} \qquad \text{(Equation 7)}$$

where R is resistance (Ω), L is the length of ACFC (m) parallel to electric current flow, and CSA_E is the effective cross sectional area perpendicular to electric current flow (m^2).

$$CSA_E = \frac{D_A}{\rho_f}W \qquad \text{(Equation 8)}$$

where D_A is the areal density of ACFC (0.176 kg/m^2, Johnsen *et al*., 2011a), ρ_f is the density of graphitic carbon (1,500 kg/m^3, Hayes, 1981), and W is the width of ACFC (m) perpendicular to

electric current flow. A linear least square regression between resistivity and temperature was used to determine resistivity as a function of temperature (Equation 3).

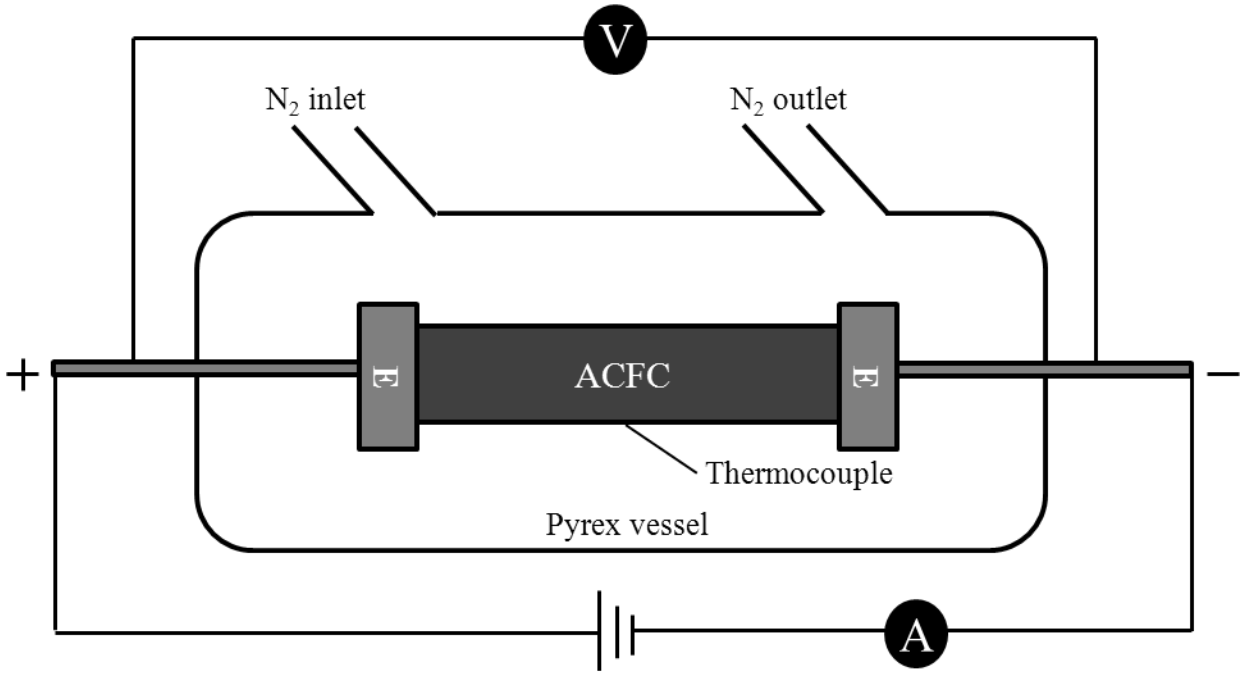

V	Volt meter
A	Ammeter
E	Electrode

Figure 16: 2-point probe apparatus for characterizing electrical resistivity of rectangular activated carbon fiber cloth (ACFC) samples

For this chapter, ACFC resistivity was determined with a different method than that discussed in Chapter 2. There are two primary differences between the resistivity measurements described in this section compared to section 2.2.2.3. First, a 2-point probe was used to measure sample resistance in this section compared to the 4-point probe from Chapter 2. The 2-point probe was selected for this section because it is a simpler apparatus and because resistivity was determined at elevated temperatures (≥ 50 °C) such that the effects of contact resistance were

consistent between experiments (demonstrated in the results of section 4.3.5). Second, the effective thickness of the samples was calculated in this section compared to a measured thickness in Chapter 2. This difference is primarily for comparison with previous studies in literature. Fundamental studies of ACFC resistivity, like that presented in Chapter 2, have used the measured thickness (Hashisho *et al*., 2009) while application based studies, like that presented in Chapter 4 and 5, have used the effective thickness (Sullivan *et al*., 2001) of ACFC samples to determine ACFC resistivity.

4.2.2. Physical Configuration of ACFC Cartridges

Annular ACFC cartridges were constructed by wrapping a rectangular strip of ACFC around a 1.9 cm outer diameter stainless steel annular electrode located at each end of the strip (Table 10). The length of the ACFC strips for each cartridge was 25 cm with varying widths and correspondingly varying numbers of layers for each cartridge. The ACFC was clamped to electrodes with stainless steel hose clamps resulting in an effective cartridge length for the current to flow (i.e., the distance between the hose clamps).

Table 10: Activated carbon fiber cloth (ACFC) rectangle and assembled cartridge properties

Cartridge number	**Effective cartridge length (cm)**	**ACFC width (cm)**	**Layers (#)**	**CSA_E (cm^2)[a]**	**Cartridge outer diameter (cm)**	**ACFC mass (g)**
1	21	68	9	0.8	2.8	30
2	21	162	18	2	3.7	74
3	22	260	26	3.2	4.5	114

[a]Equation 8

4.2.3. Adsorption and Regeneration Apparatus and Methods

Adsorption and regeneration cycles for the individual ACFC cartridges occurred in a 1.5 L interior volume Pyrex vessel (Figure 17). Gas flow rates were controlled with mass flow controllers (air: Aalborg, model GFC571S; isobutane/N_2: Tylan Inc.). A fifty SLPM air stream of house compressed air that passed through silica gel and a high efficiency particulate air filter to remove water and particles, respectively, was used for all adsorption experiments. Gas streams for isobutane adsorption cycles were generated by mixing isobutane (Aeropres Corp., 97.8 % isobutane, vapor withdrawal) with this air stream. The downstream adsorbate concentration was measured with a PID that was calibrated as described in section 3.2.1 (RAE Systems, Inc., PDM-10A). For adsorption cycles, a 50 SLPM air stream containing 2,000 ppm_v isobutane was directed into the vessel until the vessel's exhaust stream reached a breakthrough concentration of 1,000 ppm_v isobutane as measured with a photoionization detector. To regenerate the ACFC, the vessel was purged of O_2 with 15 L N_2 (S.J. Smith, 99.95 % N_2) at 5 SLPM. The N_2 flow rate was then reduced to 0.5 SLPM and a feedback controller was activated to heat the ACFC. The controller was designed with LabVIEW™ 6.1 software and controlled DC voltage to an SCR (Robicon, Model 440 102.10), which supplied up to 120 V rectified AC that was then reduced with a variable voltage transformer (Variac, Powerstat) and applied to the ACFC for heating. Direct-contact Type K thermocouples (0.81 mm diameter, Omega Inc.) measured ACFC temperature during heating. RMS voltage and current applied to the ACFC were measured with a potentiometer (Omega, Inc.) and a current transformer (Split Core) connected to an ammeter (Omega, Inc.), respectively. All measurements were stored with National Instruments Fieldpoint™ hardware.

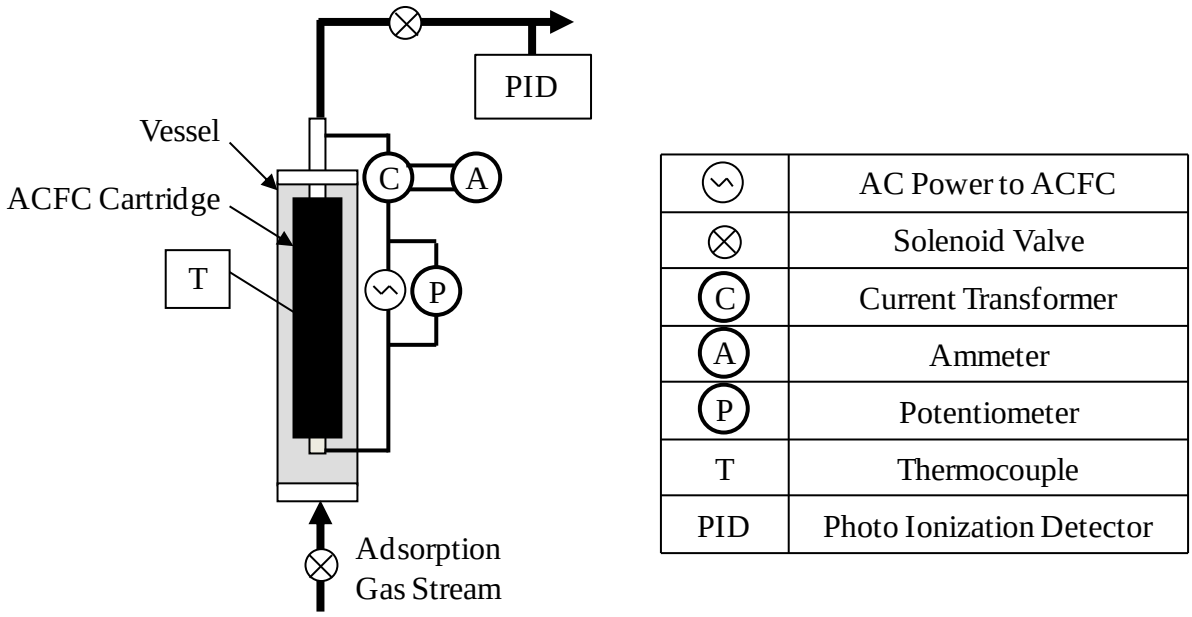

Figure 17: Schematic of experimental apparatus for adsorption and regeneration experiments with an activated carbon fiber cloth (ACFC) cartridge

The following section describes the experiments to determine cartridge resistance as a function of temperature. ACFC was heated to temperature set-points for 5 min to allow time for stabilization of voltage and current, and then a 100 sample arithmetic mean was calculated for measured voltage and current values. Resistance was calculated based on the mean voltage and current values. Equations 3, 7, and 8 that were used to determine the resistivity of a flat sheet of ACFC, were also used to model the resistance of the ACFC cartridge based on the ACFC's resistivity, measured temperature, and geometry to evaluate closure between the measured and modeled resistance values.

4.2.4. Resistance-feedback Controller

Resistance-feedback control converts a temperature set-point to a resistance set-point to control ACFC heating based on the ACFC's real-time resistance values, determined using

remote amperage and voltage measurements. This method eliminates the need for local temperature measurements. In this chapter, ACFC voltage and current values were used as feedback for proportional plus integral control of the voltage applied to the ACFC to achieve and maintain the temperature set-point (Figure 18). Conditioning of measured resistance values was used to reduce variability in the real-time calculated resistance values to achieve stable temperature control based on resistance. Conditioning involved the removal of outlier resistance values ($< 0\ \Omega$ or $> 4\ \Omega$, constituting < 2.5 % of data) before resistance values were used for control. The 0 to 4 Ω range was selected to encompass set-points corresponding to ACFC ranging from 0 to 400 °C for the cartridges in Table 10. A ten point (i.e., one Hz) moving mean of these filtered values was used as the feedback signal for control of voltage applied to the ACFC. The settling time (i.e., defined here as 4 % of the temperature or resistance set-point values) and AAE (Equation 6) between measured and set-point or modeled values, were used to quantify controller performance.

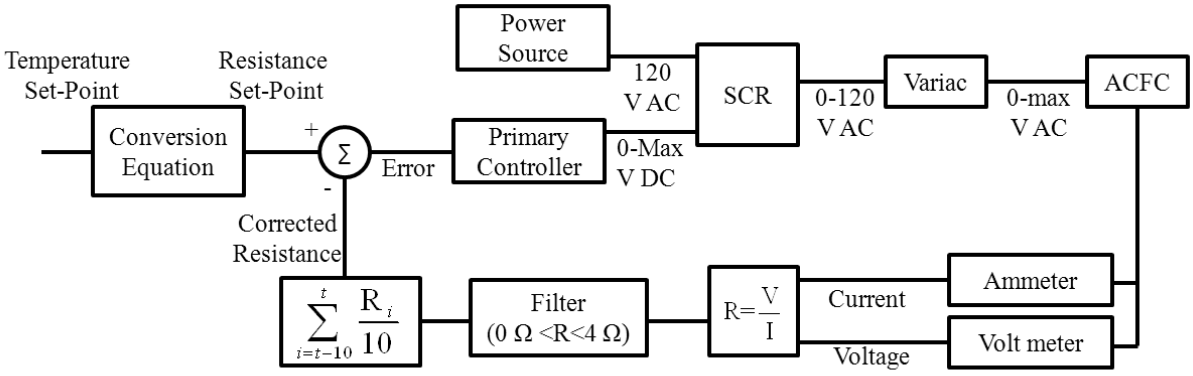

SCR	Silicon Controlled Rectifier
V DC	Direct Current Voltage
V AC	Alternating Current Voltage
ACFC	Activated Carbon Fiber Cloth
R	Resistance
I	Current
t	Time

Figure 18: Control loop for an ACFC regeneration controller with resistance-feedback

4.3. Results and Discussion

4.3.1. Resistivity of Flat ACFC Rectangles

For ACFC in this chapter, the mean ± standard deviation values of resistivity at 0 °C and thermal coefficient (Equation 3, $r^2 \geq 0.96$) were determined as $1.46 \cdot 10^{-3}$ Ω-m ± $0.08 \cdot 10^{-3}$ and $-2.00 \cdot 10^{-3}$ °C^{-1} ± $0.16 \cdot 10^{-3}$, respectively. These values are similar to values reported for ACFC (ACC5092-20) with increased activation, which has resistivity and thermal coefficient values of $1.84 \cdot 10^{-3}$-$2.35 \cdot 10^{-3}$ Ω-m and $-3.0 \cdot 10^{-3}$ °C^{-1}, respectively (Sullivan *et al.*, 2001). For both activation levels, resistivity calculations involved determining an effective cross sectional area that considers pore volume. However, increasing porosity can also increase the effective length for current flow if the current travels around the ACFC pores, which would explain the larger calculated resistivity values for ACFC with higher activation levels. A higher activation level

also results in a larger specific surface area for heat transfer, which explains the larger thermal coefficient when comparing ACC5092-20 to the ACFC in this study.

The resistivity and thermal coefficient values of activated carbon monoliths (composed of activated carbon powder and binder) ranged from 0.58 to 0.71 Ω-m and $-2.7 \cdot 10^{-3}$ to $2.8 \cdot 10^{-3}$ °C^{-1}, respectively (Lu *et al*., 2006; Yu *et al*., 2004). For ACFCs with cellulose (Lu *et al*., 2006; Ramos *et al.,* 2008) and Novoloid (Subrenat *et al.,* 2001) precursors, the resistivity values ranged from 0.3 to $86.6 \cdot 10^{-3}$ Ω-m and thermal coefficient values ranged from -0.5 to $-16.2 \cdot 10^{-3}$ °C^{-1}. These resistivity values vary by more than three orders of magnitude suggesting these activated carbons have significantly different absolute power requirements for electrothermal heating.

4.3.2. Resistivity of Annular ACFC Cartridges

Each ACFC cartridge (Table 10) was electrothermally heated and resistance values were measured at specified temperatures. Measured resistance values were then compared to corresponding modeled resistance values from Equations 3, 6, 7, and 8 (Figure 19). The AAE values between the predicted and measured resistance values were 10.5 %, 1.2 %, and 7.0 % for cartridges 1, 2, and 3, respectively. These small AAE values suggest ACFC cartridges can be designed to achieve resistance values for a specific application depending on the desired temperature range and the ACFC mass, resistivity, and geometry. Linear regressions of the measured resistance and temperature resulted in regression coefficients $r^2 > 0.97$ for all cartridges showing linearity in the measured values. This relationship is valuable, because it allows for ACFC temperature prediction with resistance measurements.

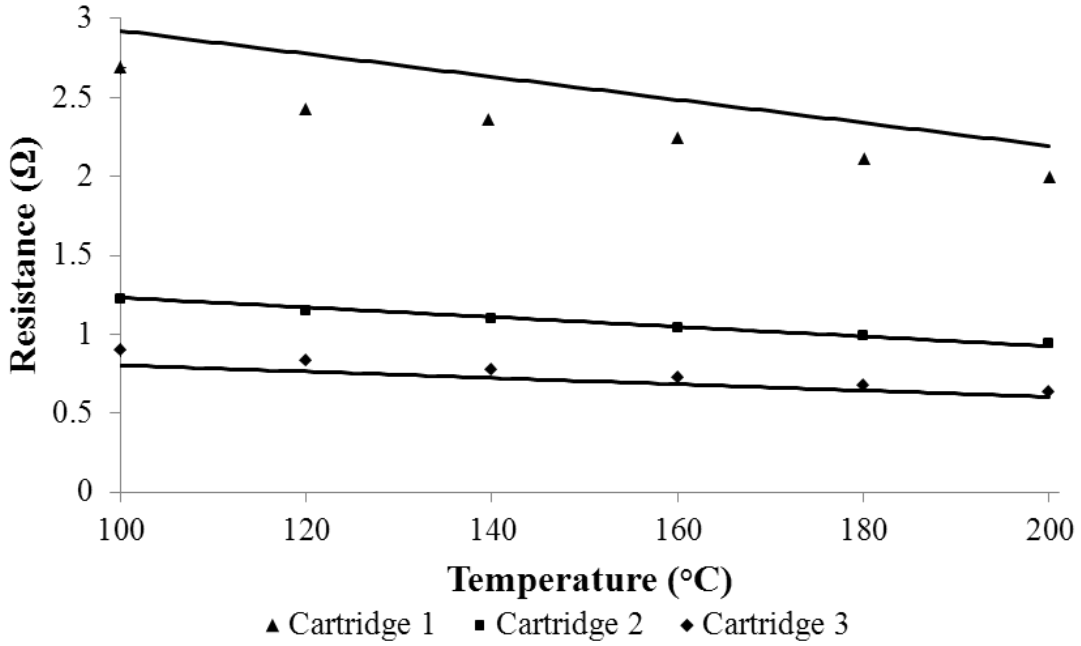

Figure 19: Measured (symbols) compared to modeled (lines) resistance values for activated carbon fiber cloth cartridges

4.3.3. Dynamic Resistance-feedback Control

A linear regression relating measured resistance (R, Ω) and temperature (T, °C) values was determined for cartridge 1 (Figure 19, $R = -6.9 \cdot 10^{-3} \cdot T + 3.4$, $r^2 = 0.993$) so that temperature set-points can be converted to resistance set-points for resistance-feedback control. This linear regression of the measured data was used instead of modeled values to achieve more accurate control, because the AAE between the regression and the measured resistance values was smaller (0.8 %) than the AAE between the modeled and measured resistance values (10.5 %). The linear regression was used to determine resistance set-points ranging from 2.67 Ω to 1.98 Ω, corresponding to typical regeneration temperatures from 100 °C to 200 °C.

Resistance-feedback control was then used to heat cartridge 1 to select temperature set-points for 5 min intervals to allow the measured ACFC temperature to reach the set-point temperature (Figure 20). The ACFC was heated and after initially reaching each resistance set-

point, measured resistance values were within 1 % AAE of the set-point resistance values showing accurate resistance control. Once the resistance value reached the set-point value, measured ACFC temperature was compared with modeled temperature that was predicted based on the corresponding resistance set-point. Measured and modeled temperatures agreed within 2.3 % for each set-point. Although the largest AAE value for temperature occurred at the smallest resistance set-point value (i.e., largest temperature), no overall trends were observed between AAE and temperature set-point. This close agreement between expected and measured values suggests that remote resistance measurements can be used to determine and control ACFC temperature during electrothermal regeneration.

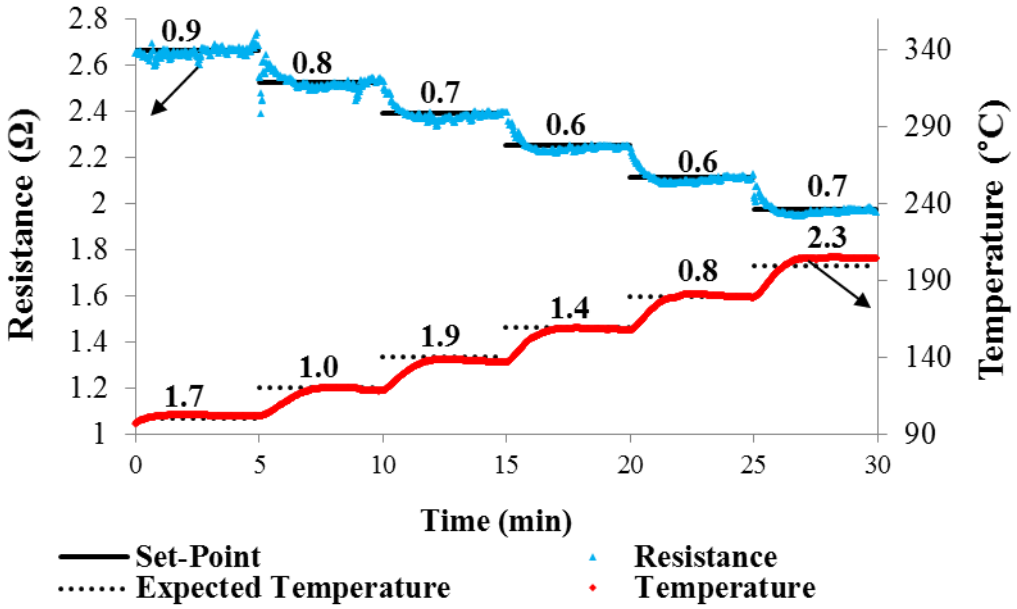

Figure 20: Resistance-feedback control when heating cartridge 1 without adsorbate, in which black lines describe set-points or predicted values and blue/red data points describe measured values and labeled absolute average percent difference (AAE, %) values at each set-point that were calculated starting when resistance reached each set-point value

4.3.4. Resistance-feedback Control with Adsorbed Isobutane

Cartridge 1, without and with adsorbate (0.1074 ± 0.0002 g isobutane/g ACFC, provided as mean ± standard deviation), was electrothermally heated for 40 min with resistance-feedback control to a set-point of 2.32 Ω, which is equivalent to 150 °C for ACFC without adsorbate (Figure 21). Controller performance is evaluated based on agreement between: 1) measured and set-point resistance values that are directly controlled based on resistance measurements and 2) measured and set-point temperature values that are indirectly controlled based on the relationship between temperature and resistance (Table 11). Because resistance was controlled to 2.32 Ω for all tests, differences between temperature profiles for the cases with and without isobutane are attributed to the adsorbate's influence on the relationship between the adsorbent's temperature and resistance (analyzed further in section 5.3.2.2). For electrothermal heating based on resistance-feedback, the regenerated ACFC (without isobutane) achieved the predicted set-point temperature within 2 min. The difference in temperature of the adsorbent with and without isobutane was 13.0 % at 2 min of heating and 2.1 % at 9 min of heating. The mean difference in temperature during the remaining 31 min of regeneration was 1.2 %. The larger differences in temperature at the beginning of the regeneration cycle likely occurred because the remaining adsorbed isobutane decreased the ACFC's electrical resistance (Johnsen *et al.*, 2011a). Then, as the isobutane desorbed from the ACFC, the temperature profiles converged. This decreased temperature that occurs when adsorbate is present results in a settling time for temperature that was 874 % larger for ACFC with adsorbate than without. However, during the same tests, the difference between settling times for resistance values with or without initial adsorbate was small (8.5 %), which is expected because control was directly based on resistance-feedback. Although the settling time for temperature increased when adding adsorbate, the maximum AAE value

between measured and predicted temperatures was still < 13 % after 2 min of heating. This value is an allowable temperature difference from the set-point for certain adsorbent regeneration applications. For example, during ACFC regeneration, the toluene concentration profiles were unchanged at temperatures ranging from 150 to 200 °C (Das *et al.,* 2004). Additionally, the AAE value was reduced as adsorbate loading was reduced. This relationship suggests applications that adsorb smaller concentrations of isobutane (< 2,000 ppm_v) or for shorter adsorption cycles (< 50 % breakthrough) can achieve closer control to the regeneration set-point temperature when resistance-feedback control is used without considering the impact of the adsorbate on ACFC's resistance. A resistance-feedback controller applicable for larger amounts of adsorbate would benefit from the addition of logic that considers the relationship between resistance, temperature, and adsorbed mass.

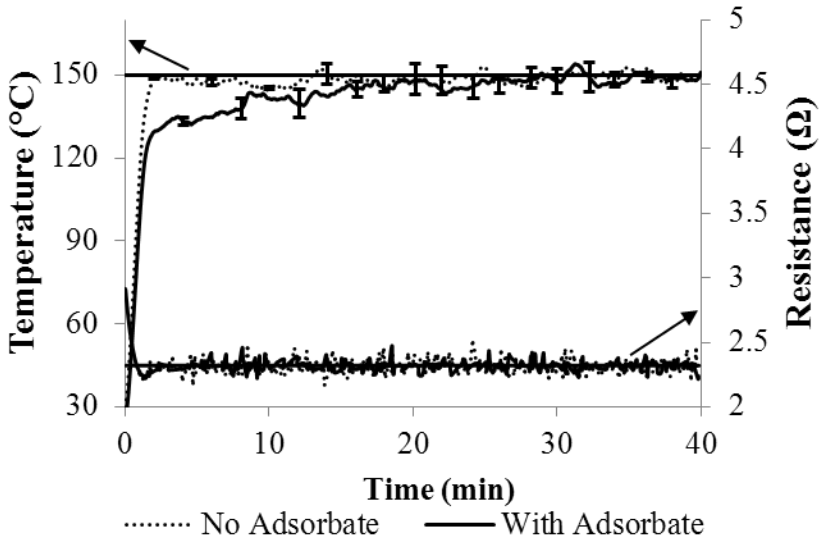

Figure 21: Temperature (standard deviations as vertical bars) and resistance values when heating cartridge 1 with and without adsorbate using resistance-feedback control, where horizontal solid lines represent the temperature and resistance set-point values during the regeneration cycle

Table 11: Resistance-feedback control responses from heating cartridge 1 to 2.32 Ω, as shown in Figure 21, where for each condition (with and without adsorbate loading), values are provided for the resistance response (directly controlled and measured) and the temperature response (measured during resistance control)

Response parameter	**No adsorbate loading[b]**	**Adsorbate loading[c]**
Resistance set-point (Ω)	2.32	2.32
Resistance settling time (s)	33	36
Resistance AAE (%)[a]	1.0	0.8
Temperature initial value (°C)	30	30
Temperature set-point (°C)	150	150
Temperature settling time (s)	100	874
Temperature AAE (%)[a]	0.7	12.7

*****Absolute average percent difference (AAE)

[a]ACFC without adsorbate first reached the set-point temperature in 2 min. AAE values for heating both with and without adsorbate were thus calculated for 1 min starting after 2 min of heating, [b]Dotted resistance and temperature lines from Figure 21, [c]Solid resistance and temperature lines from Figure 21

4.3.5. ACFC Longevity

This section characterizes the effects of repeated power application on ACFC performance. ACFC's electrical resistance and isobutane adsorption were initially characterized to describe the cartridge before heating. A linear regression was determined comparing resistance (R, Ω) to temperature (T, °C) based on measurements for cartridge 3 (Figure 19, $T = -381 \cdot R + 439$, $r^2 = 0.992$) to determine the initial resistance of the cartridge. This linear regression was used instead of modeled values for longevity tests because the purpose of the longevity tests is to determine the consistency of ACFC resistance over time so it is important to have measured initial values instead of modeled values to isolate the changes in resistance that occur over time from model error. The initial adsorption breakthrough curve (i.e., ends at 50 % breakthrough) revealed an adsorption capacity of 0.118 g isobutane/g ACFC.

The ACFC cartridge, with intermittent adsorbed isobutane (as described below), was then heated and cooled for a series of heating cycles. A heating cycle involved applying electrical power to control the ACFC temperature to 175 °C for 7 min in 0.5 SLPM N_2 to simulate regeneration conditions for ESA of isobutane with ACFC. Power was then turned off, and the next heating cycle began once the cartridge cooled to 60 °C, which was selected as a realistic ESA temperature limit to switch from a cooling cycle to an adsorption cycle. Nine hundred heating cycles were performed, but data are presented for the initial conditions (i.e., heating cycle without adsorbate present and first adsorption cycle) and the last 400 cycles to provide a concise and representative description of the dataset. The intermediate cycles were consistent with the 400 presented heating cycles. These 400 heating cycles were composed of a series of seven different sets of ≥ 50 continuous heating cycles. Each set of continuous cycles occurred over > 20 h and the variation in number of cycles between sets is due to availability of personnel to manually terminate the set. An adsorption cycle was performed after each set of continuous heating cycles was terminated and the ACFC cooled to ambient temperature. The adsorption cycles demonstrated consistent adsorption capacities at 50 % breakthrough of 0.117 g isobutane/g ACFC ± 0.002 (i.e., mean ± standard deviation) as shown in Figure 22. The measured downstream isobutane concentration is > 0 ppm_v at the start of each adsorption cycle, which is attributed to remaining isobutane in the sampling line after PID calibration. However, this measurement artifact does not have a significant effect on the total measured adsorbed mass (i.e., total adsorbed mass during the first half of the adsorption cycle in Figure 22 is within 2.2 % of the total adsorbed mass if 100 % capture efficiency were achieved), which was the adsorption property considered in this chapter.

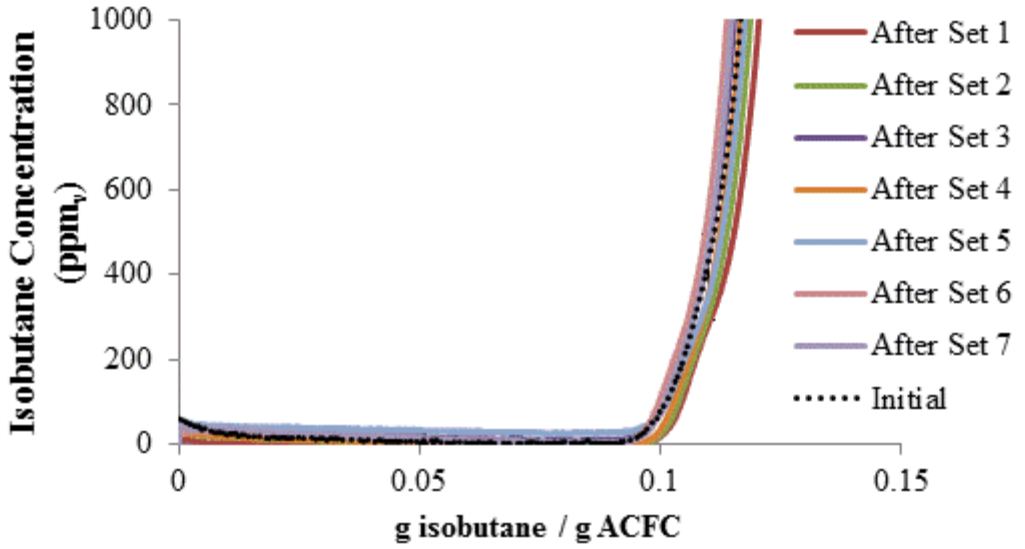

Figure 22: Breakthrough curves with 2,000 ppm$_v$ isobutane in an air stream after completing select sets of continuous heating cycles

Figure 23a includes the mean measured resistance of cartridge 3 (symbols) when the ACFC's measured temperature was 175 °C ± 0.5 °C (i.e., mean ± standard deviation) during each heating cycle. Each set of continuous heating cycles was compared to the expected initial resistance value for ACFC without adsorbate at 175 °C (horizontal line, Figure 23a). The largest difference between the expected resistance value and measured values was 3.4 %, while the AAE for all cycles of all sets was 1.2 %, which demonstrates consistent agreement between resistance values over > 47 h of electrothermal heating. Figure 23b includes an alternative representation of the data from Figure 23a, in which the set-point temperature (175 °C, horizontal line) is compared to the predicted adsorbent temperature values (symbols). These temperature values were predicted by inputting the measured resistance values from Fig. 8A into the previously mentioned linear regression for cartridge 3. The measured resistances correspond to predicted temperatures (i.e., based on previously mentioned fitted measured values from Figure 19) ranging from 169 °C to 180 °C, within 6 °C of the set-point value. The consistency of the predicted temperature based on resistance values with the actual temperature (175 °C ± 0.5 °C,

provided as mean ± standard deviation) demonstrates encouraging results for using resistance-feedback control over repeated electrothermal heating cycles.

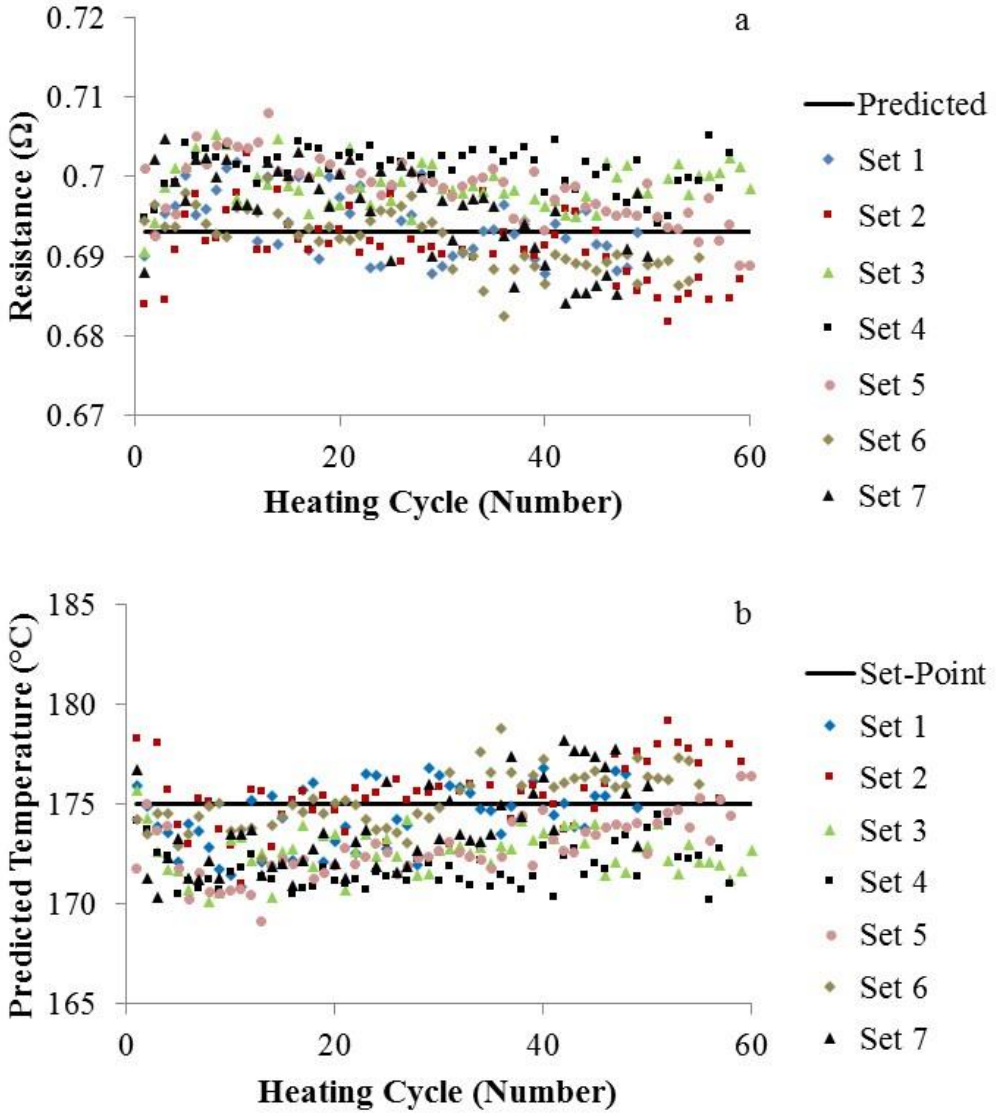

Figure 23: Mean measured resistance of activated carbon fiber cloth (ACFC) during heating cycles with a set-point of 175 °C (a, symbols) from seven sets of continuous heating cycles compared to the predicted resistance for this temperature (a, horizontal line), where ACFC temperature is predicted from measured resistance values from part a (b, symbols) and set-point temperature (b, horizontal line) and isobutane adsorption occurs before each set of continuous heating cycles

The mean resistance for each heating cycle increased during the first five cycles of each set of continuous heating cycles that occur after an adsorption cycle (corresponding to the first 35 min of heating after the initial adsorption cycle) due to isobutane desorbing from the ACFC. This corresponds with trends described in Figure 21, which shows increases in temperature at a fixed resistance indicating isobutane desorption over 40 min of heating. Linear regressions were performed to relate the mean resistance to the cycle number for the first five cycles of each of the sets of continuous heating cycles, and then linear regressions were also performed on the remaining cycles (starting with cycle six) for each of the sets of continuous heating cycles. Thus, two linear regressions were performed for each set, which included a regression of the first five cycles and a regression of the remaining cycles. Means of the linear regression coefficients over the seven sets of continuous heating cycles were calculated during the first five cycles and also for the remaining cycles. The mean slope of the resistance was positive during the first five cycles (0.0026 Ω/cycle ± 0.0008, provided as mean ± standard deviation, with mean $r^2 = 0.52$), which is attributed to the desorbing isobutane. The remaining cycles have a mean resistance slope that is close to zero (-0.00016 Ω/cycle ± 0.00009, provided as mean ± standard deviation, with mean $r^2 = 0.40$) suggesting the isobutane was largely desorbed by the sixth heating cycle. Although this resistance slope is small, the linear correlation between resistance and cycle is statistically significant at a 0.05 significance level for each set. This trend may be due to reorientation of the ACFC when alternating between adsorption and regeneration cycles. During the adsorption cycle, high flow rate air (i.e., 50 SLPM) travels from the exterior to the interior of the cartridge, which slightly compresses the cartridge and stretches the fibers; thus, the length for current flow increases, increasing resistance. During the continuous heating cycles, low flow rate N_2 (i.e., 0.5 SLPM) flows from the interior to the exterior of the cartridge, allowing the

ACFC to gradually expand to its initial shape, reducing the length for current flow and thus the resistance. This expansion and compression may explain the decreasing resistance in the later heating cycles and the consistency in resistance between sets. The observed trend in resistance values may also be due to adsorbed water or O from the air used during adsorption cycles that gradually desorbed during the following continuous heating cycles that used N_2 instead of air. Consistent resistance values are required to achieve set-point temperatures using resistance-feedback control, so the demonstrated consistency in resistance values (i.e., 1.2 % AAE between the resistance value from an initial heating cycle and measured resistance values from > 900 succeeding heating cycles) is promising for long-term applications of "remote resistance control" for ESA.

Chapter 5: Monitoring and Control of Electrothermal Swing Adsorption based on Electrical Properties of the Adsorbent

5.1. Abstract

ACFC-ESA includes adsorption and regeneration cycles, which are typically controlled based on measurements from hydrocarbon sensors, requiring their initial purchase, maintenance, and periodic calibration. ESA also typically utilizes measurements from local temperature sensors (e.g., thermocouples) to control electrothermal heating during regeneration cycles and to determine when the cooling portion of a regeneration cycle is complete. This chapter presents a new automated system to monitor and control ACFC-ESA that is based entirely on remote electrical measurements, which eliminates the need for hydrocarbon and local temperature sensors. For this system, the ACFC's electrical resistance was initially characterized based on adsorbent temperature and amount of adsorbed organic gas/vapor. These relationships were then used to develop control logic to monitor and control ESA cycles based on measured resistance and applied power values. Continuous sets of adsorption, regeneration, and cooling cycles were performed sequentially based entirely on remote electrical measurements achieving ≥ 99.5 % isobutane capture efficiency at inlet concentration of 2,000 and 4,000 ppm_v isobutane in air demonstrating proof of concept of a novel cyclic ESA system that does not require hydrocarbon or local temperature sensors. This tested control method resulted in a regeneration cycle that is 3.2 times longer than the adsorption cycle when tested at the same conditions as a traditional ESA system suggesting this control technique requires additional ACFC compared to traditional ESA. An alternative control method was developed based on electrical properties of the adsorbent that begins an adsorption cycle when the ACFC is at elevated temperatures (i.e., 60 °C) as occurs with traditional ESA. This alternative control method has an adsorption cycle that

is 18 % longer than the regeneration cycle (i.e., requiring the same mass of ACFC compared to traditional ESA) and achieved an isobutane capture efficiency of 98.4 % demonstrating that this method is competitive with traditional ESA but requires less sensors (i.e., no hydrocarbon or temperature sensors).

5.2. Experimental Apparatus and Methods

5.2.1. Adsorption Isotherms

5.2.1.1. *Apparatus*

Adsorption isotherms were generated using a gravimetric microbalance system. The microbalance setup consists of a gas generation system, a gravimetric balance, and a data acquisition system (Figure 24). The gas generation system produces a controlled concentration gas stream either by injecting specified volumes of liquid adsorbate into an ultra-high purity N_2 carrier gas using a syringe pump and hypodermic needle or by supplying a controlled flow rate of gaseous adsorbate into the N_2 carrier gas. The N_2 was passed through a gas drier/purifier containing $CaSO_4$ before being mixed with the adsorbate to remove contaminants. All gas flow rates were controlled with mass flow controllers (Tylan Inc. or Alicat Scientific Inc.), which were calibrated with a gas flow meter (BIOS DryCal, Model DC-2). The temperature of the sample was measured with a thermocouple (1.6 mm diameter, Omega Inc.) and controlled with electric heating tape and a variable voltage transformer (Variac, Staco Energy Products Co.). The gravimetric balance (Cahn, Model C-2000) measured the mass of the samples before and after adsorption of select adsorbates. The mass and temperature values were displayed on a data

acquisition system (Metrabyte, Model DASH-08/EXP-16) and then manually recorded for analysis.

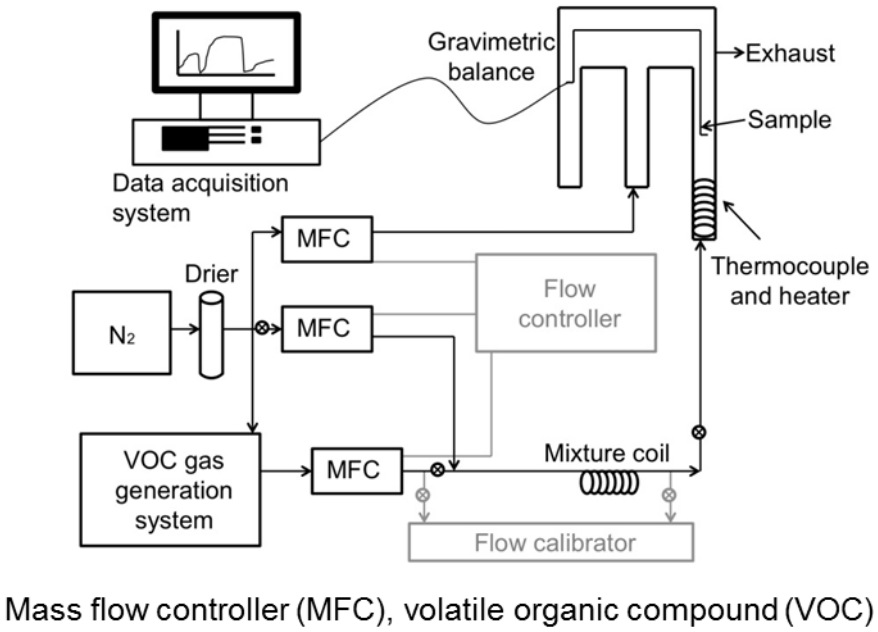

Figure 24**:** Experimental apparatus for gravimetric measurement of adsorption isotherms (figure reproduced from Mallouk and Rood, 2011)

5.2.1.2. *Procedure*

The adsorption capacity of isobutane, acetone, and toluene at select inlet concentrations onto ACFC-15 were determined with gravimetric adsorption isotherms. Triplicates were performed for each isotherm using different samples of ACFC-15. Prior to starting the experiment, the ACFC was heated to 100 °C in an oven for at least 8 h to remove adsorbed volatile materials and the gravimetric balance was zeroed and calibrated with a 10 mg reference weight. The adsorbent sample was then placed on the sample pan of the balance and heated to 45 °C for at least 2 h (until the mass stabilized) to ensure removal of volatile adsorbed materials.

The adsorbent was then allowed to cool to ambient temperature and the mass was recorded. Dry N_2 flowed through the sample chamber at 0.3- 0.5 SLPM for the duration of the experiments. An organic compound of known concentration (relative pressure) was then passed through the balance chamber and adsorbed onto the ACFC sample (i.e., causing the ACFC to gain mass). The system was assumed to be at equilibrium once the ACFC mass stabilized (i.e., < 0.2 mg change in 5 min) and the mass (ACFC plus adsorbed organic) was recorded. The adsorption capacity was then determined at a select concentrations as the ratio of the adsorbed mass of organic compound to the initial mass of the ACFC.

5.2.1.3. *Isotherms Modeling and Isosteric Heat of Adsorption*

The adsorption capacity of isobutane, acetone, and toluene onto ACFC-15-V was modelled at select relative pressures using both the DR and the Toth isotherm equations for comparison. A combination of the DR isotherm equation and the Clausius-Clapeyron equation was then used to determine the isosteric heat of adsorption for these adsorbates at select adsorption capacities.

The DR equation models adsorption based on Polanyi theory and assumes that adsorbed vapor condenses into a liquid within the pores of microporous adsorbents (Dubinin, 1989).

$$q = q_O exp\left[-\left(\frac{R_g T ln\left(\frac{P_o}{P}\right)}{E}\right)^2\right] \quad \text{(Equation 9)}$$

where q is the mass of adsorbate per mass of adsorbent (mg/g), q_O is the mass of adsorbate per mass of adsorbent at saturation (mg/g), R_g is the ideal gas law constant (kJ/mol-K), T is the adsorbent temperature (K), P_o is the saturation partial pressure of the adsorbate (kPa), P is the

partial pressure of the adsorbate (kPa), and E is the characteristic adsorption energy of the adsorbate (kJ/mol).

The Toth equation is an empirically derived isotherm that has performed well for characterizing the adsorption of gases onto microporous adsorbents, such as activated carbon materials (Park, 2011; Yu, 2002; Wang, 2012).

$$q = q_0 \frac{b_1 P}{\left[1+(b_1 P)^{b_2}\right]^{1/b_2}} \quad \text{(Equation 10)}$$

where b_1 is the Langmuir affinity constant (kPa^{-1}) and b_2 is a dimensionless constant (-). b_1, b_2, and q_0 are adjusted to fit adsorption experiments performed at different inlet gas concentrations for a specific adsorbate/adsorbent combination.

The fitting parameters for the DR (q_0, E) and Toth (q_0, b_1, and b_2) equations were determined by minimizing the AAE (Equation 6) between the predicted and measured adsorption capacity values using the generalized reduced gradient nonlinear least-square method in Microsoft Excel. The optimized AAE was then used to compare the accuracy of the models.

A combination of the DR and Clausius-Clapeyron equations was used to determine the isosteric heat of adsorption (ΔH_s, kJ/mol) for a given adsorbate-adsorbent pair based on the corresponding adsorption isotherm values (Ramirez *et al*., 2005).

$$\Delta H_s = \frac{R_g T^2}{P_{i,s}} \frac{dP_{i,s}}{dT} + E\left(ln\left(\frac{q_o}{q}\right)\right)^{\frac{1}{n_h}} + \frac{\propto TE}{2}\left(ln\left(\frac{q_o}{q}\right)\right)^{\frac{1}{n_h}-1} \quad \text{(Equation 11)}$$

where n is the heterogeneity parameter (-) (n_h = 2 for ACFC used by Ramirez *et al*., 2004), and α_a is the thermal coefficient of limiting adsorption (K^{-1}).

$$\alpha_a = \frac{1}{T_c - T_b} ln\left(\frac{\rho_b}{\rho_c}\right) \quad \text{(Equation 12)}$$

where ρ_b and ρ_c are the densities of the adsorbate (g/cm^3) at the normal boiling temperature (T_b, K) and the critical temperature (T_c, K), respectively.

5.2.2. ACFC-ESA Apparatus and Methods

5.2.2.1. *Experimental Apparatus*

Adsorption and regeneration experiments were performed with the apparatus and methods described in 4.2.3 with the following modifications. The PID was calibrated with ten controlled adsorbate inlet concentrations before each test (i.e., 0, 50, 100, 200, 500, 1000, 1500, 2000, 3000, and 4000 ppm_v isobutane remainder air). This calibration technique includes three additional low concentration calibration points (i.e., ≤ 200 ppm_v isobutane) when compared to tests from the previous chapters to ensure accurate PID calibration at low concentrations, which is required for determining abatement system capture efficiency (i.e., presented in this chapter). For acetone and toluene adsorption, gas streams were generated by injecting specified volumes of liquid adsorbate into a dried (i.e., < 5 % RH) particle free house air stream using a syringe pump and hypodermic needle. A small voltage (< 2 VAC) was applied to the ACFC during adsorption cycles and the cooling portion of regeneration cycles so that voltage and current could be measured to determine resistance. A one min moving mean of the electrical resistance of the ACFC cartridge was determined at one Hz and recorded during these cycles. The real-time adsorbed mass (m_A, g) was determined during adsorption cycles.

$$m_A = \sum_{i=0}^{t_f} M\left[\frac{PQ_a y}{R_g T}\right](t_i - t_{i-1}) \qquad \text{(Equation 13)}$$

where M is the molecular weight of adsorbate (g/mol), P is the adsorption gas stream pressure (atm), Q_a is the flow rate of the adsorption gas stream (SLPM), y is the mole fraction of the adsorbate in the gas stream (-), R_g is the ideal gas law constant (atm-L/mol-K), T is the ambient temperature (K), t is the time (min), and t_f is the time at the end of the adsorption cycle (min).

5.2.2.2. *Desorption Modeling*

Mass and energy balances were performed to model the desorption of isobutane from an ACFC cartridge during electrothermal heating. Modeling was based on the study by Sullivan *et al*., 2004a with the following changes: 1) liquid condensate of isobutane on the vessel walls was not considered in this study because isobutane exists as a gas at the tested operating conditions; 2) the Antoine equation was used to predict the vapor pressure of isobutane instead of the Wagner equation because the tested regeneration temperatures were greater than the critical temperature of isobutane, which causes infeasible results when using the Wagner equation; and 3) the heat capacity of the Pyrex adsorption vessel wall was considered in this study, which was not considered by Sullivan *et al*., 2004a. The parameters described in this section are summarized in Table 19 of Appendix A.

A mass balance was performed to equate the adsorbed isobutane to the sum of the gas phase isobutane within the vessel and the gas phase isobutane that exits the vessel.

$$\rho_{li} m_{ACFC} \frac{dW_i}{dt} = \frac{PV_v(M_{iso})}{R_g T} \frac{dy}{dt} + \frac{Q_{N_2} tP(M_{iso})y}{R_g T dt} \qquad \text{(Equation 14)}$$

where ρ_{li} is the liquid density of isobutane (kg/m^3), m_{ACFC} is the mass of ACFC (kg), W_i is the volume of adsorbed isobutane per unit mass of adsorbent (m^3/kg), t is the time (s), P is the pressure (atm), V_v is the vessel volume (m^3), M_{iso} is the molecular weight of isobutane (kg/kmol), R_g is the ideal gas law constant (m^3-atm/K-kmol), T is the ACFC temperature (K), y is the bulk mole fraction of isobutane in the N_2 purge gas (-), and Q_{N_2} is the N_2 flow rate (m^3/s). Isobutane does not condense at ambient temperature and pressure (23 °C and 1 atm) so the mass balance does not include a term for condensed isobutane. The bulk mole fraction of isobutane in the gas phase was determined using a combination of the DR and Antoine equations.

$$y = \frac{exp\left[A_1 + \frac{A_2}{T} + A_3 \ln(T) + A_4 T^{A_5}\right]}{Pexp\left[\frac{101.325 \cdot E}{R_g T}\sqrt{-ln\left(\frac{W_i}{W_o}\right)}\right]} \quad \text{(Equation 15)}$$

where A_i (i.e., i = 1,2,3,4, or 5) are the Antoine equation constants for isobutane (-), E is the adsorption energy for isobutane onto ACFC (kJ/kmol) and W_o is the total adsorbent micropore volume per mass of adsorbent (m^3/kg).

An energy balance was then used to describe the consumption of the applied energy for regeneration heating. The applied electrical energy includes five terms, which are: 1) the heat of adsorption, 2) the heat capacities of the major system components, and 3) conductive, 4) convective, and 5) radiative heat transfer. The heat of adsorption term describes the energy required to desorb the VOC from the ACFC. The heat capacity term describes the energy to heat the ACFC cartridge fittings, vessel wall, ACFC, adsorbate, and carrier gas. The final three terms describe conductive, convective and radiative heat transfer.

$$\frac{d(P_{IV})}{dt} = m_{ACFC}\Delta H_s \frac{dq}{dt} + \left[\sum m_f c_f + m_w c_w + m_{ACFC}\left(c_{ACFC} + q c_l + (q_i - q)c_g\right) + m_{N_2} c_{N_2}\right]\frac{dT}{dt} + hA_{conv}\frac{d(T - T_\infty)}{dt} + \varepsilon\sigma A_{rad}\frac{d(T^4 - T_\infty^4)}{dt} + \frac{\omega_{cond} A_{cond}}{L_{cond}}\frac{d(T - T_\infty)}{dt} \quad \text{(Equation 16)}$$

where P_{IV} is the electrical power applied to the ACFC cartridge (kW, current times voltage), ΔH_s is the isosteric heat of adsorption for the adsorbate/adsorbent pair (kJ/kg), q is the mass of adsorbate per mass of adsorbent ($W_i D_{li}$, kg/kg), m_f is the mass of the adsorbent cartridge fittings (kg), m_w is the mass of the vessel wall (kg), m_{N_2} is the mass of the N_2 purge gas (kg), c_i is the heat capacity of the fittings (kJ/kg-K), where $i = f, w, ACFC, l, g,$ and N_2 for the fittings, vessel wall, ACFC, liquid adsorbate, gas phase adsorbate, and N_2 purge gas, respectively, q_i is the initial mass of adsorbed isobutane per mass of adsorbent (kg/kg), h is the convective heat transfer coefficient (kW/m^2-K), A_i is area for heat transfer (m^2), where $i = conv, rad,$ and $cond$ for convective, radiative, and conductive heat transfer, respectively, T_∞ is the ambient temperature (K), ε is the emissivity of the ACFC (-), σ is the Stephen-Boltzmann constant (kW/m^2-K^4), ω_{cond} is the thermal conductivity for the stainless steel tubing entering the vessel (kW/m-K), and L_{cond} is the conduction length along the stainless steel tubing (m). The convective heat transfer coefficient from the ACFC to the gas in the annular space is then estimated.

$$h = \frac{Nu_L \omega_{conv}}{L_{conv}} \qquad \text{(Equation 17)}$$

$$Nu_L = \left\{ 0.825 + \frac{0.387 Ra_L^{1/6}}{\left[1+(0.492/Pr)^{9/16}\right]^{8/27}} \right\}^2 \qquad \text{(Equation 18)}$$

$$Ra_L = \frac{2g(T-T_\infty)L_{conv}^3}{\alpha_d \gamma (T+T_\infty)} \qquad \text{(Equation 19)}$$

where Nu_L is the Nusselt number (-), ω_{conv} is the thermal conductivity of the N_2 purge gas (kW/m-K), L_{conv} is the length of the cartridge (m), Ra_L is the Rayleigh number (-), Pr is the

Prandtl number (-), g is the acceleration of gravity (m/s^2), α_d is the thermal diffusivity at the N_2 gas temperature (m^2/s), and γ is the temperature dependent viscosity of the N_2 purge gas (m^2/s).

5.2.2.3. *Cyclic ESA based on Electrical Measurements Methodology*

Cyclic ESA based on electrical measurements involves sequential operation of adsorption, regeneration, and cooling cycles. For all cyclic experiments, the adsorption cycle involved passing a 50 SLPM gas stream containing 2,000 or 4,000 ppm_v isobutane in air through the ACFC cartridge. A small voltage was applied to the ACFC during the adsorption cycle (i.e., < 2 VAC) to determine a one minute moving mean of ACFC's electrical resistance (i.e., at 1 Hz) for control. The adsorption cycle was automatically ended after the occurrence of a specified change in electrical resistance that was determined as the product of the isobutane adsorption capacity and the change in ACFC resistance per change in adsorbed mass (i.e., determined in section 5.3.1). The set-point for the change in resistance for isobutane adsorption cycles was 0.07 and 0.09 dΩ for inlet isobutane concentrations of 2,000 and 4,000 ppm_v, respectively. After the first adsorption cycle, the set-point for the change in electrical resistance is multiplied by a correction factor to account for the reduced adsorption capacity due to the adsorbate that remains on the ACFC from incomplete regeneration and to account for differences between the modelled and measured values (i.e., 0.75 correction factor for heating to 150 °C for 10 min, as described in 5.3.1.5). During the adsorption cycle, the downstream adsorbate concentration was measured with a PID to characterize the system capture efficiency but these measurements were not used for ESA control.

After breakthrough, the regeneration cycle was initiated. First, the vessel was purged with 15 L N_2 at 5 SLPM to inert the environment. The N_2 was then reduced to 0.5 SLPM and a

controller was activated that adjusts the power applied to the ACFC to achieve a power set-point profile (i.e., electrothermal heating). Selection of the power set-point profile is based on modeled values and is described in detail in section 5.3.2.4. The controller was designed with computer software and controlled 0-5 VDC to an SCR, which supplied up to 120 VAC that was then reduced with a variable voltage transformer (Variac, Powerstat) and applied to the ACFC to achieve the required power profile.

After the regeneration heating was complete the ACFC was cooled in 0.5 SLPM N_2. During cooling the voltage applied to the ACFC was reduced (< 2 VAC) and ACFC resistance was determined (i.e., one minute moving mean measured at 1 Hz). Cooling continued until the ACFC's electrical resistance reached a value corresponding to a temperature of 60 °C (i.e., determined from Figure 19), which is a temperature set-point that has been previously used for starting an adsorption cycle (Mallouk *et al*., 2010). At this resistance set-point (i.e., corresponding to 60 °C), a 50 SLPM air stream was passed through the ACFC to provide rapid cooling. ACFC cooling continued until the change in ACFC resistance over time reached zero (i.e., ≤ 0.00001 Ω/s) indicating the ACFC was at a stable temperature.

An alternative control method was used to start a simultaneous adsorption/cooling cycle at elevated temperatures (60 °C, described in 5.3.3.3). This method used the same regeneration heating control as previously described. For the cooling cycle, once the ACFC reached the resistance set-point corresponding to a temperature of 60 °C, a 50 SLPM gas stream with adsorbate was passed through the ACFC to simultaneously start an adsorption cycle while providing rapid cooling. This simultaneous adsorption/cooling cycle continues until the change in ACFC's resistance over time is negative (i.e., ≤ -0.0001 Ω/s) and then reaches zero (i.e., ≥ 0 Ω/s), indicating adsorption is the dominant factor affecting ACFC resistance compared to

temperature and then that adsorption is complete, respectively (described in detail in 5.3.1.4). The changes in ACFC electrical resistance over time that are used to determine the end of a cooling cycle and also the end of a simultaneous adsorption/cooling cycle require extensive data averaging to eliminate noise that results from calculating the time derivate of resistance. A multimeter that measures resistance (Fluke, Model 45) was used during cooling and adsorption cycles to reduce measurement error from calculating resistance from independent voltage and current measurements. A 2-point probe was used for multimeter resistance measurements to avoid adding additional sensors/probes within the adsorption vessel (i.e., the goal of this research is to eliminate the need for sensors so adding probes would be counterproductive). The resistance is sampled at 0.5 Hz. A one minute moving mean of the resistance was used to determine smoothed electrical resistance values. The change in these smoothed resistance values over time were then averaged (i.e., one minute moving mean of the time derivative of smoothed resistance) and stored for control.

5.3. Results and Discussion

A simpler and less expensive method to monitor and control ACFC-ESA systems is presented that is based entirely on remote electrical measurements, which eliminates the need for hydrocarbon and local temperature sensors. For this method, ACFC's electrical resistance is initially characterized based on adsorbent temperature and amount of adsorbed material. These relationships are then used to develop control logic to monitor and control ESA cycles based on measured resistance and applied power values. First, ACFC electrical resistance was characterized during adsorption cycles. Then, ACFC electrical resistance and applied power for

heating were characterized during regeneration cycles. Finally, the system was automatically controlled in cyclic operation mode based on ACFC resistance and applied power for heating.

5.3.1. Characterization of an ESA Adsorption Cycle

The electrical resistance of ACFC and mass that is adsorbed during an adsorption cycle is characterized here so that an adsorption cycle can be automatically controlled based on electrical resistance measurements. First, adsorption isotherms are presented to characterize the adsorption of select adsorbates onto the ACFC at ideal conditions. Then, the adsorption capacity and electrical resistance of an ACFC cartridge are characterized during adsorption. For practical applications, ESA must be able to operate over a wide range of conditions so the relationship between adsorbed mass and resistance is also characterized for different adsorbates, adsorption cycles starting at different temperatures, and adsorption cycles starting with varying amounts of remaining previously adsorbed material.

5.3.1.1. *Adsorption Isotherms and Isosteric Heat of Adsorption*

Measured and modeled isobutane, acetone, and toluene adsorption isotherms at 25 °C are presented in Figure 25 and Table 12. Adsorption capacities at partial pressures of 0.003 to 0.3 are presented for isobutane, while a wider range of partial pressures is presented for acetone and toluene (i.e., 0.003 to 0.8), because a pure isobutane gas stream at 25 °C and 1 atm has a partial pressure of 0.3 (i.e., 100 % isobutane). For each adsorbate, adsorption capacity increased with increasing concentration following type I isotherm behavior, which is common for the adsorption of gases onto microporous adsorbents (Ramirez *et al*., 2004). The DR and Toth equation

isotherm models are both effective for modeling the adsorption capacity for the adsorbates in this study (i.e., AAE ≤ 15 %). The Toth equation describes the measured data better than the DR equation for isobutane and acetone (i.e., AAE between modeled and measured values is 2.2 and 2.6 for the Toth equation and is 4.3 and 14.6 for the DR equation for isobutane and acetone, respectively). The DR equation was less accurate than the Toth equation at the highest and lowest partial pressures within the tested ranges (e.g., 33 % and 14 % error at P/P_o = 0.05 for acetone adsorption modeled with the DR and Toth equations, respectively). However, the DR equation provided a better fit than the Toth equation for toluene adsorption, which is likely due to the smaller range of adsorption capacities for the toluene isotherm (i.e., 324 to 460 mg/g) when compared to the isobutane and acetone isotherms (62 to 303 and 48 to 420 mg/g, respectively).

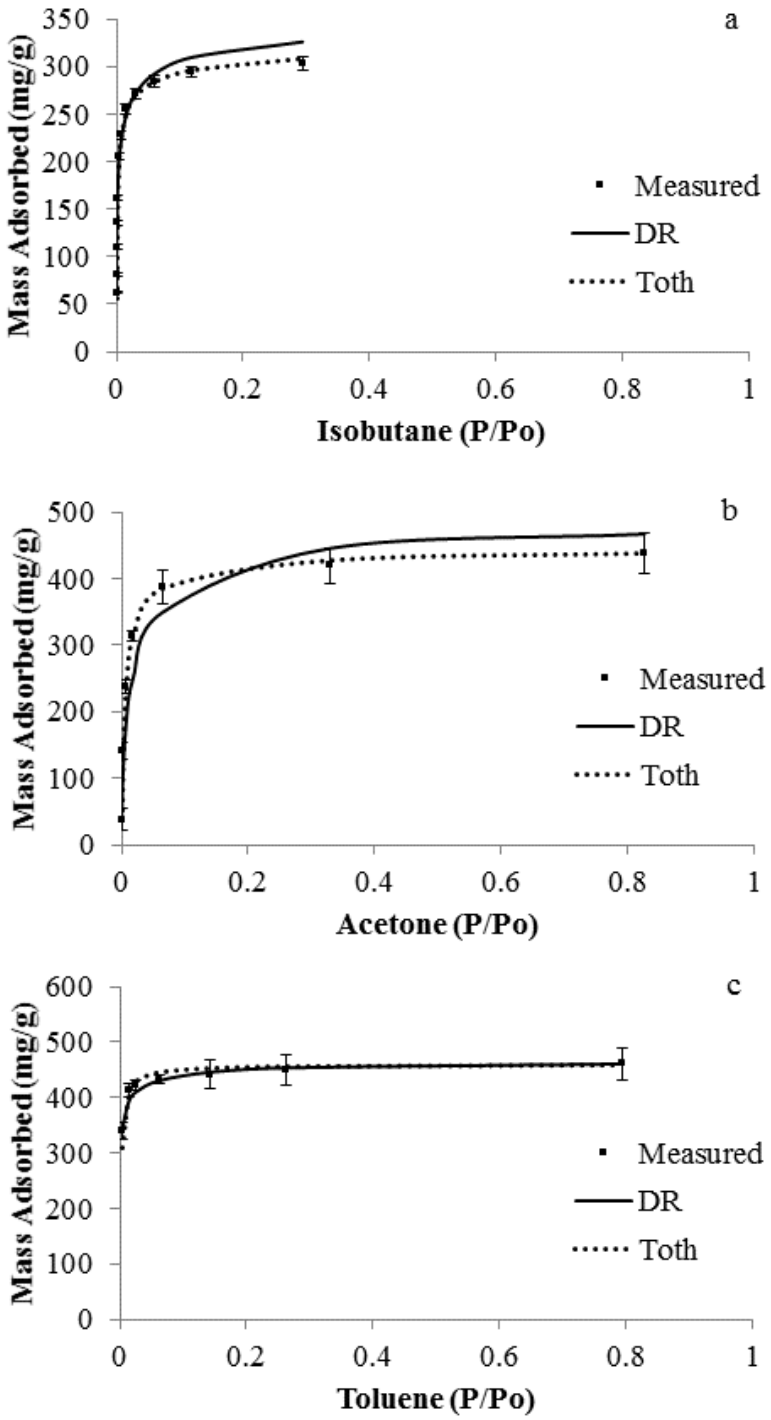

*Dubinin-Radushkevich (DR) equation

Figure 25: Adsorption capacity of isobutane (a), acetone (b), and toluene (c) at select partial pressures onto ACFC-15-V at 25 °C

Table 12: Fitting parameters and absolute average percent difference (AAE) between modelled and measured adsorption capacities during the adsorption of isobutane acetone, and toluene at select partial pressures onto ACFC-15-V at 25 °C

Adsorbate	**DR equation[a]**			**Toth equation[b]**			
	q_O **(mg/g)**	E **(kJ/mol)**	**AAE (%)[c]**	q_O **(mg/g)**	b_1 **(kPa^{-1})**	b_2 **(-)**	**AAE (%)[c]**
Isobutane	334	18.0	4.3	342	49	0.3	2.2
Acetone	467	12.5	14.6	449	11	0.7	2.6
Toluene	461	26.4	1.4	460	302	0.8	2.6

[a]Equation 9, [b]Equation 10, [c]Equation 6

The modeled saturation adsorption capacities (i.e., q_O from the DR and Toth equations) were compared to the micropore volume of the adsorbent. More specifically, the quotient of q_O and the liquid density of the adsorbates was determined (W_O, cm^3/g) and compared with the measured micropore volume for ACFC-15-V (i.e., 0.59 cm^3/g). For the DR equation, the percent error between the modeled adsorbed volume (i.e., W_O) and the measured micropore volume was -4.8, 0.0, and -9.8 % for isobutane, acetone, and toluene, respectively. For the Toth equation, the percent error between these parameters was -2.5,-3.7, and -10.0 % for isobutane, acetone, and toluene, respectively. These results are promising because all modeled W_O values are less than or equal to the measured micropore volume. Additionally, all modeled values were within 10 % of the micropore volume suggesting pore filling occurs at saturation.

Isosteric heat of adsorption values are presented in Figure 26. The isosteric heat of adsorption values for isobutane and acetone follow three phases: 1) first decreasing with adsorption capacity, 2) then constant with adsorption capacity, and 3) then increasing with adsorption capacity. These three phases are not visible for toluene because the minimum measured adsorption capacity for toluene was 324 mg/g, such that all measured values are likely in the third phase. The higher isosteric heat of adsorption values at low adsorption capacities are

attributed to stronger interactions between the adsorbate and adsorbent at low surface loadings, while those at higher adsorption capacities are attributed to stronger lateral interactions between adsorbate molecules at high surface loadings (Ramirez *et al*., 2004). The isosteric heat of adsorption for toluene is larger than acetone, which is attributed to toluene's low saturation vapor pressure compared to acetone (3.8 and 30.7 kPa, respectively). The sharp increase in the isosteric heat of adsorption for isobutane is primarily due to the small difference between the boiling point and critical temperature of isobutane (147 °C) when compared to the other adsorbates (179 °C and 208 °C for acetone and toluene, respectively), which results in a 40 % larger thermal coefficient (α_a) for isobutane than either acetone or toluene.

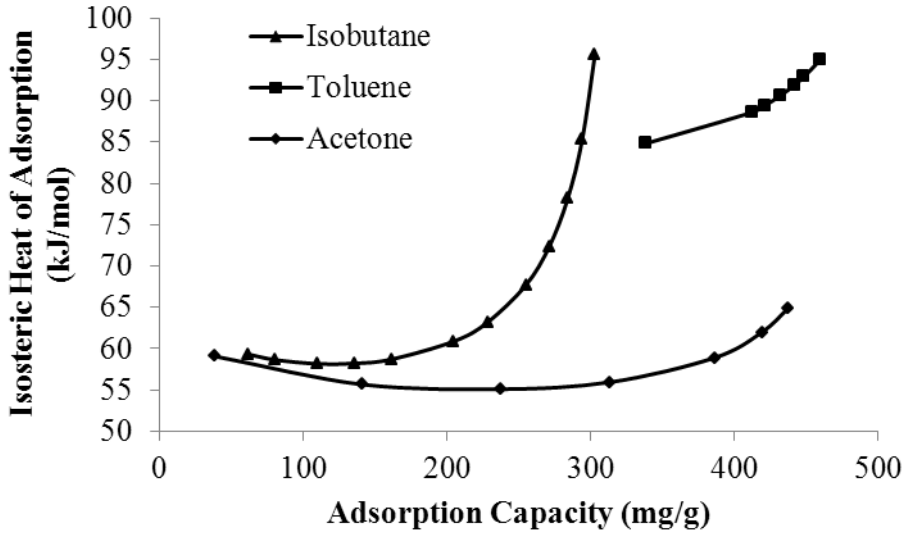

Figure 26: Isosteric heat of adsorption of isobutane, acetone, and toluene at select adsorption capacities when adsorbed onto ACFC-15-V at 25 °C

5.3.1.2. *Characterization of the Adsorption of 2,000 ppm_v Isobutane onto an ACFC Cartridge at Ambient Temperature*

The adsorption of 2,000 ppm_v isobutane in air onto an ACFC cartridge was characterized at 25 °C. The mean isobutane concentration from eight adsorption experiments performed over 28 days (i.e., occurred until 50 % breakthrough was reached) is presented in Figure 27. The isobutane adsorption capacity at 10 % breakthrough was consistent at 0.106 ± 0.001 g/g ACFC (mean ± standard deviation). This measured adsorption capacity was within 22 % of that predicted with the Toth model based on equilibrium values determined with a microbalance (i.e., 0.136 g/g from 5.3.1.1). The measured ACFC cartridge adsorption capacity was within 13 % of that from a previous study with a larger ACFC cartridge (i.e., 0.094 g isobutane/g ACFC for a 183.3 g ACFC cartridge) (Mallouk *et al*., 2010). The mean adsorption capacities from this study and Mallouk *et al*., 2010 were within one standard deviation suggesting differences in adsorption capacity can be attributed to measurement error. Additionally, the regeneration cycle preceding the adsorption cycle in this work involved heating the ACFC for 30 min at 175 °C compared to 10 min at 200 °C in Mallouk *et al.*, 2010. Thus, the larger adsorption capacity in this work compared to Mallouk *et al.*, 2010 may also be due to the ACFC being more regenerated from the increased regeneration time.

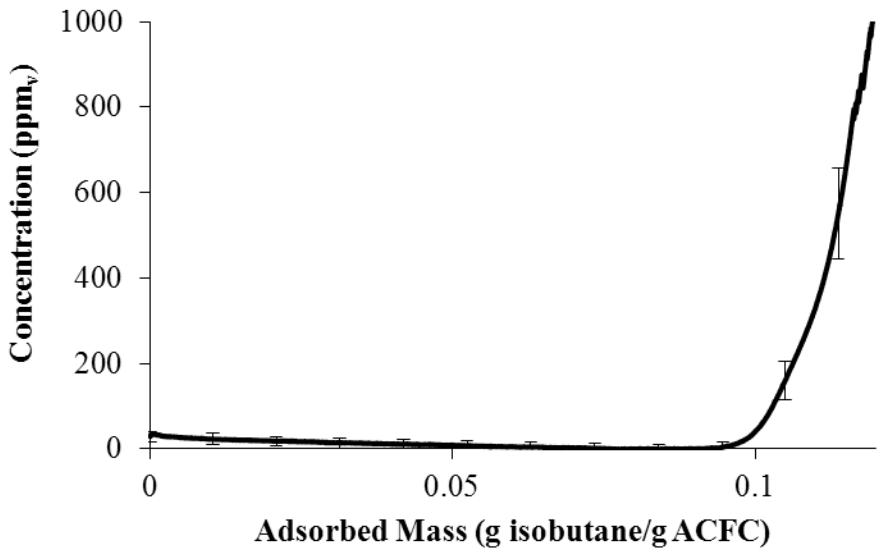

Figure 27: Activated carbon fiber cloth (ACFC) adsorption breakthrough curve with an inlet gas stream with 2,000 ppm_v isobutane in dried and particle free air

ACFC's electrical resistance was characterized during adsorption and desorption of isobutane at ambient temperatures (no regeneration heating) to demonstrate a reversible change in electrical resistance with physically adsorbed/desorbed mass. Resistance and adsorbed mass values were acquired while passing carrier air (initial condition, Figure 28a), then carrier air with isobutane (adsorption cycle, Figure 28b), and then carrier air (desorption into air without heating, Figure 28c) through the ACFC cartridge. When air was initially passed through the cartridge (Figure 28a), the resistance remained constant for 80 min with a mean value of 1.31 Ω and coefficient of variance of 1.2 %. Then, as isobutane was adsorbed, the resistance linearly decreased with increasing adsorbed mass ($r^2 = 0.97$, Figure 28b). As isobutane was desorbed into the air stream, the adsorbent's resistance returned to the initial value, a mean of 1.31 Ω and a coefficient of variance of 1.7 % for the final 80 min in Figure 28c. These results demonstrate that the resistance of an ACFC cartridge can be altered with VOC adsorption and then return to its initial value after desorbing the VOC.

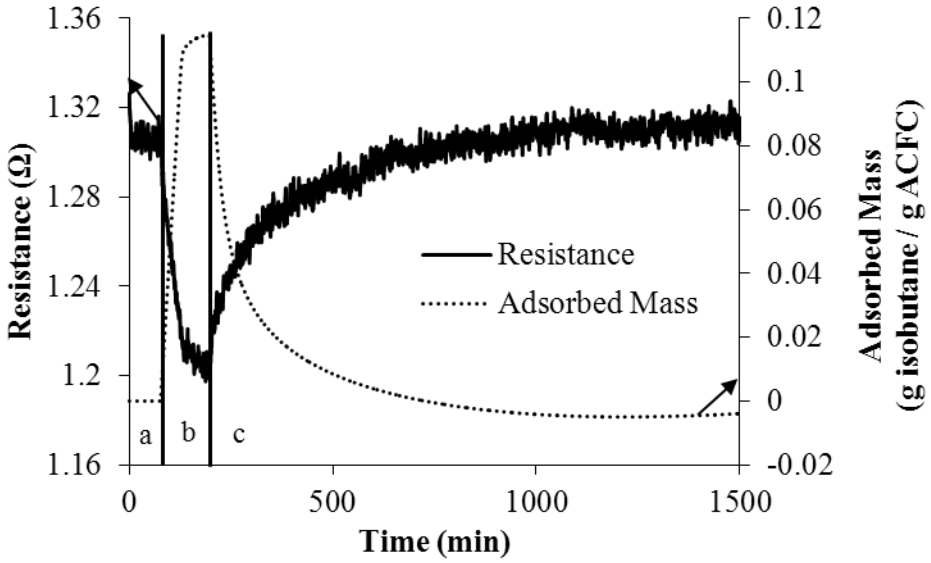

Figure 28: Electrical resistance and adsorbed mass while 50 SLPM air (a), air with 2,000 ppm_v isobutane (b), and air (c) were passed through an activated carbon fiber cloth (ACFC) cartridge

Figure 28 was selected as a representative figure to show the trends of the decrease in electrical resistance that occurs during isobutane adsorption and increase in electrical resistance to the initial resistance value during desorption. However, the initial resistance of the regenerated ACFC cartridge (25 °C) varied from 1.25 to 1.90 Ω for experiments performed over the duration of 2 yr. This variation in the initial resistance values is attributed to alterations in the contact resistance between the ACFC and the electrodes and adds complexity in determining the adsorbed mass based on electrical resistance measurements. The total measured resistance is the sum of the ACFC resistance and contact resistance. Assuming the contact resistance is constant over a single adsorption cycle (as was demonstrated in Figure 28 for the 25 h adsorption and desorption cycle), the decrease in resistance that occurs during an adsorption cycle will be consistent regardless of the total resistance (i.e., ACFC plus contact resistance). The decrease in resistance during isobutane adsorption from Figure 28, which has an initial cartridge resistance

of 1.31 Ω was compared with that from isobutane adsorption experiments with the same ACFC cartridge with a different mean initial cartridge resistance (i.e., 1.48 Ω). The change in resistance was -0.76 ± 0.01 Ω (i.e., mean ± standard deviation) at 10 % breakthrough when the cartridge had an initial resistance of 1.48 Ω, which is comparable to the -0.77 Ω change in resistance to achieve 10 % breakthrough when the initial resistance was 1.31 Ω. These results provide evidence that the change in resistance during isobutane adsorption is consistent although the initial resistance varies due to variations in contact resistance. This result confirms that adsorbate breakthrough can potentially be predicted based on electrical resistance measurements if both the ratio of electrical resistance change per adsorbed mass and the adsorption capacity of the ACFC are known. Each of these properties can be characterized by performing adsorption experiments with a small sample of adsorbent (e.g., 1 g ACFC) as described in section 5.3.1.1 and 5.3.1.3.

5.3.1.3. *Effect of Adsorbate and Adsorbate Concentration on the Resistance of an ACFC Cartridge during Adsorption*

The electrical resistance of an ACFC cartridge was characterized during the adsorption of isobutane and acetone at inlet concentrations of 2,000 and 4,000 ppm_v (Figure 29). Linear regressions of the relationship between the change in electrical resistance and adsorbed mass are provided in Table 13. ACFC's electrical resistance decreased by 0.71 Ω/(g adsorbed/g ACFC) (r^2 = 0.99) and 0.32 Ω/(g adsorbed/g ACFC) (r^2 = 0.99) during the adsorption of isobutane and acetone at an inlet concentration of 2000 ppm_v (Table 13). Increasing the inlet adsorption concentration from 2,000 to 4,000 ppm_v increases the VOC adsorption capacity, which increases the total resistance change over the adsorption cycle. However, the resistance change per

adsorbed mass was within 5.6 % for inlet concentrations of 2,000 and 4,000 ppm_v for isobutane and acetone, suggesting resistance change per adsorbed mass is independent of the inlet adsorbate concentration for the tested concentrations. As described in Chapter 2, adsorbed isobutane attracts ACFC's nanographite domains, decreasing the spacing between ACFC nanographite domains resulting in the observed decrease in electrical resistance with isobutane adsorption. Acetone has a similar carbon backbone but also contains a hydroxyl group, which repels the hydrophobic nanographite domains lessoning the net attraction between the adsorbate and domains when compared to isobutane adsorption. Additionally, acetone has a higher boiling point than isobutane (i.e., 56 °C and -12 °C, respectively) such that acetone molecules are more attracted to each to each other than isobutane, which likely reduces the attraction to the ACFC nanographitic domains. This reduced attraction for acetone compared to isobutane explains the reduction in the change in ACFC electrical resistance during acetone adsorption when compared to isobutane adsorption. The resistivity of the adsorbed molecules is not expected to affect ACFCs resistivity because the adsorbed molecules are gases, which have infinite resistivity unless ions are present. Adsorbate that liquefies within ACFC's micropores can also potentially affect ACFCs resistivity. However, the tested adsorbates are still electric insulators in the liquid state (i.e., as indicated by the resistivity values shown in Table 3) suggesting the Coulomb-gap variable range hopping model (Fung *et al*., 1994) is still valid after physical adsorption of the tested adsorbates.

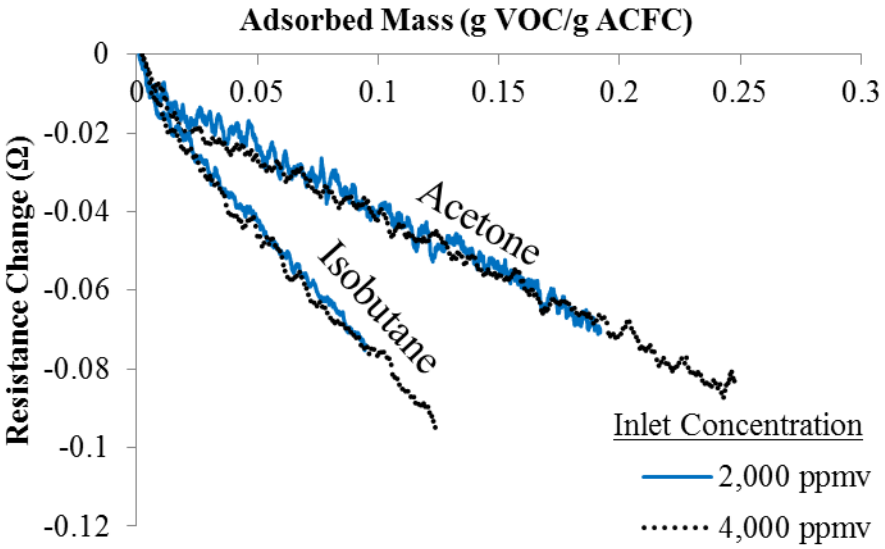

*Volatile organic compond (VOC)

Figure 29: Electrical resistance change during isobutane and acetone adsorption at select concentrations at 25 °C onto an activated carbon fiber cloth (ACFC) cartridge

Table 13: Linear regressions of the change in activated carbon fiber cloth (ACFC) cartridge resistance compared to adsorbed volatile organic compound (VOC) mass, determined from data presented in Figure 29 and Figure 30

VOC	Concentration (ppm_v)	C_1 (Ω)[a]	C_2 (Ω-g ACFC/g VOC)[a]	r^2 (-)[b]
Isobutane	2,000	-0.001	-0.713	0.99
Isobutane	4,000	-0.010	-0.685	0.99
Acetone	2,000	-0.007	-0.321	0.99
Acetone	4,000	-0.012	-0.303	0.99
Toluene	2,000	-0.005	-0.354	0.98
Toluene	4,000	-0.013	-0.300	0.96

[a]resistance change = $C_1 + C_2 \cdot$ (adsorbed VOC mass), [b]r is the linear correlation coefficient describing the dependence of ACFC's resistance on adsorbed VOC

Toluene was then adsorbed onto the ACFC cartridge. A comparison of the change in cartridge resistance during the adsorption of toluene and isobutane is provided in Figure 30 (i.e., linear regressions of data from Figure 30 are provided in Table 13). Results from the adsorption of acetone and toluene are provided in separate figures so the data are easier to interpret (i.e.,

Figure 29 and Figure 30, respectively) as the values for the resistance change per unit adsorbed mass of acetone and toluene overlap from 0-0.25 g/g (i.e., resistance change per unit mass adsorbed for toluene was within 5 % of that for acetone). The decrease in ACFCs electrical resistance from toluene adsorption is smaller than that of isobutane adsorption (g/g), which is attributed to the high boiling point toluene molecules (i.e., 111 °C compared to -12 °C of isobutane) being strongly attracted to each other, likely weakening the attraction between the toluene molecules and ACFCs nanographite domains. Toluene also has a larger molecular weight than acetone and isobutane (92.1 g/mol, 58.1 g/mol and 58.1 g/mol, respectively) resulting in toluene having a 20% lower surface diffusivity within the ACFC micropores than acetone or isobutane, which may also effect the change in resistance per adsorbed mass. However, there is not a clear trend between adsorbate molecular size or surface diffusivity and the change in ACFC resistance per unit mass adsorbed. It would be beneficial to perform future work with a wider range of adsorbates to determine if adsorbate molecular size and surface diffusivity effect the change in ACFC resistance per unit mass adsorbed.

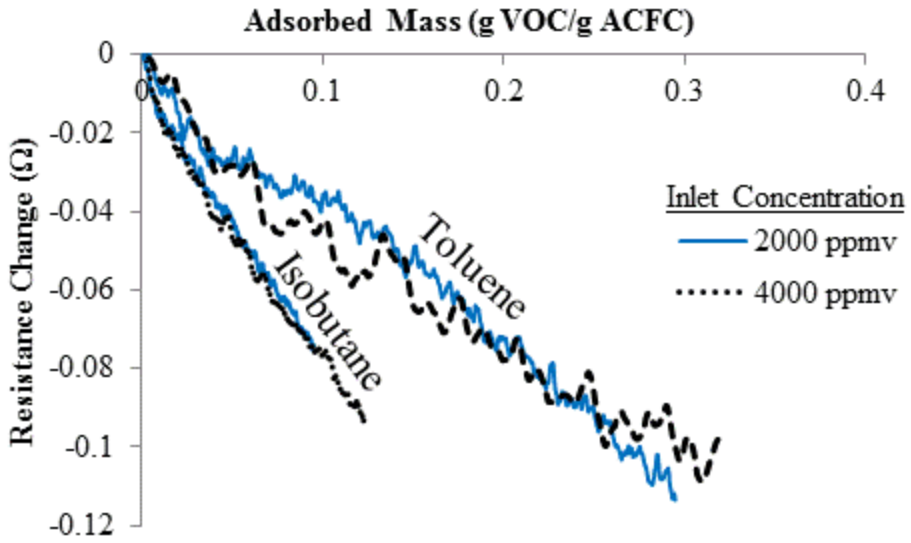

*Volatile organic compond (VOC)

Figure 30: Electrical resistance change during isobutane and toluene adsorption at select concentrations at 25 °C onto an activated carbon fiber cloth (ACFC) cartridge

It is possible that the change in ACFC resistance per adsorbed mass is effected by whether the adsorbed molecules form a monolayer on the surface of the adsorbent or micropore filling occurs. The surface area of the adsorbed isobutane, acetone, and toluene is larger than the surface area of the ACFC and the adsorbed volume at saturation is within 10% of the micropore volume indicating that micropore filling occurs (i.e., as previously discussed in section 5.3.1.1). For example, a monolayer of adsorbed isobutane would result in 0.01 g isobutane/g ACFC (i.e., assuming spherical molecules), while Figure 29 and Figure 30 demonstrate adsorption capacities > 0.1 g/g ACFC. It would be beneficial for future studies to analyze the change in ACFC resistance at lower adsorbate concentrations, in which the adsorption capacity is closer to that of monolayer coverage, to determine if the change in resistance per unit mass adsorbed can be used to detect whether surface coverage or micropore filling is occurring.

The ACFC cartridge was fully regenerated after isobutane and acetone adsorption cycles (Figure 29) using electrothermal heating to 150 °C for 1 h (i.e., adsorption capacity remained constant before and after regeneration). The ACFC cartridge was electrothermally heated to 200 °C for 1 h after toluene adsorption cycles (Figure 30), because toluene was not fully desorbed at 150 °C. Even after heating at 200 °C, the toluene adsorption capacity was 30% less than that of the first adsorption cycle indicating the cartridge was not fully regenerated. It is expected that increasing the regeneration heating temperature will fully regenerate the ACFC (i.e., a single layer of ACFC that experienced adsorption of 100 ppb_v toluene was fully regenerated through heating to 150 °C for 1 h in Yao *et al*., 2009) but regeneration heating temperatures above 200 °C were not tested due to safety concerns. The increased electrothermal heating temperature that is required for toluene desorption (i.e., compared to acetone and isobutane) is attributed to toluene being less volatile than acetone and isobutane (i.e., boiling points of toluene, acetone, and isobutane are 111 °C, 56 °C, and -12 °C, respectively).

5.3.1.4. *Effect of Initial ACFC Temperature on the Resistance of an ACFC Cartridge during Adsorption*

An ESA adsorption cycle typically starts before the ACFC temperature cools to ambient temperature (after regeneration heating) so tests were performed to describe adsorption cycles that start at elevated temperatures (i.e., simultaneous cooling/adsorption). Figure 31 and Figure 32 provide the electrical resistance, temperature, and downstream isobutane concentration for adsorption cycles that start when the ACFC temperature has cooled to 40 and 60 °C after

regeneration heating, respectively (i.e., with blank cycles that have the same conditions without isobutane for comparison).

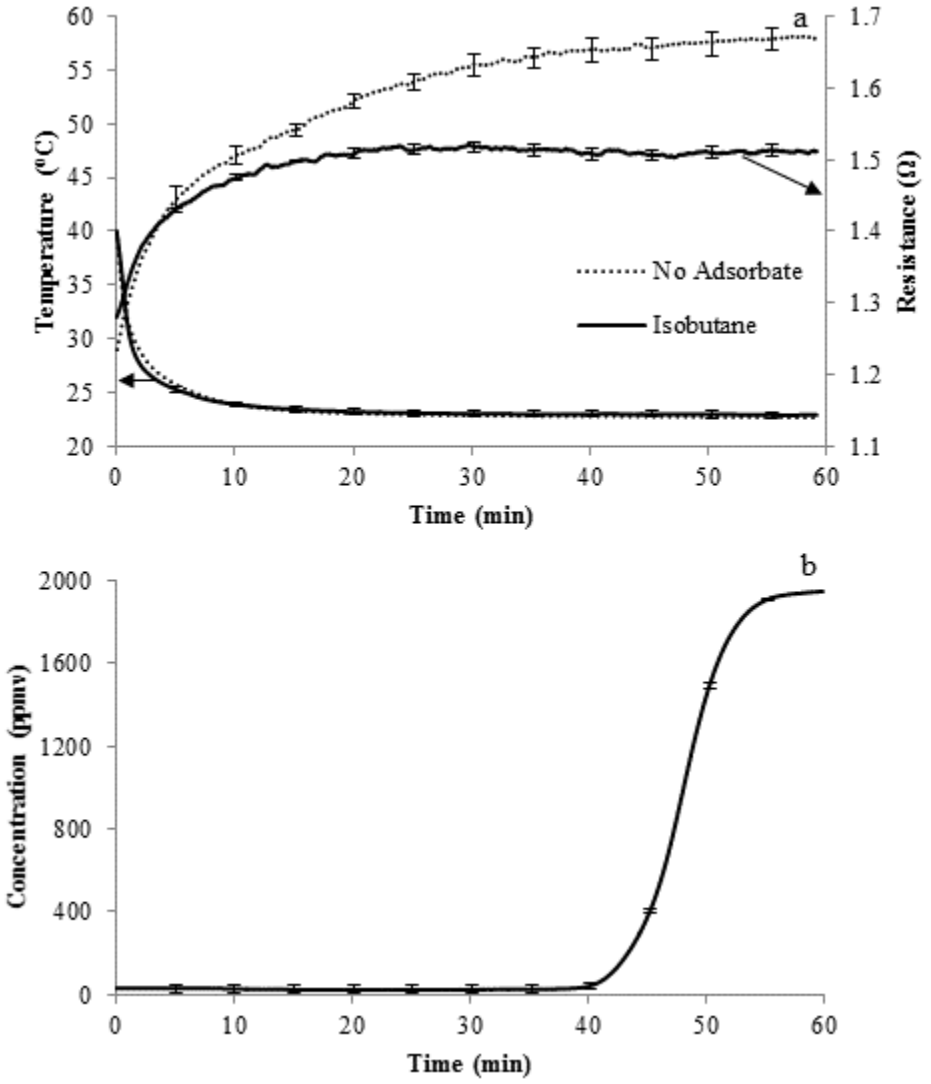

Figure 31: Electrical resistance (a) and temperature (a) and downstream isobutane concentration (b) during an adsorption cycle of 2,000 ppm_v isobutane that starts when the activated carbon fiber cloth (ACFC) cools to 40 °C (after regenerating the ACFC to 150 °C) with standard deviations represented by vertical error bars

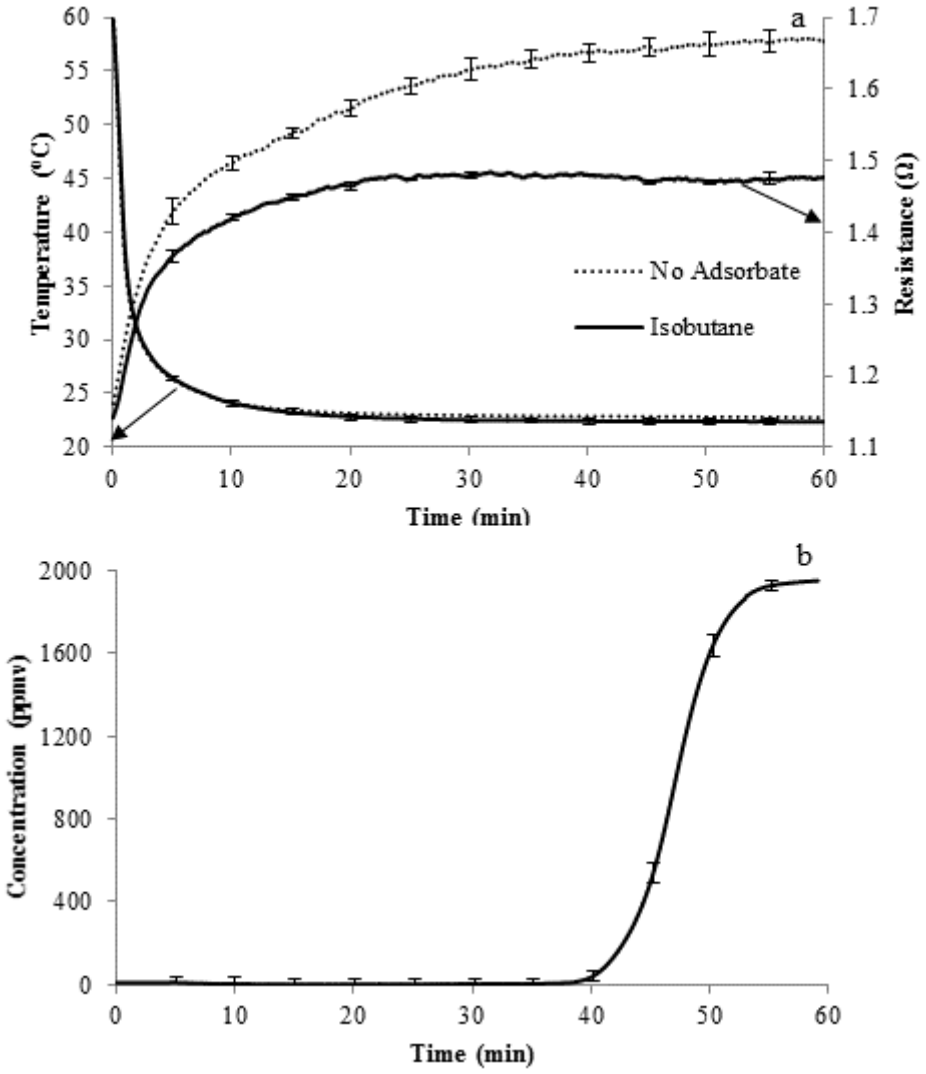

Figure 32: Electrical resistance (a) and temperature (a) and downstream isobutane concentration (b) during an adsorption cycle of 2,000 ppm_v isobutane that starts when the activated carbon fiber cloth (ACFC) cools to 60 °C (after regenerating the ACFC to 150 °C) with standard deviations represented by vertical error bars

The temperature profiles for the blank cooling cycles and simultaneous cooling/adsorption cycles were within one standard deviation suggesting the effects of ACFC temperature on the electrical resistance of the ACFC were the same for the blank cooling cycles and the simultaneous cooling/adsorption cycles. The electrical resistance profiles of the blank and adsorption cycles are indistinguishable until the ACFC cools to a temperature of 25 to 30 °C

demonstrating that ACFC electrical resistance is dominated by temperature during initial cooling. Figure 33 provides a magnified view of the electrical resistance of the adsorption cycle from Figure 32 to accentuate features in the resistance profile. Figure 33a shows the region where temperature dominates the change in resistance (resistance changes by > 0.3 Ω so it is not visible in Figure 33a). The decrease in electrical resistance from the adsorption of isobutane then competes with the increase in resistance from cooling in Figure 33b and c resulting in the ACFC resistance being smaller during the adsorption cycle than the blank cycle. In Figure 33b, the effect of cooling is larger than the effect of adsorption so the resistance increases with time. Then, as the temperature stabilizes to ambient temperature in Figure 33c, adsorption has a larger effect on resistance than temperature and the resistance decreases with time. Finally, the electrical resistance is constant with time in Figure 33d as isobutane adsorption ends and the ACFC temperature remains stable. These results demonstrate that controlling an ACFC simultaneous adsorption/cooling cycle requires careful consideration of the four regions shown in Figure 33. Also, the noise in resistance measurement can mask the signal (i.e., especially for regions b, c, and d) so careful data smoothing is required to control simultaneous cooling/adsorption based on resistance measurements.

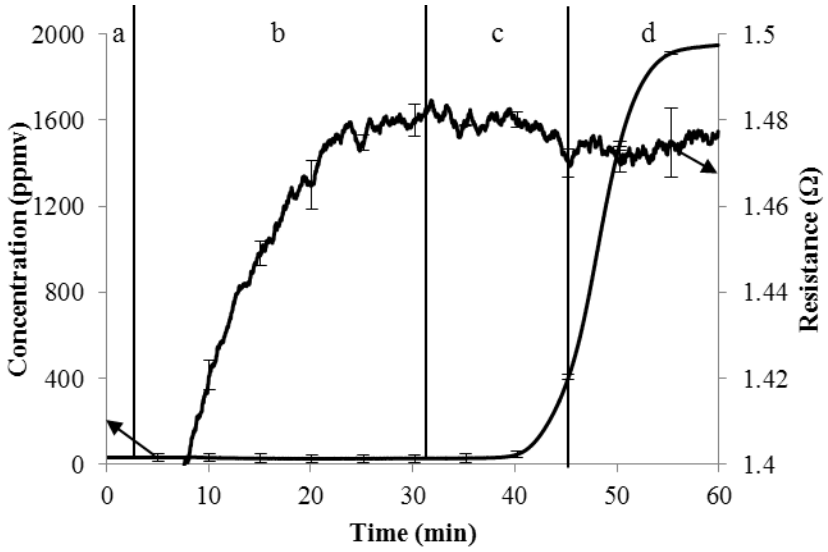

Figure 33: Electrical resistance and downstream isobutane concentration during an adsorption cycle of 2,000 ppm_v isobutane that starts when the activated carbon fiber cloth (ACFC) cools to 60 °C (after regenerating the ACFC to 150 °C) with a-d representing regions with different resistance behavior and standard deviations represented by vertical error bars

5.3.1.5. *Effect of Previously Adsorbed Mass on the Resistance of an ACFC Cartridge during Adsorption*

For ESA applications, ACFC is not completely regenerated resulting in the presence of remaining adsorbed material at the start of an adsorption cycle. This remaining adsorbed mass was modeled by inputting the measured applied power profile from the regeneration heating cycle into the ACFC desorption model described in section 5.2.2.2. The regeneration modeling results are discussed in detail in section 5.3.2.4, while the modeled adsorbed mass that remains after a regeneration cycle is discussed here. The remaining adsorbed mass was also experimentally determined based on the difference between the equilibrium and measured adsorption capacities (i.e., measured adsorption capacity values after previous adsorption/regeneration cycles) to compare the modeled values to experimental values. For a regeneration cycle that involves heating ACFC with an initially adsorbed 0.108 g isobutane/g

ACFC to 150 °C for 10 min, the predicted and measured remaining adsorption capacity for the next adsorption cycle are 0.102 and 0.086 ± 0.002 g isobutane /g ACFC (mean ± standard deviation), respectively. For a regeneration cycle that involves heating ACFC with an initially adsorbed 0.108 g isobutane/g to 110 °C for 0.5 min, the predicted and measured remaining adsorption capacity for the next adsorption cycle are 0.076 and 0.069 ± 0.002 g isobutane /g ACFC (mean ± standard deviation), respectively. The modeled values were reasonably close to the measured values (i.e., within 19 %) for these tested conditions demonstrating that this model can provide moderately accurate predictions of the remaining adsorption capacity after a regeneration cycle.

5.3.2. Characterization and Control of an ESA Regeneration Cycle

The electrical resistance of ACFC and power application were characterized during an ACFC regeneration cycle. First, ACFC's electrical properties were characterized during regeneration heating cycles with varying amounts of initially adsorbed mass. Then, three parameters were evaluated for determining when to end a regeneration heating cycle (i.e., temperature, applied power, and modeled energy). Finally, the relationship between ACFC temperature and electrical resistance was characterized during cooling after the completion of regeneration heating.

5.3.2.1. *Varying Initially Adsorbed Mass Before Regeneration*

ACFC with varying amounts of initially adsorbed isobutane was heated to a regeneration resistance value corresponding to 150 °C for ACFC with no adsorbate (i.e., resistance feedback controller described in chapter 4) and ACFC temperature and power were measured (Figure 34).

An initially adsorbed isobutane mass of 0, 0.11, and 0.13 g/g was provided by adjusting the inlet isobutane concentration during the preceding adsorption cycle (i.e., no adsorbate, 2,000 ppm_v and 4,000 ppm_v, respectively). The initially adsorbed isobutane altered the temperature and power profiles (i.e., when heating to a resistance set-point), but the difference between profiles for the tests with 0.11 and 0.13 g isobutane adsorbed/g were within one standard deviation and thus not distinguishable. The total energy required to heat the ACFC with 0, 0.11, and 0.13 g isobutane/g ACFC for 30 min was 145.5 ± 7.7, 158.9 ± 12.4, and 160.5 ± 13.3 kJ, respectively (mean ± standard deviation). The mean energy required to heat ACFC to a resistance set-point increased with adsorbed mass ($r^2 = 0.998$). However, the overlapping standard deviations in energy values between tests indicate that energy measurements cannot be used to identify adsorbed mass for a single regeneration cycle.

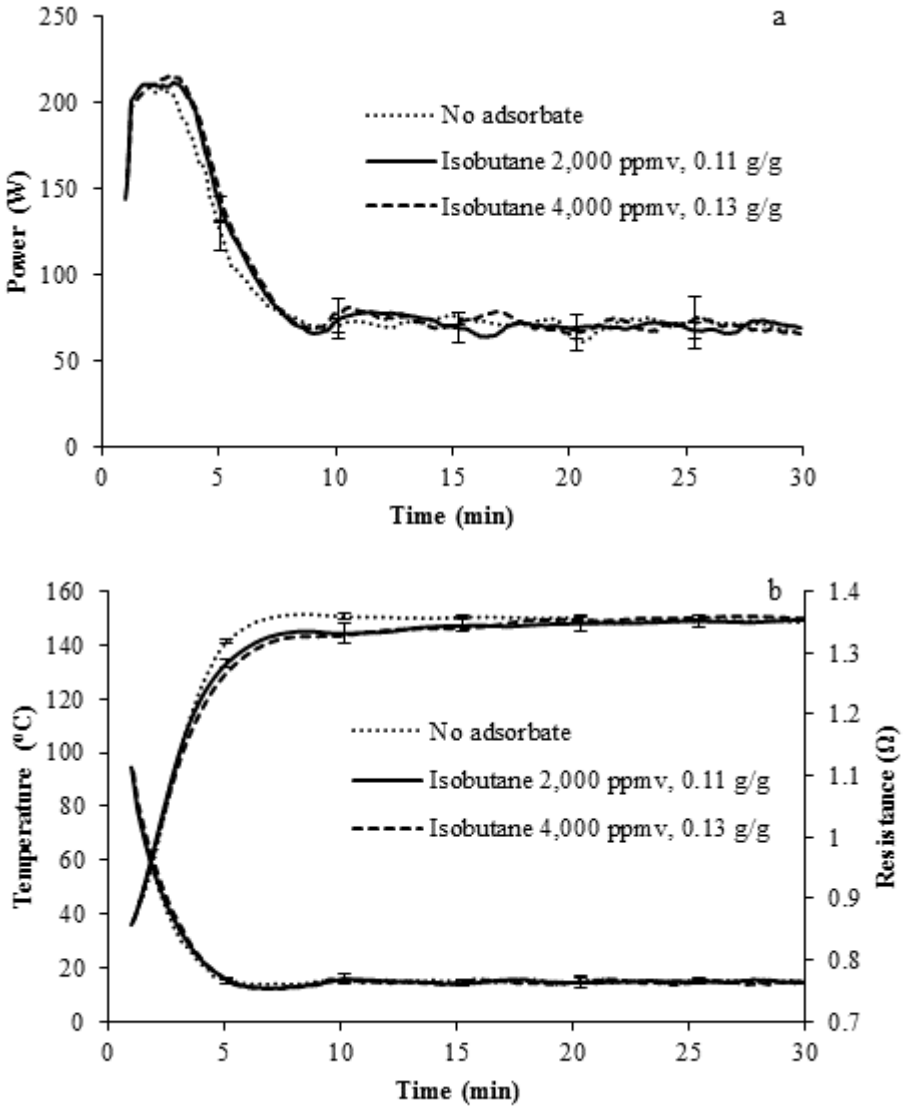

Figure 34: Power (a), temperature (b), and electrical resistance (b) for activated carbon fiber cloth heated to a resistance set-point corresponding to 150 °C based on resistance feedback with varying amounts of initially adsorbed isobutane

5.3.2.2. *Automatically End Regeneration Cycle Based on Temperature*

Power was applied to the ACFC to achieve a resistance set-point for regeneration heating (i.e., resistance feedback controller described in chapter 4) and the heating cycle was automatically ended once the ACFC temperature was within 2 % of the set-point temperature. ACFC was heated to a resistance set-point corresponding to a set-point temperature (i.e., 100 and

150 °C) with blank heating cycles for comparison (i.e., heating ACFC without adsorbed isobutane), as shown in Figure 35. The resistance profiles were similar when heating ACFC with and without initially adsorbed isobutane because the power application was controlled to achieve a resistance set-point, as described in more detail in chapter 4. When heating to within 2 % of 150 °C (Figure 35a), the mean heating time was 17.6 ± 0.2 min (mean ± standard deviation) showing consistency between heating cycles. After these heating cycles, the adsorption capacity for 2,000 ppm_v isobutane was 77.5 ± 0.2 % (i.e., mean ± standard deviation) of the initial ACFC adsorption capacity showing the cartridge was adequately regenerated for ESA applications. The ACFC was also heated to within 2 % of 100 °C (Figure 35b) to determine the robustness of this control method. The mean heating time was 193 ± 79 min, which is more than twice the time required to heat to within 2 % of 150 °C due to the lower heating temperature (i.e., mean ± standard deviation). After these heating cycles (i.e., to 100 °C) , the adsorption capacity for 2,000 ppm_v isobutane was 80.1 ± 6 % (i.e., mean ± standard deviation) of the initial ACFC adsorption capacity, which is consistent with the 77.5 % when heating to 150 °C. The higher variation in results when heating to 100 °C is attributed to the more gradual desorption of isobutane at the lower temperature, which creates larger time periods for noise in the electrical resistance signal to reach a value that surpasses the temperature set-point.

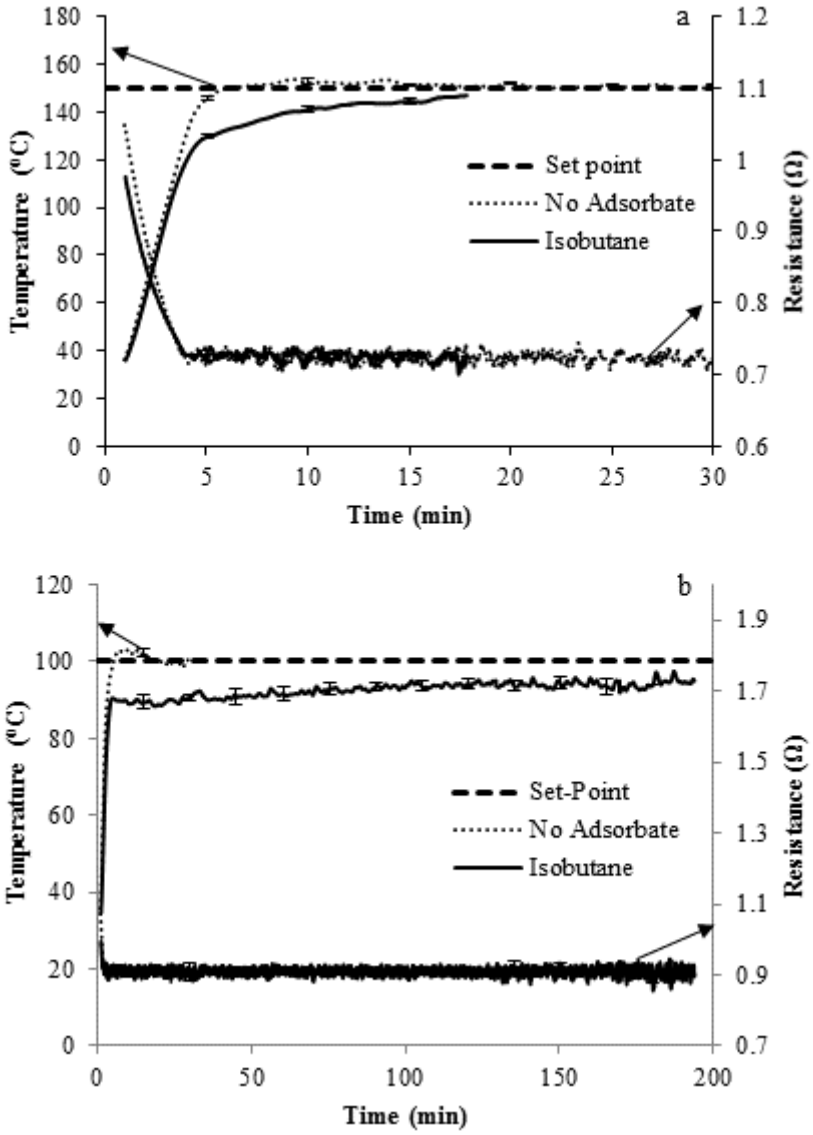

Figure 35: Temperature and electrical resistance for activated carbon fiber cloth (ACFC) heated to a resistance set-point corresponding to 150 °C (a) and 100 °C (b) based on resistance feedback that was automatically terminated when the ACFC temperature was within 2 % of the set-point temperature

The similarity in ACFC regeneration (80.1 and 77.5 % regenerated when heating to 100 and 150 °C, respectively) shows promise for using this control method, especially when considering that achieving these temperatures resulted in drastically different heating times (i.e., 193 and 17.6 min for 100 and 150 °C, respectively). One trade-off for this method is that it requires careful consideration of electrical resistance signal noise to improve consistency of

regeneration cycle duration for low regeneration temperatures (e.g., 100 °C for isobutane). It should also be noted that while this control method eliminates the need for hydrocarbon sensors, it is only applicable for ESA systems that have a direct-contact thermocouple for temperature measurement.

5.3.2.3. *Automatically End Regeneration Cycle Based on Power*

Power was applied to the ACFC to achieve a resistance set-point (resistance feedback controller described in chapter 4) and the heating cycle was automatically ended once the power applied to the ACFC (5 min mean) decreased to a specified power set-point (Figure 36 and Figure 37**)**. This power set-point was determined by modeling the steady-state power required to maintain the ACFC (without adsorbate) at the set-point temperature. From Figure 36 and Figure 37, the power required to initially heat the ACFC to the set-point temperature is larger when isobutane is present, which is attributed to the additional energy required to heat and desorb isobutane. The heating times for heating ACFC to 150 and 100 °C with this control method were 11.8 ± 1.0 min and 7.2 ± 0.1 min, respectively (i.e., mean ± standard deviation). This heating time provided adequate regeneration (71.3 ± 0.1 % regenerated, provided as mean ± standard deviation) for the 150 °C set-point. However, for the 100 °C set-point, the following adsorption cycles resulted in instantaneous adsorbate breakthrough.

This control method (i.e., heating to a resistance set-point until reaching a power set-point representing the steady-state power to heat ACFC without isobutane) is not effective for determining when to end regeneration heating cycles with the existing controller. Based on modeled values, only 20 % of the total energy used for ACFC regeneration heating to 150 °C (i.e., total energy includes energy to heat ACFC, system components, adsorbate, and carrier gas,

energy for desorbing the adsorbate and energy for conductive, convective, and radiative heat transfer) is used to heat/desorb the isobutane, as described in Figure 37. However, the applied power is automatically rapidly adjusted to maintain the resistance set-point resulting in mean steady-state standard deviations of power values of 14 % and 23 % for ACFC with and without isobutane, respectively. An alternative regeneration heating control method that uses power feedback measurements to achieve a power set-point (i.e., instead of a resistance feedback) reduces noise in the power values and is presented in the next section.

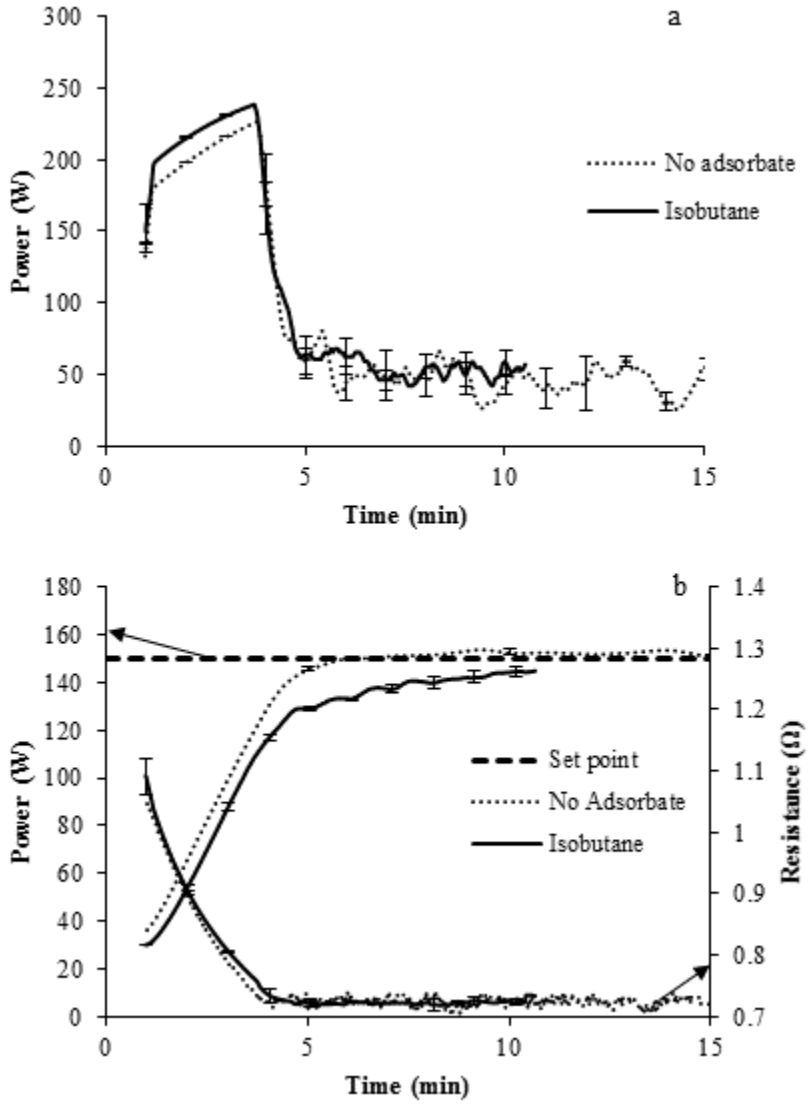

Figure 36: Power (a), temperature (b), and electrical resistance (b) for activated carbon fiber cloth heated to a resistance set-point corresponding to 150 °C based on resistance feedback that automatically terminates when power is < 70 W (i.e., 0.61 W/g ACFC)

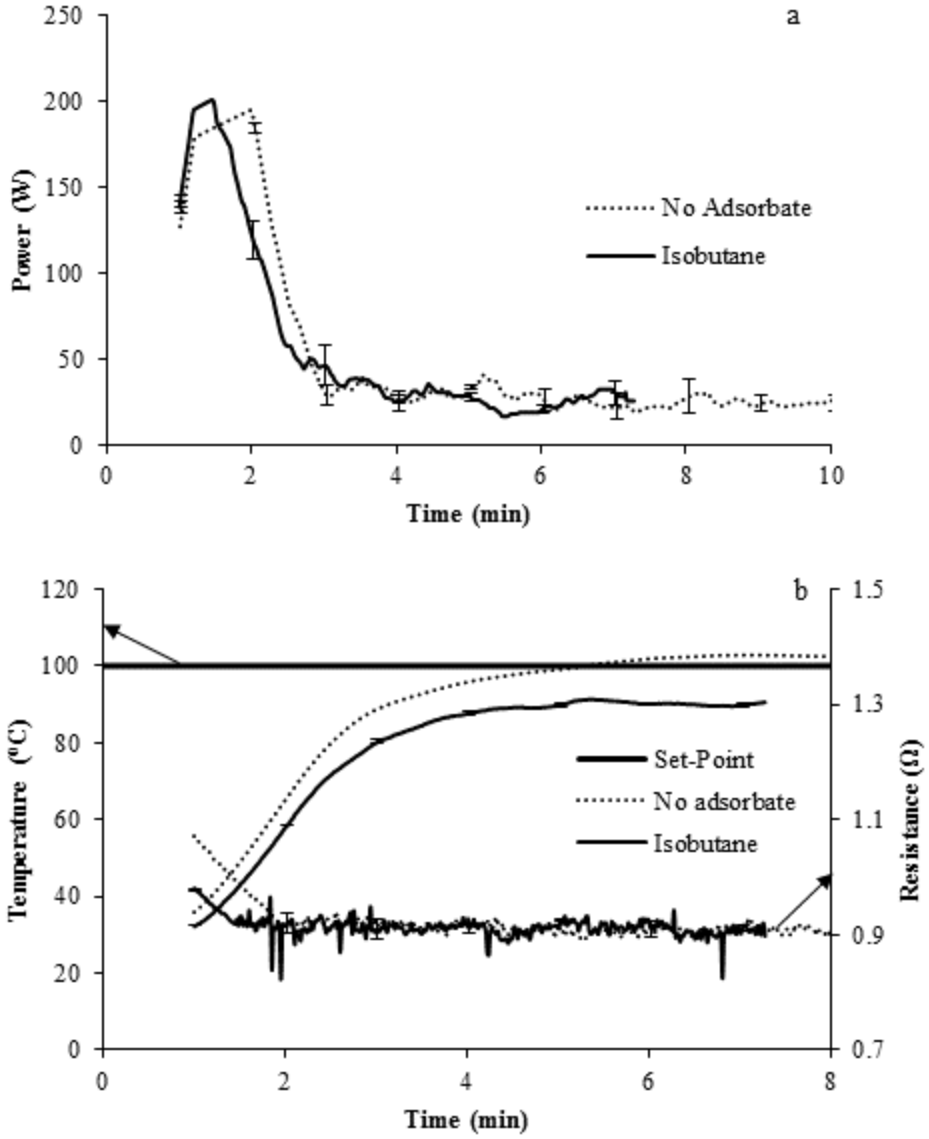

Figure 37: Power (a), temperature (b), and electrical resistance (b) for activated carbon fiber cloth heated to a resistance set-point corresponding to 100 °C based on resistance feedback that automatically terminates when power is < 42 W (i.e., 0.37 W/g ACFC)

5.3.2.4. *Automatically End Regeneration Cycle Based on Energy*

A method is presented to determine the power profile to apply to ACFC that is determined based on modeled values from mass and energy balances. First, a desired regeneration temperature profile is determined. A heating rate of 40 °C/min was selected to heat the ACFC to the set-point temperature until the ACFC reached a maximum temperature of 150 °C for comparison with previous regeneration tests. The desorption of isobutane was modeled based on the desired temperature profile (i.e., model described in 5.2.2.2) and is presented in Figure 38. A total regeneration heating cycle time of 10 min was selected as adequate for ACFC regeneration because, based on modeled values, 95 % of the isobutane is desorbed in 10 min (Figure 38).

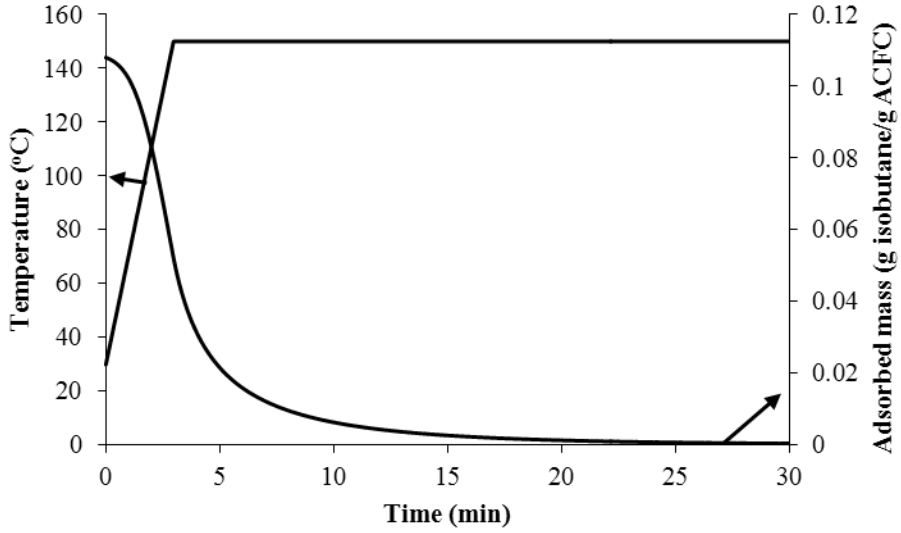

Figure 38: Selected temperature profile for regeneration of activated carbon fiber cloth (ACFC) with 0.11 g isobutane initially adsorbed/g ACFC and modeled mass of isobutane that remains on the ACFC when heating to the selected temperature profile

The energy and mass balance model was then used to determine the applied power profile that is required to achieve the temperature profile from Figure 39 (i.e., heat to 150 °C at 40 °C/min and maintain the temperature at 150 °C for a total heating time of 10 min). The modeled applied power reached a maximum of 300 W during the initial 3 min of heating and was 70 W to maintain the ACFC at 150 °C after the isobutane is completely desorbed. The ACFC was heated using this modeled power profile as a set-point and the actual power profile and temperature profile were measured, as shown in Figure 39. The AAE between the set-point and measured temperature profiles was 2.0 %, providing closure between the modeled and controlled/measured values.

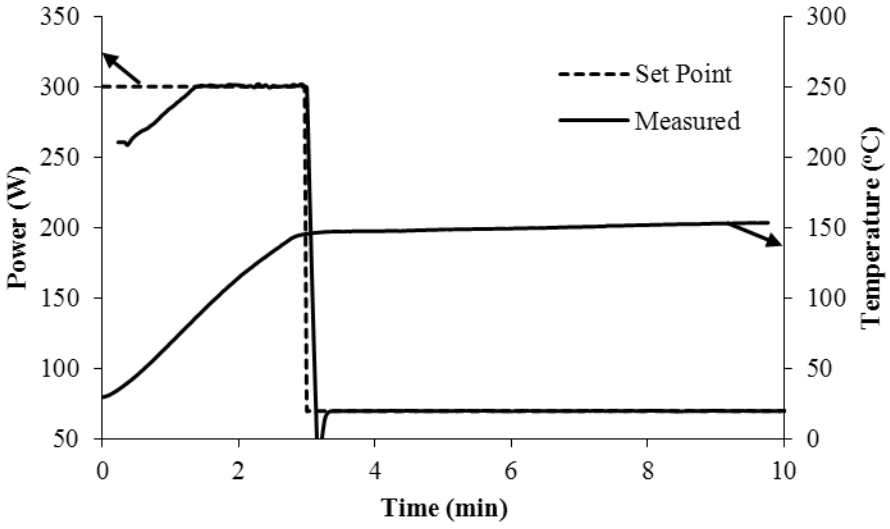

Figure 39: Measured power and temperature when heating activated carbon fiber cloth with isobutane to a modeled power set-point profile

The temporal variation of modeled energy for the temperature profile from Figure 39 is provided in Figure 40. Sixteen percent of the total energy used for heating was used to desorb the isobutane. During the initial heating phase, 61 % of the energy is attributed to the heat capacity of the adsorbent, adsorbate, and fittings. Then, after reaching the set-point temperature

of 150 °C, 66 % of the total energy is lost to radiation (41 %) and convection (23 %) suggesting using a reflective material for the vessel can substantially reduce the energy requirements for maintaining the ACFC at a constant temperature.

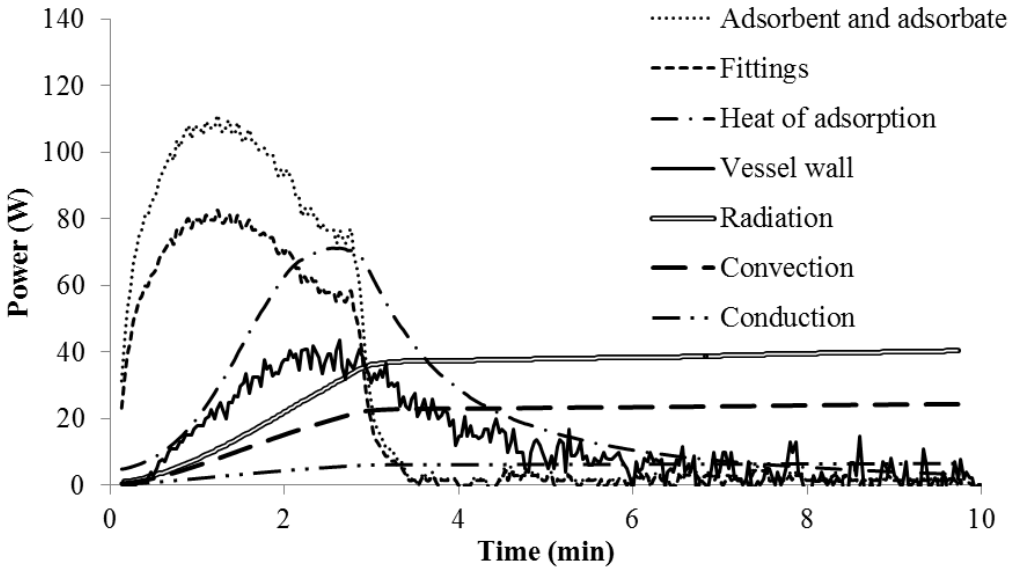

Figure 40: Temporal variation of modeled energy to heat activated carbon fiber cloth with adsorbed isobutane to the temperature profile presented in Figure 39

The energy requirements to achieve 95% regeneration of ACFC (i.e., 0.11 g isobutane with initially adsorbed/g ACFC) were considered for a range of regeneration heating temperatures. Regenerating (i.e., 95% regeneration) the ACFC with lower temperatures tends to require more time and energy (e.g., heating to 100 °C requires 60 min and consumes 161 kJ compared to heating to 150 °C, which requires 10 min and consumes 86.3 kJ). Increasing the regeneration heating temperature reduces the heating time and energy consumption until a heating temperature of 200 °C (i.e., 5 min and 77.2 kJ). Heating to a regeneration temperature that is higher than 200 °C increases the total energy requirements to achieve 95% regeneration. Thus, heating to 200 °C for 5 min is considered the optimal heating profile to achieve 95% regeneration for these conditions.

5.3.2.5. *Characterize Cooling after Electrothermal Heating*

The mean temperature and resistance profiles during the cooling portion of the regeneration cycle that occurred after heating ACFC with and without isobutane (i.e., 0.11 g/g initial condition) to 160 °C for 30 min are provided in Figure 41. The measured temperature and resistance values were within one standard deviation of each other for tests with and without initially adsorbed isobutane (error bars in Figure 41A), suggesting the remaining isobutane does not need to be considered for the tested conditions. Figure 41 is also representative of the cooling cycles that followed regeneration heating of ACFC that had adsorbed isobutane, acetone, and toluene at inlet concentrations of 2,000 and 4,000 ppm_v in air suggesting that remaining adsorbed mass does not need to be considered for characterizing the resistance of ACFC during cooling.

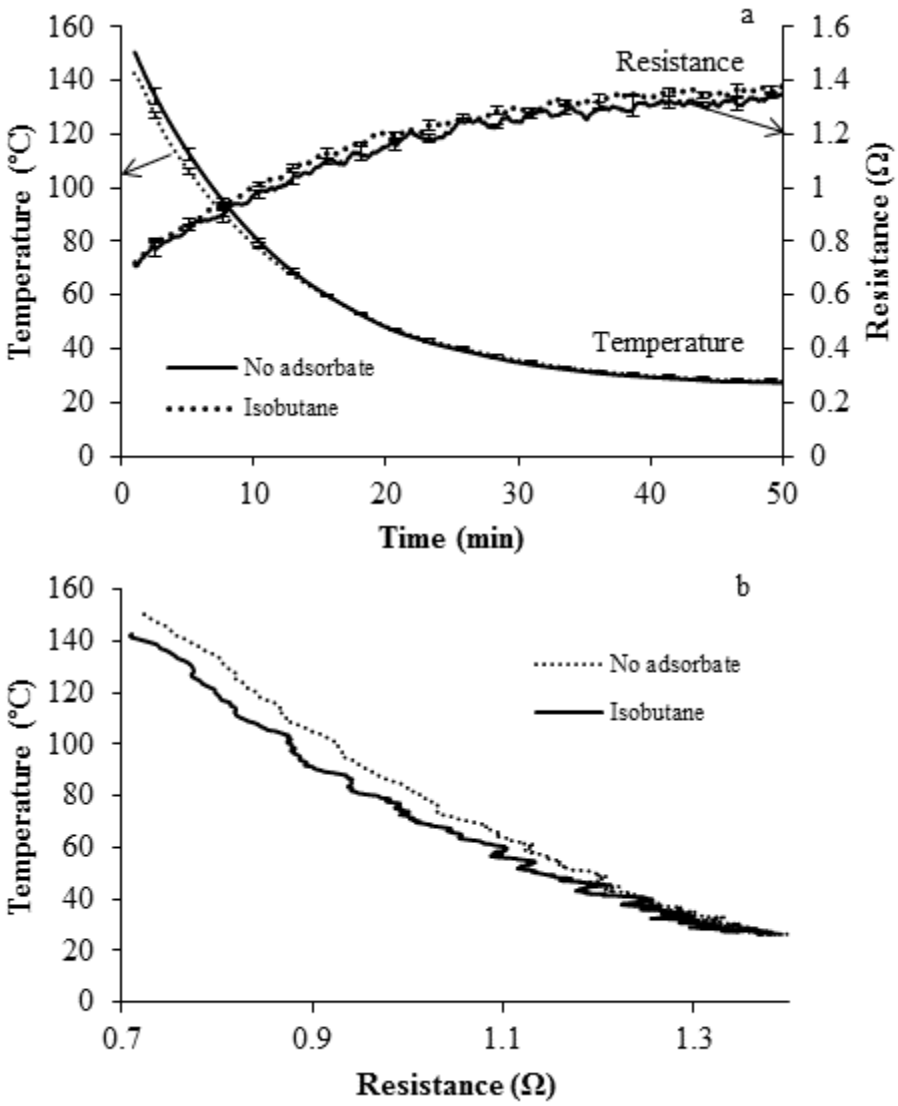

Figure 41: Temperature (a) and electrical resistance (a) and temperature versus electrical resistance (b) for activated carbon fiber cloth cooling from 160 °C to ambient temperature (20 °C)

5.3.3. Demonstration of Cyclic ESA of Isobutane Based on Resistance Measurements

Experimental results demonstrating control of an ESA system based entirely on resistance and power measurements are presented. First, ESA was operated based on electrical measurements to capture 2,000 ppm_v isobutane, where an adsorption cycle starts when the ACFC is at ambient temperature (i.e., proof of concept of ESA controlled based on electrical

measurements). Then, the ESA system was operated with alternative inlet concentrations and initial adsorption temperatures to demonstrate robustness of this control method.

5.3.3.1. *Cyclic ESA of 2,000 ppm_v Isobutane at Ambient Temperature*

Automated ESA of 2,000 ppm_v isobutane at ambient temperature was first performed using a 10 min regeneration heating cycles at 150 °C (Figure 42), based on modeled applied power values from section 5.3.2.4. ESA was successfully accomplished with 96.8 % capture efficiency in this automated mode. The duration (i.e., mean ± standard deviation) of the adsorption cycle was 33.9 ±7.7 min and the regeneration cycle was 79.2 ± 3.6 min (i.e., heating plus cooling time) suggesting that continuous capture of isobutane with this method would require additional ACFC. As shown in Figure 42b, there was early breakthrough of isobutane during each of the adsorption cycles (after the initial cycle), which is attributed to the ACFC cartridge not being fully regenerated from the 10 min heating cycle. Thus, increasing the duration of the regeneration heating cycle is expected to improve the overall system capture efficiency.

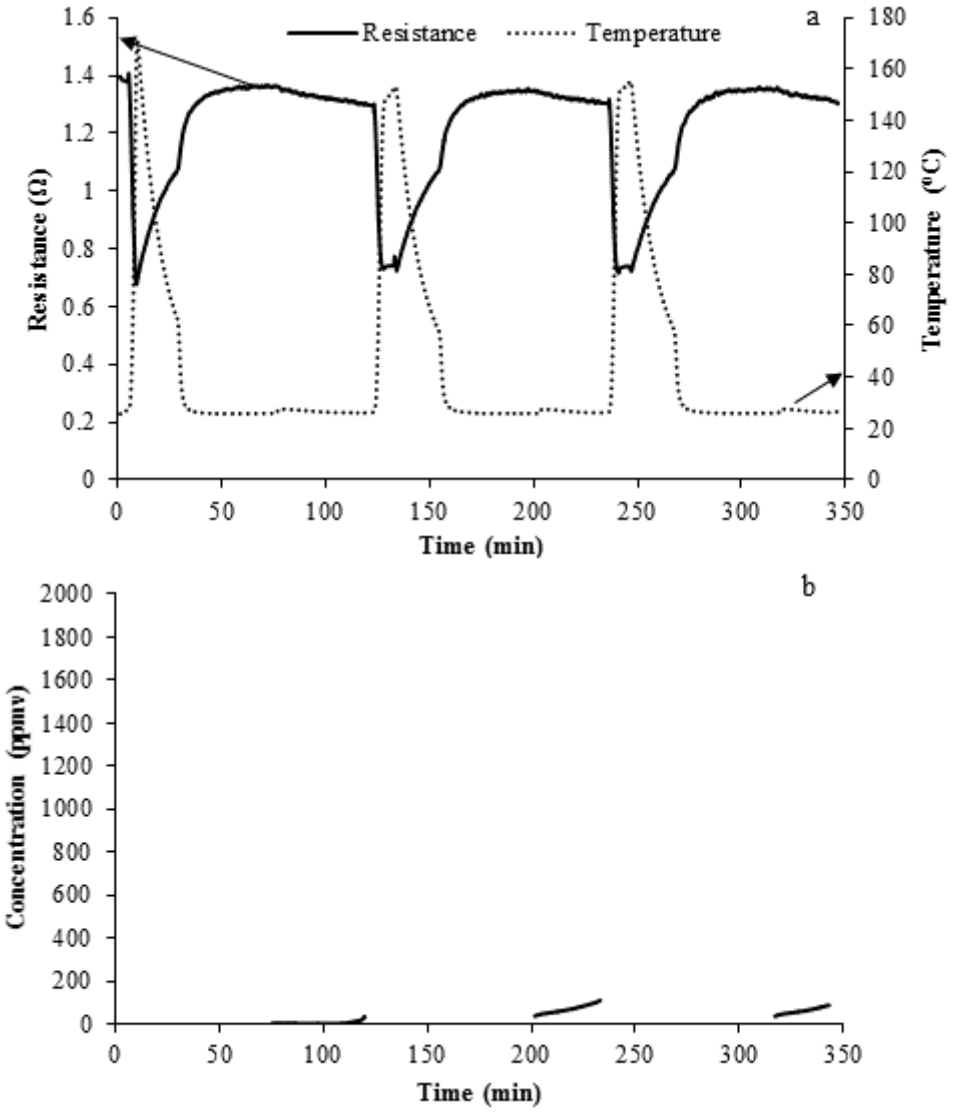

Figure 42: Temperature (a), electrical resistance (a), and outlet isobutane concentration downstream of the adsorption vessel (b) for activated carbon fiber cloth (ACFC) during automated electrothermal swing adsorption of 2,000 ppm_v isobutane at ambient temperature with 10 min heating cycles based on electrical measurements

Automated ESA of 2,000 ppm_v isobutane at ambient temperature was then performed with 30 min regeneration heating cycles at 150 °C to improve the overall system capture efficiency (Figure 43). The increased regeneration heating time eliminated the early breakthrough observed in Figure 42, improving the isobutane capture efficiency to 99.6 %. This capture efficiency is an improvement over the 98% capture efficiency achieved while operating

the system with hydrocarbon and direct contact temperature sensors because adsorption cycles ended before adsorbate breakthrough occurred (Mallouk *et al*., 2010). However, the modeled energy requirements for heating to 150 °C for 30 min (i.e., conditions in this study) are larger than heating to 225 °C for 10 min as performed by Mallouk *et al*., 2010 (i.e., 166.3 and 127.7 kJ, respectively). The total time (i.e., mean ± standard deviation) for the adsorption cycle (32.0 ± 6.4 min) was unaffected by the added heating time while the time for the regeneration cycle (102.6 ± 10.0 min) increased compared to that from Figure 42. The 22.9 min increase in the total time for regeneration when using a 30 min heating time compared to the 10 min heating time corresponds well with the 20 min increase in heating time.

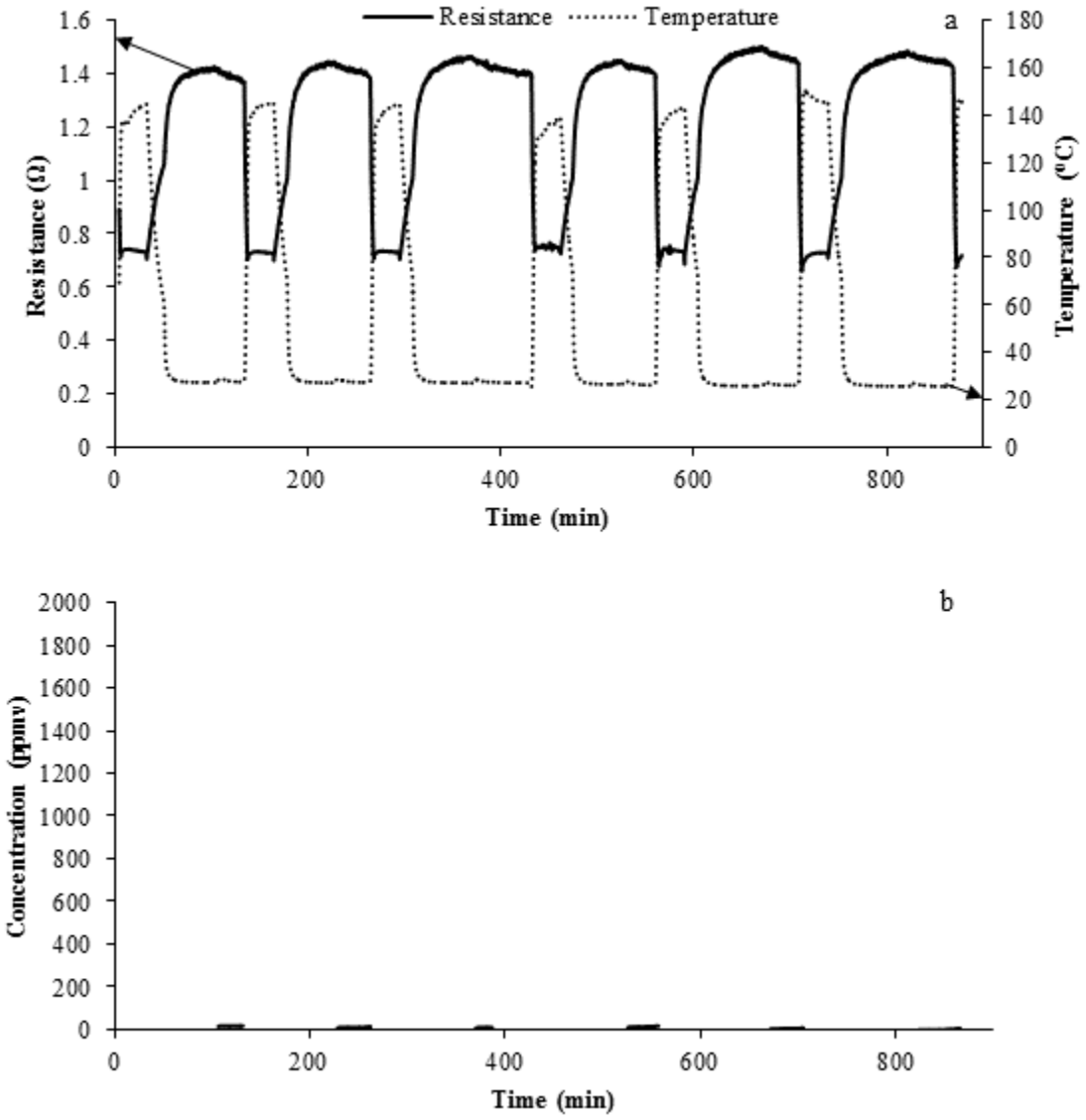

Figure 43: Temperature (a), electrical resistance (a), and outlet isobutane concentration downstream of the adsorption vessel (b) for activated carbon fiber cloth during automated electrothermal swing adsorption of 2,000 ppm_v isobutane at ambient temperature with 30 min heating cycles based on electrical measurements

5.3.3.2. *Cyclic ESA of 4,000 ppm_v Isobutane at Ambient Temperature*

Automated ESA of 4,000 ppm_v isobutane at ambient temperature was performed with 30 min regeneration heating cycles at 150 °C to test robustness of the proposed control method with an alternative isobutane inlet concentration (Figure 44). The automated ESA system achieved a

99.7 % capture efficiency of isobutane (i.e., inlet concentration of 4,000 ppm_v). The system operation was consistent when controlling ESA with a higher isobutane inlet concentration (4,000 ppm_v compared to 2,000 ppm_v) based on electrical measurements, while the adsorption cycle was shorter due to the increased mass flow rate of isobutane. The duration (i.e., mean ± standard deviation) of the adsorption and regeneration cycles were 17.9 ± 4.8 min and 97.7 ± 21.0 min, respectively.

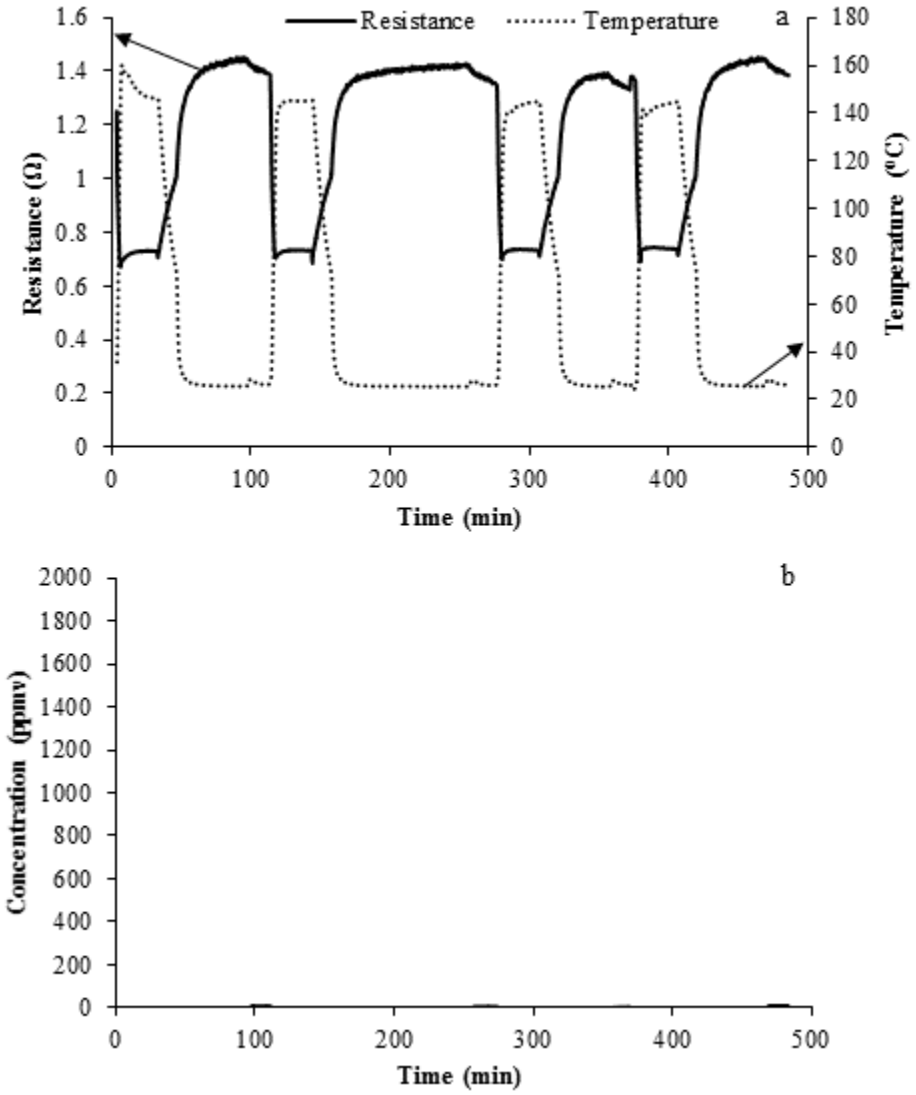

Figure 44: Temperature (a), electrical resistance (a), and outlet isobutane concentration downstream of the adsorption vessel (b) for activated carbon fiber cloth during automated electrothermal swing adsorption of 4,000 ppm_v isobutane at ambient temperature with 30 min heating cycles based on electrical measurements

5.3.3.3. *Cyclic ESA of 2,000 ppm_v Isobutane with Elevated Initial Temperature for an Adsorption Cycle*

Automated ESA of 2,000 ppm_v isobutane was performed, in which a simultaneous adsorption/cooling cycle started when the ACFC resistance reached a resistance set-point

corresponding to 60 °C after a 30 min regeneration heating cycle at 150 °C (Figure 45). The major benefit to this method of operation is that it reduces the duration of the cooling portion of a regeneration cycle such that the adsorption cycle is longer than the regeneration cycle (i.e., 58.5 ± 2.1 min and 48.1 ± 1.1 min, respectively, provided as mean ± standard deviation) allowing for a dual vessel system to continuously capture isobutane. However, the isobutane capture efficiency for this method of operation (98.4 %) was slightly reduced when compared to that of the adsorption cycles starting at ambient temperature (99.5 %). This decrease in capture efficiency is attributed to isobutane breakthrough at the beginning and end of the adsorption cycles (Figure 45b). The beginning of the adsorption cycle has isobutane breakthrough because ACFC has reduced adsorption capacity at elevated temperatures (60 °C). The end of the adsorption cycle has isobutane breakthrough because the cycle was automatically ended once the time derivative of electrical resistance reached zero (after decreasing during adsorption) indicating that the adsorbent was nearly saturated and adsorbate breakthrough occurred. By contrast, an adsorption cycle that begins at ambient temperature (i.e., described in sections 5.3.3.1 and 5.3.3.2) is ended when the electrical resistance decreases to a set-point value, which can be selected to occur before breakthrough occurs. This method to end adsorption based on reaching a resistance value is not an option for an adsorption cycle that begins at an elevated temperature because the ACFC resistance is dynamic for this cycle (i.e., increases from cooling, then decreases from adsorption, and then stabilizes once adsorption is complete, as described in 5.3.1.4). Thus, an adsorption cycle that starts at elevated temperatures can be controlled based on electrical resistance measurements but this method does not allow for ending adsorption before breakthrough occurs.

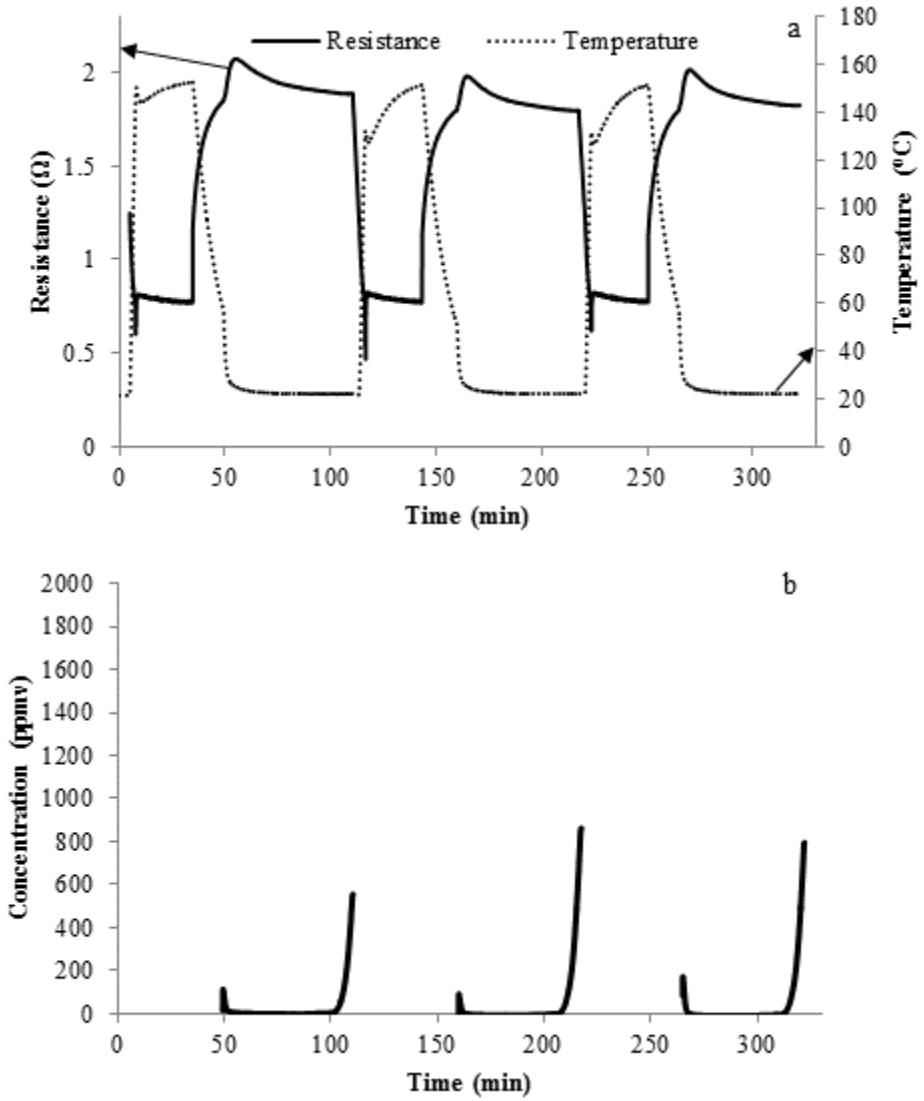

Figure 45: Temperature (a), electrical resistance (a), and outlet isobutane concentration downstream of the adsorption vessel (b) for activated carbon fiber cloth during automated electrothermal swing adsorption of 2,000 ppm_v isobutane at 60 °C with 30 min heating cycles based on electrical measurements

Chapter 6: Environmental and Economic Sustainability of ACFC-ESA Compared to Alternative Volatile Organic Compound Abatement Systems

6.1. Abstract

This chapter presents an LCA and cost assessment that compares the environmental and economic impacts, respectively, of using select abatement systems for treating gaseous emissions from the production of packaging materials. The impacts from using an RTO are compared to those of using GAC and ACFC systems. The life cycle inventory reveals that although the operational electricity requirements for the ACFC system are > 2.5 times larger than those of the other systems, the total operational energy (i.e., inclusion of electricity, steam, and natural gas) consumption for the ACFC system is less than the other systems (i.e., 19.2, 8.7, and 3.4 TJ/yr for the RTO, GAC system, and ACFC system, respectively). Select fuels (i.e., fuel mixes for the five states with the largest isobutane emissions from packaging manufacturing and natural gas) for electricity production were considered and using natural gas for electricity production provided the lowest impacts for all abatement systems. When using natural gas for electricity production, the GAC and ACFC systems performed similarly for 7 of 9 environmental impact categories (i.e., within one standard deviation of each other) and had lower impacts than the RTO for every category. The net present value (NPV) of the GAC and ACFC systems were positive compared to the $4.1M net cost to operate the RTO for 20 yr. A Monte Carlo uncertainty analysis and a sensitivity analysis were performed to identify areas to improve model and system design. The environmental impacts of the RTO and GAC system were primarily affected by the isobutane emission rate (i.e., from the manufacturing production exhaust to the abatement system) and steam consumption, respectively. The environmental impacts of the ACFC system were primarily affected by the production of electricity and N_2 used for thermal regeneration

cycles. Overall, the adsorption systems were more environmentally and economically competitive than the RTO due to recovered isobutane for the process and are thus recommended for treating the exhaust gas stream from this packaging manufacturing application.

6.2. Methods

6.2.1. Pollution Abatement Description

This chapter focuses on the abatement of gaseous emissions from packaging material manufacturing. A simplified diagram is presented to describe the input and output materials for packaging material manufacturing and air pollution abatement of the resulting exhaust gas (Figure 46). The key inputs for the manufacturing process are a polymer and an inert liquid blowing agent (e.g., isobutane). The liquid blowing agent is injected into the liquid polymer and volatilizes creating gaseous voids in the solidifying polymer resulting in a low density packaging material (e.g., sheet foam). Typically, > 50 % of the blowing agent is emitted during manufacturing and the remainder is released as fugitive emissions during warehousing, transportation, and after the product is sold (USEPA, 1990). The gaseous blowing agent that is released during manufacturing disperses into the surrounding air creating an exhaust gas stream that is treated with an abatement system. This study considers the operating conditions from a packaging manufacturing facility with gaseous emissions of isobutane. This study also provides a comparison of the environmental and economic impacts of using a commercially available RTO (i.e., destructive isobutane abatement) to a commercially available GAC system (i.e., provides recovered liquid isobutane) and the ACFC-ESA system in this research (i.e., provides recovered liquid isobutane) to determine the most desirable isobutane abatement option.

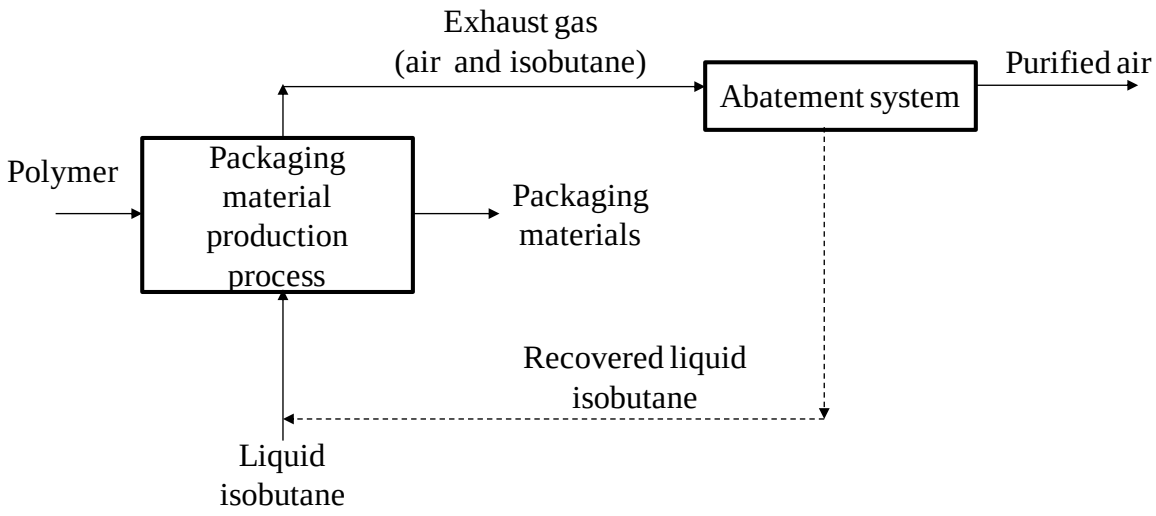

Figure 46: Packaging material production process and exhaust gas abatement with relevant input and output materials (dashed lines applicable for abatement systems with liquid isobutane recovery)

6.2.1.1. *Thermal Oxidation*

A RTO (Combuchanger Model 1-15.0AS3+, ABB Air Preheater, Inc.) is considered the benchmark for treating the gaseous isobutane emissions from packaging material manufacturing for this study because it is a typical and commercially available abatement system for treating isobutane emissions (Figure 47). The primary system components include a blower to move the packaging manufacturing exhaust gas stream, natural gas burners for start-up, an oxidizer bed filled with gravel, and a heat exchanger. During start-up, the natural gas burners are activated for up to 6 h to raise the incinerator bed temperature to 900 °C. The burners are then deactivated and the blower is used to direct the isobutane-laden air stream through the heat exchanger and into the incinerator bed in the "up flow" direction indicated in Figure 47. Natural gas is continually injected into the gas stream to ensure isobutane oxidation occurs. Oxidation of the gas stream occurs near the inlet of the oxidizer bed causing the temperature of the bed to increase with a preferential increase at the bottom of the bed near the inlet. Once the temperature of the

bottom half of the oxidizer bed reaches 1100 °C, the direction of the gas flow is changed to the "down flow" configuration, which increases the temperature at the top half of the bed and allows the bottom half of the bed to cool. The gas stream is then oxidized in the "down flow" configuration until the top half of the oxidizer bed reaches 1100 °C. This switching of the gas stream direction allows oxidation to continuously occur at 900 °C to 1100 °C, which is a desirable temperature range that results in 95 % thermal efficiency for oxidation and > 98% combustion of isobutane.

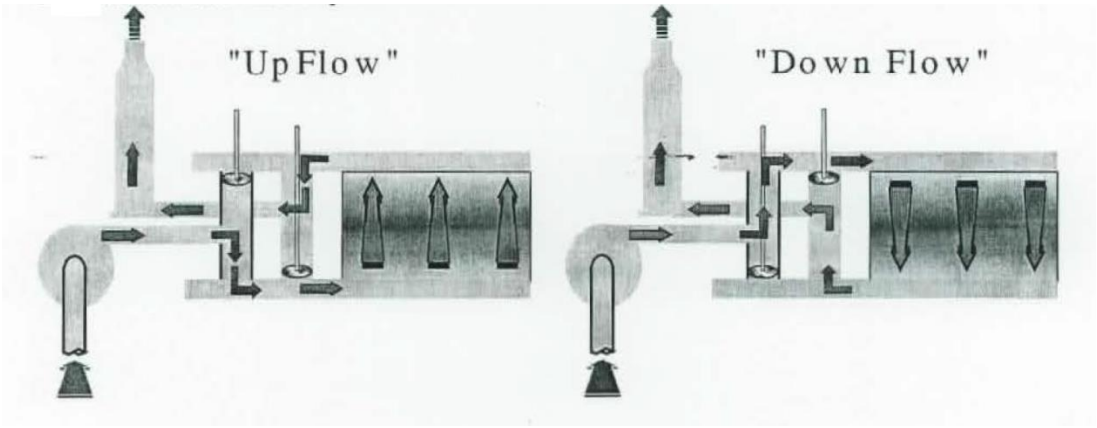

Figure 47: Schematic of a regenerative thermal oxidizer for treating packaging manufacturing emissions with arrows indicating gas stream flow direction (figure reproduced from ABB Air Preheater Inc., 2000)

6.2.1.2. *GAC Adsorption*

A steam regenerated GAC system was designed to achieve 98 % isobutane capture and recovery efficiency of packaging manufacturing emissions (Figure 48). The system was designed based on the USEPA control cost manual (USEPA, 2002). The primary system components include a blower to move the packaging manufacturing exhaust gas stream, two adsorption vessels filled with GAC, a steam generator, a condenser, and a compressor. The blower directs the exhaust gas stream from the production process to one of the adsorption beds

where the isobutane is adsorbed onto GAC providing purified exhaust air. The second adsorption vessel is regenerated using steam (i.e., thermal regeneration) and the steam/isobutane gas flow is passed through a condenser (i.e., heat exchanger with cooling water) that liquefies/separates the water vapor from the isobutane gas. The resulting isobutane gas stream is then compressed to provide liquid isobutane for the packaging material manufacturing process. After regeneration heating with steam, air is passed through the regenerated adsorption vessel for GAC drying/cooling. The adsorption vessels alternate between adsorption and regeneration cycles so that one vessel is always available to adsorb isobutane from the gas stream (i.e., adsorption cycle) while the other vessel experiences a regeneration cycle.

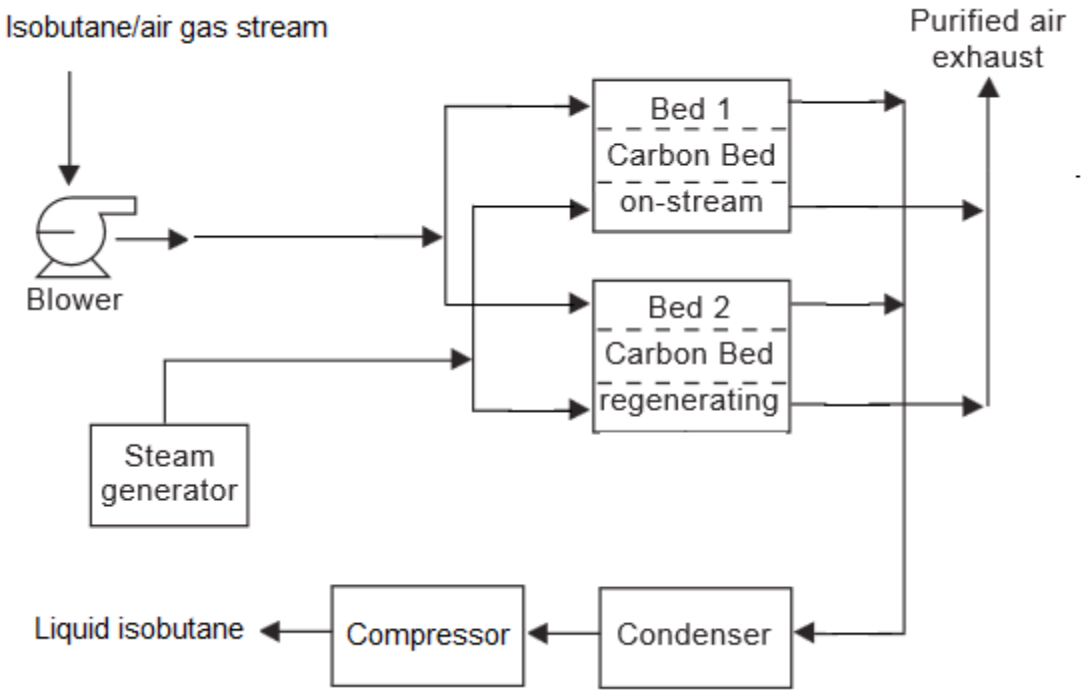

Figure 48: Design for continuously operated fixed bed granular activated carbon adsorption system (modified figure from USEPA, 2002)

6.2.1.3. *ACFC Adsorption*

A dual vessel ACFC-ESA system was designed to achieve 98 % capture and recovery efficiency of isobutane from the packaging manufacturing exhaust gas stream (Figure 49). The primary system components include a blower to move the packaging manufacturing exhaust gas stream, two adsorption vessels, a liquid N_2 reservoir, AC power for electrothermal heating, and a compressor. The blower directs the gas stream from the manufacturing process to one of the adsorption vessels where the isobutane is adsorbed onto ACFC providing purified exhaust air. N_2 is passed through the second adsorption vessel to create an inert environment and then the adsorbent is regenerated using electrothermal heating. The resulting N_2/isobutane exhaust gas is passed through a compressor to provide liquid isobutane for the packaging material manufacturing process. After regeneration heating, N_2 continues to pass through the vessel for cooling. The adsorption vessels alternate between adsorption and regeneration cycles so that one vessel is always available to adsorb isobutane from the gas stream (i.e., adsorption cycle) while the other vessel experiences a regeneration cycle.

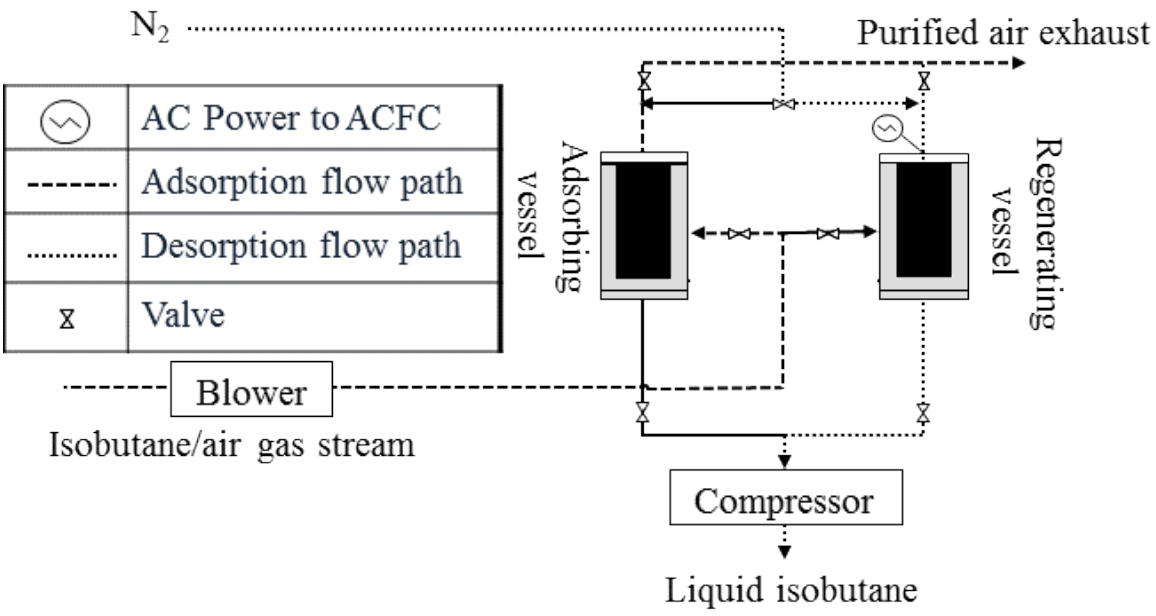

Figure 49: Dual vessel activated carbon fiber cloth (ACFC) electrothermal swing adsorption system for treating isobutane emissions from packaging manufacturing (adsorbing and regenerating vessels alternate when the corresponding cycles are completed)

6.2.2. LCA

A LCA was performed to compare the environmental impacts from directly emitting isobutane emissions from packaging manufacturing to treating isobutane emissions with a RTO, GAC system, and ACFC system. The LCA was performed according to ISO standards (ISO 14040, 2006; ISO 14044, 2006). This section includes a description of the LCA goal and scope, inventory assessment, impact assessment, and normalization.

6.2.2.1. *Goal and Scope*

6.2.2.1.1. Goal

As previously mentioned, this study compares a commercially available steam regenerated GAC system and a novel ACFC-ESA system (i.e., system analyzed throughout this

dissertation) to directly emitting isobutane and thermally oxidizing isobutane emissions from packaging manufacturing. This LCA is a study that involves the treatment of emissions that were determined based on the conditions at a packaging manufacturing facility over a 20 yr period. This research is intended to be an evaluation of air pollution abatement systems for packaging manufacturing that can be applied to more general studies. The goals of this LCA are to 1) determine the life cycle inventory inputs that have the largest environmental impacts for each VOC abatement system, 2) compare the environmental impacts of these VOC abatement systems, 3) determine the uncertainty and sensitivity of this LCA model, and 4) identify areas to improve the design of the VOC abatement system.

6.2.2.1.2. Functional Unit and System Boundaries

The functional unit for this study is the treatment of 162.5 million m^3 of an exhaust gas stream from packaging manufacturing that contains isobutane in air (i.e., annual treatment of 5.7 m^3/s) to achieve 98 % isobutane removal efficiency. This functional unit allows for comparison of the same total mass of treated isobutane for each system and has also been selected as the functional unit for previous studies for comparing air pollution abatement systems (i.e., total volume of a treated gas stream) (Abromaitis *et al*., 2011, Saffarian, 2009). The 98 % removal efficiency requirement is a typical maximum achievable control (i.e., abatement) technology removal efficiency for packaging manufacturing emissions (Indiana Title V1 Permit, 2012). This required removal efficiency considers the isobutane emissions during packaging manufacturing but not fugitive isobutane emissions that result from isobutane release from the packaging material after manufacturing. The system boundaries for this study are provided in Figure 50. These boundaries include the abatement system processes but do not include the

packaging material production process, fugitive emissions of isobutane after packaging manufacturing, or abatement system construction/final disposal. The packaging material production process is not included because it is not affected by abatement system selection. The fugitive emissions of isobutane are not considered because they do not reach the abatement systems and are thus the same regardless of abatement system selection. The construction/final disposal of the abatement system capital materials are not considered because these values are assumed to be minimal and similar between abatement systems (i.e., verified in section 6.3.2), which is an assumption used for other LCA studies (Fruergaard *et al*., 2010; Saffarian, 2009; Sauer *et al*., 2002). The impacts from the production, transportation, use, disposal, and emissions from the process materials/fuels are considered.

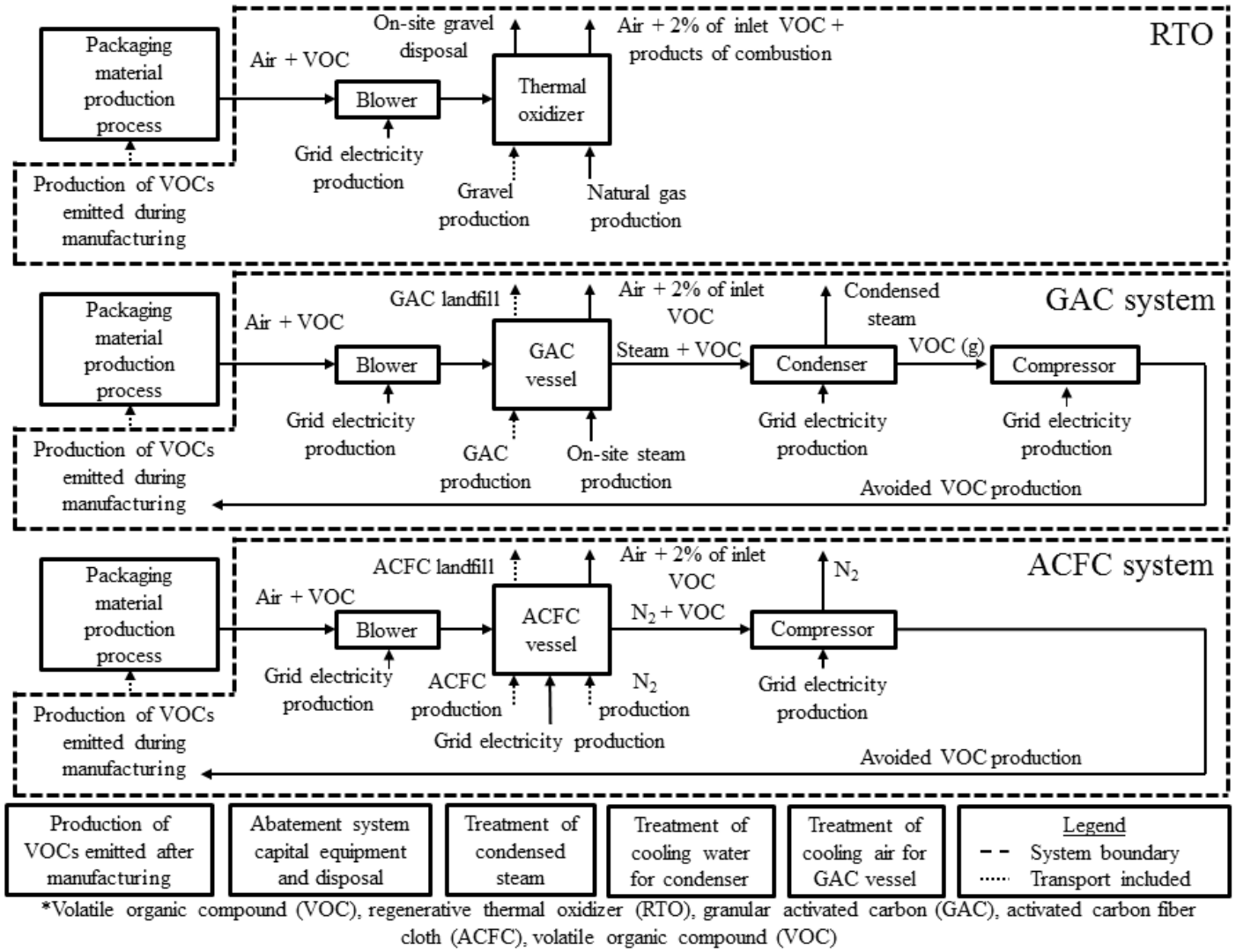

*Volatile organic compound (VOC), regenerative thermal oxidizer (RTO), granular activated carbon (GAC), activated carbon fiber cloth (ACFC), volatile organic compound (VOC)

Figure 50: System boundary of VOC abatement systems (i.e., RTO, GAC system, and ACFC system) for treating isobutane emissions from packaging manufacturing

6.2.2.1.3. Allocation and Assumptions

The following allocations and assumptions were used for this LCA. The environmental impacts from energy/materials were allocated evenly over the lifetime of the abatement system without any depreciation rate. The following assumptions were used for specific processes/materials:

- The emissions from burning isobutane were determined based on butane, which was determined using AP-42 emissions standards (USEPA, 1996), because isobutane and butane are isomers and are expected to result in similar emissions.
- The emissions from isobutane oxidation (i.e., isobutane and natural gas mixture) are assumed to be the same as the emissions from independently burning isobutane and natural gas because impacts from burning mixtures were not available in the LCA software database. This assumption does not significantly affect the LCA because the impacts from the emissions that result from burning isobutane were two orders of magnitude lower than the impacts from producing isobutane indicating that the emissions from burning isobutane are not a significant component for the total impacts for this LCA.
- The isobutane that was not treated by the abatement systems was assumed to be directly emitted into the atmosphere because no secondary treatment systems were present.
- Recovered liquid isobutane was considered as an avoided product because it can be reused as a blowing agent for the packaging manufacturing process.
- Gravel disposal was considered to be performed on site and the material is inert so no disposal impacts were considered.

- The impacts for ACFC production were determined assuming a polyacrylonitrile fiber precursor was activated with the same process used to produce GAC from coal (as described in Table 26 of Appendix B). ACFC is produced using polyacrylonitrile fibers so this is a reasonable surrogate for Novoloid (i.e., Novoloid impacts are not available). Additionally, the activation process for synthetic fibers and GAC both include pyrolysis followed by activation in CO_2 or steam so using the impacts for GAC activation to represent ACFC activation is reasonable.
- It was assumed that all activated carbon (i.e., GAC and ACFC) is treated as inert waste and is sent to a landfill because activated carbon is inert and remaining adsorbed isobutane is non-toxic.
- Impacts from treating cooling air and water were not considered because it was assumed that these resources would be re-circulated.
- Treatment of the condensed water from the steam/isobutane mixture from GAC regeneration was not considered because it was assumed that minimal isobutane would condense into the water (i.e., small Henry's law constant for isobutane into water at 25 °C of 0.00086 mol/kg-atm (Yaws and Yang, 1992)). Additionally, isobutane is non-toxic so it is not a regulated drinking water contaminant that requires treatment.
- Select fuels were considered for the production of electricity and are discussed in the results section.

6.2.2.2. *Inventory Analysis*

The inventory analysis for this LCA involved obtaining information for the operating conditions for packaging material manufacturing as well as information for treating the

manufacturing gas stream with each abatement system. Data were obtained from an Indiana based packaging material manufacturing company using a questionnaire and email correspondence with an engineer at the facility (Anonymous, 2013). These data included the process operating schedule and conditions, isobutane removal requirements for the abatement systems, and information about the existing RTO (Table 20 of Appendix B). The RTO, GAC, and ACFC systems were analyzed/designed to provide the remaining system inputs for the life cycle inventory. Shipping distances for abatement system operating materials are provided in Table 23 of Appendix B. A detailed description of all inputs that were used to describe and design the abatement systems are provided in Appendix B.

6.2.2.2.1. RTO

Many of the system design inputs for the RTO were either readily available from correspondence with personnel at the Indiana packaging manufacturing facility or expert estimates (i.e., facility engineers) were available because the RTO system is currently being continuously operated (Table 20 of Appendix B). For example, values for the annual consumption of natural gas (V_{ng}, m^3/yr), incinerator bed gravel (m_{RTOg}, kg/yr), and required isobutane removal efficiency (f_r, -) were available from the packaging manufacturing facility. Input values that were not available included the power requirements for the RTO system blower and the shipping details for the operating materials (i.e., isobutane and gravel). The electricity energy requirements (E_{RTO}, kWh/yr) for the RTO blower were determined with an empirical equation provided by the USEPA that assumes a motor efficiency of 0.6 (USEPA, 2002).

$$E_{RTO} = 0.163 \cdot Q_e \Delta p t_{op} \quad \text{(Equation 20)}$$

where Q_e is the packaging manufacturing exhaust gas flow rate (m^3/s), Δp is the pressure drop across the abatement system (e.g., includes the incinerator and heat exchanger) (cm H_2O), and t_{op} is the annual abatement system operating time (h/yr). The isobutane and gravel shipping information were estimated based on the location of gravel quarries and gas specialty facilities within Indiana. It was conservatively assumed that these materials were shipped 500 km by truck because shipping was not a significant portion of the environmental impacts for the abatement system (i.e., the impacts from shipping the operating materials were < 5% of the abatement system impacts for each impact category).

6.2.2.2.2. GAC System

The GAC system design process is primarily based on the USEPA control cost manual guidelines for the design of fixed bed GAC systems (USEPA, 2002). The GAC system model input parameters in this section are provided in Table 21 of Appendix B. First, the adsorbent requirements were determined. Equilibrium adsorption capacity values for isobutane onto GAC were represented with adsorption capacity values of butane onto Kureha spherical bead activated carbon because these isotherms were readily available over a wide range of temperatures and inlet concentrations that can be used to represent the packaging manufacturing exhaust gas (Zhu *et al*., 2005). Kureha spherical bead activated carbon has a micropore volume and BET surface area of 0.56 cm^3/g and 1,300 m^2/g, respectively, which are typical values for GACs, indicating it will likely have similar isobutane adsorption capacities when compared to GAC. The bead activated carbon adsorption capacities were fitted with the Toth equation (Equation 10) using a temperature dependent term for the Langmuir affinity constant b_1 (kPa^{-1}) (Zhu *et al*., 2005).

$$b_1 = b_o exp\left[\frac{\Delta H_s}{R_g T_R}\left(\frac{T_R}{T} - 1\right)\right] \quad \text{(Equation 21)}$$

where b_o is the Langmuir affinity constant (kPa^{-1}) at reference temperature T_R (298 K), ΔH_s is the isosteric heat of adsorption of isobutane onto the carbon (kJ/kmol), R_g is the ideal gas law constant (kJ/kmol-K), and T is the adsorbent temperature (K). This temperature dependent Langmuir affinity constant allows for the prediction of isobutane adsorption capacity over a range of abatement system operating temperatures. The equilibrium adsorption capacity (q, kg adsorbed/kg adsorbent) was determined using the concentration of isobutane in the packaging manufacturing exhaust gas (C_{isoe}, ppm_v) with equations 10 and 11. The equilibrium adsorption capacity was then multiplied by a correction factor (f_a = 0.5) to determine the working adsorption capacity (q_w, kg adsorbed/kg adsorbent) for the GAC abatement system (USEPA, 2002). The mass of GAC (m_{GAC}, kg) that was required for each adsorption vessel was then determined based on the working adsorption capacity.

$$m_{GAC} = \frac{\dot{m}_D t_{GACads}}{q_w} \quad \text{(Equation 22)}$$

where $\dot{m}_D$ is the design isobutane mass emission rate (kg/h) and t_{GACads} is the duration of a GAC adsorption cycle (h). Horizontal cylindrical vessel dimensions were determined assuming a carbon bulk packing density of 480 kg/m^3 within the vessel (i.e., carbon and void space, USEPA, 2002).

$$d_{GACv} = 0.026\frac{m_{GAC} v_{GACs}}{Q_e} \quad \text{(Equation 23)}$$

$$L_{GACv} = \frac{414}{m_{GAC}}\left(\frac{Q_e}{v_s}\right)^2 \quad \text{(Equation 24)}$$

where d_{GACv} is the vessel diameter (m), v_{GACs} is the superficial velocity of gas through the GAC (m/s), and L_{GACv} is the vessel length (m). The GAC thickness was then determined for the horizontal cylindrical vessels (H_{GACv}, m) (USEPA, 2002).

$$H_{GACv} = \frac{0.0021 \cdot m_{GAC}}{d_{GACv} L_{GACv}} \quad \text{(Equation 25)}$$

The pressure drop across the GAC bed was determined (Δp_{GACv}, cm H_2O) using an empirically derived equation for GAC and the total system pressure drop was determined assuming there is one cm H_2O pressure drop across the remaining system components (Δp_{GACs}, cm H_2O) (USEPA, 2002).

$$\Delta p_{GACv} = H_{GAC}(75 \cdot v_{GACs} + 0.57 \cdot v_{GACs}^2) \quad \text{(Equation 26)}$$

$$\Delta p_{GACs} = \Delta p_{GACv} + 1 \quad \text{(Equation 27)}$$

The energy for the adsorption blower (E_{GACab}, kWh/yr) was determined using equation 20 with the pressure drop across the GAC system (Δp_{GACs}). Next, the regeneration steam requirement was determined (m_{steam}, kg) based on the mass of GAC and total time for steam regeneration throughout the 20 yr lifespan of the system.

$$m_{steam} = S_{st} m_{GAC} \frac{t_{op}}{t_{GACads}} \quad \text{(Equation 28)}$$

where S_{st} is the mass of steam required per mass of adsorbent (kg steam/kg carbon). The mass of steam was then multiplied by the energy required to produce one kg steam (S_{est}, MJ/kg) to determine the fuel requirements for steam production (i.e., MJ of natural gas and heavy fuel oil to produce steam). The condenser operating time (t_{GACcw}, h/yr) and cooling water flow rate requirements were then determined (Q_{cw}, LPM) (USEPA, 2002).

$$t_{GACcw} = (1 - f_{dc}) t_{op} \frac{t_{GACdes}}{t_{GACads}}$$ (Equation 29)

$$Q_{cw} = \frac{S_{cw} m_{steam}}{60 \cdot t_{GACcw}}$$ (Equation 30)

where f_{dc} is the fraction of time that drying/cooling occurs during the regeneration cycle (-), t_{GACdes} is the duration of the desorption cycle (h), and S_{cw} is the volume of cooling water that is required per mass of steam (L/kg steam). The energy requirements for the condenser (E_{GACcw}, kWh/yr) were determined by solving equation 20 using the condenser cooling water flow rate (Q_{cw}, LPM), pressure drop for the cooling water condenser (Δp_{GACcw}, cm H_2O), and condenser operating time (t_{GACcw}, h/yr). The operating time for the regeneration cycle drying/cooling air blower (t_{GACdc}, h/yr) and the air flow rate requirements for the drying/cooling air were then determined (Q_{dc}, LPM) (USEPA, 2002).

$$t_{GACdc} = (f_{dc}) t_{op} \frac{t_{GACdes}}{t_{GACads}}$$ (Equation 31)

$$Q_{dc} = \frac{S_{dc} m_{GAC}}{60 \cdot f_{cw} t_{GACdes}}$$ (Equation 32)

where S_{dc} is the volume of drying/cooling air that is required per mass of adsorbent (L/kg). The energy for the drying/cooling air blower (E_{GACdc}, kWh/yr) was determined by solving equation 20 using the drying/cooling air flow rate (Q_{dc}, LPM), GAC system pressure drop (Δp_{GACs}, cm H_2O), and cooling/drying air operating time (t_{GACdc}, h/yr). Next, the compressor requirements were determined. First, the density of the pure isobutane at the inlet of the compressor was determined using the ideal gas law (ρ_{GACic}, kg/m^3). Then, the mean isobutane desorption flow rate that reaches the GAC compressor was determined assuming pure isobutane reaches the compressor (Q_{GACiso}, m^3/s).

$$Q_{GACiso} = \frac{\dot{m}_{op} t_{op}}{3600 \cdot t_{GACcw} \rho_{GACic}} \quad \text{(Equation 33)}$$

where $\dot{m}_{op}$ is the mean isobutane emission rate from the packaging manufacturing process (kg/h). The pressure to condense desorbing isobutane (i.e., assuming pure isobutane) was determined using the Antoine equation (P_{GACiso}, atm). The isobutane compression energy requirements (E_{GACco}, kWh/yr) were then determined assuming adiabatic compression and a compressor efficiency of 60 %, as recommended by the EPA control cost manual (USEPA, 2001), which has also been demonstrated for both single stage and multi-stage gas compression (Brun and Kurz, 2001)

$$E_{GACco} = \frac{Q_{GACiso} \rho_{GACic} t_{GACcw}}{2.8 \cdot 10^{-7} \cdot M_{iso}} \frac{R_g T_{ic}}{0.6} \frac{k_{iso}}{k_{iso}-1} \left[\left(\frac{P_{GACiso}}{P} \right)^{\left[\frac{k_{iso}-1}{k_{iso}} \right]} - 1 \right] \quad \text{(Equation 34)}$$

where M_{iso} is the molecular weight of isobutane (kg/kmol), R is the ideal gas law constant (kJ/kmol-K), T_{ic} is the temperature at the inlet of the compressor (K), k_{iso} is the ratio of the specific heat of isobutane at constant pressure to that at constant volume (-), and P is the total ambient pressure at the outlet of the compressor (1 atm). The total electrical energy requirements for the GAC system include the electricity consumption for the adsorption blower, regeneration condenser pump, regeneration bed drying/cooling blower, and regeneration compressor (E_{GACtot}, kWh/yr).

$$E_{GACtot} = E_{GACab} + E_{GACcw} + E_{GACdc} + E_{GACco} \quad \text{(Equation 35)}$$

6.2.2.2.3. ACFC System

The ACFC system design is based on a combination of scaling values from bench-scale tests and using the USEPA control cost manual for the design of fixed bed GAC systems (USEPA, 2002). The ACFC system model input parameters in this section are provided in Table 22 of Appendix B. First, the ACFC requirements were determined. ACFC adsorption capacity values were predicted with the Toth model (i.e., based on experimental results from 5.3.1.1) with an additional temperature dependent Langmuir affinity constant term that is described in equation 21. Experimental bench-scale adsorption isotherms for isobutane onto ACFC at 31.5 °C and 40 °C confirm the temperature dependent Toth equation predictions of ACFC adsorption capacity (i.e., within 10 %) for isobutane partial pressures from 0.00007 to 0.13. The equilibrium adsorption capacity was then multiplied by a correction factor (f_a = 0.5) to determine the working adsorption capacity (q_w, kg adsorbed/kg adsorbent) for the ACFC abatement system (USEPA, 2002). This correction factor value was selected based on the USEPA control cost manual guidelines for designing GAC adsorption systems and is also selected as a conservative estimate based on a study of bench-scale ACFC working adsorption capacities for isobutane, which ranged from 50-80% of the equilibrium adsorption capacity (Mallouk and Rood, 2013). Varying this correction factor from 0.5-0.8 alters the LCA results by < 2% in all impact categories suggesting this parameter has minimal effects on the output of the model for this range of values (i.e., 0.5-0.8). The ACFC requirement for each adsorption vessel (m_{ACFC}, kg) was determined using equation 23 with a one hour ACFC adsorption cycle ($t_{ACFCads}$, h). This design adsorption time for the ACFC system is shorter than that of the GAC system (i.e., 6 h) because the GAC system requires additional time for steam heating and for

GAC drying after heating. The volume of ACFC in the vessel (V_{ACFCv}, m^3) was then determined based on the mass and density of the ACFC.

$$V_{ACFCv} = 1000 \cdot m_{ACFC} \frac{H}{D_A} \quad \text{(Equation 36)}$$

where H is the height (thickness) of a layer of ACFC (m) and D_A is the areal density of ACFC (g/m^2). The number of cylindrical ACFC cartridges that are required to achieved the desired ACFC volume in each adsorption vessel (N_{ACFCc}) was then determined.

$$d_{ACFCo} = d_{ACFCi} + 2(N_{ACFCl} H) \quad \text{(Equation 37)}$$

$$N_{ACFCc} = \frac{V_{ACFCv}}{H_{ACFCc} \pi [(d_{ACFCo})^2 - (d_{ACFCi})^2]} \quad \text{(Equation 38)}$$

where d_{ACFCo} is the outer diameter of an ACFC cartridge (m), d_{ACFCi} is the inner diameter of an ACFC cartridge (m), N_{ACFCl} is the number of layers of ACFC per cartridge (-), and H_{ACFCc} is the height of an ACFC cartridge (m) such that d_{ACFCi}, N_{ACFCl}, and H_{ACFCc} are design parameters. The number of rows of cartridges in the width (N_{ACFCcw}) and length (N_{ACFCcl}) direction of the adsorption vessel were then determined.

$$N_{ACFCcw} = \frac{W_{ACFCv} - d_{ACFCbc}}{d_{ACFCo} + d_{ACFCbc}} \quad \text{(Equation 39)}$$

$$N_{ACFCcl} = \frac{N_{ACFCc}}{N_{ACFCcw}} \quad \text{(Equation 40)}$$

where W_{ACFCv} is the maximum vessel width that was selected to allow for road transportation of the abatement system (m) and d_{ACFCbc} is the distance between ACFC cartridges (m). The vessel length (L_{ACFCv}, m) and height (H_{ACFCv}, m) were determined based on the ACFC cartridge dimensions and distance between ACFC cartridges.

$$L_{ACFCv} = (d_{ACFCo} + d_{ACFCbc})N_{ACFCcw} + d_{ACFCbc} \quad \text{(Equation 41)}$$

$$H_{ACFCv} = H_{ACFCc} + 2 \cdot d_{ACFCbc} \quad \text{(Equation 42)}$$

The superficial velocity (v_{ACFCs}, cm/s) and pressure drop across the ACFC adsorption vessel (Δp_{ACFCs}, cm H_2O) were determined assuming the system pressure drop is the sum of the pressure drop across the ACFC cartridge and an additional 1 cm H_2O for other system components.

$$v_{ACFCs} = \frac{100 \cdot Q_e}{N_{ACFCc}(H_{ACFCc} \cdot \pi d_{ACFCi})} \quad \text{(Equation 43)}$$

$$\Delta p_{ACFCs} = \Delta p_{ACFCl} L_{ACFCv} v_{ACFCs} + 1 \quad \text{(Equation 44)}$$

where Δp_{ACFCl} is the pressure drop through a single sheet of ACFC per superficial velocity of the gas stream passing through the ACFC cartridge ($\frac{cm\ H_2O}{cm/s}$). The volume of isobutane (V_{iso}, m^3) that is desorbed during a regeneration cycle is determined using the ideal gas law and a mass balance for isobutane (i.e., adsorbed mass equals desorbed mass at steady-state).

$$V_{iso} = \frac{1000 \cdot \dot{m}_{op} t_{ACFCads}}{M_{iso}} \frac{R_g T}{P} \quad \text{(Equation 45)}$$

The volume of N_2 that is required for a regeneration cycle (V_{N_2}, m^3/g isobutane) was determined as the sum of the N_2 used to inert the vessel, that used during regeneration heating, and that used while the ACFC is cooling before an adsorption cycle.

$$V_{N_2} = \frac{3 \cdot W_{ACFCv} L_{ACFCv} H_{ACFCv} + 2 \cdot V_{iso} \frac{100 - C_{isod}}{C_{isod}}}{1000 \cdot \dot{m}_{op} t_{ACFCads}} \quad \text{(Equation 46)}$$

where C_{isod} is the mean isobutane concentration during the desorption heating cycle (%). The numerator of equation 46 includes two terms: 1) the N_2 requirement to inert the vessel and 2) the N_2 requirement to regenerate the vessel (i.e., both regeneration heating and cooling). The first term describes the N_2 requirements to pass three vessel volumes of N_2 through the ACFC vessel to purge the vessel of O_2 before electrothermal heating occurs. The second term describes the N_2 that is required for regeneration. This term includes the N_2 requirements for electrothermal heating (i.e., determined based on C_{isod}) and is multiplied by a factor of two to account for N_2 consumed during cooling (i.e., conservative assumption). The N_2 mass requirements (m_{N_2}, kg/yr) were then determined using the ideal gas law. The energy requirements for the adsorption cycle blower (E_{ACFCab}) were determined with equation 20 using the pressure drop across the ACFC system (Δp_{ACFCs}). The energy requirements for electrothermal heating (E_{ACFCeh}, kWh/yr) were determined based on the mass of isobutane that needs to be desorbed during a regeneration cycle and the total time for regeneration heating over the 20 y lifespan of the system.

$$E_{ACFCeh} = \frac{S_{eh}}{M_{iso}} \dot{m}_{op} t_{op} \qquad \text{(Equation 47)}$$

where S_{eh} is the electrothermal heating energy per mole of isobutane desorbed (kJ/mol). S_{eh} was determined based on the results presented in Figure 15 assuming the ACFC is heated to 150 °C for 10 min during a regeneration cycle, which was adequate for maintaining a working adsorption capacity that is > 50 % of the equilibrium capacity (i.e., for bench-scale tests). The compressor requirements for liquefying/separating the isobutane from the isobutane/N_2 gas stream were determined. First, the density of the isobutane at the inlet of the compressor was determined using the ideal gas law and the gas stream composition (ρ_{ACFCic}, g/m^3).

$$\rho_{ACFCic} = \frac{P[C_{isod}M_{iso}+(100-C_{isod})M_{N_2}]}{100 \cdot R_g T} \quad \text{(Equation 48)}$$

where M_{N_2} is the molecular weight of N_2 (g/mol). Then, the isobutane desorption flow rate was determined based on the mass of isobutane that is desorbed and the duration of the regeneration heating cycle ($Q_{ACFCiso}$, m^3/h).

$$Q_{ACFCiso} = \frac{100 \cdot \dot{m}_{op} t_{op}}{t_{GACcw} \rho_{ACFCic} C_{isod}} \quad \text{(Equation 49)}$$

The pressure requirements for condensing isobutane from the desorption stream were determined using the Antoine equation and correcting for the purity of isobutane in the isobutane/N_2 gas stream (i.e., assuming negligible N_2 condensation) ($P_{ACFCisod}$, atm).

$$P_{ACFCiso} = \frac{100 \cdot P_{GACiso}}{C_{isod}} \quad \text{(Equation 50)}$$

The isobutane compression energy requirements were then determined assuming adiabatic compression and a compressor efficiency of 60 % (Brun and Kurz, 2001; USEPA, 2001) (E_{ACFCco}, kWh/yr).

$$E_{ACFCco} = \frac{Q_{ACFCiso} \rho_{ACFCic} t_{op} f_c}{2.8 \cdot 10^{-7} \cdot M_{iso}} \frac{R_g T_{ic}}{0.6} \frac{k_{iso}}{k_{iso}-1} \left[\left(\frac{P_{ACFCiso}}{P} \right)^{\left[\frac{k_{iso}-1}{k_{iso}} \right]} - 1 \right] \quad \text{(Equation 51)}$$

where f_c is the percentage of time that the compressor is operating (-). The total annual electrical energy requirements for the ACFC system were determined as the sum of the energy for the adsorption blower, electrothermal heating, and compressor.

$$E_{ACFCtot} = E_{ACFCab} + E_{ACFCeh} + E_{ACFCco} \quad \text{(Equation 52)}$$

6.2.2.3. *Impact Assessment*

The impact assessment for this LCA was performed using the Tools for Reduction and Assessment of Chemical and other Environmental Impacts (TRACI) method. TRACI was designed for US impacts and is a midpoint model, which minimizes subjective forecasting (Bare *et al*., 2003). The midpoint impact categories in TRACI include ozone depletion (kg CFC-11 eq), global warming (kg CO_2 eq), smog (kg O_3 eq), acidification (H^+ moles eq), eutrophication (kg N eq), carcinogenics (CTUh), non carcinogenics (CTUh), respiratory effects (kg PM 10 eq), and ecotoxicity (CTUe). SimaPro version 7.3.3 with EcoInvent version 3 was used to convert the inventory analysis values into the environmental impacts of the abatement systems (SimaPro, 2012). The EcoInvent version 3 database values that were used for each inventory parameter are provided in Table 25 of Appendix B, while a more description of the customized values for the activated carbon (i.e., both GAC and ACFC) and state electricity fuel mixes (i.e., described later in this section) are provided in Table 26 and Table 27 of Appendix B, respectively. Smog is considered the primary impact factor of concern for this study because this study focuses on the abatement of isobutane, which is directly regulated (e.g., Indiana Title V1 Permit, 2012) because it reacts in the atmosphere to create smog. Also, direct emission of isobutane into the atmosphere creates smog impacts but does create impacts in any of the other previously mentioned environmental impact categories (i.e., determined with EcoInvent version 3) supporting that smog is the primary impact factor of concern when considering isobutane abatement. As previously mentioned, the environmental impacts are presented on an annual basis that is determined using equal allocation of the impacts over the 20 yr lifespan of the abatement systems.

The environmental impact assessment for each abatement system is presented for a range of scenarios that consider different fuel mixes for electricity production. Electricity impacts were first determined using the Indiana fuel mix because data obtained for this study was based on Indiana packaging manufacturing. The electricity impacts were also determined using the electricity fuel mix from the US states with the largest VOC emissions from the production of sheet foam to expand the applicability of this study (Table 27 of Appendix B). These states include North Carolina, Georgia, Indiana (i.e., already considered), Michigan, and Illinois, which have annual VOC emissions from sheet foam manufacturing of 1,516, 1,011, 951, 946, and 936 tonne, respectively (i.e., 39% of the total US VOC emissions from sheet foam manufacturing) (USEPA, 2013). Electricity produced from natural gas was also selected as an alternative design option with reduced environmental impacts.

6.2.2.4. *Normalization*

Normalization of environmental impacts is considered an optional step for LCAs (ISO 14040, 2006; ISO 14044, 2006) and was performed in this research to provide a metric for the comparison of impact factors. Normalization was performed based on US per capita normalization factors that were established based on data from 2008 (Ryberg *et al*., 2014). Thus, the normalized impacts are presented as the US per capita equivalent impacts of using each abatement systems to treat the packaging manufacturing exhaust gas.

6.2.3. Cost Assessment

A cost assessment was performed based on the USEPA control cost manual to determine the economic impacts for each abatement system (USEPA, 2002). All monetary values are presented as 2014 US$ and cost input parameters are provided in Table 24 of Appendix B. Cost information was available for the RTO (i.e., data from Indiana packaging manufacturing facility). The adsorption systems are conceptual designs so cost information was not available for these systems. It was assumed that the performance testing, start-up, and operation labor costs are the same for the adsorption systems and the RTO, while all other adsorption system costs were predicted using the USEPA control cost manual. The net present value (NPV, $) of each abatement system was determined, by considering the capital costs and annual operating costs (i.e., includes offsets from isobutane recovery and maintenance costs) over the life span of each abatement system.

$$\text{NPV} = B_{cap} + \sum_{i=0}^{t_l} \frac{B_{ann}}{(1+r_{int})^i} \qquad \text{(Equation 53)}$$

where B_{cap} is the capital cost for the abatement system ($), B_{ann} is the annual cost for the abatement system ($/yr), r_{int} is the interest rate (-), and t_l is the lifespan of the system (20 yr). The adsorption systems have a positive annual cash flow after the initial purchase of capital materials so their internal rate of return was determined by setting the NPV in equation 53 equal to zero and solving for r_{int}.

6.2.4. Uncertainty and Sensitivity Analyses

The values for each LCA input variable were determined (as previously described), while the uncertainty of the input values (i.e., distribution/range of values) was unknown. It was assumed that all variables follow a normal distribution (unless otherwise stated) so that the uncertainty of each input parameter could be estimated using a Pedigree matrix (Weidema and Wesnaes, 1996). This assumption was made due to the lack of available data to more thoroughly characterize the distribution of each input parameter. The distributions of the input parameters are provided in Table 20-Table 24 of Appendix B. According to the Pedigree matrix, the input values were assigned a coefficient of variance of 0.05 for verified data from site-specific measurements, 0.10 for estimates based on detailed design data or design values, 0.2 for scaled values or values based on other similar systems, 0.3 for expert estimates (e.g., engineer at packaging manufacturing facility), and 0.5 for non-expert estimates. A coefficient of variance of 0.10 was used for all cost data because cost values were directly obtained from the packaging manufacturing facility or were obtained using the well documented USEPA control cost manual methods. Lognormal distributions were assigned to the shipping distances to avoid negative values because shipping distances had large coefficient of variance values (i.e., based on non-expert (author) estimates that involved determining the distance between IN packaging manufacturing facilities and facilities that produce products that are consumed by the abatement systems and landfills to receive consumed products/waste) and negative shipping distances are not feasible.

After determining distributions for each input parameter, an uncertainty analysis of the impacts of each abatement system (i.e., model outputs) was performed using a Monte-Carlo simulation with 100,000 runs (Oracle Crystal Ball, Fusion Edition). Sensitivity analysis was also

simultaneously performed using this Oracle Crystal Ball software to determine the effect of each input variable on the abatement system impacts. This software provides rank correlation coefficients between every input and output value for the model. A higher rank correlation coefficient indicates that the input variable has a more significant effect on both the uncertainty and sensitivity of the output value. For each input, the square of the rank correlation coefficient was normalized to the sum of the squares of the rank correlation coefficients of all the model inputs to provide the percentage of the contribution of variance for a single input to a single output. All sensitivity values in this study are provided as the percentage of the contribution of variance for a single input to a single output.

6.3. Results and Discussion

6.3.1. Life Cycle Inventory

The life cycle inventory is provided in

Table 14. A detailed list of the parameters used to obtain the life cycle inventory values is provided in Appendix B (i.e., methods described in 6.2.2.2). This life cycle inventory provides insights into differences in the material requirements for the isobutane abatement systems. For example, the isobutane production and shipping requirements for the adsorption systems are two orders of magnitude lower than those for the RTO because the adsorption systems recover isobutane, which is considered avoided product and thus reduces requirements for isobutane production and shipping. When comparing the adsorption systems, the GAC system requires 36 times more mass of activated carbon than the ACFC system. This difference in activated carbon requirement is due to 1) GAC having a lower adsorption capacity than ACFC, 2) GAC requiring periodic replacement (i.e., every 5 yr), and 3) the GAC system having a longer adsorption cycle

than the ACFC system (i.e., for the same mass of activated carbon, steam regeneration has a longer duration than electrothermal heating due to the added time for heating and drying). The operating electricity requirements for the ACFC system are greater than 2.5 times those of the other systems. However, when considering the total annual abatement system operating energy consumption (i.e., electricity, steam, and natural gas), the ACFC system is more competitive than the other systems (i.e., 19.2, 8.7, and 3.4 TJ/yr for the RTO, GAC, and ACFC systems, respectively). Thus, while each abatement system uses different forms of energy for regeneration, the ACFC system is the most energy efficient abatement system for this application.

Table 14: Life cycle inventory analysis inputs (normalized values from 20 yr lifespan of abatement systems to represent annual values)

Name	**RTO system**	**GAC system**	**ACFC system**
Isobutane (kg/yr)	264,000	5,290	5,290
Activated carbon (kg/yr)	-	1,990	62
Electricity (MJ/yr)	1,396,000	1,030,000	3,360,000
Steam (kg/yr)	-	2,163,000	-
Natural gas (MJ/yr)	17,800,000	-	-
N_2 (kg/yr)	-	-	317,000
Gravel (kg/yr)	28,100	-	-
Isobutane shipping (tonne-km/yr)	132,000	2,640	2,640
N_2 shipping (tonne-km/yr)	-	-	158,600
Activated carbon shipping (tonne-km/yr)	-	18,000	750
Gravel shipping (tonne-km/yr)	14,100	-	-

*****Regenerative thermal oxidizer (RTO), granular activated carbon (GAC), activated carbon fiber cloth (ACFC)

6.3.2. Impact Assessment

The environmental impacts from directly emitting isobutane from packaging manufacturing compared to using select abatement systems to treat these emissions are presented

in Figure 51 (i.e., for electricity produced using the Indiana fuel mix). Figure 51 includes impact values that are normalized to the packaging manufacturing exhaust treatment option with the highest impacts in each impact category for comparison between treatment options while magnitudes of the impacts are provided in Table 28-Table 31 of Appendix B. The RTO has the largest impacts for every category except smog, eutrophication, and carcinogenics. The abatement systems reduce the smog impacts to less than 25 % of those from directly emitting isobutane to the atmosphere because they are designed to reduce isobutane emissions, which reacts in the atmosphere to form smog, demonstrating the importance of using abatement systems. The ACFC system has the largest eutrophication and carcinogenics impacts, which are primarily due to electricity and N_2 consumption. Isobutane consumption was the largest component of the environmental impacts from the RTO for nearly every category (i.e., 8 of 9 impact categories), while 98 % of the isobutane consumption was avoided with the adsorption and recovery systems. When comparing the adsorption systems for this scenario, the GAC system performed better than the ACFC system in every impact category except ozone depletion. Figure 51 reveals that the impacts of the ACFC system are dominated by electricity usage, while the impacts for the GAC system were dependent on electricity and steam consumption (i.e., depending on the impact category). These results support examining alternative electricity fuel mixes for electricity production to potentially reduce the total environmental impacts of the adsorption systems.

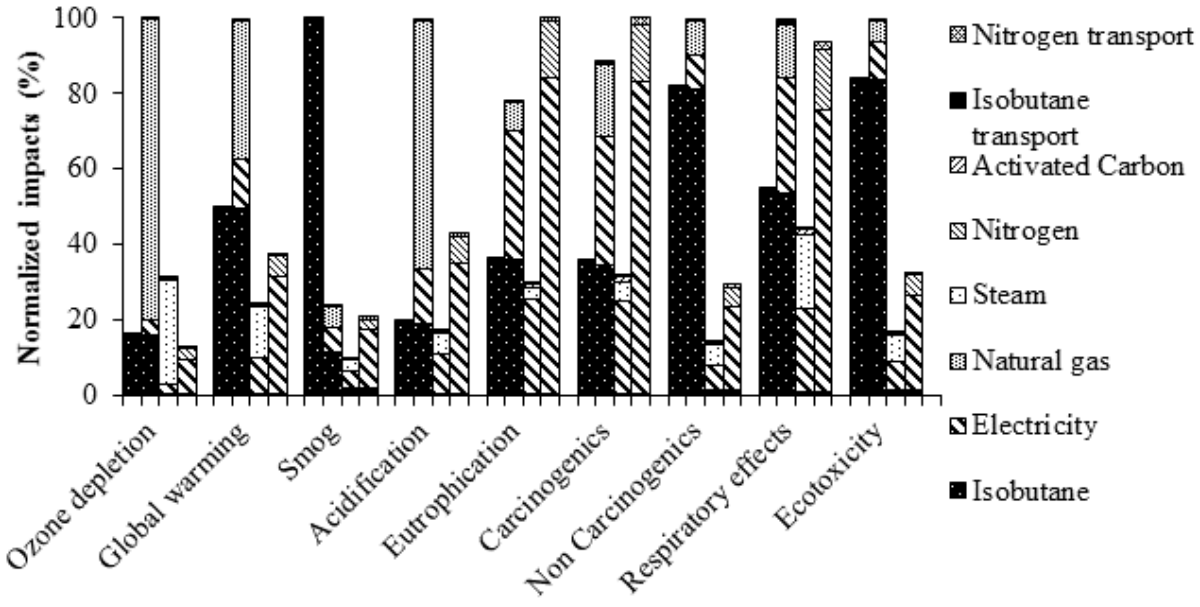

Figure 51: Environmental impacts of select isobutane abatement systems (i.e., no system, regenerative thermal oxidizer system, granular activated carbon system, and activated carbon fiber cloth system from left to right) for treating isobutane emissions from packaging manufacturing normalized to the system with the highest impacts for each impact category, in which electricity is produced from the average Indiana fuel mix

The environmental impacts from using select abatement systems to treat the packaging manufacturing exhaust gas stream were then determined using the electricity impacts resulting from electricity being produced from the average fuel mix from North Carolina, Georgia, Michigan, and Illinois (i.e., presented in Figure 52, Figure 53, Figure 54, and Figure 55, respectively). These figures include impact values that are normalized to the packaging manufacturing exhaust treatment option with the highest impacts in each impact category for comparison between treatment options while magnitudes of the impacts are provided in Table 28-Table 31 of Appendix B (i.e., as was presented in Figure 51). As previously mentioned, these states (i.e., North Carolina, Georgia, Michigan, and Illinois) and Indiana were considered because they have the highest VOC emissions from sheet foam production. For all 4 states (i.e.,

North Carolina, Georgia, Michigan, and Illinois), of which < 44% of their electricity is produced using coal, smog is reduced by > 80% when using an abatement system and the RTO has the largest impacts in all other impact categories. These state fuel mix results demonstrate reduced impacts for the ACFC system compared to when using the Indiana fuel mix (i.e., 88% coal in Figure 51, in which the ACFC system has the largest impacts in 2 categories). Additionally, when comparing the adsorption systems, the GAC system has lower impacts than the ACFC system in 8 of the 9 impact categories (i.e., all categories except ozone depletion) for all state fuel mixes.

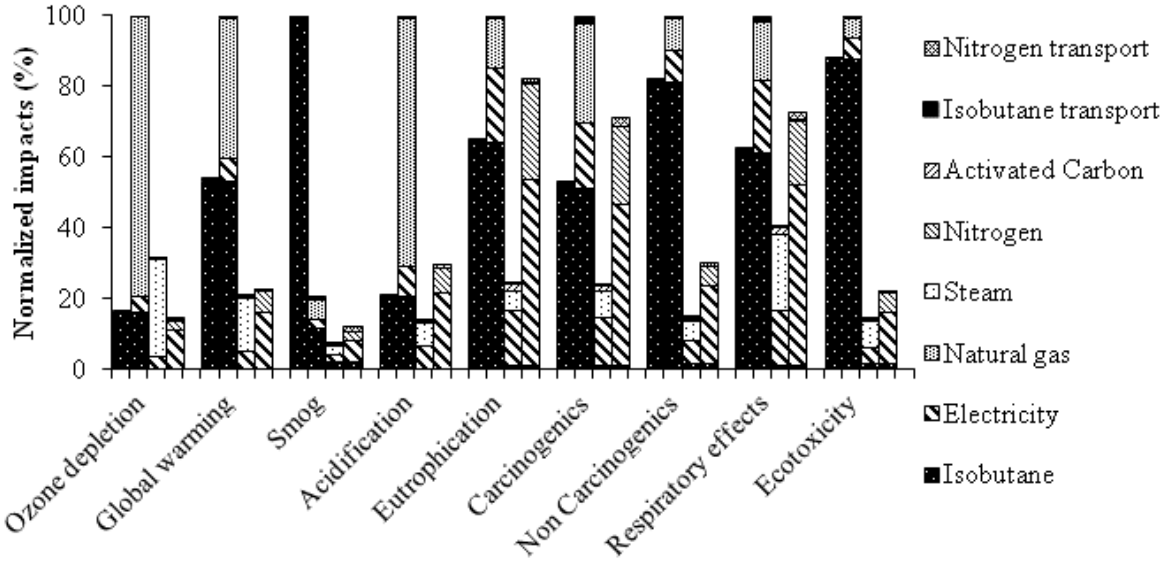

Figure 52: Environmental impacts of select isobutane abatement systems (i.e., no system, regenerative thermal oxidizer system, granular activated carbon system, and activated carbon fiber cloth system from left to right) for treating isobutane emissions from packaging manufacturing normalized to the system with the highest impacts for each impact category, in which electricity is produced from the average North Carolina fuel mix

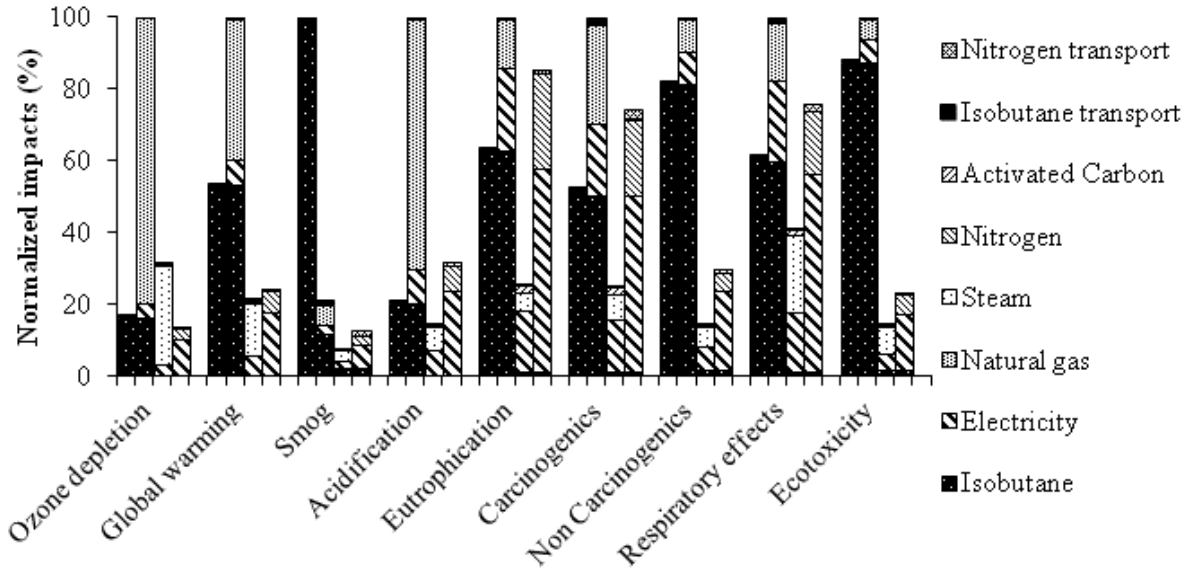

Figure 53: Environmental impacts of select isobutane abatement systems (i.e., no system, regenerative thermal oxidizer system, granular activated carbon system, and activated carbon fiber cloth system from left to right) for treating isobutane emissions from packaging manufacturing normalized to the system with the highest impacts for each impact category, in which electricity is produced from the average Georgia fuel mix

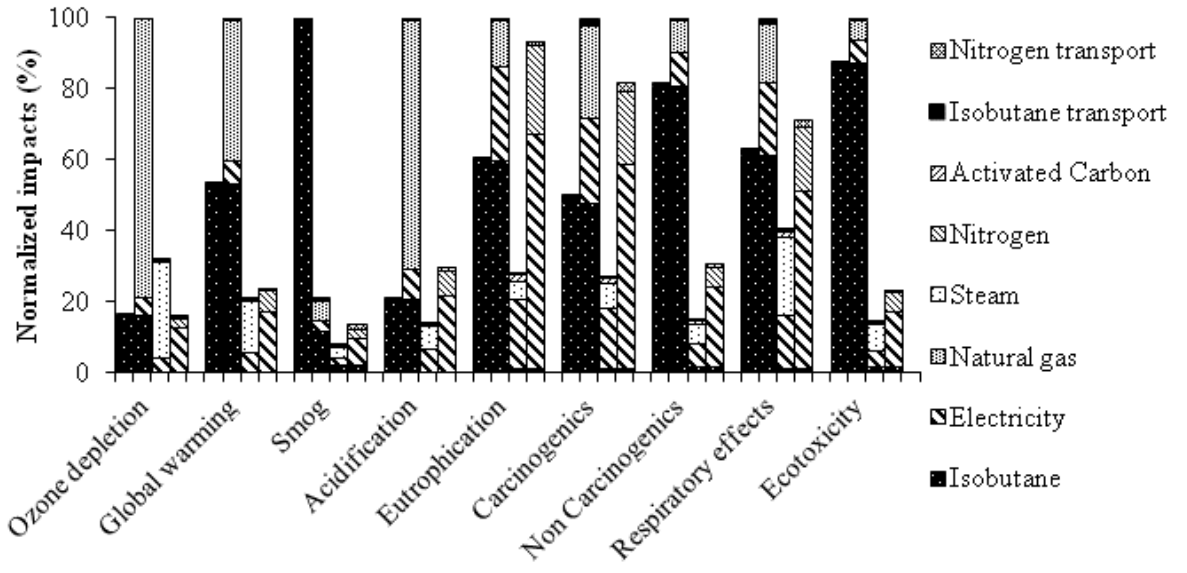

Figure 54: Environmental impacts of select isobutane abatement systems (i.e., no system, regenerative thermal oxidizer system, granular activated carbon system, and activated carbon fiber cloth system from left to right) for treating isobutane emissions from packaging manufacturing normalized to the system with the highest impacts for each impact category, in which electricity is produced from the average Michigan fuel mix

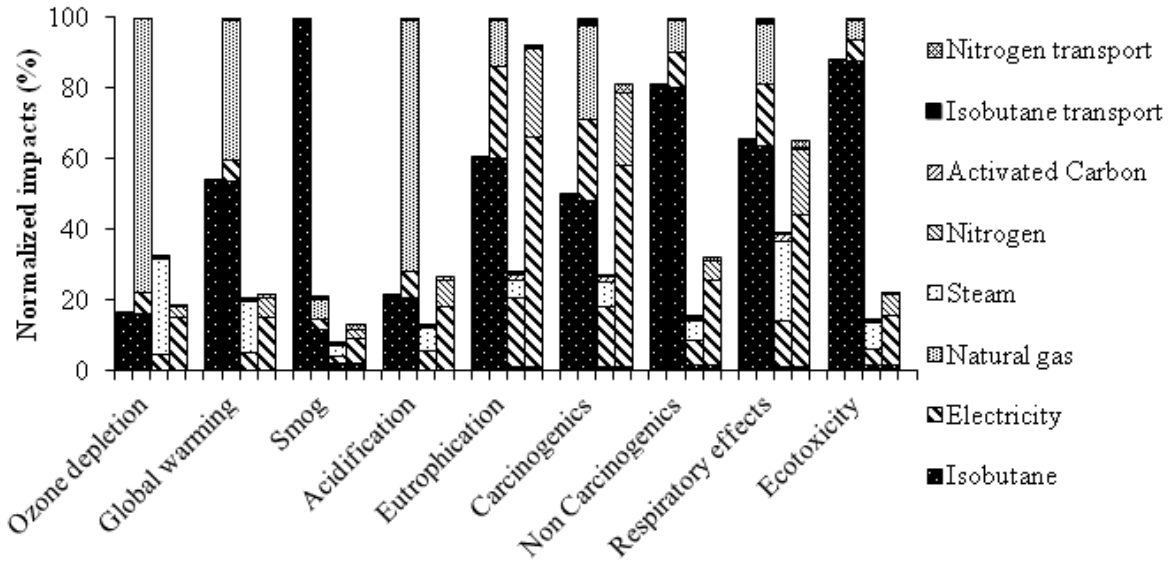

Figure 55: Environmental impacts of select isobutane abatement systems (i.e., no system, regenerative thermal oxidizer system, granular activated carbon system, and activated carbon fiber cloth system from left to right) for treating isobutane emissions from packaging manufacturing normalized to the system with the highest impacts for each impact category, in which electricity is produced from the average Illinois fuel mix

The environmental impacts from using select abatement systems with electricity produced from natural gas are presented in Figure 56. Figure 56 includes impact values that are normalized to the packaging manufacturing exhaust treatment option with the highest impacts in each impact category for comparison between treatment options while magnitudes of the impacts are provided in Table 28-Table 31 of Appendix B (i.e., as was presented in Figure 51). Using natural gas instead of one of the average state fuel mixes to produce electricity reduces the environmental impacts from electricity consumption in 5 of the impact categories, including smog (i.e., primary impact category of concern for isobutane abatement), so it is considered a best case fuel scenario for electricity production. For this scenario, the abatement systems reduce the smog impacts compared to directly emitting isobutane by > 80 %, again demonstrating the importance of using an isobutane abatement system. The RTO has the largest

impacts in every category except smog, when compared to direct isobutane emission or using the adsorption systems to treat the exhaust as stream. This scenario results in the ACFC system being more competitive with the GAC system (i.e., ACFC system has lower ozone depletion impacts than the GAC system and is within 25 % of the GAC impacts in 6 other categories) than when using the Indiana electricity fuel mix, which is primarily coal. The impacts for the ACFC and GAC systems are compared in more detail in section 6.3.5 using uncertainty analysis.

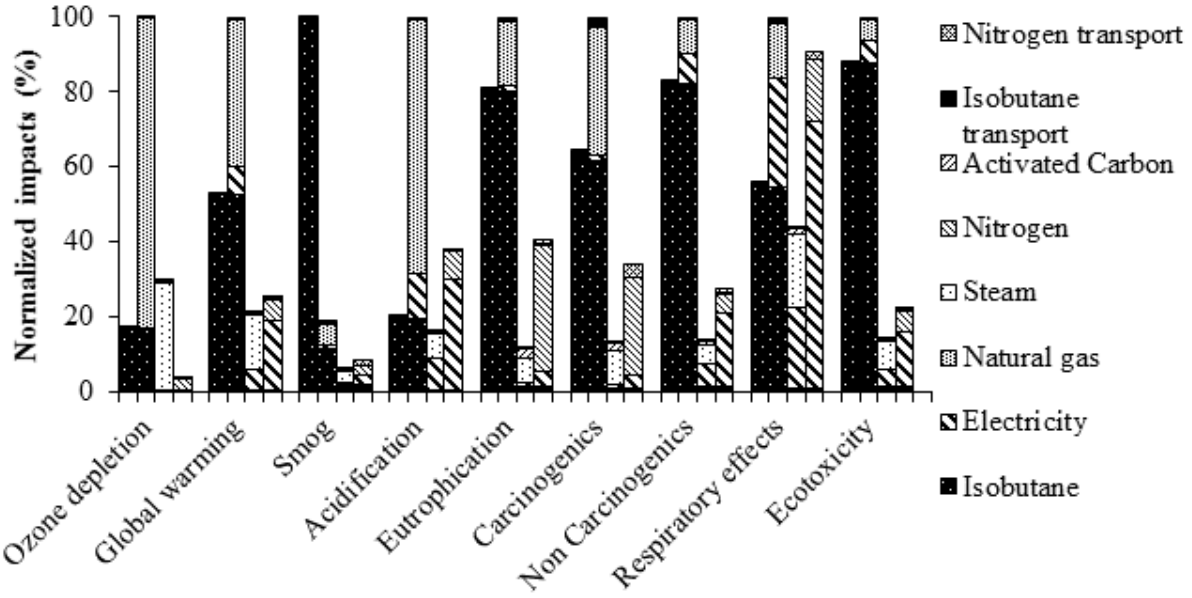

Figure 56: Environmental impacts of select isobutane abatement systems (i.e., no system, regenerative thermal oxidizer system, granular activated carbon system, and activated carbon fiber cloth system from left to right) for treating isobutane emissions from packaging manufacturing normalized to the system with the highest impacts for each impact category, in which electricity is produced from natural gas

The mass of the capital materials used to construct the abatement systems was unknown. Five materials that are typically used to construct components of abatement systems were selected (i.e., steel, copper, concrete, polybutadiene, and poly(methyl methacrylate)) and the mass of each of these materials that is required to contribute 2 % to any impact category when

using the state fuel mixes in Table 27 of Appendix B or natural gas to produce electivity (i.e., Figure 51-Figure 56) was considered (Table 15). The mass of capital materials that was required to increase the impacts of the abatement systems by 2 % was larger than that used for abatement systems (i.e., > 2,000 kg for each material) justifying the assumption that the capital materials have negligible environmental impacts for this LCA.

Table 15: Mass of capital material required to increase the impacts of treating isobutane emissions from packaging manufacturing with select abatement systems (i.e., regenerative thermal oxidizer, granular activated carbon, and activated carbon fiber cloth systems) by 2 % for any environmental impact category when considering electricity produced from the North Carolina, Georgia, Indiana, Michigan, and Illinois fuel mixes or natural gas

Material	**Example Use**	**Mass (kg)**
Steel	Abatement system exterior wall	63,000
Copper	Wires	2,000
Concrete	Supporting structure	800,000
Polybutadiene	Solenoid valve components	3,100,000
Poly(methyl methacrylate)	Adsorption vessel wall	1,000,000

6.3.3. Normalization

The US per capita impacts from emitting packaging manufacturing exhaust compared to treating the exhaust with select abatement systems (i.e., for electricity produced from natural gas as shown in Figure 56) are presented in Figure 57. The impact categories with the largest per capita impacts were global warming, smog, acidification, carcinogenics, and ecotoxicity suggesting these may be the most relevant impact categories for this study. The adsorption systems have reduced impacts in these impact categories compared to direct emissions or RTO treatment by at least 50 %, which suggests these adsorption systems are particularly beneficial for the impact categories that are most relevant on a US per capita basis. It should be noted that comparing impact categories based on US per capita impacts only provides selective evidence of

the most relevant impact categories for this study because relevance is subjective and depends on weighting values for many factors (e.g., human health, material usage, air quality).

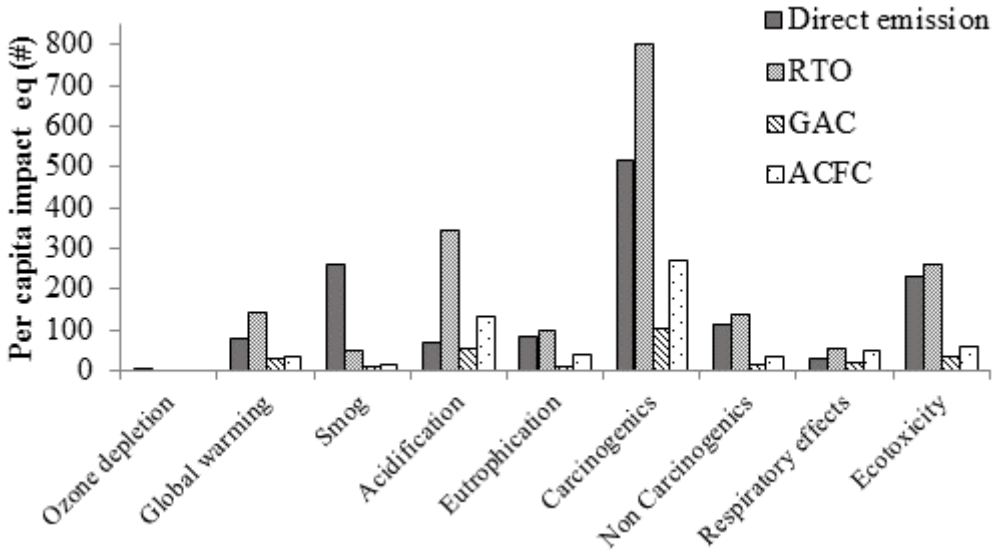

*Regenerative thermal oxidizer (RTO), granular activated carbon (GAC), activated carbon fiber cloth (ACFC)

Figure 57: United States per capita environmental impacts of emitting packaging manufacturing emissions compared to treating these emissions with select abatement systems, in which electricity is produced from natural gas

6.3.4. Cost Assessment

A cost assessment comparing the economic value of the abatement systems is presented in Table 16 (i.e., inputs to cost assessment provided in Table 24 of Appendix B). The RTO has a lower capital cost ($464,000) than the adsorption systems ($693,000 and $713,000 for the GAC and ACFC systems, respectively) making this system an attractive short-term capital cost option. However, the reduced annual costs from using the adsorption systems to recover isobutane result in the adsorption systems providing a positive annual return compared to the RTO, which costs $300,000/yr to operate. Over the expected 20 yr abatement system life span, the NPV of the

adsorption systems are positive, while the RTO costs $4,000,000 indicating the adsorption systems are more economically competitive than the RTO for this application. The positive annual return for the adsorption systems results in an internal rate of return of 11 % and 8 % for the ACFC and GAC systems, respectively. Thus, implementing an adsorption system eliminates the annual RTO cost and additionally provides an internal rate of return of $\geq$ 8 % over the 20 yr lifespan of the abatement system.

Table 16: Life cycle costs for abatement systems used to treat isobutane emissions from packaging manufacturing for 20 yr

Capital costs	**RTO system**	**GAC system**	**ACFC system**
Total carbon cost ($)	-	(87,389)	(122,031)
Vessel Cost ($)	(277,000)[a]	(67,007)	(37,050)
Pumps/piping ($)	(50,000)[a]	(257,636)	(265,453)
Tax and freight ($)	(10,000)[a]	(32,963)	(33,963)
Foundations and supports ($)	(10,000)[a]	(35,600)	(36,680)
Handling and erection ($)	-	(62,299)	(64,190)
Electrical ($)	(10,000)[a]	(17,800)	(18,340)
Piping ($)	(50,000)[a]	(8,900)	(9,170)
Insulation ($)	-	(4,450)	(4,585)
Painting ($)	-	(4,450)	(4,585)
Engineering ($)	-	(57,849)	(59,605)
Start-up ($)	(12,000)[a]	(12,000)[a]	(12,000)[a]
Performance testing ($)	(45,000)[a]	(45,000)[a]	(45,000)[a]
Total capital investment ($)	(464,000)	(693,342)	(712,651)

Annual costs	**RTO system**	**GAC system**	**ACFC system**
Operating labor ($/yr)	(18,883)[a]	(18,883)[a]	(18,883)[a]
Carbon replacement labor ($/yr)	-	(121)	-
Carbon replacement ($/yr)	-	(23,019)	-
Electricity ($/yr)	(28,309)	(20,809)	(68,069)
Steam ($/yr)	-	(30,107)	-
Cooling water ($/yr)	-	(2,275)	-
N_2 ($/yr)	-	-	(7,740)
Natural gas ($/yr)	(147,074)	-	-
Other replacement parts ($/yr)	(30,000)[a]	-	-
Overhead ($/yr)	(11,330)	(11,330)	(11,330)
Administrative charges ($/yr)	(9,280)	(13,867)	(14,253)
Property tax ($/yr)	(4,640)	(6,933)	(7,127)
Insurance ($/yr)	(4,640)	(6,933)	(7,127)
Capital recovery ($/yr)	(40,970)	(63,267)	(67,274)
Avoided cost for isobutane ($/yr)	-	277,000	277,000
Total annual costs ($/yr)	(295,125)	79,455	75,198
Net present value ($)	4,141,900	(296,800)	(224,500)

*****Regenerative thermal oxidizer (RTO), granular activated carbon (GAC), activated carbon fiber cloth (ACFC)

[a]Values provided from personnel at Indiana packaging manufacturing facility

6.3.5. Uncertainty and Sensitivity Analyses

An uncertainty and sensitivity analyses was performed to compare the abatement systems when using natural gas to produce electricity (i.e., previously described in Figure 56). Natural gas was selected for the uncertainty and sensitivity analyses because it provides lower environmental impacts for each abatement system (i.e., lower impacts in 5 impact categories compared to the state average electricity fuel mixes) and is thus considered the best design option of the analyzed scenarios for these abatement systems. Additionally, the US average levelized cost for electricity from new natural gas plants is 7 cents/kWh compared to 11 cents/kWh for coal plants or 9 cents/kWh for nuclear plants indicating it is more economical to produce future electricity from natural gas than coal or nuclear plants (USEIA, 2014b). The impact values and corresponding uncertainties for treating the packaging manufacturing exhaust gas with each abatement system is compared to that of directly emitting the exhaust gas in Figure 58. The impacts from using the RTO are equivalent (within one standard deviation) or worse than directly emitting the exhaust gas for 8 of the 9 impact categories. The RTO reduces smog compared to emitting untreated exhaust due to the 98 % reduction in emissions of isobutane, which reacts to create smog. Although the impact standard deviations were large (i.e., > 20 % for select impact categories), the adsorption systems have impacts that were greater than one standard deviation less than the RTO for 7 of the 9 impact categories including smog, which is the primary objective of the isobutane abatement systems. This result presents convincing evidence that treating the packaging exhaust gas stream with the adsorption systems reduces environmental impacts when compared to using the RTO. When comparing the adsorption systems, the GAC system performs worse for ozone depletion while the ACFC system is worse for eutrophication. The mean values for the impacts of the GAC system are smaller than the

ACFC system for 8 impact categories but overall the impacts are similar (i.e., 7 of the 9 categories are within one standard deviation). In summary, the adsorption systems perform similarly and have smaller impacts than the RTO or directly emitting isobutane.

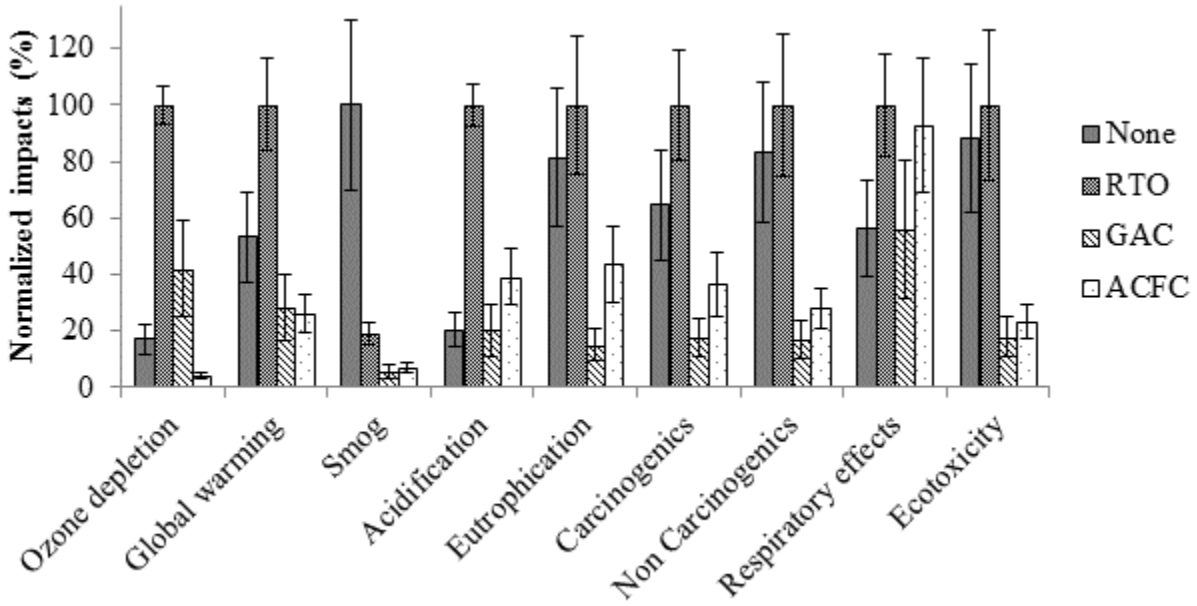

*Regenerative thermal oxidizer (RTO), granular activated carbon (GAC), activated carbon fiber cloth (ACFC)

Figure 58: Environmental impacts of using select abatement systems to treat isobutane emissions from packaging manufacturing, in which electricity is produced from natural gas and error bars describe standard deviations

The percentages of the contributions of the input parameters (i.e., defined in section 6.2.2.2 and Appendix B) to the environmental impacts of each abatement system are presented in Table 17. This table excludes directly emitting isobutane because the impacts for this scenario were dictated by the isobutane emission rate from the packaging manufacturing process (i.e., > 99% of the contribution for all impact categories was attributed to the isobutane emission rate). This table also excludes input parameters that contribute < 2 % to the sensitivity and uncertainty of the environmental impacts to focus on the most prominent inputs, which describe > 95 % of the total contribution. The impacts from the RTO were primarily affected by the mean isobutane

emission rate from the packaging manufacturing process ($\dot{m}_{op}$, > 60 % of effect on all impacts). The RTO impacts (Figure 56) were mainly attributed to isobutane consumption so it follows that changes in the isobutane emission rate (i.e., total isobutane consumption) has a large effect on the system impacts. Thus, future work to improve prediction of the impacts of the RTO should include direct measurement of the isobutane emission rate to reduce uncertainty.

Table 17: Percentage of the contribution of input parameters to the environmental impacts of isobutane abatement systems used to treat packaging manufacturing emissions

Parameter	Ozone depletion (%)	Global warming (%)	Smog (%)	Acidification (%)	Eutrophication (%)	Carcinogenics (%)	Non carcinogenics (%)	Respiratory effects (%)	Ecotoxicity (%)
RTO system									
Isobutane emission rate ($\dot{m}_{op}$)	60.8	97.8	97.8	68.7	99.8	98.8	99.5	89.3	99.7
Natural gas consumption (V_{ng})	39.1	1.3	-	20.1	-	-	-	-	-
RTO pressure drop (Δp_{RTO})	-	-	-	10.3	-	-	-	9.8	-
Total	99.9	99.9	98.5	99.1	99.9	99.5	99.9	99.2	99.9
GAC system									
Fraction of equilibrium adsorption capacity (f_a)	31.4	34.4	34.5	30.9	35.8	35.0	32.6	32.4	33.9
Saturation adsorption capacity (q_O)	31.3	34.0	34.2	30.3	35.6	34.8	32.0	31.8	33.4
Steam per adsorbent (S_{st})	30.5	18.3	20.6	6.0	16.7	20.5	8.1	8.4	14.2
Temperature (T)	6.2	6.9	6.9	6.2	7.2	7.0	6.6	6.5	6.8
Superficial velocity (v_{GACs})	-	5.3	2.6	24.2	-	-	17.7	18.9	9.3
Total	99.3	98.9	98.8	97.7	95.2	97.2	96.9	98.0	97.6
ACFC system									
Isobutane emission rate ($\dot{m}_{op}$)	45.9	89.3	64.0	89.8	44.8	43.7	89.9	90.0	89.2
Desorption isobutane concentration (C_{isod})	35.0	4.2	18.2	3.0	36.2	35.5	3.7	2.8	5.2
Saturation adsorption capacity (q_O)	6.8	-	2.5	-	6.8	6.7	-	-	-
Fraction of equilibrium adsorption capacity (f_a)	6.8	-	2.4	-	6.9	6.8	-	-	-
Temperature (T)	3.2	-	-	-	3.2	3.2	-	-	-
Electrothermal heating energy per adsorbate (S_{eh})	-	5.2	-	5.9	-	-	4.9	6.0	4.1
N_2 shipping distance	-	-	9.4	-	-	2.3	-	-	-
Total	97.7	98.7	96.5	98.7	97.9	98.2	98.5	98.7	98.5

*****Regenerative thermal oxidizer (RTO), granular activated carbon (GAC), activated carbon fiber cloth (ACFC), variables and variable input distributions described in Table 20-Table 23 of Appendix B

The impacts from using the GAC system are most affected by the fraction of the equilibrium adsorption capacity used during an adsorption cycle (f_a) and the saturation adsorption capacity (q_O), which are both used to determine the effective adsorption capacity of isobutane onto the GAC (Table 17). The values from Table 17 indicate that the adsorption capacity input parameters have the largest effect on the system impacts while Figure 56 demonstrates that regeneration steam consumption is a major component contributing to the GAC impacts. This trend is due to the adsorption capacity input parameters being used to predict the steam consumption. The steam scaling factor for the GAC model (S_{st}) is directly related to the mass of adsorbent (i.e., kg steam required/kg adsorbent) such that increasing GAC adsorption capacity (i.e., kg/kg) reduces the steam requirement for a given mass of adsorbed isobutane, which reduces the steam consumption and the corresponding impacts. This GAC system model can be improved in the future by improving the steam requirement predictions with a term that includes more parameters (e.g., adsorbent mass, adsorbed mass, and adsorbate composition).

The ACFC system impacts are dominated by electricity usage and N_2 consumption (Figure 56), while the input parameters that have the largest effect on the ACFC system impacts are the mean isobutane emission rate ($\dot{m}_{op}$) and the isobutane concentration at the inlet of the compressor (C_{isod}) (Table 17). The mean isobutane emission rate affects the impacts from electricity usage because the scaling factor used to predict ACFC regeneration heating (S_{eh}) assumes that the electrothermal heating energy is proportional to the mass of isobutane that is adsorbed during the preceding adsorption cycle. Thus, for this model, increasing the isobutane emission rate increases the total mass of isobutane that must be removed from the ACFC, which increases the electricity requirements for electrothermal regeneration. This ACFC system design

model can be improved in future work by predicting electrothermal heating with a term that includes more parameters (e.g., adsorbent mass, adsorbed mass, and adsorbate composition). The isobutane concentration at the inlet of the compressor has the largest effect on the ACFC system eutrophication impacts (Table 17), which is dominated by N_2 consumption (Figure 56), because isobutane concentration is used to determine the N_2 requirements for electrothermal regeneration. This ACFC system model can be improved in the future by improving the prediction of N_2 consumption with a term that models the isobutane concentration at the inlet of the compressor (e.g., using the DR equation, regeneration temperature, and N_2 gas flow rate). In summary, the ACFC system impacts can be reduced by reducing the electricity and N_2 requirements for electrothermal heating, which are most sensitive to the mean isobutane emission rate and the isobutane concentration at the inlet of the compressor, respectively.

The purified gas (i.e., 98 % isobutane removed) that is exhausted from the abatement systems can potentially be reused for the packaging manufacturing process resulting in a closed loop system for the carrier gas. This provides a unique opportunity for the ACFC system, because N_2 (i.e., instead of air) can be used as the inert background gas for packaging production, which would eliminates the N_2 that is required for regeneration heating. Instead the system will require enough N_2 to initially fill the abatement system and packaging manufacturing system and will only require additional N_2 to account for system leaks. The impacts of treating the exhaust gas stream (i.e., electricity produced using natural gas) relative to the reduction in system nitrogen consumption (i.e., from using recirculated N_2 as the carrier gas) normalized to the impacts from treating the exhaust gas stream with a granular activated carbon (GAC) system are presented in Figure 59. For an 82 % reduction in N_2 consumption (i.e., corresponding to carrier gas recirculation with 18% N_2 loss from system leaks), the ACFC system outperforms the

GAC system in 5 of the 9 impact categories and is within 100 % of the GAC system in 3 other categories. Thus, future work that studies the feasibility of N_2 carrier gas recirculation can potentially reduce the impacts of the ACFC system so that it is more competitive with the GAC system.

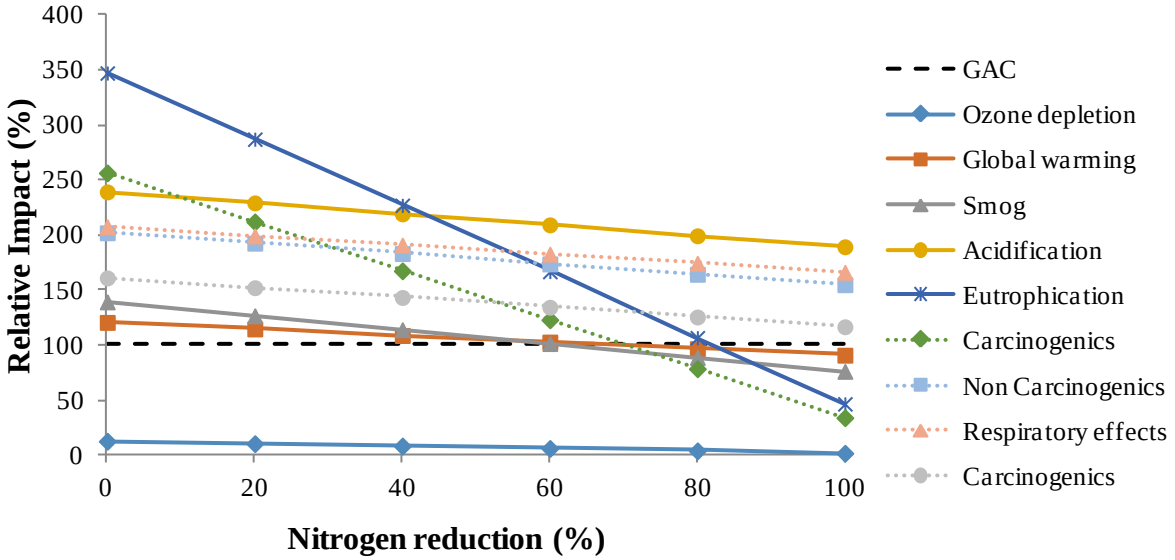

Figure 59: Impacts of treating a packaging manufacturing exhaust gas stream using an activated carbon fiber cloth system relative to reduction in system N_2 consumption normalized to the impacts from treating the exhaust gas stream with a granular activated carbon (GAC) system

The NPVs and corresponding uncertainties for each abatement system are provided in Figure 60. The uncertainty of the NPV for the RTO (i.e., standard deviation of $240,000) is smaller than that of the adsorption systems (i.e., standard deviations > $1M) because the NPV of the adsorption systems is more affected by the operating conditions than that of the RTO (i.e., supported by results presented in Table 18). However, the NPVs of the adsorption systems are greater than two standard deviations from that of the RTO suggesting they are more economical options for treating the packaging manufacturing exhaust gas despite being more affected by the operating conditions than the NPV of the RTO.

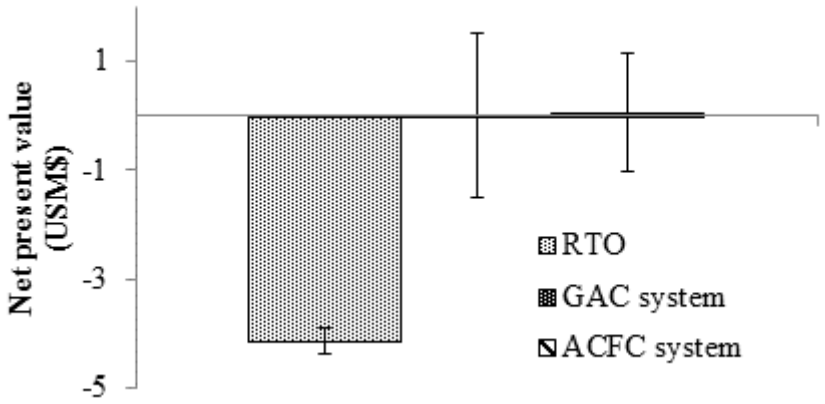

*Regenerative thermal oxidizer (RTO), granular activated carbon (GAC), activated carbon fiber cloth (ACFC)

Figure 60: Net present value of abatement systems to treat isobutane emissions from packaging manufacturing for 20 yr, in which electricity is produced from natural gas and error bars indicate standard deviations

The percentages of the contributions of the input parameters (i.e., defined in section 6.2.2.2 and Table 24 of Appendix B) to the NPV of each abatement system are presented in Table 18. The costs for the RTO are primarily affected by the cost for natural gas (i.e., price of natural gas and natural gas usage (V_{ng})). By contrast, the adsorption systems are most affected by the mean isobutane emission rate ($\dot{m}_{op}$) because this parameter directly affects the amount of isobutane that can be recovered (i.e., avoided product cost). These results demonstrate that the RTO is the more economically competitive when natural gas usage is minimized and natural gas is inexpensive, while the adsorption systems are more economically competitive for applications as isobutane emission rates increase.

Table 18: Percentage of the contribution of input parameters to the net present value of select volatile organic compound abatement systems used to treat packaging manufacturing emissions

Parameter	RTO system (%)	GAC system (%)	ACFC system (%)
Isobutane emission rate ($\dot{m}_{op}$)	-	58.0	60.2
Price of isobutane	-	6.2	11.0
Fraction of equilibrium adsorption capacity	-	12.9	10.5
Saturation adsorption capacity (q_O)	-	12.9	9.7
Temperature (T)	-	2.4	2.9
Price of ACFC	-	-	2.0
ACFC system adsorption cycle duration ($t_{ACFCads}$)	-	-	2.0
Abatement system expected lifetime (t_l)	-	3.9	-
Price of natural gas	60.0	-	-
Natural gas consumption (V_{ng})	14.7	-	-
RTO unit cost	9.3	-	-
RTO pressure drop (Δp_{RTO})	8.5	-	-
Operating labor and maintenance cost	2.4	-	-
Total	94.9	96.3	98.4

*****Regenerative thermal oxidizer (RTO), granular activated carbon (GAC), activated carbon fiber cloth (ACFC), variables and variable input distributions described in Table 20-Table 24 of Appendix B

Chapter 7: Summary and Conclusions

For this research, a new ACFC-ESA system was developed, tested, and assessed that provides real-time detection of adsorbed mass while eliminating the need for hydrocarbon and direct-contact temperature sensors. This system provides real-time monitoring of ACFC temperature and adsorbed VOC mass based on electrical properties of the ACFC to control adsorption cycles, regeneration cycles, and cyclic ESA based on these electrical values. This study provides significant improvements to the state of knowledge of vapor/gas control with ESA as summarized in the following sections. The summary, conclusions, and future work for Chapters 2-6 are presented in section 7.1-7.5, respectively. A prioritized list of future work related to this dissertation is presented in section 7.6.

7.1. Effect of ACFC Micropore Volume and Surface Oxygen Content on the Electrical Resistivity of ACFC during an Adsorption Cycle

The electrical resistivity of ACFC samples with select micropore volumes and surface O contents was characterized during isobutane adsorption and was related to the nanographitic structure of the samples (Johnsen *et al*., 2013a; Johnsen *et al*., 2013b; Johnsen *et al*., 2014a; Johnsen *et al*., 2014b). This is the first research to describe the effects of isobutane adsorption on the electrical resistivity of ACFC and to relate these effects to ACFCs nanographitic structure, micropore volume, and surface O content. This research reveals that increasing ACFC micropore volume results in a larger change in resistivity after an isobutane adsorption cycle due to increased adsorption capacity with increasing micropore volume, while increasing surface O improves ACFC's ability to sense adsorbed mass based on resistivity up to a threshold O value (i.e., 3.8 at. %). These results can be used to identify desirable ACFC properties to detect

adsorbed mass based on resistivity measurements so that ACFC can be nano-tailored to sense adsorbed VOC. Real-time detection of adsorbed VOC based on electrical resistivity measurements allows an adsorption cycle to be automatically ended before VOC breakthrough occurs, improving ACFC-ESA capture efficiency (i.e., reducing VOC emissions to the atmosphere) and removing the need for hydrocarbon detectors (i.e., providing a simpler ACFC-ESA system with lower cost). It would be beneficial for future studies to be performed to describe the effects of competitive adsorption on the electrical resistivity of ACFC so that measured resistivity values can be used to determine when to end an adsorption cycle for applications with competitive adsorption. Understanding the change in electrical resistivity during competitive adsorption also requires better understanding of the effect of the adsorbate structure (e.g., molecule size), composition, surface diffusivity, and relative pressure on ACFC's electrical resistivity beyond this research. Future research that considers a range of adsorbate relative pressures and relates the change in ACFC resistivity during adsorption to properties of the adsorbate would greatly expand the applicability of sensing adsorbed mass based on electrical resistivity. It would also be beneficial for future studies to determine if the change in resistance per unit mass adsorbed can be used to detect whether surface coverage or micropore filling is occurring. Additionally, future work should be performed to develop a physical model that relates ACFC resistivity to micropore volume, surface oxygen content, and adsorbed mass.

7.2. Evaluation of the Effect of Heating Temperature and Power Profiles on Regeneration Heating Cycle Energy Efficiency

ACFC electrothermal heating was evaluated with a range of regeneration heating temperature and applied power profiles (Johnsen *et al*., 2011a). This is the first research to

develop ACFC electrothermal heating controllers to evaluate the effects of temperature oscillations, power oscillations, and magnitudes of the initial heating rate during electrothermal heating on the total regeneration energy efficiency (i.e., kJ/mol isobutane desorbed). This research reveals that energy requirements for regeneration were independent of differences in temperature/power oscillations, while increasing the maximum power application at lower ACFC temperatures decreased the regeneration energy consumption (i.e., 36% decrease in energy consumption for 100% increase in maximum power application). These results can be used to select regeneration temperature and power profiles that reduce energy consumption for a regeneration heating cycle, which can be used to reduce the total energy consumption for ACFC-ESA making this abatement system more economically feasible. Future work is needed to model the relationship between regeneration energy consumption and maximum power application to determine the optimal power supply for electrothermal regeneration of ACFC for select VOC abatement applications.

7.3. Automated Temperature Control of ACFC during a Regeneration Heating Cycle based on Resistance Measurements

A new method was developed and demonstrated to model the resistance of an ACFC cartridge and then control an automated ACFC regeneration heating cycle based on ACFC electrical resistance measurements (Johnsen and Rood, 2011b; Johnsen and Rood, 2012a). This new method was used to control ACFC temperature to within 2.3 % of electrothermal heating regeneration set-point temperatures demonstrating accurate temperature control without requiring direct-contact temperature sensors (e.g., thermocouples). Additionally, when

electrothermal heating ACFC to 175°C for 900 cycles, the resistance and adsorption capacity of an ACFC cartridge remained within 3 % and 2 %, respectively, demonstrating longevity of this resistance control method. This research provides a method to predict the resistance of an ACFC cartridge and a method to electrothermally heat the cartridge based on rapid electrical resistance measurements, removing the need for direct-contact temperature sensors providing a simple, cost-efficient, and long-term regeneration technique for ESA systems. Increasing the maximum power application for electrothermal heating at lower ACFC temperatures was shown to reduce the regeneration energy consumption (Chapter 2), so it would be beneficial for future work to characterize this new resistance control method with a range of maximum power application values to reduce energy consumption.

7.4. Monitoring and Control of Electrothermal Swing Adsorption based on Electrical Properties of the Adsorbent

A new automated system to monitor and control ACFC-ESA that is based entirely on remote electrical measurements (i.e., eliminates the need for hydrocarbon and local temperature sensors) was developed and demonstrated (Johnsen and Rood, 2012b). First, the electrical resistance of small samples of ACFC (i.e., 1 g) were characterize based on adsorbent temperature and mass of adsorbed organic gas/vapor. These relationships were then used to develop control logic to monitor and control ESA cycles for ACFC cartridges (i.e., 115 g) based on measured resistance and applied power values. Continuous sets of adsorption, regeneration, and cooling cycles were performed sequentially based entirely on remote electrical measurements achieving $\geq$ 99.5 % isobutane capture efficiency at inlet concentrations of 2,000 and 4,000 ppm_v isobutane in air, demonstrating proof of concept of this novel cyclic ESA system that does not require

hydrocarbon or local temperature sensors (i.e., reducing system cost and complexity). This new ESA system has improved capture efficiency compared to existing ESA systems because the adsorption cycles end before adsorbate breakthrough occurs providing a more economically competitive ESA system. Future studies should be performed to operate the new ESA system with increased capture efficiency with the regeneration temperature profile that was used to operate the previous ESA system (Mallouk *et al*., 2010) to compare this system to a benchmark (i.e., ESA controlled with hydrocarbon and direct-contact temperature sensors) for regeneration electricity requirements. It would be beneficial for future studies to characterize this new ESA system that is operated based on electrical properties of the adsorbent with alternative adsorbates and competitive adsorption to expand the applicability of this system. Additionally, future work should be performed to describe the effect of ACFC cartridge geometry on the energy requirements for the heating portion of a regeneration cycle and the duration of the cooling portion of the regeneration cycle to provide recommendations for cartridge design to reduce system energy consumption and ACFC requirements. For example, a pleated cartridge provides increased area for convective and radiative cooling per cartridge volume and thus can reduce ACFC regeneration cooling time but may increase regeneration heating requirements.

7.5. Environmental and Economic Sustainability of ACFC-ESA Compared to Alternative Volatile Organic Compound Abatement Systems

A life cycle assessment and a cost assessment were performed to compare the impacts from treating a packaging manufacturing exhaust gas stream with the ACFC-ESA system from this research to more conventional air pollution abatement systems (i.e., RTO and GAC systems). The ACFC and GAC systems were environmentally and economically competitive

with each other and were an improvement over the RTO due to the recovered isobutane for the packaging manufacturing process. The environmental impacts of the ACFC system were primarily affected by electricity and N_2 consumption during regeneration heating suggesting ACFC system design improvements should focus on methods to reduce the consumption of these resources. This research is valuable because it demonstrates the feasibility of using this new ESA control method based on a life cycle assessment and a cost assessment and identifies key areas for ACFC-ESA design improvement. It would be beneficial to perform future work to improve the LCA model and ACFC-ESA system design. The GAC system model (i.e., a component of the LCA model) can be improved in the future by improving the modeled values for regeneration steam requirements (e.g., using a term that includes adsorbent mass, adsorbed mass, and adsorbate composition). The ACFC system model (i.e., a component of the LCA model) can be improved in the future by improving the prediction of N_2 consumption with a term that models the isobutane concentration at the inlet of the compressor (e.g., using the DR equation, regeneration temperature, and N_2 gas flow rate). Additionally, future work that studies the feasibility of N_2 carrier gas recirculation can potentially reduce the impacts of the ACFC system so that it is more competitive with the GAC system. Future LCAs should also be performed to 1) compare this new ACFC-ESA system controlled based on electrical properties of the adsorbent to the existing ACFC-ESA system that requires hydrocarbon and direct-contact temperature sensors, 2) compare the use of adsorbents with select micropore volumes and surface oxygen contents, and 3) compare abatement devices for alternative applications that emit VOCs that can be treated using disposal or recovery (e.g., treatment of VOC emissions from spray coating operations).

7.6. Prioritized list of future work to improve monitoring and control of electrothermal swing adsorption based on electrical properties of the adsorbent

The future work that is recommended in sections 7.1-7.5 is provided here in prioritized tiers (i.e., highest, middle, and lowest priority) as a guideline for future research. All future work objectives within a tier are considered to have equal priority.

Highest priority tier - Research areas that allow this new ACFC system to be used for a wider range of applications or that involve ACFC system design improvements (i.e., have been determined to be key areas to improve the system design based on LCA results).

- Determine the effects of adsorbate structure, composition, surface diffusivity, and relative pressure on the change in ACFC resistivity during an adsorption cycle (section 7.1)
- Characterize the effects of competitive adsorption on the electrical resistivity of ACFC (section 7.1)
- Develop a physical model that relates ACFC resistivity to micropore volume, surface oxygen content, and adsorbed mass (section 7.1)
- Model the relationship between regeneration energy consumption and maximum power application to determine optimal heating temperature profiles (section 7.2)
- Evaluate N_2 carrier gas recirculation for cyclic operation (section 7.4)
- Develop a LCA to compare abatement devices for alternative applications that emit VOCs that can be treated using disposal or recovery (section 7.5)

Middle priority tier - Research areas that benchmark the new ACFC system, involve potential ACFC system design improvements (i.e., scope of improvements are uncertain), or provide potential model improvements (i.e., scope of improvements are uncertain).

- Describe the effect of ACFC cartridge geometry on the energy requirements during cyclic operation (section 7.4)
- Operate the new ESA system with the regeneration temperature profile that was used to operate the previous ESA system to benchmark this system (section 7.4)
- Improve the LCA modeled values for GAC regeneration steam requirements and ACFC N_2 requirements (section 7.5)
- Develop a LCA to compare this new ACFC-ESA system controlled based on electrical properties of the adsorbent to the existing ACFC-ESA system that requires hydrocarbon and direct-contact temperature sensors (section 7.5)

Lowest priority tier – Research based on a hypothesis without experimental evidence (i.e., high level of uncertainty), that has been conceptually developed and is an incremental change compared to existing results, or that unlikely to significantly improve ACFC system performance based on LCA evidence.

- Determine if the change in resistance per unit mass adsorbed can be used to detect whether surface coverage or micropore filling is occurring during adsorption (section 7.1)
- Characterize electrothermal heating using resistance control with a range of maximum power application values (section 7.3)

- Operate this new ESA system in cyclic mode with alternative adsorbates and with competitive adsorption (section 7.4)
- Develop a LCA to compare using adsorbents with select micropore volumes and surface oxygen contents for this ACFC system (section 7.5)

Appendix A: Desorption modeling parameters

Table 19: Input parameters for desorption mass and energy balances for electrothermal regeneration of an activated carbon fiber cloth (ACFC) cartridge

Parameter	Description	Value	Reference
A_1	Antoine equation constant 1 (-)	100.18	(Perry and Green, 1997)
A_2	Antoine equation constant 2 (-)	-4814.9	(Perry and Green, 1997)
A_3	Antoine equation constant 3 (-)	-13.541	(Perry and Green, 1997)
A_4	Antoine equation constant 4 (-)	0.0201	(Perry and Green, 1997)
A_5	Antoine equation constant 5 (-)	1	(Perry and Green, 1997)
A_{cond}	Area for conductive heat transfer (m^2)	0.000214	$\pi \cdot ({d_{to}}^2 - {d_{ti}}^2)$
A_{conv}	Area for convective heat transfer (m^2)	0.0314	$\pi \cdot H_{ACFCc} \cdot d_{ACFCo}$
A_{rad}	Area for radiative heat transfer (m^2)	0.0314	$\pi \cdot H_{ACFCc} \cdot d_{ACFCo}$
c_{ACFC}	Heat capacity (ACFC) (kJ/kg-K)	0.91	(Lo *et al*., 2002)
c_f	Heat capacity (stainless steel fittings) (J/g-K)	0.47	(Incropera and Dewitt, 1981)
c_g	Heat capacity (isobutane gas) (kJ/kg-K)	0.75	(Welty *et al*., 2007)
c_l	Heat capacity (liquid isobutane) (kJ/kg-K)	1.04	(Lide, 1993)
c_{N_2}	Heat capacity (gaseous N_2) (kJ/kg-K)	2.23	(Lange, 1992)
c_w	Heat capacity (Pyrex vessel) (kJ/kg-K)	1.64	(Lange, 1992)
E	Adsorption energy (kJ/kmol)	18,000	Equation 9
g	Acceleration of gravity (m/s^2)	9.8	-
ΔH_s	Isosteric heat of adsorption (isobutane onto ACFC) (kJ/kg)	1.0e-3	Equation 11
h	Convective heat transfer coefficient (W/m^2-K)	f(T)	(Incropera and Dewitt, 1981)
L_{cond}	Length for conductive heat transfer (m)	0.0635	Measured length of tube exiting ACFC cartridge
L_{conv}	Length for convective heat transfer (m)	0.25	Measured height of cartridge

Table 19 (continued)

Parameter	Description	Value	Reference
M_{iso}	Molecular weight (isobutane)	58.1	-
m_{ACFC}	Mass (ACFC) (kg)	0.115	Gravimetric balance
m_f	Mass (cartridge fittings) (kg)	0.212	Gravimetric balance
m_w	Mass (vessel wall) (kg)	0.381	Gravimetric balance
Nu_L	Nusselt number (-)	f(T)	Equation 18
P	Pressure (atm)	1	Ambient pressure
P_{IV}	Electrical power (kW)	0-0.3	Equation 16
Pr	Prandtl number (-)	f(T)	(Incropera and Dewitt, 1981)
Q_{N_2}	Flow rate (N_2) (SLPM)	8.3e-6	Controlled with mass flow controller
q	Mass of isobutane adsorbed per mass of adsorbent (kg/kg)	0-0.347	Calculated from W_i
q_o	Saturation mass of isobutane adsorbed per mass of adsorbent (kg/kg)	0.347	Calculated from W_{io}
Ra_L	Rayleigh number (-)	f(T)	Equation 19
R_g	Ideal gas law constant (m^3-atm/kmol-K)	0.0821	-
T	ACFC temperature (K)	297-473	Measured with thermocouple or selected as set-point
T_∞	Ambient temperature (K)	297-300	Measured with thermocouple
t	Time (s)	0-3600	Measured with computer
V_v	Volume (vessel) (m^3)	1.4e-3	Measured with water displacement
W_i	Volume of isobutane adsorbed per mass of adsorbent (m^3/kg)	0-5.8e-4	Calculated from DR equation
W_o	Total ACFC micropore volume per mass of adsorbent (m^3/kg)	5.8e-4	Calculated from isotherm
y	Mole fraction of isobutane in the gas stream (-)		Equation 15
α_d	Thermal diffusivity (m^2/s)	f(T)	(Incropera and Dewitt, 1981)
γ	Kinematic gas viscosity (m^2/s)	f(T)	(Incropera and Dewitt, 1981)

*****Dubinin-Radushkevich (DR) equation

Table 19 (continued)

Parameter	Description	Value	Reference
ε	Emissivity (ACFC) (-)	0.9	(Incropera and Dewitt, 1981)
ρ_{li}	Liquid density (isobutane) (kg/m^3)	598	(Haynes and Hiza, 1977)
σ	Stephen-Boltzmann constant ($kW/m^2\text{-}K^4$)	5.68e-11	(Incropera and Dewitt, 1981)
ω_{conv}	Thermal conductivity coefficient (N_2) (kW/m-K)	f(T)	(Incropera and Dewitt, 1981)
ω_{cond}	Thermal conductivity coefficient (stainless steel) ($kW/m^{2\text{-}}K$)	1.5e-2	(Incropera and Dewitt, 1981)

Appendix B: Life cycle assessment parameters

Table 20: Operating conditions and existing air pollution abatement system data for treatment of packaging manufacturing exhaust gas

Variable	Parameter	Value	CV
C_{isoe}	Isobutane concentration in exhaust gas (ppm_v)[a,b]	2,400-3,900	-
f_r	Abatement system isobutane removal efficiency (-)[c]	0.98	-
m_{RTOg}	Annual RTO incinerator bed gravel consumption (kg/yr)[d]	28,100	0.05
$\dot{m}_{op}$	Mean isobutane emission rate (kg/h)[a]	30.4	0.3
$\dot{m}_D$	Design isobutane emission rate (kg/h)[c]	47.2	-
Δp_{RTO}	RTO pressure drop (cm H_2O)[e]	48.3	0.2
Q_e	Exhaust gas flow rate (m^3/s)[a,b]	5.2-6.1	-
T	Temperature (°C)	25	0.2
t_l	Life time of abatement system (yr)[c]	20	-
t_{op}	Abatement system operating time (h/yr)[c]	8,712	-
V_{ng}	Annual RTO natural gas consumption (therm/yr)[d]	170,000	0.05

*Coefficient of variance (CV)

[a]Site engineer estimate, [b]uniform distribution was used for uncertainty with the indicated range provided by the site engineer, [c]site specific requirement for Indiana packaging manufacturing facility, [d]site specific data for Indiana packaging manufacturing facility, [e](USEPA, 2002)

Table 21: Granular activated carbon (GAC) system input data for determining life cycle inventory values

Variable	Parameter	Value	CV
b_1	Langmuir affinity constant (kPa^{-1})[a]	23.8	-
b_2	Toth constant (-)[a]	0.36	-
f_a	Ratio of equilibrium adsorption capacity to working adsorption capacity (-)[b]	0.5	0.2
f_{dc}	Fraction of time that drying/cooling occurs during a GAC regeneration cycle (%)[b]	0.4	0.2
ΔH_s	Isosteric heat of adsorption (kJ/kmol)[a]	42,500	0.2
Δp_{GACcw}	Cooling water pressure drop (cm H_2O)[b]	3048	0.2
q_O	Saturation concentration of isobutane on GAC (kg/kg)[a]	0.335	0.2
S_{cw}	Cooling water for condenser (L/kg steam)[b]	28.6	0.2
S_{dc}	Cooling air after regeneration (L air/kg adsorbent)[b]	6,320	0.2
S_{st}	Steam for regeneration (kg/kg adsorbent)[c]	0.3	0.2
S_{est}	Energy to produce steam (MJ/ kg)[d]	2.65	-
T_{ic}	Temperature of gas at the inlet of compressor (^oC)[e]	30	0.1
t_{GACads}	Duration of adsorption cycle (h)[e]	6	0.1
t_{GACdes}	Duration of desorption cycle (h)[e]	5	0.1
v_{GACs}	GAC bed superficial velocity (m/s)[b]	0.43	0.2

*Coefficient of variance (CV)

[a](Zhu *et al*., 2005), [b](USEPA, 2002), [c](Bansal and Goyal, 2005), [d]Energy to produce steam at 450 psig with feed water at 38 ^oC, [e]Design selection

Table 22: Activated carbon fiber cloth (ACFC) system input data for determining life cycle inventory values

Variable	Parameter	Value	CV
b_1	Langmuir affinity constant (kPa^{-1})[a]	49	-
b_2	Toth constant (-)[a]	0.38	-
C_{isod}	Mean concentration of adsorbate at inlet of compressor (%)[b]	40	0.2
d_{ACFCbc}	distance between ACFC cartridges (m)[c]	0.0508	0.1
d_{ACFCi}	ACFC cartridge inner diameter (m)[c]	0.0762	0.1
f_a	Ratio of equilibrium adsorption capacity to working adsorption capacity (-)[d]	0.5	0.2
f_c	Fraction of time the compressor is active during regeneration cycle (%)[e]	0.17	0.2
H_{ACFCc}	ACFC cartridge height (m)[c]	2	0.1
ΔH_s	Heat of adsorption (kJ/kmol)[a]	64,000	0.2
N_{ACFCl}	ACFC layers per cartridge (#)[c]	40	0.1
Δp_{ACFCl}	Pressure drop across a single sheet of ACFC ($\frac{cm\ H_2O}{cm/s}$)[f]	0.042	0.2
q_O	Saturation concentration of isobutane on ACFC (kg/kg)[a]	0.342	0.2
S_{eh}	Energy for electrothermal heating (kJ/mol)[b]	646	0.2
T_{ic}	Temperature of gas at inlet of compressor (^oC)[c]	30	-
$t_{ACFCads}$	Duration of ACFC adsorption cycle (h)[c]	1	0.1
W_{ACFCv}	Maximum vessel ACFC width (m)[c]	2.4	0.1

*Coefficient of variance (CV)

[a]Results from section 5.3.1.1, [b]results from section 3.3, [c]design selection, [d](USEPA, 2002), [e](Mallouk *et al*., 2011), [f](Sullivan *et al*., 2001)

Table 23: Shipping distances for operating materials for determining life cycle inventory values

Parameter	Value	CV
Isobutane shipping to plant by truck (km)	500	0.5
Gravel shipping to plant by truck (km)	500	0.5
N_2 shipping to plant by truck (km)	500	0.5
Carbon (GAC and ACFC) shipping to plant by truck (km)	3000	0.5
Carbon (GAC and ACFC) shipping to plant by freight (km)	8000	0.5
Carbon (GAC and ACFC) to landfill by truck (km)	50	0.5

*Coefficient of variance (CV), granular activated carbon (GAC), activated carbon fiber cloth (ACFC)

Table 24: Input data for air pollution abatement system cost assessments

Parameter	Value	CV
GAC ($/kg)[a]	2.2	0.1
ACFC ($/kg)[b]	98	0.1
Electricity from grid ($/kWh)[c]	0.073	0.1
Natural gas ($/kg)[c]	0.44	0.1
Steam ($/kg)[d]	0.023	0.1
Cooling water ($/L)[d]	$6.1 \cdot 10^{-5}$	0.1
Isobutane ($/L)[c]	0.56	0.1
Liquid N_2 ($/$m^3$)[c]	19.7	0.1
GAC replacement fee ($/kg)[d]	0.11	0.1
Discount rate (-)[e]	0.045	0.1
RTO[c]		
RTO ($)	277,000	0.1
Plumbing ($)	20,000	0.1
Tax and freight ($)	10,000	0.1
Instrumentation ($)	30,000	0.1
Foundation and supports ($)	10,000	0.1
Electric ($)	10,000	0.1
Piping ($)	50,000	0.1
Start-up ($)	12,000	0.1
Permitting ($)	20,000	0.1
Stack testing ($)	25,000	0.1
Replacement parts ($/yr)	30,000	0.1
Operation labor and maintenance ($/yr)	18,883	0.1

*Coefficient of variance (CV), granular activated carbon (GAC), activated carbon fiber cloth (ACFC), regenerative thermal oxidizer (RTO)

[a](USEPA, 2002), [b](Cheng, 2010), [c]Site specific data for Indiana packaging manufacturing facility, [d](USEPA, 2002), [e]30 yr mean interest rate of United States federal funds (USFED, 2014)

Table 25: EcoInvent 3 database values used for life cycle assessment

Parameter	EcoInvent 3 database material/process
Isobutane production	Butanes from butenes, at plant RER/U
Isobutane direct emission	Isobutane[a]
Isobutane emissions from burning	Heat, natural gas, at boiler modulating <100kW/RER U[b]
GAC	Described in Table 26
ACFC	Described in Table 26
Electricity (US average)	Electricity, medium voltage, at grid/US U
Electricity (Georgia)	Described in Table 27
Electricity (Indiana)	Described in Table 27
Electricity (Illinois)	Described in Table 27
Electricity (Michigan)	Described in Table 27
Electricity (North Carolina)	Described in Table 27
Electricity from natural gas	Electricity, natural gas, at power plant/US U
Natural gas combustion	Heat, natural gas, at boiler modulating <100kW/RER U
Gravel production	Gravel, unspecified at mine/CH U
Steam production	Steam, for chemical processes, at plant/RER U, modified[c]
N_2 production	Nitrogen, liquid, at plant/RER U, modified[c]
Road transport	Transport, lorry >16t, fleet average/RER U
Boat transport	Operation, transoceanic freight ship/OCE U
Activated carbon landfill (GAC and ACFC)	Disposal, inert waste, 5 % water, to inert landfill/CH U

*Granular activated carbon (GAC), activated carbon fiber cloth (ACFC), United States (US), Europe (RER), unit process (U), Switzerland (CH), Oceanic (OCE)

[a]Contains impacts from direct isobutane emission, [b]database values were modified to only include emissions to air from burning natural gas such that the database air emissions for particulate matter, SO_2, NO_x, N_2O, CO_2, and CO were updated to the values for burning butane (USEPA, 2011b). [c]Database material was modified to be produced using US average electricity

Table 26: Materials to produce 1 kg of granular activated carbon (GAC) and 1 kg of activated carbon fiber cloth (ACFC)

Parameter	Value	EcoInvent 3 database material/process
Feedstock for 1 kg of GAC		
Coal production (kg)[a]	1	Hard coal coke, at plant/RER U
Feedstock for 1 kg of ACFC		
Polyacrylonitrile fiber production (kg)[b]	3[c]	Polyacrylonitrile fibres, from acrylonitrile and methacrylate, prod. Mix, PAN w/o additives EU-27 S
Production materials for 1 kg of activated carbon (GAC or ACFC)		
Coal combustion (MJ)[a]	60.8	Hard coal coke, burned in stove, 5-15kW/RER U
Natural gas combustion (MJ)[a]	13.2	Heat, natural gas, at boiler modulating <100kW/RER U
Electricity consumption (MJ)[a]	5.8	Electricity, high voltage, at grid/US U
Deionized water (kg)[a]	12	Water, deionised, at plant/CH U

*Europe (RER), unit process (U), European Union (EU-27), system process (S), Switzerland (CH)

[a]Values for GAC production (Gabarrell *et al*., 2012), [b]Polyacrylonitrile fiber used as surrogate for Novoid, [c]Required feedstock based on ACFC-15 yield (Hayes, 1994)

Table 27: Electricity production source profile for the five states with the largest volatile organic compound emissions from extruded foam manufacturing

Electricity source	**EcoInvent 3 database material/process**	**North Carolina[a]**	**Georgia[a]**	**Indiana[a]**	**Michigan[a]**	**Illinois[a]**
Natural gas (%)	Electricity, natural gas, at power plant/US U	26.9	29.9	5.3	12.1	1.2
Coal (%)	Electricity, hard coal at power plant/US U	31.8	35.1	88.7	43.5	42.6
Nuclear (%)	Electricity, nuclear, at power plant/US U	33.1	27.2	0.0	35.0	48.6
Hydroelectric (%)	Electricity, hydropower, at power plant/CH U	4.6	4.0	0.3	1.6	0.0
Other renewables (%)[b]	Electricity, at wind power plant 800kW/RER U	3.4	3.7	5.5	7.6	7.6

*United States (US), unit process (U), Switzerland (CH), Europe (RER)
[a](USEIA, 2014a), [b]Other renewables are represented with wind power

Table 28: Annual environmental impacts from directly emitting isobutane from packaging manufacturing

Parameter	**Ozone depletion (kg CFC-11 eq)**	**Global warming (kg CO_2 eq)**	**Smog (kg O_3 eq)**	**Acidification (mol H^+ eq)**	**Eutrophication (kg N eq)**	**Carcinogenics (CTUh)**	**Non Carcinogenics (CTUh)**	**Respiratory effects (kg PM_{10} eq)**	**Ecotoxicity (CTUe)**
Isobutane production	5.00E-02	1.85E+06	3.57E+04	1.93E+05	1.80E+03	2.51E-02	1.18E-01	7.23E+02	2.53E+06
Isobutane emission	0	0	3.25E+05	0	0	0	0	0	0
Isobutane lorry	3.77E-04	1.76E+04	3.61E+03	6.81E+03	2.38E+01	1.08E-03	1.23E-03	1.98E+01	1.55E+04
Total	5.04E-02	1.87E+06	3.65E+05	2.00E+05	1.83E+03	2.61E-02	1.19E-01	7.43E+02	2.55E+06

Table 29: Annual environmental impacts from treating isobutane emissions from packaging manufacturing with a regenerative thermal oxidizer

Parameter	**Ozone depletion (kg CFC-11 eq)**	**Global warming (kg CO_2 eq)**	**Smog (kg O_3 eq)**	**Acidification (mol H^+ eq)**	**Eutrophication (kg N eq)**	**Carcinogenics (CTUh)**	**Non Carcinogenics (CTUh)**	**Respiratory effects (kg PM_{10} eq)**	**Ecotoxicity (CTUe)**
Isobutane production and combustion emissions	5.00E-02	1.85E+06	3.57E+04	1.93E+05	1.80E+03	2.51E-02	1.18E-01	7.23E+02	2.53E+06
Isobutane emission	0	0	6.50E+03	0	0	0	0	0	0
Electricity at grid (Indiana fuel mix)	1.07E-02	4.23E+05	2.19E+04	1.40E+05	1.64E+03	2.37E-02	1.28E-02	3.90E+02	2.99E+05
Electricity at grid (North Carolina fuel mix)	1.20E-02	2.43E+05	9.83E+03	8.95E+04	6.64E+02	1.00E-02	1.30E-02	2.71E+02	1.79E+05
Electricity at grid (Georgia fuel mix)	1.20E-02	2.43E+05	9.83E+03	8.95E+04	6.64E+02	1.00E-02	1.30E-02	2.71E+02	1.79E+05
Electricity at grid (Michigan fuel mix)	1.52E-02	2.35E+05	1.13E+04	8.09E+04	8.15E+02	1.24E-02	1.35E-02	2.40E+02	1.81E+05
Electricity at grid (Illinois fuel mix)	1.89E-02	2.02E+05	1.07E+04	6.66E+04	7.96E+02	1.23E-02	1.45E-02	1.98E+02	1.65E+05
Electricity at grid (Natural gas)	2.46E-04	2.65E+05	3.74E+03	1.20E+05	3.59E+01	5.37E-04	1.13E-02	3.85E+02	1.70E+05
Natural gas consumption	2.46E-01	1.38E+06	1.98E+04	6.66E+05	3.84E+02	1.38E-02	1.30E-02	1.95E+02	1.70E+05
Gravel production	1.17E-05	7.90E+01	1.32E+02	3.18E+01	2.37E-01	1.11E-05	2.06E-05	1.64E-01	1.47E+02
Isobutane lorry	3.77E-04	1.76E+04	3.61E+03	6.81E+03	2.38E+01	1.08E-03	1.23E-03	1.98E+01	1.55E+04
Gravel lorry	4.01E-05	1.87E+03	3.84E+02	7.24E+02	2.53E+00	1.15E-04	1.31E-04	2.11E+00	1.65E+03

Table 29 (continued)

Parameter	Ozone depletion (kg CFC-11 eq)	Global warming (kg CO_2 eq)	Smog (kg O_3 eq)	Acidification (mol H^+ eq)	Eutrophication (kg N eq)	Carcinogenics (CTUh)	Non Carcinogenics (CTUh)	Respiratory effects (kg PM_{10} eq)	Ecotoxicity (CTUe)
Total (Electricity from Indiana fuel mix)	3.08E-01	3.67E+06	8.80E+04	1.01E+06	3.85E+03	6.37E-02	1.45E-01	1.33E+03	3.02E+06
Total (Electricity from North Carolina fuel mix)	3.09E-01	3.49E+06	7.60E+04	9.56E+05	2.88E+03	5.00E-02	1.46E-01	1.21E+03	2.90E+06
Total (Electricity from Georgia fuel mix)	3.09E-01	3.49E+06	7.60E+04	9.56E+05	2.88E+03	5.00E-02	1.46E-01	1.21E+03	2.90E+06
Total (Electricity from Michigan fuel mix)	3.12E-01	3.48E+06	7.74E+04	9.48E+05	3.03E+03	5.24E-02	1.46E-01	1.18E+03	2.90E+06
Total (Electricity from Illinois fuel mix)	3.16E-01	3.45E+06	7.68E+04	9.33E+05	3.01E+03	5.23E-02	1.47E-01	1.14E+03	2.88E+06
Total (Electricity from natural gas)	2.97E-01	3.52E+06	6.99E+04	9.87E+05	2.25E+03	4.06E-02	1.44E-01	1.33E+03	2.89E+06

Table 30: Annual environmental impacts from treating isobutane emissions from packaging manufacturing with a granular activated carbon system

Parameter	**Ozone depletion (kg CFC-11 eq)**	**Global warming (kg CO_2 eq)**	**Smog (kg O_3 eq)**	**Acidification (mol H^+ eq)**	**Eutrophication (kg N eq)**	**Carcinogenics (CTUh)**	**Non Carcinogenics (CTUh)**	**Respiratory effects (kg PM_{10} eq)**	**Ecotoxicity (CTUe)**
Activated carbon production	5.91E-04	1.85E+04	6.43E+02	5.89E+03	5.42E+01	8.43E-04	1.10E-03	2.14E+01	1.13E+04
Isobutane production	9.62E-04	2.04E+04	7.14E+02	3.34E+03	3.06E+01	4.30E-04	2.21E-03	1.34E+01	4.95E+04
Isobutane emission	0	0	6.50E+03	0	0	0	0	0	0
Electricity at grid (Indiana fuel mix)	7.85E-03	3.10E+05	1.60E+04	1.03E+05	1.20E+03	1.73E-02	9.34E-03	2.86E+02	2.19E+05
Electricity at grid (North Carolina fuel mix)	9.73E-03	1.61E+05	6.54E+03	5.93E+04	4.42E+02	6.74E-03	9.65E-03	1.81E+02	1.21E+05
Electricity at grid (Georgia fuel mix)	8.80E-03	1.78E+05	7.19E+03	6.55E+04	4.86E+02	7.33E-03	9.49E-03	1.98E+02	1.31E+05
Electricity at grid (Michigan fuel mix)	1.11E-02	1.72E+05	8.24E+03	5.92E+04	5.97E+02	9.04E-03	9.87E-03	1.76E+02	1.32E+05
Electricity at grid (Illinois fuel mix)	1.39E-02	1.48E+05	7.81E+03	4.87E+04	5.83E+02	8.97E-03	1.06E-02	1.45E+02	1.21E+05
Electricity at grid (Natural gas)	1.80E-04	1.94E+05	2.74E+03	8.79E+04	2.63E+01	3.93E-04	8.30E-03	2.82E+02	1.25E+05
Steam production	8.54E-02	5.06E+05	1.08E+04	5.99E+04	1.51E+02	3.63E-03	7.76E-03	2.60E+02	2.16E+05
Isobutane lorry	7.54E-06	3.52E+02	7.22E+01	1.36E+02	4.76E-01	2.15E-05	2.46E-05	3.97E-01	7.54E-06
Activated carbon lorry	1.70E-05	7.92E+02	1.63E+02	3.07E+02	1.07E+00	4.86E-05	5.54E-05	8.94E-01	1.70E-05
Activated carbon transoceanic freight	2.40E-05	1.43E+02	5.53E+01	1.95E+02	1.89E-01	1.05E-06	3.10E-06	5.72E-01	2.40E-05
Activated carbon lorry to landfill	2.83E-07	1.32E+01	2.71E+00	5.11E+00	1.79E-02	8.09E-07	9.23E-07	1.49E-02	2.83E-07
Landfill activated carbon	5.62E-06	1.41E+01	3.02E+00	5.86E+00	1.83E-02	5.82E-07	6.77E-07	2.28E-02	8.40E+00

Table 30 (continued)

Parameter	Ozone depletion (kg CFC-11 eq)	Global warming (kg CO_2 eq)	Smog (kg O_3 eq)	Acidification (mol H^+ eq)	Eutrophication (kg N eq)	Carcinogenics (CTUh)	Non Carcinogenics (CTUh)	Respiratory effects (kg PM_{10} eq)	Ecotoxicity (CTUe)
Total (Electricity from Indiana fuel mix)	9.49E-02	8.56E+05	3.50E+04	1.72E+05	1.44E+03	2.23E-02	2.05E-02	5.82E+02	4.97E+05
Total (Electricity from North Carolina fuel mix)	9.68E-02	7.07E+05	2.55E+04	1.29E+05	6.79E+02	1.17E-02	2.08E-02	4.77E+02	4.00E+05
Total (Electricity from Georgia fuel mix)	9.58E-02	7.24E+05	2.61E+04	1.35E+05	7.24E+02	1.23E-02	2.06E-02	4.94E+02	4.09E+05
Total (Electricity from Michigan fuel mix)	9.82E-02	7.18E+05	2.72E+04	1.29E+05	8.34E+02	1.40E-02	2.10E-02	4.72E+02	4.10E+05
Total (Electricity from Illinois fuel mix)	1.01E-01	6.94E+05	2.68E+04	1.19E+05	8.20E+02	1.39E-02	2.17E-02	4.41E+02	3.99E+05
Total (Electricity from natural gas)	8.72E-02	7.40E+05	2.17E+04	1.58E+05	2.64E+02	5.37E-03	1.95E-02	5.78E+02	4.03E+05

Table 31: Annual environmental impacts from treating isobutane emissions from packaging manufacturing with an activated carbon fiber cloth system

Parameter	**Ozone depletion (kg CFC-11 eq)**	**Global warming (kg CO_2 eq)**	**Smog (kg O_3 eq)**	**Acidification (mol H^+ eq)**	**Eutrophication (kg N eq)**	**Carcinogenics (CTUh)**	**Non Carcinogenics (CTUh)**	**Respiratory effects (kg PM_{10} eq)**	**Ecotoxicity (CTUe)**
Activated carbon production	4.91E-05	1.35E+03	5.48E+01	3.13E+02	4.07E+00	6.07E-05	6.38E-05	1.21E+00	2.21E+03
Isobutane production	9.62E-04	2.04E+04	7.14E+02	3.34E+03	3.06E+01	4.30E-04	2.21E-03	1.34E+01	4.95E+04
Isobutane emission	0	0	6.5E+03	0	0	0	0	0	0
Electricity at grid (Indiana fuel mix)	2.63E-02	1.04E+06	5.38E+04	3.44E+05	4.02E+03	5.82E-02	3.13E-02	9.58E+02	7.35E+05
Electricity at grid (North Carolina fuel mix)	3.26E-02	5.40E+05	2.20E+04	1.99E+05	1.48E+03	2.26E-02	3.24E-02	6.08E+02	4.08E+05
Electricity at grid (Georgia fuel mix)	2.95E-02	5.96E+05	2.41E+04	2.20E+05	1.63E+03	2.46E-02	3.18E-02	6.65E+02	4.40E+05
Electricity at grid (Michigan fuel mix)	3.74E-02	5.76E+05	2.76E+04	1.99E+05	2.00E+03	3.03E-02	3.31E-02	5.89E+02	4.43E+05
Electricity at grid (Illinois fuel mix)	4.65E-02	4.96E+05	2.62E+04	1.63E+05	1.96E+03	3.01E-02	3.55E-02	4.86E+02	4.05E+05
Electricity at grid (Natural gas)	6.03E-04	6.51E+05	9.19E+03	2.95E+05	8.81E+01	1.32E-03	2.79E-02	9.46E+02	4.18E+05
N_2 production	9.07E-03	1.99E+05	9.35E+03	7.04E+04	7.64E+02	1.07E-02	7.71E-03	2.15E+02	1.60E+05
Isobutane lorry	7.54E-06	3.52E+02	7.22E+01	1.36E+02	4.76E-01	2.15E-05	2.46E-05	3.97E-01	3.09E+02
N_2 lorry	5.32E-07	2.48E+01	5.10E+00	9.62E+00	3.36E-02	1.52E-06	1.74E-06	2.80E-02	2.19E+01
Activated carbon lorry	4.52E-04	2.11E+04	4.33E+03	8.17E+03	2.85E+01	1.29E-03	1.47E-03	2.38E+01	1.86E+04
Activated carbon transoceanic freight	7.52E-07	4.49E+00	1.73E+00	6.13E+00	5.93E-03	3.29E-08	9.71E-08	1.79E-02	7.27E-01
Activated carbon lorry to landfill	8.87E-09	4.14E-01	8.50E-02	1.60E-01	5.60E-04	2.54E-08	2.89E-08	4.67E-04	3.64E-01
Landfill activated carbon	1.76E-07	4.42E-01	9.46E-02	1.84E-01	5.75E-04	1.82E-08	2.12E-08	7.16E-04	2.63E-01

Table 31 (continued)

Parameter	**Ozone depletion (kg CFC-11 eq)**	**Global warming (kg CO_2 eq)**	**Smog (kg O_3 eq)**	**Acidification (mol H^+ eq)**	**Eutrophication (kg N eq)**	**Carcinogenics (CTUh)**	**Non Carcinogenics (CTUh)**	**Respiratory effects (kg PM_{10} eq)**	**Ecotoxicity (CTUe)**
Total (Electricity from Indiana fuel mix)	3.69E-02	1.28E+06	7.48E+04	4.27E+05	4.85E+03	7.07E-02	4.28E-02	1.21E+03	9.66E+05
Total (Electricity from North Carolina fuel mix)	4.32E-02	7.83E+05	4.30E+04	2.81E+05	2.31E+03	3.51E-02	4.39E-02	8.62E+02	6.38E+05
Total (Electricity from Georgia fuel mix)	4.01E-02	8.39E+05	4.52E+04	3.02E+05	2.46E+03	3.70E-02	4.33E-02	9.19E+02	6.71E+05
Total (Electricity from Michigan fuel mix)	4.79E-02	8.19E+05	4.87E+04	2.81E+05	2.83E+03	4.28E-02	4.46E-02	8.43E+02	6.74E+05
Total (Electricity from Illinois fuel mix)	5.70E-02	7.39E+05	4.72E+04	2.46E+05	2.78E+03	4.25E-02	4.70E-02	7.40E+02	6.36E+05
Total (Electricity from natural gas)	1.11E-02	8.94E+05	3.02E+04	3.77E+05	9.16E+02	1.38E-02	3.93E-02	1.20E+03	6.49E+05

Appendix C: Nomenclature

Abbreviations

AAE	Absolute average percent difference
AC	Alternating current
ACFC	Activated carbon fiber cloth
BET	Brunauer Emmett Teller
CH	Switzerland
DC	Direct current
DR	Dubinin-Radushkevich
ESA	Electrothermal swing adsorption
ESR	Electron spin resonance
EU-27	European Union
FID	Flame ionization detector
GAC	Granular activated carbon
LCA	Life cycle assessment
MSA	Microwave swing adsorption
NPV	Net present value
OCE	Oceanic
PID	Photoionization detector
P-I-D	Proportional integral derivative
PSA	Pressure swing adsorption
RER	Europe
RMS	Root mean square
RTO	Regenerative thermal oxidizer
S	System process
SCR	Silicon controlled rectifier
TRACI	Tools for the reduction and assessment of chemical and other environmental impacts
U	Unit process
UCTE	Union for the Coordination of Transmission of Electricity (Europe)
US	United States
USEPA	United States Environmental Protection Agency
VOC	Volatile organic compound
XRD	X-ray diffraction

Variables

A_1, A_2, A_3, A_4, A_5	Antoine equation constants
A_{cond}	Area for conductive heat transfer
A_{conv}	Area for convective heat transfer
A_{rad}	Area for radiative heat transfer
B_{ann}	Annual operating cost for abatement system
B_{cap}	Capital cost for abatement system
b_0	Toth equation Langmuir affinity constant at a reference temperature of 25 °C
b_1	Toth equation Langmuir affinity constant
b_2	Toth equation constant
C	BET equation constant
C_{isod}	Mean isobutane concentration during an ACFC regeneration heating cycle
C_{isoe}	Isobutane concentration in packaging manufacturing exhaust gas
CSA_E	Effective cross sectional area
c_{ACFC}	Heat capacity per mass of ACFC
c_f	Heat capacity per mass of ACFC cartridge fittings
c_g	Heat capacity per mass of gaseous adsorbate
c_l	Heat capacity per mass of liquid adsorbate
c_{N_2}	Heat capacity per mass of N_2 gas
c_w	Heat capacity per mass of vessel wall
D_A	Areal density
d_{ACFCbc}	Distance between ACFC cartridges
d_{ACFCi}	Inner diameter of annular ACFC cartridge
d_{ACFCo}	Outer diameter of annular ACFC cartridge
d_{GACv}	Diameter of cylindrical GAC vessel
d_{ti}	Inner diameter of stainless steel electrode connected to ACFC cartridge
d_{to}	Outer diameter of stainless steel electrode connected to ACFC cartridge
d_{002}	Interlayer spacing within ACFC nanographite domains
E	Characteristic adsorption energy of the adsorbate
E_{ACFCab}	ACFC adsorption blower annual electrical energy requirements
E_{ACFCco}	ACFC compressor annual electrical energy requirements
E_{ACFCeh}	ACFC electrothermal heating annual electrical energy requirements
$E_{ACFCtot}$	Total annual ACFC electrical energy requirements
E_{GACab}	GAC adsorption blower annual electrical energy requirements

Variables

E_{GACco}	GAC compressor annual electrical energy requirements
E_{GACcw}	GAC condenser annual electrical energy requirements
E_{GACdc}	GAC drying/cooling blower annual electrical energy requirements
E_{GACtot}	Total annual GAC electrical energy requirements
E_{RTO}	Total annual RTO electrical energy requirements
f_a	Ratio of equilibrium adsorption capacity to working adsorption capacity
f_c	Fraction of time the compressor is active during regeneration cycle
f_{dc}	Fraction of time that drying/cooling occurs during a GAC regeneration cycle
f_r	Abatement system isobutane removal efficiency
g	Acceleration of gravity
H	Height (thickness) of single layer of ACFC
H_{ACFCc}	Height of ACFC cartridge
H_{ACFCv}	Height of ACFC vessel
H_{GACv}	Bed thickness for cylindrical GAC vessel
ΔH_s	Isosteric heat of adsorption for an adsorbate/adsorbent
h	Convective heat transfer coefficient
I	Electrical current
k_{iso}	Ratio of the specific heat of isobutane at constant pressure to that at constant volume
L	Length
L_{ACFCv}	Length of ACFC vessel
L_{cond}	Length for conductive heat transfer through stainless steel tubing
L_{conv}	Length for convective heat transfer through ACFC cartridge
L_{GACv}	Length of cylindrical GAC vessel
L_I	Length between interior electrodes
M	Molecular weight
M_{iso}	Molecular weight of isobutane
M_{N_2}	Molecular weight of N_2
m_a	Adsorbed mass
$m_{a,iso}$	Adsorbed mass of isobutane
m_{ACFC}	Mass of ACFC
m_d	Desorbed mass
m_f	Mass of ACFC cartridge fittings
m_{GAC}	Mass of GAC
m_{N_2}	Annual mass of N_2 consumed with ACFC system

Variables

m_{RTOg}	Annual RTO incinerator bed gravel consumption
m_{steam}	Annual mass of steam for GAC system
m_w	Mass of ACFC vessel wall
$\dot{m}_D$	Design mass emission rate for isobutane exhausted from packaging manufacturing
$\dot{m}_{op}$	Mean mass emission rate for isobutane exhausted from packaging manufacturing
N_{ACFCc}	Number of ACFC cartridges per adsorption vessel
N_{ACFCcl}	Number of rows of ACFC cartridges in the length direction of an adsorption vessel
N_{ACFCcw}	Number of rows of ACFC cartridges in the width direction of an adsorption vessel
N_{ACFCl}	Number of ACFC layers per cartridge
Nu_L	Nusselt number
n	Number of matched pairs
n_h	Heterogeneity parameter
$O_{\%}$	Oxygen atomic percent
P	Pressure and partial pressure of single adsorbate
$P_{ACFCiso}$	Pressure required to condense desorbed isobutane from the ACFC system
P_{GACiso}	Pressure required to condense desorbed isobutane from the GAC system
P_{IV}	Electrical power
P_o	Partial pressure of adsorbate at saturation conditions
Pr	Prandtl number
Δp	Pressure drop across system component
Δp_{ACFCl}	Pressure drop across a single sheet of ACFC per superficial velocity of gas flow
Δp_{ACFCv}	Pressure drop across ACFC vessel
Δp_{GACcw}	Pressure drop across GAC cooling water condenser
Δp_{GACs}	Pressure drop across GAC system
Δp_{GACv}	Pressure drop across GAC adsorption bed
Δp_{RTO}	Pressure drop across RTO
Q_a	Flow rate of adsorption gas stream
$Q_{ACFCiso}$	Mean isobutane desorption flow rate at inlet of ACFC compressor
Q_{cw}	Cooling water flow rate for GAC condenser
Q_{dc}	GAC drying/cooling air flow rate
Q_e	Packaging manufacturing exhaust gas flow rate
Q_{GACiso}	Mean isobutane desorption flow rate at inlet of GAC compressor
Q_{N_2}	Flow rate of N_2
q	Mass of adsorbed material per mass of adsorbent at

Variables

	equilibrium
q_i	Initial mass of adsorbed material per mass of adsorbent
q_O	Mass of adsorbed material per mass of adsorbent at saturation conditions
q_w	Working adsorption capacity
R	Electrical resistance
Ra_L	Rayleigh number
R_g	Ideal gas law constant
r	Correlation coefficient
r_{int}	Interest rate
S_{cw}	Volume of cooling water per mass of steam
S_{dc}	Volume of drying/cooling air per mass of GAC
S_{eh}	Electrothermal heating energy per mole of isobutane desorbed
S_{est}	Energy to produce steam
S_{st}	Mass of steam per mass of GAC
T	Temperature
T_b	Boiling point temperature
T_c	Critical temperature
T_{ic}	Temperature of isobutane at compressor inlet
T_R	Reference temperature
T_∞	Ambient temperature
t	Time
t_f	Final integration time
$t_{ACFCads}$	Duration of ACFC system adsorption cycle
t_{GACads}	Duration of GAC system adsorption cycle
t_{GACcw}	Annual operating time for the GAC condenser and compressor
t_{GACdc}	Annual operating time for the GAC drying/cooling blower
t_{GACdes}	Duration of GAC system desorption cycle
t_l	Expected lifetime of abatement system
t_{op}	Annual abatement system operating time
V	Electrical voltage
V_{ACFCv}	Volume of ACFC within an adsorption vessel
V_{iso}	Volume of isobutane desorbed during a regeneration cycle
V_{N_2}	Volume of N_2 used during a regeneration cycle
V_{ng}	Annual RTO natural gas consumption
V_v	Vessel volume
v_{ACFCs}	Superficial velocity through ACFC adsorption bed
v_{GACs}	Superficial velocity through GAC adsorption bed

Variables

W	Width
W_{ACFCv}	Width of an ACFC vessel
W_i	Volume of isobutane adsorbed per mass of adsorbent
W_o	Total adsorbent micropore volume per mass of adsorbent
x_i	Values from data set i
Y_{iso,t_i}	Isobutane to N_2 mole ratio at time i
y	Mole fraction of adsorbate in gas stream
α_a	Thermal coefficient of limiting adsorption
α_d	Thermal diffusivity
α_R	Thermal coefficient of resistivity
γ	Gas viscosity
ε	ACFC emissivity
λ	X-ray wavelength
θ	X-ray incidence angle
ρ_{ACFCic}	Density of isobutane at the inlet of the ACFC compressor
ρ_b	Density of adsorbate at its boiling point temperature
ρ_c	Density of adsorbate at its critical temperature
ρ_f	Fiber density
ρ_{GACic}	Density of isobutane at the inlet of the GAC compressor
ρ_{li}	Density of liquid isobutane
ρ	Electrical resistivity
ρ_R	Electrical resistivity at reference temperature
σ	Stephen-Boltzmann constant
ω_{cond}	Thermal conductivity coefficient for stainless steel tubing
ω_{conv}	Thermal conductivity of N_2 purge gas

References

ABB Air Preheater Inc. Combuchanger Model 1-15.0AS3+ design specifications. Wellsville, NY, USA. Issued Jan 2000.

Abromaitis V, Ochmanaite V, Denafas G, Martuzevicius D. LCA-based comparison of VOC removal from exhaust gases by plasma and "conventional" end-of-pipe methods. 8th International Conference on Environmental Engineering, Vilnius, Lithuania, May 19-20 2011, p. 1-5.

Altwicker ER, Canter LW, Cha SS, Chuang KT, Liu DHF, Ramachandran G, Raufer RK, Reist PC, Sanger AR, Turk A, Wagner CP. Air pollution in Environmental Engineers' Handbook. Boca Raton, FL: CRC Press LLC 1999.

An H, Feng B. Desorption of CO_2 from activated carbon fibre-phenolic resin composite by electrothermal effect. International Journal of Greenhouse Gas Control. 2010;4(1):57-63.

Anonymous. Engineer from Indiana Packaging Manufacturing Facility. Personal correspondence. 2013.

Askalany AA, Salem M, Ismail IM, Ali AHH, Morsy MG. A review on adsorption cooling systems with adsorbent carbon. Renewable & Sustainable Energy Reviews. 2012;16(1):493-500.

Atkinson JD, Zhang Z, Yan Z, Rood MJ. Evolution and impact of acidic oxygen functional groups on activated carbon fiber cloth during NO oxidation. Carbon. 2013;54:444-453.

Bansal RC, Goyal M. Activated Carbon Adsorption. Boca Raton, FL, USA: Taylor & Francis Group CRC Press 2005.

Bare JC, Norris G, Pennington DW, McKone T. TRACI − The tool for the reduction and assessment of chemical and other environmental impacts. Journal of Industrial Ecology. 2003;6(3).

Baudu M, Le Cloirec P, Martin G. Thermal regeneration by joule effect of activated carbon used for air treatment. Environmental Technology. 1992;13(5):423-35.

Bourdin V, Gray PG, Grenier P, Terrier MF. An apparatus for adsorption dynamics studies using infrared measurement of the adsorbent temperature. Review of Scientific Instruments. 1998;69(5):2130-6.

Brun K, Kurz R, Measurement uncertainties encountered during gas turbine driven compressor field testing. Journal of Engineering for Gas Turbines Power. 2001;121(3):62-9.

Brunauer S, Deming LS, Deming WE, Tellef E. On a theory of the van der Waals adsorption of gases. Journal of the American Chemical Society. 1940;62(7):1723-32.

Cheng, TL. Taiwan Carbon Technology Co., Ltd., price quote for AW1103. Personal correspondence. Oct, 2010.

Cooper D, Alley FC. Air pollution control: A design approach. Boston, MA, USA: PWS Engineering 1986.

Dacey JR, Quinn DF, Gallagher, JT. Effect of adsorbed vapors on electrical conductivity of saran carbon. Carbon. 1966;4(1):73-80.

Das D, Gaur V, Verma N. Removal of volatile organic compound by activated carbon fiber. Carbon. 2004;42(14):2949-2962.

Daud W, Ali WSW, Sulaiman MZ. Effect of activation temperature on pore development in activated carbon produced from palm shell. Journal of Chemical Technology and Biotechnology. 2003;78(1):1-5.

De Benedetti B, Toso D, Baldo GL, Rollino S. EcoAudit: A renewed simplified procedure to facilitate the environmentally informed material choice orienting the further life cycle analysis for ecodesigners. Materials Transactions. 2010;51(5):832-7.

Del Vecchio ND, Barghi S, Puskas JE. New method for monitoring of adsorption column saturation and regeneration I. Demonstration of the measurement principle. Chemical Engineering Communications. 2002;189(3):352-71.

Del Vecchio ND, Barghi S, Primak S, Puskas JE. New method for monitoring of adsorption column saturation and regeneration II: on-line measurement. Chemical Engineering Science. 2004;59(12):2389-400.

Do DD. Adsorption analysis: Equilibria and kinetics. London, UK: Imperial College Press 1998.

Do DD, Do HD. Surface diffusion of hydrocarbons in activated carbon: comparison between constant molar flow, differential permeation and differential adsorption bed methods. Adsorption. 2001;7(3):189-209.

Dombrowski KD, Lehmann CMB, Sullivan PD, Ramirez D, Rood MJ, Hay KJ. Organic vapor recovery and energy efficiency during electric regeneration of an activated carbon fiber cloth adsorber. Journal of Environmental Engineering. 2004;130(3):268-75.

DOW Answer Center, Accessed Jun 2014. https://dow-answer.custhelp.com/app/answers/detail/a_id/3777.

Dubinin MM. Fundamentals of the theory of adsorption in micropores of carbon adsorbents: Characteristics of their adsorption properties and microporous structures. Carbon. 1989;27(37):457-67.

Enoki T, Takai K. Unconventional electronic and magnetic functions of nanographene-based host-guest systems. Dalton Transactions. 2008(29):3773-81.

Emamipour H, Hashisho Z, Cevallos D, Rood MJ, Thurston DL, Hay KJ, Kim BJ, Sullivan PD. Steady-state and dynamic desorption of organic vapor from activated carbon with electrothermal swing adsorption. Environmental Science & Technology. 2007;41(14):5063-9.

Enoki T, Takai K, Kiguchi M. Magnetic Edge State of Nanographene and Unconventional Nanographene-Based Host-Guest Systems. Bulletin of the Chemical Society of Japan. 2012;85(3):249-64.

Fabuss BM, Dubois WH. Carbon adsorption electrodesorption process. 63rd Annual Meeting of the Air Pollution Control Association. St. Louis, MO, USA 1970:p 18.

Fruergaard T, Hyks J, Astrup T. Life-cycle assessment of selected management options for air pollution control residues from waste incineration. Science of the Total Environment. 2010;408(20):4672-80.

Fung AWP, Wang ZH, Dresselhaus MS, Dresselhaus G, Pekala RW, Endo M. Coulomb-gap magnetotransport in granular and porous carbon structures. Physical Review B. 1994;49(24):17325-35.

Fung AWP, Rao AM, Kuriyama K, Dresselhaus MS, Dresselhaus G, Endo M, Shindo N. Raman scattering and electrical conductivity in highly disordered activated carbon fibers. Journal of Materials Research. 1993a;8(3):489-500.

Fung AWP, Dresselhaus MS, Endo M. Transport properties near the metal-insulator transition in heat-treated activated carbon fibers. Physical Review B. 1993b;48(20):14953-62.

Gabarrell X, Font M, Vicent T, Caminal G, Sarrá M, Blánquz P. A comparative life cycle assessment of two treatment technologies for the Grey Lanaset G textile dye: biodegradation by Trametes versicolor and granular activated carbon adsorption. The International Journal of Life Cycle Assessment. 2012;17(5):613-24.

Gales L, Mendes A, Costa C. Removal of acetone, ethyl acetate and ethanol vapors from air using a hollow fiber PDMS membrane module. Journal of Membrane Science. 2002;197(1-2):211-22.

Hao S, Takai K, Kang F, Enoki T. Electronic and magnetic properties of acid-adsorbed nanoporous activated carbon fibers. Carbon. 2008;46(1):110-6.

Hao S, Takai K, Joly J, Yokota K, Kiguchi M, Enoki T. Magnetic properties and interplay between nanographitic host and nitric acid guest in nanographene-based nanoporous carbon. Bulletin of the Chemical Society of Japan. 2012;85(3):376-88.

Handbook of chemistry and physics 64th edition. Boca Raton, FL, USA: CRC Press 1983-1984.

Hashisho Z, Rood MJ, Botich L. Microwave-swing adsorption to capture and recover vapors from air streams with activated carbon fiber cloth. Environmental Science & Technology. 2005;39(17):6851-9.

Hashisho Z, Rood MJ, Barot S, Bernhard J. Role of functional groups on the microwave attenuation and electric resistivity of activated carbon fiber cloth. Carbon. 2009;47(7):1814-23.

Hayes J. American Kynol, price quote for ACFC-5092-15. Personal correspondence. Oct, 2010.

Hayes J. Activated carbon fibers and textiles: Properties and applications. American Kynol Inc. brochure. 1994.

Hayes J, Sakai N. Cyclohexanone recovery on activated carbon fiber. 94th Annual Meeting of the Air & Waste Management Association. Orlando, Fl, USA 2001.

Hayes J. Novoloid fibers. Encyclopedia of Chemical Technology, Vol 16. John Wiley and Sons 1981:125-38.

Haynes WM, Hiza MJ. Measurements of the orthobaric liquid densities of methane, ethane, propane, isobutane, and normal butane. Journal of Chemical Thermodynamics. 1977;9(2):179-87.

Heaney BM. Electrical Conductivity and Resistivity. Boca Raton, FL, USA: CRC Press 2003.

Hunter P, Oyama ST. Control of volatile organic compound emissions: Conventional and emerging technologies. NY, USA: John Wiley 2000.

Incropera FP, Dewitt DP. Fundamentals of Heat Transfer. NY, USA: John Wiley & Sons 1981.

Indiana Department of Environmental Management. Title V Operating Permit. T099-31133-00028, 2012.

ISO: Environmental management life cycle assessment principles and framework, EN ISO 14040, 2006.

ISO: Environmental management life cycle assessment requirements and guidelines, EN ISO 14044, 2006.

Johnsen DL, Mallouk KE, Rood MJ. Control of electrothermal heating during regeneration of activated carbon fiber cloth. Environmental Science & Technology. 2011a;45(2):738-43.

Johnsen DL, Rood MJ. Temperature control of activated carbon fiber cloth regeneration with resistance feedback. 104th Annual Meeting of the Air & Waste Management Association. Orlando, FL, USA, 2011b:No. 148, pp. 12.

Johnsen DL, Rood MJ. Temperature Control during Regeneration of Activated Carbon Fiber Cloth with Resistance-Feedback. Environmental Science & Technology. 2012a;46(20):11305-12.

Johnsen DL, Emamipour H, Rood MJ. Monitor and control of an electrothermal swing adsorption based on remote electrical measurements. 105th Annual Meeting of the Air & Waste Management Association. San Antonio, TX, USA, 2012b:No. 75, pp. 14.

Johnsen DL, Emamipour H, Rood MJ. Effects of activated carbon fiber cloth's physical structure, chemical composition, and adsorbed material on its electrical resistance. 106th Annual Meeting of the Air & Waste Management Association. Chicago, IL, USA, 2013a:No. 12476, pp. 14.

Johnsen DL, Emamipour H, Zhang Z, Yan Z, Rood MJ. Relationship between activated carbon fiber cloth's structure and electrical resistance. Carbon. Rio de Janeiro, Br, 2013b:No. 120, pp. 4.

Johnsen DL, Emamipour H, Zhang Z, Yan Z, Rood MJ. Effect of isobutane adsorption on the electrical resistivity of activated carbon fiber cloth with select physical and chemical properties. Carbon. 2014a;76:435-45.

Johnsen DL, Zhang Z, Emamipour H, Yan Z, Rood MJ. Effect of isobutane adsorption on the electrical resistivity of activated carbon fiber cloth with select physical and chemical properties. 107th Annual Meeting of the Air & Waste Management Association. Long Beach, CA, USA, 2014b: No. 32326.

Joly VLJ, Takai K, Enoki T. Oxygen guest molecules in the nanopores of nanographite-network. Journal of Physics and Chemistry of Solids. 2010;71(4):575-8.

Kaneko K, Ishii C, Ruike M, Kuwabara H. Origin of superhigh surface area and microcrystalline graphitic structures of activated carbons. Carbon. 1992;30(7):1075-88.

Kempinski M, Kempinski W, Kaszynski J, Sliwinska-Bartkowiak M. Model of spin localization in activated carbon fibers. Applied Physics Letters. 2006;88(14).

Kempinski M, Kempinski W, Sliwinska-Bartkowiak M. Size modification of nanographite system of activated carbon fibers studied by EPR. Acta Physica Polonica A. 2005;108(2):339-43.

Khan FI, Ghoshal AK. Removal of volatile organic compounds from polluted air. Journal of Loss Prevention in the Process Industries. 2000;13(6):527-45.

Kobayashi N, Enoki T, Ishii C, Kaneko K, Endo M. Gas adsorption effects on structural and electrical properties of activated carbon fibers. Journal of Chemical Physics. 1998;109(5):1983-90.

Lange's Handbook of Chemistry. 10th edition. NY, USA: McGraw-Hill 1992.

Leson G, Winer AM. Biofiltration - an innovative air-pollution control technology for VOC emissions. Journal of the Air & Waste Management Association. 1991;41(8):1045-54.

Lide DR. Handbook of Chemistry and Physics. Boca Raton, FL, USA: CRC Press 1993.

Liu W, Zhao G. Effect of temperature and time on microstructure and surface functional groups of activated carbon fibers prepared from liquefied wood. Bioresources. 2012;7(4):5552-67.

Lo S, Ramirez D, Rood MJ, Hay KJ. Characterization of the physical and thermal properties of a series of activated carbon fiber cloths. 95th Annual Meeting of the Air & Waste Management Association. Baltimore, MD, USA 2002:pp. 17.

Lordgooei M, Carmichael KR, Kelly TW, Rood MJ, Larson SM. Activated carbon cloth adsorption-cryogenic system to recover toxic volatile organic compounds. Gas Separation & Purification. 1996;10(2):123-30.

Luo L, Ramirez D, Rood MJ, Grevillot G, Hay KJ, Thurston DL. Adsorption and electrothermal desorption of organic vapors using activated carbon adsorbents with novel morphologies. Carbon. 2006;44(13):2715-23.

Mallouk KE, Johnsen DL, Rood MJ. Capture and recovery of isobutane by electrothermal swing adsorption with post-desorption liquefaction. Environmental Science & Technology. 2010;44(18):7070-5.

Mallouk KE, Rood MJ. Characterization of Adsorption of Select Organic Gases on Activated Carbon Fiber Cloth. 105th Annual Meeting of the Air & Waste Management Association. San Antonio, TX, USA, No.65, 2012:pp. 12.

Mallouk KE, Rood MJ. Performance of an electrothermal swing adsorption system with postdesorption liquefaction for organic gas capture and recovery. Environmental Science & Technology. 2013;47(13):7373-9.

Masel RI. Principles of adsorption and reaction on solid surfaces. NY, USA: Wiley; 1996.

McIntosh R, Haines RS, Benson GC. The effect of physical adsorption on the electrical resistance of activated carbon. Journal of Chemical Physics. 1946;15(1):17-27.

Mrozowski S. Semiconductivity and diamagnetism of polycrystalline graphite and condensed ring systems. Physical Review. 1952;85(4):609-20.

Noll KE. Fundamentals of air quality systems: Design of air pollution control devices. Annapolis, MD, USA: American Academy of Environmental Engineers 1999.

Noll KE, Gounaris V, Hou W. Adsorption technology for air and water pollution control. Chelsea, MI, USA: Lewis Publishers, Inc. 1984.

Oshida K, Kogiso K, Matsubayashi K, Takeuchi K, Kobayashi S, Endo M, Dresselhaus MS, Dresselhaus G. Analysis of pore structure of activated carbon fibers using high resolution transmission electron microscopy and image processing. Journal of Materials Research. 1995;10(10):2507-17.

Park JW, Lee SS, Choi DK, Lee YW, Kim YM. Adsorption equilibria of toluene, dichloromethane, and trichloroethylene onto activated carbon fiber. Journal of Chemical and Engineering Data. 2002;47(4):980-3.

Perry RH, Green DW. Perry's Chemical Engineers' Handbook, 7th edition. NY, USA: McGraw Hill 1997.

Petkovska M, Tondeur D, Grevillot G, Granger J, Mitrovic M. Temperature-swing gas separation with electrothermal desorption step. Separation Science and Technology. 1991;26(3):425-44.

Ponec V, Knor Z, Cerný S. Adsorption on solids. London, UK: Butterworths 1974.

Ramirez D, Emamipour H, Vidal EX, Rood MJ, Hay KJ. Capture and recovery of methyl ethyl ketone with electrothermal-swing adsorption systems. Journal of Environmental Engineering. 2011;137(9):826-832.

Ramirez D, Sullivan PD, Rood MJ, Hay KJ. Equilibrium adsorption of phenol-, tire-, and coal-derived activated carbons for organic vapors. Journal of Environmental Engineering. 2004;130(3):231-41.

Ramos ME, Bonelli PR, Cukierman AL. Physico-chemical and electrical properties of activated carbon cloths effect of inherent nature of the fabric precursor. Colloids and Surfaces a-Physicochemical and Engineering Aspects. 2008;324(1-3):86-92.

Ruthven DM. Principals of adsorption and adsorption processes. USA: John Wiley & Sons 1984.

Ryberg M, Vieira MDM, Zgola M, Bare J, Rosenbaum RK. Updated US and Canadian normalization factors for TRACI 2.1. Clean Technology and Environmental Policy. 2014;16:329-39.

Saffarian S. A LCA study of activated carbon adsorption and incineration in air pollution control. University of Boras, Master of Science thesis, 2009.

Sato H, Kawatsu N, Enoki T, Endo M, Kobori R, Maruyama S, Kaneko K. Physisorption-induced change in the magnetism of microporous carbon. Carbon. 2007;45(1):214-7.

Sauer B, Franklin W, Miner R, Word D, Upton B. Environmental tradeoffs: Life cycle approach to evaluate the burdens and benefits of emission control systems in the wood panel industry. Forest Products Journal. 2002;52(3):50-9.

Saysset S, Grevillot G, Lamine AS. Adsorption of volatile organic compounds on carbonaceous adsorbent and desorption by direct Joule effect. Re´cents Progre`s en Ge´nie des Proce´de´s, No. 68, *Proc. of 2nd European Congress of Chemical Engineering*, Montpellier, France, Oct 5-7, 1999, European Federation of Chemical Engineering, Lyon, France, 389-396.

Shibayama Y, Sato H, Enoki T, Bi XX, Dresselhaus MS, Endo M. Novel electronic properties of a nano-graphite disordered network and their iodine doping effects. Journal of the Physical Society of Japan. 2000;69(3):754-67.

Shell Oil, Shell chemicals toluene data sheet. CAS# 108-88-3. Issued 2007.

Shell Oil, Shell chemicals acetone data sheet. CAS# 67-64-1. Issued 2010.

SimaPro LCA software version 7.3.3. 2012.

Smeltzer WW, McIntosh R. The effect of physical adsorption on the electrical resistance of active carbon. Canadian Journal of Chemistry. 1953;15(1):11.

Snyder JD, Leesch JG. Methyl bromide recovery on activated carbon with repeated adsorption and electrothermal regeneration. Industrial & Engineering Chemistry Research. 2001;40(13):2925-33.

Subrenat A, Baleo JN, Le Cloirec P, Blanc PE. Electrical behaviour of activated carbon cloth heated by the joule effect: desorption application. Carbon. 2001;39(5):707-16.

Subrenat A, Le Cloirec P, Blanc PE. Removal of VOC by adsorption-desorption cycles using activated carbon cloth filter: Regeneration by Joule effect. Adsorption Science and Technology. World Scientific, Singapore. 2000, ISBN 981-02-4263-8, 361–365.

Subrenat A, Le Cloirec P. Thermal Behavior of activated carbon cloths heated by Joule effect. Journal of Environmental Engineering. 2003;129(12):1077-84.

Subrenat A, Le Cloirec P. Volatile organic compound (VOC) removal by adsorption onto activated carbon fiber cloth and electrothermal desorption: An industrial application. Chemical Engineering Communications. 2006;193(4):478-86.

Sullivan PD, Rood MJ, Grevillot G, Wander JD, Hay KJ. Activated carbon fiber cloth electrothermal swing adsorption system. Environmental Science & Technology. 2004a Sep;38(18):4865-77.

Sullivan PD, Rood MJ, Hay KJ, Qi S. Adsorption and electrothermal desorption of hazardous organic vapors. Journal of Environmental Engineering. 2001;127(3):217-23.

Sullivan PD, Rood MJ, Dombrowski KD, Hay KJ. Capture of organic vapors using adsorption and electrothermal regeneration. Journal of Environmental Engineering. 2004b;130(3):258-67.

Sullivan PD, Stone BR, Hashisho Z, Rood MJ. Water adsorption with hysteresis effect onto microporous activated carbon fabrics. Adsorption-Journal of the International Adsorption Society. 2007;13(3-4):173-89.

Sumanasekera GU, Chen G, Takai K, Joly J, Kobayashi N, Enoki T, Eklund PC. Charge transfer and weak chemisorption of oxygen molecules in nanoporous carbon consisting of a disordered network of nanographene sheets. Journal of Physics-Condensed Matter. 2010;22(33).

Sun J, Chen S, Rood MJ, Rostam-Abadi M. Correlating N_2 and CH_4 adsorption on microporous carbon using a new analytical model. Energy & Fuel 1998;12(6):1071–8.
Suzuki T, Kaneko K. Structural change of activated carbon fibers with desorption by insitu X-ray diffraction. Carbon. 1988;26(5):744-5.

Tobias H, Cohen H, Soffer A. The electrical-conductivity of carbon-fibre adsorbents. Journal of the Chemical Society-Faraday Transactions I. 1986;82:2627-34.

USEIA, Electric power monthly: State net electricity profile by source. 2014a.

USEIA, Annual energy outlook, 2014. Published May 2014. Last accessed Jun 2014b. http://www.eia.gov/forecasts/aeo/.

USEPA, 2011 US national emissions inventory. Version 1, released Sep 2013.

USEPA, An Introduction to indoor air quality (IAQ) volatile organic compounds (VOCs). Revised Mar 2011a. Last accessed Jun 2014. http://www.epa.gov/iaq/voc.html.

USEPA, AP 42 emissions standards. Section 1.5: Liquefied petroleum gas combustion. 1996.

USEPA, Control of VOC emissions from polystyrene foam manufacturing. Office of Air Quality Planning and Standards, EPA-450/3-90-020. Research Triangle Park, NC, USA. 1990.

USEPA, Clean air technology center (CATC). General information on CATC products, Packed-bed/packed-tower wet scrubber fact sheet. Last accessed Jun 2014. http://www.epa.gov/ttncatc1/products.html.

USEPA, Definition of volatile organic compounds (VOC). 40 CFR 51.100(s). 2009.

USEPA, Emissions factors & AP 42, Compilation of air pollutant emission factors. 2011b. Last accessed Jun 2014. http://www.epa.gov/ttnchie1/ap42/.

USEPA, Inventory of US greenhouse gas emissions and sinks: 1990-2009. Washington DC, USA 2011c.

USEPA, National risk management research laboratory office of research and development. Life cycle assessment: Principles and practice. 2006.

USEPA, Office of Air Quality Planning and Standards. EPA air pollution control cost manual. Research Triangle Park, NC, USA. 2002.

USFED, Selected interests rates (daily) – H.15. Board of governors of the federal reserve interest rates. 2014. Last accessed Jun 2014.
http://www.federalreserve.gov/releases/h15/data.htm#fn1

Wang DC, Li YH, Li D, Xia YZ, Zhang JP. A review on adsorption refrigeration technology and adsorption deterioration in physical adsorption systems. Renewable & Sustainable Energy Reviews. 2010;14(1):344-53.

Wang Y, Ercan C, Khawajah A, Othman R. Experimental and theoretical study of methane adsorption on granular activated carbons. American Institute of Chemical Engineers Journal. 2012;58:782–788.

Wark K, Warner CF, Davis WT. Air pollution: Its origin and control. Menlo Park, CA, USA: Addison-Wesley 1998.

Weidema BP, Wesnaes, Data quality management for life cycle inventories-an example of using data quality indicators. Journal of Cleaner Production. 1996;4(3-4):167-74.

Welty J, Wicks C, Rorrer G, Wilson R. Fundamentals of momentum, heat and mass transfer 5th edition. NY, USA: John Wiley & Son 2007.

Yang RT. Gas separation by adsorption processes. London, UK: Imperial College Press 1999.

Yao M, Zhang Q, Hand DW, Perrarn D, Taylor R. Adsorption and regeneration on activated carbon fiber cloth for volatile organic compounds at indoor concentration levels. Journal of the Air & Waste Management Association. 2009;59(1):31-6.

Yaws CL, Yang HC. Thermodynamic and physical property data. Houston, TX, USA: Gulf Publishing Company 1992, 181-206.

Yu FD, Luo LA, Grevillot G. Adsorption isotherms of VOCs onto an activated carbon monolith: Experimental measurement and correlation with different models. Journal of Chemical and Engineering Data. 2002;47(3):467-73.

Yu FD, Luo LA, Grevillot G. Electrothermal desorption using joule effect on an activated carbon monolith. Journal of Environmental Engineering. 2004;130(3):242-8.

Yu P, Cardona M. Fundamentals of semiconductors: Physics and materials properties. Springer 2004.

Zerbonia RA, Brockmann CM, Peterson PR, Housley D. Carbon bed fires and the use of carbon canisters for air emissions control on fixed-roof tanks. 93rd Annual Meeting of the Air & Waste Management Association. Salt Lake City, UT, USA, 2000: No. 256.

Zhu W., Kapteijn F., Groen J.C., Moulijn J.A. Adsorption on Kureha activated carbon: Isotherms and kinetics. Adsorption. 2005;11(1):637-41.

Ziegler JG, Nichols NB. Optimum settings for automatic controllers. Journal of Dynamic Systems Measurement and Control-Transactions of the ASME. 1993;115(2B):220-2.